Inducing and suppressing the alternative lengthening of telomeres mechanism in cancer cells

Dissertation

submitted by Delia Braun

2018

Dissertation

submitted to the
Combined Faculties for the Natural Sciences and for Mathematics
of the Ruperto-Carola University of Heidelberg, Germany
for the degree of
Doctor of Natural Sciences

presented by
Dipl.-Chem. Delia Maria Braun
born in Offenburg, Germany
Oral examination: 24.07.2018

Inducing and suppressing the alternative lengthening of telomeres mechanism in cancer cells

Referees: Prof. Dr. Karsten Rippe
Prof. Dr. Brian Luke

This work was performed from September 2012 to January 2018 under the supervision of Prof. Dr. Karsten Rippe in the Division Chromatin Networks at the DKFZ and the Bioquant Center in Heidelberg, Germany.

Declaration

I hereby declare that I have written the submitted dissertation “Inducing and suppressing the alternative lengthening of telomeres mechanism in cancer cells” myself and in this process, have used no other sources or materials than those explicitly indicated. I hereby declare that I have not applied to be examined at any other institution, nor have I used the dissertation in this or any other form at any other institution as an examination paper, nor submitted it to any other faculty as a dissertation.

_____ _____

(Place, Date) Delia Braun

Für Philipp und Lina

Table of contents

Materials and Methods 19

List of publications

During this thesis, the following publications with my contribution appeared:

Braun DM, Chung I, Kepper N, Deeg KI, and Rippe K (2018). *TelNet* – a database of human and yeast genes involved in telomere maintenance. *BMC Genetics* **19**(32): 1-10.

Sieverling L, Hong C, Koser SD, Ginsbach P, Kleinheinz K, Hutter B, Braun DM, Cortes-Ciriano I, Xi R, Kabbe R, Park PJ, Eils R, Schlesner M, Rippe K, Jones DTW, Brors B, and Feuerbach L (2018). Genomic footprints of activated telomere maintenance mechanisms in cancer. *Nature communications, in press*. Preprint: *bioRxiv* 157560. doi: 10.1101/157560.

Deeg KI, Chung I, Poos AM, Braun DM, Korshunov A, Oswald M, Kepper N, Bender S, Castel D, Lichter P, Grill J, Pfister SM, König R, Jones DTW, and Rippe K (2017). Dissecting telomere maintenance mechanisms in pediatric glioblastoma. Preprint: *bioRxiv* 129106. doi: 10.1101/129106.

Summary

Cancer cells extend critically short telomeres either by reactivating the reverse transcriptase telomerase or by employing alternative lengthening of telomeres (ALT). The ALT mechanism depends on proteins involved in DNA repair and homologous recombination (HR). High-throughput sequencing is increasingly used to analyze whole genome sequences (WGS) and gene expression in patient samples, and potentially, provides a rich resource of information on ALT. However, in ALT cancers the only recurrent mutations identified so far are in the chromatin remodeler ATRX (alpha thalassemia/ mental retardation syndrome X-linked), the histone chaperone DAXX (death domain associated protein), and the histone variant H3.3. In addition, gene expression signatures for patient stratification into ALT-positive and ALT-negative as well as a systematic approach to identify genes involved in telomere maintenance (TM) and in particular ALT via functional annotation are currently missing. One well-established hallmark of ALT is the dislocation of the PML (promyelocytic leukemia) protein to telomeres in ALT-associated PML nuclear bodies (APBs). These colocalizations are reliable biomarkers for ALT-positive tumors, but the functional role of PML during the development of ALT remains elusive. In this thesis, I have addressed the issues raised above by work in three areas: First, the *TelNet* database was developed as a comprehensive compilation of TM genes. Proteins involved in TM were collected, functionally categorized, and evaluated by applying a significance score. In addition to various search modes, a statistics page was implemented for TM pathway analysis and for prediction of the active TM mechanism (TMM). Second, ALT candidate genes were identified by gene expression analysis using four different approaches and isogenic cellular systems: (i) ALT suppression by HDAC inhibitor SAHA in U2OS cells, (ii) ALT induction by ASF1 depletion in HeLa cells with long telomeres (LT), (iii) reduced ALT induction capacity of the ASF1 depletion in HeLa LT cells by SAHA treatment, and (iv) deletion of *EST*2 (ever shorter telomeres 2), the telomerase protein subunit, in budding yeast to generate survivors that maintain telomeres by type II recombination, equivalent to the human ALT mechanism. A differential gene expression analysis comparing perturbed cells with the unperturbed control cells revealed a positive correlation of WNT and TGFβ signaling with the presence of ALT and on the other hand a negative association of TNF/ NFκB/ MAP kinase signaling. Furthermore, a role as potential ALT enhancers was predicted for *KCTD15* and *TNNC1*. In budding yeast type II survivors, approximately 30 genes showed a relatively small albeit statistically significant change in gene expression as compared to pre-senescent cells. Genes within the iron-regulon were overrepresented among downregulated genes, including *FIT1, FIT2, ARN2,* and *FRE4*, indicating stress response. Third, I investigated the functional role of PML in the ALT pathway by recruiting PML to telomeres in cells with and without ALT background. The formation of artificial APBs induced telomere

clustering and subsequently increased the abundance of extrachromosomal repeats as an ALT feature in both ALT-positive and ALT-negative cells. The results obtained in this thesis facilitate patient stratification based on deep sequencing data according to their TM mechanism and provide a better understanding of the functional role of APBs for ALT.

Zusammenfassung

Krebszellen verlängern kritisch kurze Telomere entweder durch Reaktivierung der reversen Transkriptase Telomerase oder durch alternative Telomerverlängerung (ALT). Der ALT-Mechanismus hängt von Proteinen ab, die an der DNA-Reparatur und der homologen Rekombination (HR) beteiligt sind. Die Hochdurchsatzsequenzierung wird zunehmend zur Analyse der Genomsequenz und Genexpression in Patientenproben verwendet und bietet möglicherweise eine reichhaltige Informationsquelle über ALT. Bei ALT-Karzinomen wurden bisher nur rekurrente Mutationen in den Genen des Chromatin-modellierenden Faktors ATRX, des Histon-Chaperons DAXX und der Histonvariante H3.3 identifiziert. Darüber hinaus fehlen derzeit Genexpressionssignaturen für die Stratifizierung von Patienten in ALT-positive und ALT-negative Patientengruppen. Weiterhin mangelt es an einem systematischen Ansatz zur Identifizierung von an der Telomer-Erhaltung und insbesondere an ALT beteiligten Genen mittels funktioneller Annotation. Ein bekanntes Merkmal von ALT ist die Dislokation des PML-Proteins an Telomere in ALT-assoziierten PML-Kernkörpern (APBs). Diese Ko-lokalisationen sind zuverlässige Biomarker für ALT-positive Tumore, aber die funktionelle Rolle von PML während der Entwicklung von ALT ist nicht bekannt. In dieser Arbeit habe ich die oben genannten Inhalte durch Arbeiten in drei Abschnitten behandelt: Zuerst wurde die *TelNet*-Datenbank als umfassende Zusammenstellung von TM-Genen entwickelt. Proteine, die an der Erhaltung der Telomere beteiligt sind, wurden gesammelt, funktional kategorisiert und mit einem Signifikanzwert bewertet. Zusätzlich zu verschiedenen Suchmodi wurde eine Statistikseite für die TM-Analyse und für die Vorhersage des aktiven Telomer-Erhaltungsmechanismus implementiert. Zweitens wurden ALT-Kandidatengene durch Genexpressionsanalyse unter Verwendung von vier verschiedenen Ansätzen und isogenen zellulären Systemen identifiziert: (i) ALT - Suppression durch den Histondeacetylase Inhibitor SAHA in U2OS-Zellen, (ii) ALT-Induktion durch ASF1-Depletion in HeLa-Zellen mit langen Telomeren (LT), (iii) reduzierte ALT-Induktionskapazität der ASF1-Depletion in HeLa-LT-Zellen durch SAHA-Behandlung und (iv) Deletion von katalytischen Telomerase-Einheit *EST2* in Hefe, um Hefezellen zu erhalten, die Telomere mithilfe von Rekombination erhalten, äquivalent zum humanen ALT Mechanismus. Eine differentielle Genexpressionsanalyse ergab eine positive Korrelation des WNT und TGFβ Signalwegs und auf der anderen Seite eine negative Korrelation des TNF/ NFκB/ MAP Kinase Signalwegs mit aktivem ALT Mechanismus. Darüber hinaus wurden *KCTD15* und *TNNC1* als potentielle ALT-Gene vorhergesagt. Bei ALT-Hefezellen zeigten ca. 30 Gene eine relativ geringe, wenn auch statistisch signifikante Veränderung der Genexpression im Vergleich zu pre-seneszenten Zellen.

Herunterreguliert waren Gene des Eisen-Regulons, einschließlich *FIT1*, *FIT2*, *ARN2* und *FRE4*, was auf eine Stressreaktion hinweisen könnte. Drittens untersuchte ich die funktionelle Rolle von PML im ALT Mechanismus durch Rekrutierung von PML zu Telomeren in Zellen mit und ohne aktiven ALT-Mechanismus. Die Bildung von künstlichen APBs induzierte eine Ansammlung von Telomeren und erhöhte anschließend die Menge an extrachromosomalen Telomersequenzen sowohl in ALT-positiven als auch in ALT-negativen Zellen. Die in dieser Arbeit erzielten Ergebnisse erleichtern die Stratifizierung von Patienten basierend auf Transkriptomsequenzierungsdaten gemäß ihrem TM-Mechanismus und ermöglichen ein besseres Verständnis der funktionellen Rolle von APBs für ALT.

List of figures

List of tables

Abbreviations

ABCC8 ..... ATP binding cassette subfamily C member 8
ALT ..... alternative lengthening of telomeres
aka ..... also known as
APB ..... ALT-associated PML nuclear body
ASF1A/ B ..... anti-silencing function 1A/ B histone chaperone
ATM ..... ataxia telangiectasia mutated protein
ATR ..... ataxia telangiectasia and Rad3-related protein
ATRi ..... ATR inhibitor
ATRX ..... alpha thalassemia/ mental retardation syndrome X-linked
BH/ FDR ..... method of Benjamini, Hochberg, and Yekutieli to control the false discovery rate
BiFC ..... PCA/ bimolecular fluorescent complementation
BSA ..... bovine serum albumin
C-circles ..... circular C-rich extrachromosomal telomeric repeats
CC-assay ..... C-circle assay
cDNA ..... complementary DNA
CLSM ..... confocal laser scanning microscopy
CST ..... protein complex: CDC13, STN1, TEN1
Ctrl ..... control
D-loop ..... displacement loop
DAXX ..... death-associated protein 6
DAPI ..... 4',6-diamidino-2-phenylindole
dATP ..... deoxyadenosine triphosphate
DAVID ..... database for annotation, visualization and integrated discovery (Dennis *et al.*, 2003)
dCTP ..... deoxycytidine triphosphate
DDR ..... DNA damage response
DESeq ..... Differential expression analysis for sequence count data, DESeq2 package (Love *et al.*, 2014)
dGTP ..... deoxyguanosine triphosphate
DMEM ..... dulbecco's modifed eagle medium
DMSO ..... dimethylsulfoxid
DNA ..... deoxyribonucleic acid
dNTP ..... deoxynucleoside triphosphate
DSB ..... DNA double-strand break
dTTP ..... deoxythymidine triphosphate
ECTRs ..... extrachromosomal telomeric repeats
EDTA ..... ethylenediaminetetraacetic acid
EST2 ..... ever shorter telomeres, catalytic subunit of budding yeast telomerase
EtOH ..... ethanol
FACS ..... fluorescence activated cell sorting
FBS ..... fetal bovine serum

FDR ..... false discovery rate
FISH ..... fluorescence in situ hybridization
FITC..... fluorescein isothiocyanate
FLAG ..... protein tag (DYKDDDDK)
FWHM ..... full width at half maximum
G..... plasmid encoding GFP (in the context of this thesis)
G4..... G-quadruplex
gDNA..... genomic DNA
GFP ..... green fluorescent protein
GO..... gene ontology
GRN163 ..... telomerase inhibitor (Geron, USA)
GST ..... glutathione S-transferase
H3.3..... histone 3 variant 3
H3.3-K27M ..... H3.3 with lysine 27-to-methionine mutation
HDAC ..... histone deacetylase
HDACi..... histone deacetylase inhibitor
HDR..... homology-directed repair
HeLa ..... human cervical cancer cell line (derived from cancer cells taken from Henrietta Lacks)
HeLa 1.2.11 ..... HeLa cervical carcinoma subclone 1.2.11, telomerase-positive cell line with long telomeres
HeLa LT..... HeLa cells with long telomeres (average of 20 kb)
HeLa ST ..... HeLa cells with short telomeres (average of 9 kb)
HEPES ..... 4-(2-hydroxyethyl)-1-piperazineethanesulfonic acid
HGNC..... HUGO gene nomenclature committee, http://www.genenames.org (Yates *et al.*, 2017)
HP1 ..... heterochromatin protein 1
HR ..... homologous recombination
HRP ..... horseradish peroxidase
ICGC..... international cancer genome consortium
ID..... identifier
IF ..... immunofluorescence
IGV ..... integrative genomics viewer
kb..... kilobase
kd..... knockdown
kDa ..... kilo Dalton
KNS42 ..... pediatric glioblastoma cell line, also known as ICGC_GBM73
l2fc/ log2 fc ..... fold change of log2 transformed values
lacO ..... lac operon
LC-MS/ MS ..... liquid chromatography - tandem mass spectrometry
LT ..... long telomeres (see HeLa LT)
MAPK ..... mitogen-activated protein kinase
MGBM1 ..... pediatric glioblastoma cell line, also known as 10-801, ICGC_GBM39
MMS21 ..... methyl methanesulfonate sensitivity protein 21
MRN ..... protein complex: MRE11, RAD50, NBS1
MudPIT..... multidimensional protein identification technology
NCBI..... national center for biotechnology information (Coordinators, 2017)

NHEJ ..... non-homologous end joining
NLS ..... nuclear localization signal
NTP ..... nucleotide triphosphate
p/ p-value..... probability value
padj..... corrected/ adjusted p-value (method: FDR/ BH)
pATM..... phosphorylated ATM
PBS ..... phosphate buffered saline
PCA..... protein complementation assay
PCR ..... polymerase chain reaction
PDK4 ..... pyruvate dehydrogenase kinase 4
pedGBM ..... pediatric glioblastoma
PFA ..... paraformaldehyde
PG ..... plasmid encoding a fusion of PML with GFP (in the context of this thesis)
PI ..... propidium iodide
PICh ..... proteomics of isolated chromatin segments
PLCB2 ..... phospholipase C beta 2
PML ..... promyelocytic leukemia
PML-NBs ..... PML nuclear bodies
PMSF ..... phenylmethylsulfonylfluoride
PNA ..... peptide nucleic acid
POT1 ..... protection of telomeres protein 1
qRT-PCR..... quantitative real-time PCR
QTIP ..... quantitative telomeric chromatin isolation protocol (Grolimund *et al.*, 2013)
qTRAP..... quantitative TRAP (Cerone *et al.*, 2011)
RAP1 ..... repressor/ activator protein 1
RBCC/ TRIM.... RING-finger, B-Box, and coiled-coil/ TRIpartite motif
rlog ..... regularized log transformation, DESeq2 package (Love *et al.*, 2014)
RNA..... ribonucleic acid
RNA-seq ..... RNA-sequencing
RPKM ..... reads per kilobase of exon per million mapped reads
rpm ..... rounds per minute
RT ..... room temperature
RT-qPCR..... reverse transcription quantitative real-time PCR
SAHA..... suberoylanilide hydroxamic acid (vorinostat), pan HDAC inhibitor
SDS ..... sodium dodecyl sulfate
SF188..... pediatric glioblastoma cell line, also known as ICGC_GBM40
SGD..... saccharomyces genome database (Cherry *et al.*, 2012)
siRNA ..... small/ short interfering RNA
SJ-G2 ..... pediatric glioblastoma cell line, also known as SJ-02, ICGC_GBM41
SSC ..... saline-sodium citrate
ssDNA ..... single-stranded DNA
SUMO..... small ubiquitin-related modifier
SMC 5/ 6 ..... structural maintenance of chromosomes complex 5/ 6
ST..... short telomeres (see HeLa ST)
T-loop ..... telomeric loop

T-SCE ..... telomere sister chromatid exchange
TAE ..... tris base, acetic acid, EDTA
TBS ..... Tris-buffered saline
TBST ..... Tris-buffered saline with additional Tween 20
TCGA ..... the cancer genome atlas
TelNet ..... database containing genes, proteins, and transcripts involved in telomere maintenance
TelSeq ..... method for estimating telomere length from WGS data (Ding *et al.*, 2014)
TERRA ..... telomeric repeat-containing RNA
TERT ..... telomerase reverse transcriptase
tetO ..... tet operon
TG ..... plasmid encoding a fusion of TRF1 with GFP (in the context of this thesis)
TIN2 ..... TRF1-interacting protein 2
TM ..... telomere maintenance
TMM ..... telomere maintenance mechanism
TP53 ..... tumor protein p53
TPE ..... telomere position effect
TPG ..... plasmid encoding a fusion of TRF1, PML, and GFP (in the context of this thesis)
TPP1 ..... TIN2- and POT1-interacting protein
TRAP ..... telomere repeat amplification protocol
TRF1 ..... telomere repeat binding factor 1, official symbol: TERF1
TRF2 ..... telomere repeat binding factor 2, official symbol: TERF2
Tris ..... tris(hydroxymethyl)aminomethane
U2OS ..... human bone osteosarcoma epithelial cell line
VE-821 ..... selective ATRi, 3-Amino-6-(4-(methylsulfonyl)phenyl)-N-phenylpyrazine-2-carboxamide,
vst ..... variance stabilizing transformation, DESeq2 package (Love *et al.*, 2014)
WB ..... Western blot
WGS ..... whole genome sequencing
wt ..... wild-type
γH2A.X ..... histone variant H2A.X with phosphorylated serine 139

Introduction

1 Telomeres and telomere maintenance

Telomeres form the nucleoprotein structures at the ends of linear chromosomes (Blackburn, 1984; Blackburn, 1991). The term telomere originates from the Greek telos (τέλος) "end" and méros (μέρος) "part". Telomeric DNA consists of double-stranded G-rich tandem repeats with single-stranded 3' G-overhang (Makarov *et al.*, 1997). Telomeric DNA is bound by proteins that constitute telosome, which in mammalian cells is also called the shelterin complex (Wright *et al.*, 1992; Dmitriev *et al.*, 2003; Liu *et al.*, 2004; de Lange, 2005b; Palm & de Lange, 2008). The single-stranded overhang folds back to form a protective displacement loop (D-loop) with duplex telomere DNA (Griffith *et al.*, 1999). The telomeric loop structure is termed t-loop and has been reported to exist in both mammals (de Lange, 2004) and in budding yeast (Luke-Glaser *et al.*, 2012). The telosome/ shelterin complex shields the ends of chromosomes from degradation, accidental recognition as DNA double-strand break and chromosome end fusions, thereby protecting from degradation and DNA repair (Denchi & de Lange, 2007). Telomeres are generally conserved among vertebrates and share common structural features among eukaryotes (Blackburn, 1990). The budding yeast *Saccharomyces cerevisiae* is a model organism that is well-studied with regard to telomere biology (Kupiec, 2014). However, extrapolations from budding yeast to mammals can be specious with respect to telomere biology, because the telosome complex is different between human and budding yeast (de Lange, 2005b).

1.1 Telomere structure and function

The proper function of a telomere is sustained by a minimum length and integrity of shelterin (Chan & Blackburn, 2002; de Lange, 2005b). Human telomeres in somatic cells have a length of 3-12 kb (Greider, 1993; Mondello *et al.*, 1999; Friedrich *et al.*, 2000) and consist of regular $[TTAGGG]_n$ repeats (Moyzis *et al.*, 1988). Telomeric DNA is bound by the shelterin complex consisting of six proteins (de Lange, 2005b), depicted in **Figure 1A**. TRF1 and TRF2 (DNA-binding telomere repeat factors 1 and 2) directly bind to double-stranded telomeric DNA (Smith & de Lange, 1997). TRF2 prevents end-to-end fusions, and its deletion leads to activation of DNA repair processes at telomeres mediated by ATM (van Steensel *et al.*, 1998). However, artificially induced DNA double-strand breaks at telomeres are efficiently repaired by ATM-dependent signaling (Doksani & de Lange, 2016). RAP1 (TERF interacting protein)

is interacting with TRF2 (Li *et al.*, 2000). TRF1 and TRF2 homodimers are bridged by TIN2 (TRF1-interacting nuclear factor 2) (Ye *et al.*, 2004). The single-stranded G-overhang is covered by POT1 (protection of telomeres 1) forming a heterodimer with TPP1 (also known as ACD, shelterin complex subunit and telomerase recruitment factor) (Hockemeyer *et al.*, 2007). POT1/ TPP1 is recruited to the shelterin complex via its interaction with TIN2 (Takai *et al.*, 2011). POT1 protects telomeres from the repair processes mediated by the ATR signaling pathway (Hockemeyer *et al.*, 2005).

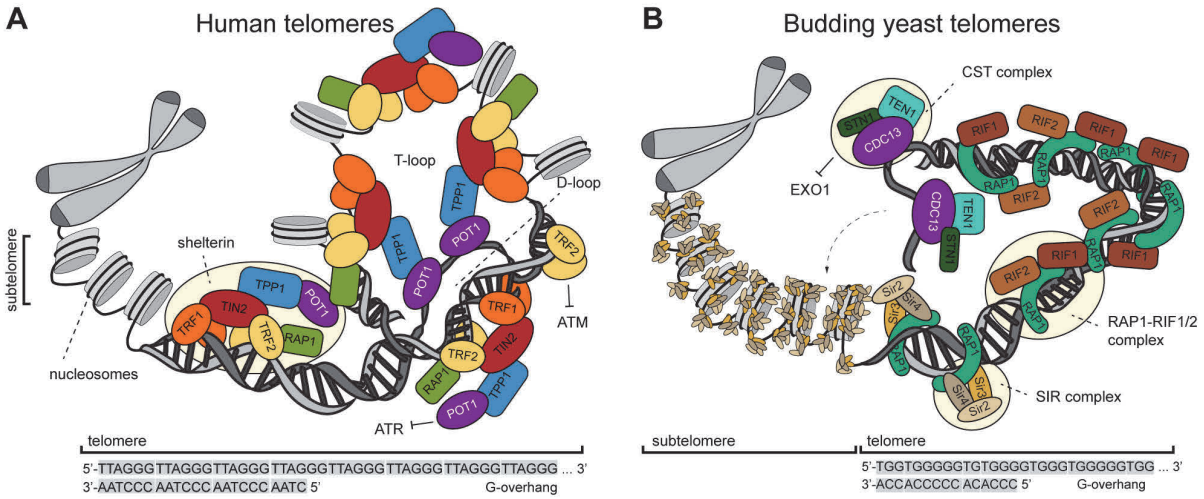

Figure 1. Telomere structure in human and budding yeast.

Telomeres and telomere binding proteins. **(A)** Human telomeres consist of TTAGGG repeats and form a t-loop by strand invasion of the G-rich overhang into duplex DNA, forming the D-loop. The shelterin complex is formed by TRF1, TRF2, TIN2, TPP1, POT1 and RAP1. TRF1 and TRF2 homodimers bind duplex telomeric DNA, while POT1/ TPP1 binds to the ssDNA of telomeres. TRF2 and POT1 protect telomeres from the DNA damage response activated by ATM and ATR signaling, respectively. **(B)** Budding yeast telomeres have an irregular telomeric sequence of TG1-3, and a fold-back structure is proposed, however not visualized yet. The subtelomere is densely packed by nucleosomes covered with SIR2/ 3/ 4. Telomeres are nucleosome-free and are bound by RAP1 that interacts with the SIR complex and RIF1/ 2. The G-rich single-stranded overhang is bound by the CST complex that protects telomeres from exonucleases, such as EXO1.

With an average length of 300 bp budding yeast telomeres are significantly shorter than human telomeres and consist of varying $[TG_{1–3}]_n$ repeats (Wellinger & Zakian, 2012). The CST complex (CDC13, STN1, TEN1) covers the telomeric overhang with CDC13 directly binding to the single-stranded repeats (Grandin *et al.*, 2001a; Gao *et al.*, 2007; Giraud-Panis *et al.*, 2010). The CST complex is essential for viability and ensures end protection by blocking exonucleases, such as EXO1 (exonuclease 1) (Grandin *et al.*, 2001b; Jia *et al.*, 2004). Double-stranded telomeric DNA is bound by RAP1 (repressor activator protein 1) (Wright & Zakian, 1995). RAP1 is essential for a proper telomere function because it protects the ends from chromosome fusions (Conrad et al. 1990; Lustig et al. 1990; Marcand et al. 2008) and degradation (Vodenicharov et al., 2010). Furthermore, RAP1 recruits RIF1/ 2 that are heterogeneously distributed over the duplex part of the telomere (Shi *et al.*, 2013). SIR2/ 3/ 4, proteins of the SIR (silence information regulator) complex also interact with RAP1 via SIR3 (Moretti *et al.*, 1994; Gotta *et al.*, 1996). In addition, proteins of the SIR complex deacetylate and bind to histones of the subtelomeres (Imai *et al.*, 2000; Liou *et al.*, 2005).

In budding yeast, only the subtelomeres are covered by nucleosomes, but telomeres are not (Wright *et al.*, 1992; Strahl-Bolsinger *et al.*, 1997). At human telomeres, canonical histones and histone variants such as macroH2A and testis-specific H2B have been identified (Dejardin & Kingston, 2009). Shelterin and nucleosomes both bind to TTAGGG repeats and might thus compete for the same binding site (Galati *et al.*, 2012; Galati *et al.*, 2015). Yeast telomeres and mammalian subtelomeres are heterochromatic. The characteristic of heterochromatin marks in the telomere comprises of HP1 (Heterochromatin protein 1), enrichment of H3K9 and H4K20 trimethylation, and heavy DNA methylation (Garcia-Cao *et al.*, 2004; Gonzalo *et al.*, 2005; Gonzalo *et al.*, 2006; Blasco, 2007). The non-coding telomere repeat containing RNA RNA (TERRA) is transcribed from subtelomeres into telomeres and might have functional roles in telomere integrity and telomerase regulation (Azzalin *et al.*, 2007; Luke *et al.*, 2008; Schoeftner & Blasco, 2008; Cusanelli & Chartrand, 2015; Rippe & Luke, 2015).

1.2 Telomere maintenance mechanisms (TMM)

As described above, the default telomere state can therefore be described as fully protected by shelterin and closed due to the protective t-loop formation (Cesare & Reddel, 2010). The limited cell proliferation of human somatic cells is mainly explained by the so-called end-replication problem (Hayflick, 1965; Olovnikov, 1973). It describes the incomplete replication of telomeres and the resulting shortening after each round of replication (Harley *et al.*, 1990; Levy *et al.*, 1992). Additionally, telomere shortening is accelerated by additional processes like oxidative stress (Saretzki & Von Zglinicki, 2002). Due to loss of telomeric repeats, shelterin is removed resulting in deprotection of telomeres and exposure of linear ends that become accessible to the DNA damage response machinery (Cesare *et al.*, 2013). By activation of ATM signaling, p53 is upregulated and replicative senescence is triggered potentially resulting in apoptosis (Lundblad & Szostak, 1989; d'Adda di Fagagna *et al.*, 2003) (**Figure 2**). In budding yeast experiments it has been shown that the shortest telomere controls induction of replicative senescence (Hemann *et al.*, 2001; Xu *et al.*, 2013). Loss of p53 and RB function allows cells to escape from senescence and continue proliferation (Chin *et al.*, 1999; Maciejowski & de Lange, 2017). Further telomere loss leads to end-to-end fusions as observed in TRF2 deficient cells (van Steensel *et al.*, 1998), leading to a state called crisis. Repetitive cycles of fusions and subsequent breakage results in genomic instability, a hallmark of cancer (Hanahan & Weinberg, 2000; de Lange, 2005a; Hanahan & Weinberg, 2011). During crisis, genetic alterations are accumulated and rare events of survivor formation have been observed (Shay & Wright, 1989). Cancer cells can escape from crisis by achieving a mechanism for extending telomeric repeats (Kim *et al.*, 1994; Counter *et al.*, 1998; Yeager *et al.*, 1999; Zhu *et al.*, 1999; Lu *et al.*, 2016; Min *et al.*, 2017). Telomere maintenance is either accomplished by reactivation of the reverse transcriptase telomerase (Greider & Blackburn, 1985; Greider, 1993; Bryan & Reddel, 1997; Chan & Blackburn, 2002) or alternative lengthening of telomeres (ALT) in the absence of

telomerase (Lundblad & Blackburn, 1993; Bryan *et al.*, 1995; Bryan *et al.*, 1997; Teng & Zakian, 1999; Dunham *et al.*, 2000; Shay *et al.*, 2012). Cell lines and primary tumors without telomere maintenance (TM) have been reported (Dagg *et al.*, 2017) and termed after the yeast terminology "ever shorter telomeres" (Lundblad & Szostak, 1989). Telomeres are very long in these cells, but telomeres shorten continuously due to ongoing proliferation.

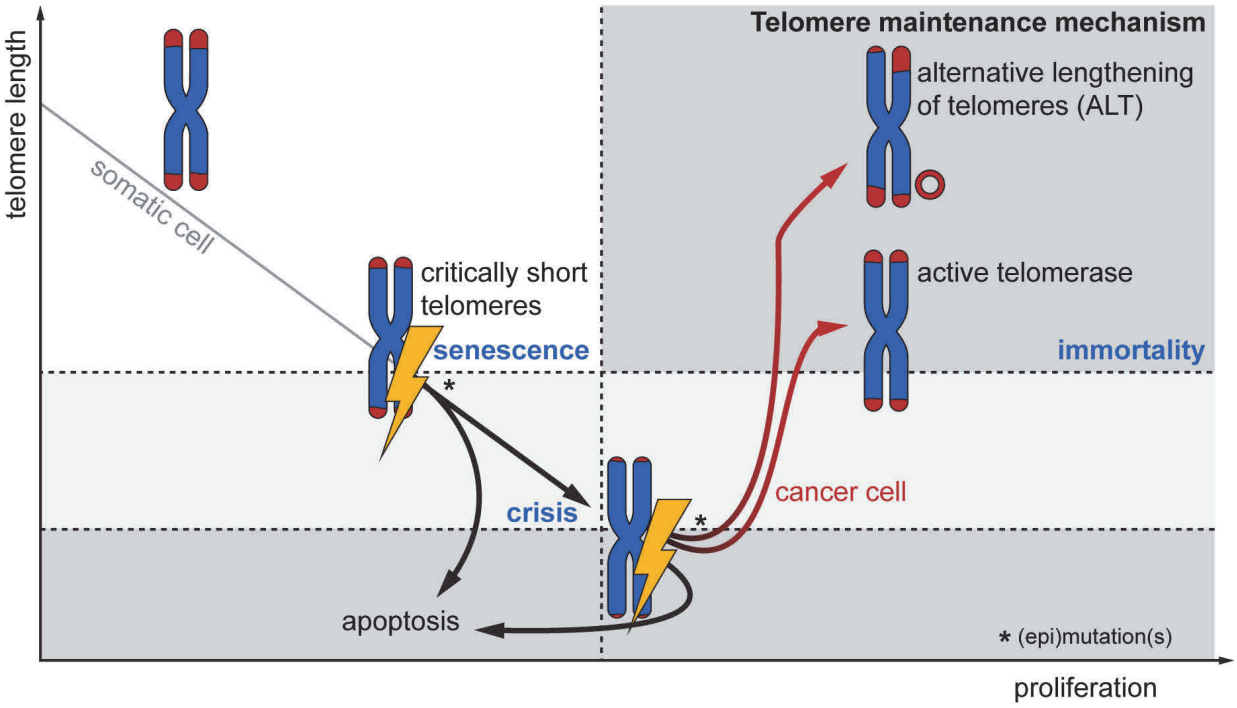

Figure 2. Telomere maintenance.

Due to the end-replication problem, cells lose telomere repeats during proliferation. Upon deprotection of telomeres, replicative senescence is triggered and followed by apoptosis. Cells can escape from senescence by (epi)mutations of for example tumor suppressor genes like p53. Further telomere shortening leads to activation of DNA damage checkpoints and cells enter a state called crisis. Additional (epi)mutations enable malignant transformation to cancer cells that either reactivate telomerase or make use of alternative lengthening of telomeres (ALT). By maintaining telomeres, cancer cells achieve unlimited proliferative potential (Hanahan & Weinberg, 2011).

Human telomerase consists of the protein TERT (telomerase reverse transcriptase) and the non-coding RNA template TERC (telomerase RNA component) and extends short telomeres by adding TTAGGG repeats (Morin, 1989). In budding yeast, telomerase is constitutively expressed and its deletion causes cellular senescence (Lundblad, 2002). Yeast cells that overcome crisis by the use of homologous recombination are called survivors and are categorized into type I and II defined by dependence on RAD50 or RAD51 (Lundblad & Blackburn, 1993; Le *et al.*, 1999; Teng & Zakian, 1999; Chen *et al.*, 2001; Lundblad, 2002). Type II survivors, dependent on RAD51, have telomeres that are heterogeneous in length, similar to human ALT cells (Le *et al.*, 1999; Teng & Zakian, 1999; Chen *et al.*, 2001). Despite the differences of telomere biology between budding yeast and human, orthologues exist for many genes involved in TM, chromatin organization and DNA repair and recombination. In budding yeast, genetic deletion screens are extensively used. Thus, transferring knowledge about TM from budding yeast will help to elucidate the alternative lengthening of telomeres (Kupiec, 2014; Lippuner *et al.*, 2014).

2 Alternative lengthening of telomeres (ALT)

In the absence of telomerase, cancer cells maintain their telomeres via the alternative lengthening of telomeres (ALT) (O'Sullivan & Almouzni, 2014; Sobinoff & Pickett, 2017; De Vitis *et al.*, 2018). Therefore, ALT has been defined as "*de novo* synthesis of telomeric DNA via a mechanism other than telomerase" (Sobinoff & Pickett, 2017). The ALT mechanism has been investigated over the past two decades and a number of molecular and cytological hallmarks have been defined that are used as biomarkers to characterize cell lines and tumor samples as described in the next section (Pickett & Reddel, 2015). In addition, it is well accepted that ALT cells use homology-directed DNA repair mechanisms to copy repeats from a template to extend telomeric DNA. However, the mechanistic details remain elusive.

2.1 Molecular and cytological hallmarks of ALT

A number of well-established molecular and cytological hallmarks of ALT are used for determining the active TMM in cancer cells (Henson & Reddel, 2010; Sobinoff & Pickett, 2017) (**Figure 3**). The extent of each feature can vary between different ALT cell lines and the relationships between the features are only partly understood.

Absence of telomerase activity

The absence of telomerase activity can be determined via lack of signal in the telomere repeat amplification protocol (TRAP) assay (Mender & Shay, 2015) (**Figure 3A**). Expression of TERT can also be accessed via RNA-seq (**Figure 3E**), however, even in telomerase-positive cells read counts are very low due to low abundance of transcripts (Fagerberg *et al.*, 2014). Expression of the RNA template TERC is also needed for active telomerase (Xi & Cech, 2014; Min *et al.*, 2017), but ALT can be active in spite of normal TERC expression levels (Zhang *et al.*, 2011).

ALT-associated PML bodies (APBs)

Telomeres aggregate with PML protein in ALT-associated PML nuclear bodies (APBs) in ALT cells (Chung *et al.*, 2012). The functional role of these biomarkers is only partly understood. APBs harbor a number of HR and DDR proteins and *de novo* telomeric synthesis was observed at telomeres in APBs, indicating that APBs are the place of telomere extension in ALT cells (Nabetani *et al.*, 2004; Chung *et al.*, 2011; Nabetani & Ishikawa, 2011). Due to the high correlation with ALT activity, APBs are an excellent marker for ALT (Henson *et al.*, 2005; Chung *et al.*, 2012). They can be visualized by staining of telomeres via TRF1/ TRF2 immunofluorescence (IF) or telomere FISH and PML IF (**Figure 3B**) (Yeager *et al.*, 1999) and a detailed description of their role for ALT is provided in **introduction section 4**.

Telomere dysfunction induced foci (TIFs)

Accumulations of DNA damage response proteins at telomeres indicate telomere dysfunction induced foci (TIFs) and are frequently found in ALT cells (Cesare *et al.*, 2009). TIFs can be visualized by immunofluorescence and detection of co-localization of telomeres with marker proteins of DNA repair as for example phosphorylated forms of ATM, the histone variant H2A.X (γH2AX) or 53BP1.

Heterogeneous telomere length

Telomeres in ALT cells are heterogeneous in length and range from very short to over 50 kb (Bryan *et al.*, 1995; Dunham *et al.*, 2000; Perrem *et al.*, 2001). The intracellular heterogeneity in telomere length might come from disproportional extension of lagging strands that are then exposed to telomere trimming processes resulting in short telomeres in turn (Min *et al.*, 2017). Furthermore, a high number of chromosomes have only very short telomeres (<0.15 kb)(Poon *et al.*, 1999), which has been used as a marker for the lack of telomerase (Hemann *et al.*, 2001; Perrem *et al.*, 2001). Methods to analyze telomere lengths have recently been reviewed (Montpetit *et al.*, 2014; Lai *et al.*, 2018). With the terminal restriction fragment (TRF) blot of telomeric DNA separated on an agarose gel qualitative heterogeneity within one sample can be visualized, but the resolution is very poor (**Figure 3C**) (Moyzis *et al.*, 1988; Aubert *et al.*, 2012). The TRF blot gives an estimate on the distribution of telomere length and the average length can be extracted (Kimura *et al.*, 2010). A higher resolution- and chromosome-specific analysis can be done with quantitative fluorescence *in situ* hybridization (Q-FISH) on metaphase chromosomes (**Figure 3D**) (Meyne & Moyzis, 1994; Uhlmann *et al.*, 2000; Poon & Lansdorp, 2001).

TERRA

The abundance of the telomeric RNA TERRA can be measured via RT-qPCR (**Figure 3F**). For measuring total TERRA levels primers that consist of UUAGGG repeats and bind to the telomeric part of TERRA can be used (Deeg, 2015). Furthermore, for chromosome-specific analysis primers that bind to proposed promotor sites in the subtelomeres of chromosomes 15q, 1q-2q-10q-13q, 9p-15q-Xq-Yq, 11q and Xp-Yp have been reported (Arnoult *et al.*, 2012; Deeg, 2015).

Extrachromosomal telomeric repeats (ECTRs)

In ALT cells, extrachromosomal telomeric repeats accumulate, which can be both linear or circular, single-stranded or double-stranded, and C-rich or G-rich. One abundant type are C-circles, which are mostly single-stranded, C-rich and circular ECTRs. The cause and mechanism of C-circle formation is not fully understood. It has been hypothesized that C-circles might be a byproduct from homologous recombination or result from telomere trimming of very long telomeres (Pickett et al., 2009). Furthermore, it has been suggested that C-circles could serve as template for telomere synthesis by rolling circle amplification (Fasching *et al.*, 2007). Recently, cytosolic DNA sensing has been linked to ALT (Chen *et al.*, 2017). A very straightforward and robust technique to quantify C-circle levels is the

C-circle assay, which makes use of the self-priming capacity of the circular partly double-stranded nature and a rolling circle amplification utilizing Φ29 polymerase (**Figure 3G**) (Henson *et al.*, 2009). Amplified C-circles can subsequently be blotted on a membrane and detected via a telomeric probe. The C-circle assay serves as reliable indicator for ALT-positive tumors, as elevated C-circle levels highly correlate with ALT activity in cell lines and tissue samples from cancer patients (Deeg *et al.*, 2017; Henson *et al.*, 2017).

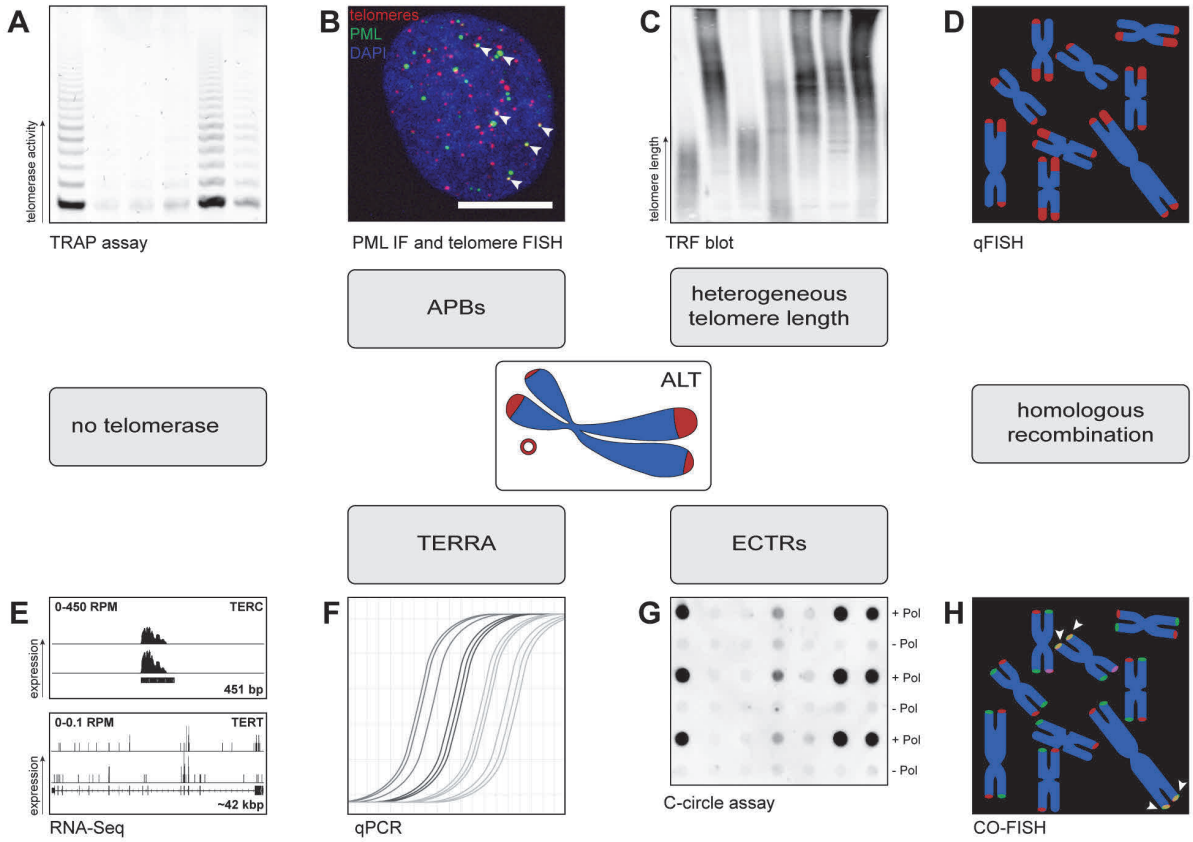

Figure 3. Measuring hallmarks of the alternative lengthening of telomeres (ALT) pathway.

(A) Telomere repeat amplification protocol (TRAP) assay to determine lack of telomerase activity. **(B)** Detection of ALT-associated PML nuclear bodies (APBs) by telomere fluorescence in situ hybridization (FISH) and immunofluorescence of PML. This can be combined with subsequent automated image acquisition and analysis to determine the number of APBs. **(C)** Telomere restriction fragment (TRF) blot to measure the absolute telomere length distribution. **(D)** Metaphase spreads and subsequent telomere FISH to yield relative telomere lengths for each chromosome. **(E)** RNA-sequencing to determine the lack of telomerase RNA (*TERC*) and protein (*TERT*) subunit expression. **(F)** Quantitative PCR with subtelomeric primers to determine the abundance of telomere repeat containing RNA (TERRA). **(G)** C-circle assay to determine the circular C-rich form of extrachromosomal telomeric repeats. **(H)** Chromosome orientation (CO)-FISH to detect telomere sister chromatid exchange (T-SCE).

Homologous recombination (HR)

De novo synthesis of telomere repeats in ALT cells is facilitated by homologous recombination (HR), namely strand invasion of single-stranded telomeres into double-stranded telomeric DNA. Intertelomeric copying of an artificially integrated gene from one telomere to another was demonstrated by integration of an exogenous gene into a telomere. This gene was then copied to another telomere

(Dunham *et al.*, 2000). The copy template can either be the same DNA strand (t-loop), another chromosome or extrachromosomal telomeric repeats. Non-replicative telomeric synthesis can be detected by BrdU assay of interphase cells and subsequent microscopy analysis. Homologous recombination events between different chromosomes can result in telomeric sister chromatid exchanges (T-SCE) (Londono-Vallejo *et al.*, 2004), which can be accessed by chromosome orientation FISH (CO-FISH) (**Figure 3H**) (Meyne & Goodwin, 1994; Bailey *et al.*, 2010; Falconer *et al.*, 2010). CO-FISH requires BrdU incorporation into newly synthesized telomeric DNA, selective digestion of BrdU containing strands, strand-specific labeling of telomeres on metaphase spreads, and subsequent imaging. During homologous recombination, another telomere might be involved in de novo telomeric synthesis, resulting in telomeric clustering, which can also be accessed by microscopy (Draskovic *et al.*, 2009; Cho *et al.*, 2014; Osterwald *et al.*, 2015).

2.2 Other ALT features

In addition to the well-established characteristics of ALT telomeres described above, a number of other features have been reported. The chromatin state of ALT telomeres appears to be altered in comparison to telomerase-positive cells. In ALT cells, telomeric chromatin was shown to be more accessible to digestion by MNase and have higher levels of TERRA transcription than telomeric chromatin in cells that maintain their chromosomal ends by telomerase (Episkopou *et al.*, 2014). Upon telomerase overexpression, H3K9me3 was increased at telomeres and TERRA levels were reduced, indicating a more relaxed chromatin state of ALT telomeres (Episkopou *et al.*, 2014). Telomeres in APBs however, are bound by all three members of the heterochromatin protein (HP1) family, indicating a condensed chromatin state at telomeres within APBs (Jiang *et al.*, 2009). Recruitment of HP1γ was sufficient to induce *de novo* formation of APBs (Chung *et al.*, 2011), while chromatin decondensation of telomeric chromatin by overexpression HMGN5 or HDAC inhibition/ depletion was shown to reduce the number of APBs (Osterwald, 2012; Jamiruddin *et al.*, 2016). These observations give rise to the assumption that epigenetic changes are linked to ALT emergence (O'Sullivan & Almouzni, 2014; Voon *et al.*, 2016).

Furthermore, the emergence of ALT in a cancer subtype is dependent on the tissue of origin. For example, a very high ALT prevalence is found in osteosarcoma (64%), leiomyosarcoma (53-58%), high-frequency microsatellite instability gastric carcinoma (57%), pancreatic neuroendocrine tumors (53%), pediatric glioblastoma multiforme (44%), diffuse astrocytoma (63%), and anaplastic astrocytoma (63%) (Heaphy *et al.*, 2011b; Chudasama *et al.*, 2018; De Vitis *et al.*, 2018). Recurrent mutations that correlate with the ALT status are found in *ATRX* (α-thalassemia mental retardation X-linked protein), *DAXX* (death-associated protein 6) and *H3F3A*, encoding for the non-canonical histone H3 variant H3.3 (Heaphy *et al.*, 2011a; Lovejoy *et al.*, 2012; Schwartzentruber *et al.*, 2012). However, single knockdown of neither of them is sufficient to induce ALT (Lovejoy *et al.*, 2012; Episkopou *et al.*, 2014; O'Sullivan

et al., 2014; Flynn *et al.*, 2015; Napier *et al.*, 2015; Udugama *et al.*, 2015; Danussi *et al.*, 2018). On the other hand, loss of ATRX was shown to facilitate ALT activation (Napier *et al.*, 2015) and reexpression of ATRX in previous ATRX-negative cell lines suppressed the ALT mechanism (Clynes *et al.*, 2015; Deeg *et al.*, 2016). This indicates that loss of a combination of multiple factors is needed for ALT activation. Introducing hTERT into ALT cells repressed some features of the ALT pathway (Perrem *et al.*, 1999). One possible explanation for this finding is that the telomerase-positive environment harbors factors that suppress homologous recombination. Proteins related to the ALT pathway have been reviewed recently (Nabetani & Ishikawa, 2011). Those investigated with regard to localization to APBs or APB formation have been summarized in (**Suppl. table S1**).

2.3 Databases with telomere maintenance (TM) information

The exact ALT mechanism and reasons for its emergence remain elusive, despite the certainty of involvement of homology-directed DNA repair (Londono-Vallejo *et al.*, 2004; Conomos *et al.*, 2013). However, a large number of proteins have been described to be related to the TM and ALT. For example, at least 53 different proteins localize to APBs in ALT cells and have a role of APB formation. They are summarized in the appendix (**Suppl. table S1**). Furthermore, experimental screens were set up to investigate proteins involved in TM yielding many hits (Dejardin & Kingston, 2009; Lee *et al.*, 2011; Uziel *et al.*, 2015). Thus, the amount of information has become substantial, and systematic approaches are needed to collect the available information. A database with a compilation of TMM proteins should provide comprehensive information on the TMM phenotype that can be accessed easily. Furthermore, the identification of TMM genes in a results list from an experimental screen or bioinformatics pipeline should be anticipated, considering the increasing use of deep sequencing for dissecting TMM (Barthel *et al.*, 2017; Chudasama *et al.*, 2018; Sieverling *et al.*, 2018). There are some publicly available databases that partly include relevant information to TM. According to HumanMine, a number of 267 genes have been annotated with a GO term containing the term “telo” (Smith *et al.*, 2012; Gene Ontology, 2015). TeloPIN (telomeric proteins interaction network), which is no longer available, contained interaction data of shelterin compounds with interaction partners (Luo *et al.*, 2015). The telomerase database (http://telomerase.asu.edu/) is dedicated to the structure and function of telomerase across organisms (Podlevsky *et al.*, 2008). Information on the localization of proteins during cell cycle progression is collected in the MiCroKiTS (midbody, centrosome, kinetochore, telomere and spindle) database (http://microkit.biocuckoo.org/) (Huang *et al.*, 2015). The websites mentioned above include parts of telomere-related information that is available from the literature. However, a database that integrates all these information, especially on proteins in the ALT mechanism is currently missing. Having such a resource would facilitate the understanding of the complex process of TM as well as the identification of novel drug targets that are related to this process.

3 Targeting telomere maintenance

Telomere maintenance (TM) is a common feature to all cancer cells. Thus, it is a highly attractive therapeutic target, since it could be exploited for the development of "pan-cancer drugs". However, targeting TM currently has several limitations. There are different pathways, and in the case of ALT, a specific molecular target is currently missing. In general, targeting TM would lead to the blocking of active telomere lengthening without causing immediate cell death. Senescence or cell death is induced in cells with critically short telomeres, resulting from telomere shortening due to cell proliferation. Depending on the initial telomere length, this can sum up to 21–24 population doublings (Min *et al.*, 2017) or in other terms 20 months' time (Uziel *et al.*, 2015). During this time of uncontrolled growth of cancer cells, the tumor mass would already be largely increased. Another problem is the evasiveness of TMM treatment, which has been observed for telomerase-depleted cells and the subsequent emergence of ALT-positive cells from crisis (Chang *et al.*, 2003; Bechter *et al.*, 2004; Chen *et al.*, 2010; Hu *et al.*, 2012; Min *et al.*, 2017). Therefore a combined treatment of telomerase and ALT has been proposed to prevent drug resistance in either direction (Shay *et al.*, 2012). Indeed, simultaneous depletion of TERT and ALT-related proteins (RAD51, NBS1 and TRF2) resulted in the reduction of cell viability of laryngeal squamous carcinoma cells (Xu *et al.*, 2016). Since TM is a common feature of all cancer cells (with a few rare exceptions), a treatment that simultaneously targets ALT and telomerase would be rated as very effective (De Vitis *et al.*, 2018).

3.1 Inhibiting telomerase

Telomerase appears to be an ideal target for cancer therapy because the majority of cancer cells depend on telomerase-mediated TM (Romaniuk *et al.*, 2014; Jager & Walter, 2016). Inhibition of telomerase can be achieved by targeting either the telomerase RNA component TERC by the antisense oligo GRN163L (Imetelstat, by Geron Corporation, Menlo Park, CA, USA) (Roth *et al.*, 2010) or the telomerase protein TERT by small-molecule inhibitors such as BIBR1532 (Pascolo *et al.*, 2002). Imetelstat has been subjected to pre-clinical and clinical trials phase I/II for treatment of e.g. breast cancer, glioblastoma or non-small lung cancer (Dikmen *et al.*, 2005; Hochreiter *et al.*, 2006; Goldblatt *et al.*, 2009; Marian *et al.*, 2010; Frink *et al.*, 2016). Unfortunately, treatment of tumors with telomerase inhibitors was faced with therapeutic limitations (Rousseau & Autexier, 2015; Shay, 2016). In a phase II clinical trial 17 from 116 patients with advanced non-small-cell lung cancer had to discontinue the treatment because of severe adverse effects (Chiappori *et al.*, 2015). The outcome of the study was a non-significant improvement of progression-free survival of patients treated with Imetelstat. A clinicial trial phase II testing Imetelstat in children suffering from recurrent medulloblastoma, high-grade glioma (HGG) or ependymoma had to be closed because of toxicity (Salloum *et al.*, 2016). Furthermore, the

presence of ALT has been detected in some of the tumors. It is not clear if these tumors already utilized the ALT mechanism prior to treatment, or if the treatment caused ALT as a resistance mechanism. since inhibiting telomerase can lead to cellular crisis, consequently allowing the emergence of ALT (Chang *et al.*, 2003; Bechter *et al.*, 2004; Chen *et al.*, 2010; Hu *et al.*, 2012; Min *et al.*, 2017).

The switch from telomerase-positive cells to ALT cells was not possible by single knockdown of *ATRX* or *DAXX* (Lovejoy *et al.*, 2012; Episkopou *et al.*, 2014; O'Sullivan *et al.*, 2014; Napier *et al.*, 2015). However, combinatorial depletion of ATRX and DAXX together with induced DNA damage and partial inhibition of telomerase has been shown to cause a TMM switch from telomerase-mediated to ALT (Hu *et al.*, 2016). Depletion of both isoforms of the histone chaperone ASF1, a and b, in telomerase-positive cells with long telomeres (HeLa LT) rapidly induced ALT within three days (O'Sullivan *et al.*, 2014). Also, both mechanisms can co-exist in one cell population (Cerone *et al.*, 2001; Grobelny *et al.*, 2001; Perrem *et al.*, 2001), demonstrating the dynamic mode of TM (De Vitis *et al.*, 2018).

3.2 Suppressing the ALT mechanism

ALT-mediated TM currently does not offer one specific molecular target and a clinically approved drug against ALT is currently missing. It is challenging to identify a druggable target specific to ALT without adverse side-effects in normal somatic cells, because here ALT-driving proteins are also present only usually not localized to telomeres. Blockage of recombination-mediated telomere lengthening can be achieved by the dominating effect as hybrid formation of telomerase-positive and –negative cells or telomerase overexpression in ALT cells led to ALT suppression (Perrem *et al.*, 1999; Ford *et al.*, 2001). It might also be necessary to target several ALT sustaining steps (Dilley & Greenberg, 2015), since depletion of different proteins related to the ALT pathway has been observed to reduce some but not all ALT hallmarks and examples are described in the following. It has been reported that SP100-related sequestering or depletion of the MRE11/ RAD50/ NBS1 (MRN) complex resulted in telomere shortening (Jiang *et al.*, 2005; Zhong *et al.*, 2007). Targeting the CST complex has been supposed to inhibit the ALT mechanism (Huang *et al.*, 2017). In addition to decreasing ECTRs and APBs, shRNA-mediated knockdown of CST members CTC1 or STN1 resulted in increased T-SCE and telomere fragility. Reduction of MUS81 has been shown to decrease T-SCE without affecting the abundance of ECTRs. (Zeng *et al.*, 2009). A therapeutic approach to induce apoptosis in ALT cells by the ATR inhibitor (ATRi) VE-821 has been tested on some ALT cell lines (Flynn *et al.*, 2015). However the observed hypersensitivity specific to ALT cells could not be confirmed (Deeg *et al.*, 2016).

As outlined above, TM might be regulated by epigenetic processes (Naderlinger & Holzmann, 2017). Indeed, treatment with histone deacetylase (HDAC) inhibitors has been described to suppress APB formation and decrease levels of ECTRs (Osterwald *et al.*, 2015). In addition, treatment with HDAC

inhibitors (HDACi) has been shown to regulate transcription of the hTERT gene (Rahman & Grundy, 2011). The HDACi trichostatin A is only used in cell culture systems because of its relatively high cytotoxicity, whereas Vorinostat (Zolinza, suberoylanilide hydroxamic acid, SAHA) has already been approved by the FDA for the treatment of relapsed and refractory cutaneous T-cell lymphoma (Eckschlager *et al.*, 2017). However, little is known about a relation of HDAC treatment to TM. A current clinical phase I/II trial treating children with solid tumors, lymphoma or leukemia that did not respond to the standard therapy involves vorinostat, a pan-inhibitor of HDACs I/II (Witt *et al.*, 2012). A therapy targeting PML might be promising, because knockdown of PML in ALT cells resulted in telomere shortening (Osterwald *et al.*, 2012; Deeg, 2015). However, depletion of the protein as an anti-tumor therapy appears unfeasible, since PML is an essential compound of PML-NBs and has a role in tumor suppression (Reineke & Kao, 2009; Marchesini *et al.*, 2015). Thus, the role of PML in TM has to be studied in more detail to consider targeting PML localization. In summary, treatment of ALT is still in its early steps and it is required to investigate the mechanistic details of ALT.

4 PML protein in the ALT pathway

4.1 Promyelocytic leukemia nuclear bodies (PML-NBs)

PML-NBs have been defined as "mobile subnuclear organelles formed by PML and SP100 protein" (Lang *et al.*, 2010). They exist in most somatic cells and have a role in various molecular processes summarized in (Guan & Kao, 2015). The PML protein forms spheres with a size of 0.1-1.0 µM and can by visualized by microscopy methods (Lang *et al.*, 2010). Several isoforms result from alternative splicing from the *PML* gene that contains 9 exons (Fagioli *et al.*, 1992; Nisole *et al.*, 2013). Because of the confusing PML nomenclature in the literature a table for a better overview referring to (Nisole *et al.*, 2013) is shown (**Table 1**). In the following, the nomenclature from Jensen *et al.* will be used (roman numerals).

Table 1. Nomenclature of PML isoforms.

(Jensen *et al.*, 2001)	NCBI name	Uniprot name	Uniprot ID	TRIM name	Other names	Protein length
PML-I	Isoform 1	PML-1	P29590-1	TRIM19 alpha		882aa
		PML-11	P29590-11		PML-1A, PML-IA	834aa
PML-II	Isoform 9	PML-2	P29590-8	TRIM19 kappa		829aa
	Isoform 11	PML-13	P29590-13		PML-2A, PML-IIA	781aa
		PML-8	P29590-3	TRIM19 gamma	PML-2G, PML-IIG	824aa

(Jensen *et al.*, 2001)	NCBI name	Uniprot name	Uniprot ID	TRIM name	Other names	Protein length
PML-III		PML-3	P29590-9			641aa
PML-IV	Isoform 6	PML-4	P29590-5	TRIM19 zeta	PML-X	633aa
	Isoform 10	PML-12	P29590-12	TRIM19 lambda	PML-4A, PML-IVA	585aa
PML-V	Isoform 2	PML-5	P29590-2	TRIM19 beta	PML-2	611aa
PML-VI	Isoform 5	PML-6	P29590-4	TRIM19 epsilon	PML-3B	560aa
	Isoform 7	PML-14	P29590-14	TRIM19 eta/ iota	PML-6B, PML-VIB	423aa
PML-VIIb	Isoform 8	PML-7	P29590-10	TRIM19 theta	PML-7, PML-VII	435aa

Names for PML isoforms from (Jensen *et al.*, 2001), NCBI and Uniprot names as well as the TRIM names and other names are given in this table. The last column shows the size of translated proteins. Table adapted from (Nisole *et al.*, 2013).

Different isoforms can have different functions. For example, PML III is capable to induce *de novo* APBs at telomeres in U2OS cells (Chung *et al.*, 2011). PML IV interacts with p53 and modifies its activity by recruiting p53 to PML nuclear bodies (Fogal *et al.*, 2000; Guo *et al.*, 2000; Pearson *et al.*, 2000). PML IV also binds to hTERT and negatively regulates its activity (Oh *et al.*, 2009). PML I, PML III, PML IV and PML V form hollow spheres, whereas nuclear bodies containing PML II and PML VI are filled out (Li *et al.*, 2017). All PML isoforms share the same N-terminus but harbor unique C-terminal regions (Jensen *et al.*, 2001) (**Figure 4**).

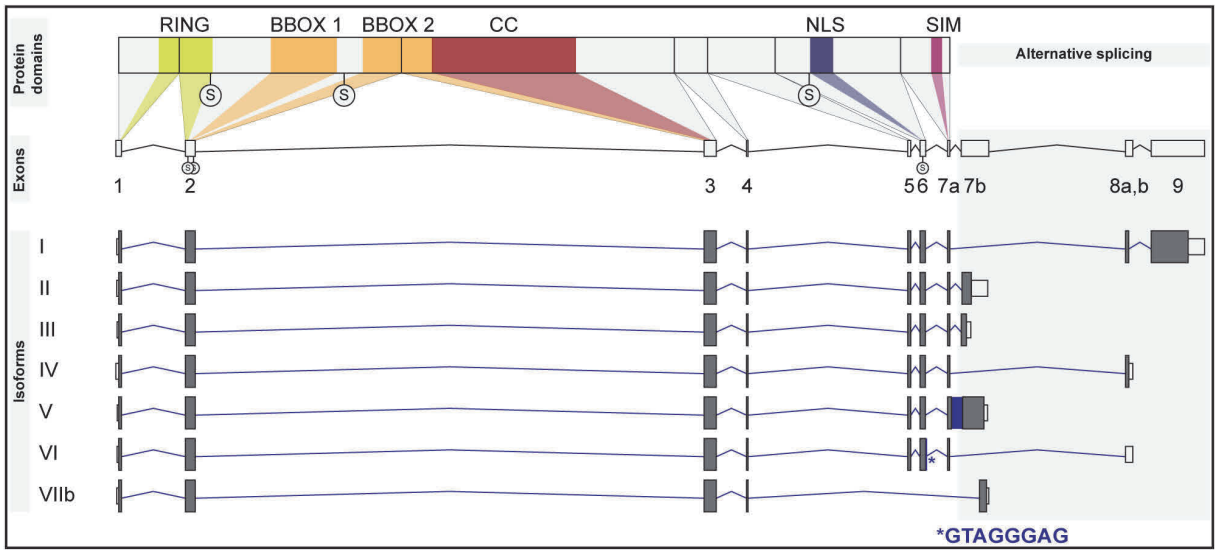

Figure 4. PML isoforms.

Upper panel shows the RBCC/ TRIM motif of the unique C-terminus, the nuclear localization signal (NLS) and the SUMO interacting motif (SIM). SUMOylation sites were marked with S in circles. Middle panel shows exons of PML. Lower panel shows exon composition of different PML isoforms. Dark blue rectangles and asterisks for smaller regions indicate retained introns. Right panel shows alternatively spliced N-terminus. Image adapted from (Nisole *et al.*, 2013) and (Jensen *et al.*, 2001).

The N-terminal region contains a RING-finger, two B-boxes and coiled-coil domain (RBCC) or TRIpartite (TRIM) motif that is present in all isoforms (Reymond *et al.*, 2001). At three lysines, K65, K160, and K190, PML can be post-translationally modified by the small ubiquitin-like modifier (SUMO) by a group of enzymes involving SUMO-activating enzymes, the SUMO-conjugating enzyme UBC9 and E3 ligases (Kamitani *et al.*, 1998; Zhong *et al.*, 2000; Jurgendohmen, 2004; Brand *et al.*,

2010). Isoforms I to V contain a SUMO interacting motif (SIM) in exon 7a (Song *et al.*, 2004; Shen *et al.*, 2006). SUMO:SIM interactions are important for multimerization of PML proteins and nuclear body formation. Furthermore, a variety of proteins is recruited to PML-NBs through SUMO-mediated interaction, that dynamically compose their structure (Lallemand-Breitenbach & de The, 2010, 2018). Van Damme *et al.* have mapped the composition of PML-NBs and reviewed the implications of SUMOylating proteins recruited to PML-NBs (Van Damme *et al.*, 2010). The functional roles of PML, such as oxidative stress response, senescence, viral infections, or stemness, are versatile and only partly understood (Dellaire & Bazett-Jones, 2004; Sahin *et al.*, 2014; Chang *et al.*, 2017). In somatic cells, PML-NBs do not contain nucleic acids (Boisvert *et al.*, 2000), however in ALT cells a subset of PML-NBs are localized around telomeric DNA forming ALT-associated PML-NBs (APBs) (Yeager *et al.*, 1999; Lang *et al.*, 2010).

4.2 ALT-associated PML nuclear bodies (APBs)

As mentioned above, APBs are defined as subset of PML protein that form a complex with telomeric DNA (Yeager *et al.*, 1999). In ALT cells, PML protein forms a shell (Lang *et al.*, 2010) around both chromosomal telomeric DNA and extrachromosomal telomeric repeats (Nabetani *et al.*, 2004; Fasching *et al.*, 2007). The average number of APBs, as determined via telomere FISH and PML IF, ranges from 4 in U2OS cells (a typical ALT-positive reference cell line), to over 8 for MGBM1 (ALT-positive glioblastoma cell line) (Deeg, 2015; Osterwald *et al.*, 2015). Aside from shelterin compounds, proteins related to the DNA repair, the recombination machinery and DNA damage response pathways localize to APBs and are summarized in the appendix (**Suppl. table S1**). Testing effects of their depletion several proteins have been identified to be essential for APB formation (**Table 2**). Some APB components (PML, TRF1, TRF2, MMS21, NBS1) have been demonstrated to be capable of inducing *de novo* formation of functional APBs by their recruitment to telomeres (Chung *et al.*, 2011).

Table 2. Essential components of ALT-associated PML nuclear bodies (APBs).

Protein	References for localization to APBs	References for decrease in APBs upon protein depletion
BLM	(Yankiwski *et al.*, 2000; Stavropoulos *et al.*, 2002; Bhattacharyya *et al.*, 2009; O'Sullivan *et al.*, 2014; Osterwald *et al.*, 2015; Sobinoff *et al.*, 2017)	decrease (Gocha *et al.*, 2014; Osterwald *et al.*, 2015)
CDKN1A (aka p21	partly (Jiang *et al.*, 2009)	decrease (Osterwald *et al.*, 2015)
DNMT1		decrease (Osterwald *et al.*, 2015)
ERCC4 (aka XPF)	(Zhu *et al.*, 2003)	decrease (Osterwald *et al.*, 2015)
FEN1		decrease (Osterwald *et al.*, 2015)
HDAC7		decrease (Osterwald *et al.*, 2015)
HDAC9		decrease (Jamiruddin *et al.*, 2016)
HP1γ (aka CBX5)	(Jiang *et al.*, 2009)	decrease (Osterwald *et al.*, 2015)

Protein	References for localization to APBs	References for decrease in APBs upon protein depletion
KAT2B (aka PCAF)		decrease (Jeitany *et al.*, 2017)
LSD1 (aka KDM1A)		decrease (Osterwald *et al.*, 2015)
MORC3		decrease (Osterwald *et al.*, 2015)
MRE11	(Zhu *et al.*, 2000; Spardy *et al.*, 2008; Cesare *et al.*, 2009)	decrease (Jiang *et al.*, 2007; Zhong *et al.*, 2007; O'Sullivan *et al.*, 2014); no sign. effect (Osterwald *et al.*, 2015)
NBS1 (aka NBN or p95)	(Wu *et al.*, 2000; Zhu *et al.*, 2000; Johnson *et al.*, 2001; Wu *et al.*, 2003; Cesare *et al.*, 2009; Wilson *et al.*, 2016)	decrease (Wu *et al.*, 2003; Jiang *et al.*, 2007; Zhong *et al.*, 2007); no effect (Osterwald *et al.*, 2015)
NR2C2	(Marzec *et al.*, 2015)	decrease (Osterwald *et al.*, 2015)
NR2F2	(Marzec *et al.*, 2015)	decrease (Osterwald *et al.*, 2015)
NSMCE2 (aka MMS21)	(Potts & Yu, 2007; Chung *et al.*, 2011)	decrease (Potts & Yu, 2007; Osterwald *et al.*, 2012; Osterwald *et al.*, 2015)
P300		decrease (Jeitany *et al.*, 2017)
PARP2	(Dantzer *et al.*, 2004)	decrease (Osterwald *et al.*, 2015)
PML	(Yeager *et al.*, 1999)	decrease (Jiang *et al.*, 2007; Osterwald *et al.*, 2012; O'Sullivan *et al.*, 2014; Osterwald *et al.*, 2015)
RAD50	(Zhu *et al.*, 2000; Jiang *et al.*, 2007)	decrease (Jiang *et al.*, 2007) (Zhong *et al.*, 2007; Osterwald *et al.*, 2015)
RAP1	(Yeager *et al.*, 1999; Wu *et al.*, 2003; Cesare *et al.*, 2009; Wilson *et al.*, 2016)	decrease (Jiang *et al.*, 2007)
RBBP8 (aka CTIP)		decrease (O'Sullivan *et al.*, 2014)
SMC5/ 6	(Potts & Yu, 2007)	decrease (Potts & Yu, 2007)
SUMO1/ 2/ 3	(Chung *et al.*, 2011)	decrease (Osterwald *et al.*, 2012; Osterwald *et al.*, 2015)
SUV420H2		decrease (Osterwald *et al.*, 2015)
TIN2	(Cesare *et al.*, 2009; Wilson *et al.*, 2016)	decrease (Jiang *et al.*, 2007; Osterwald *et al.*, 2015)
TOP2B	(Hsieh *et al.*, 2015)	decrease (Hsieh *et al.*, 2015)
TOP3A	(Temime-Smaali *et al.*, 2008)	decrease (Osterwald *et al.*, 2015)
TRF1	(Yeager *et al.*, 1999) (Zeng *et al.*, 2009; Wilson *et al.*, 2016)	decrease (Jiang *et al.*, 2007); increase (Osterwald *et al.*, 2012; Osterwald *et al.*, 2015)
TRF2	(Yeager *et al.*, 1999; Cesare *et al.*, 2009; Zeng *et al.*, 2009; Osterwald *et al.*, 2012; O'Sullivan *et al.*, 2014; Wilson *et al.*, 2016)	decrease (Jiang *et al.*, 2007; O'Sullivan *et al.*, 2014); no effect (Osterwald *et al.*, 2015)
UBE2I (aka UBC9)		decrease (Osterwald *et al.*, 2012; Osterwald *et al.*, 2015)
XRCC6		decrease (Osterwald *et al.*, 2015)

The table summarizes proteins that have been shown to co-localize with PML and telomeres in ALT cells. The first column shows the protein name and in some cases an alias. The second column contains references for the localization to APBs and the last column for the APB phenotype upon protein depletion, indicating the requirement of the specific protein for APB formation.

The functionality of APBs in the ALT pathway is controversially discussed. It has been suggested that APBs serve as a collection reservoir for sequestering linear ECTRs (Fasching *et al.*, 2007) or are associated with cellular stress and senescence (Jiang *et al.*, 2009; Jiang *et al.*, 2011). In absence of

telomerase, ALT cell lines without APBs have been reported, which raises the possibility that more than one ALT mechanism might exist. Indeed, the human fibroblast cell line, AG11395, without APBs has been reported to utilize a variant ALT mechanism similar to the budding yeast type I recombination (Fasching *et al.*, 2005; Marciniak *et al.*, 2005). Exogenous expression of the WRN helicase in the AG11395 cell line has been reported to induce APBs (Siddiqa *et al.*, 2012; Gocha *et al.*, 2014), indicating that variant ALT mechanisms exists that might require a different set of expressed proteins. Another cell line, C3-cl6, has been shown to stably maintain short telomeres in the absence of telomerase and APBs (Cerone *et al.*, 2005). In the latter case, the absence of APBs was concluded from the missing co-localization of TRF2 and PML signal. However, since the telomeres in the C3-cl6 cell line are very short, shelterin might not bind sufficiently, making an immunostaining of TRF2 difficult.

Several reports support a functional role of APBs in the ALT mechanism. First, suppression of ALT leads to absence of APBs, as is evident in hybrids formed by fusion of ALT and telomerase-positive cells (Perrem *et al.*, 2001), while induction of ALT by depletion of ASF1A and B was accompanied by the formation of APBs (O'Sullivan *et al.*, 2014). Also, disruption of APBs for example by depletion of or sequestering the MRE11/ RAD50/ NBS1 complex away from telomeres (Jiang *et al.*, 2005; Zhong *et al.*, 2007), by depletion of the structural maintenance of chromosomes (SMC) 5/ 6 complex (Potts & Yu, 2007), or by depletion of all PML isoforms in the ALT-positive cell line U2OS (Osterwald *et al.*, 2012; Deeg, 2015) results in telomere shortening. It is necessary to take into account that different PML isoforms have various effects on the formation of PML nuclear bodies and therefore APBs. Hence, if one isoform is overexpressed, the equilibrium of PML isoforms is misbalanced and the resulting consequences have to be considered. For example, exogenous expression of PML-III, -V and -VI in ALT cells decreased the number of APBs, whereas PML-IV resulted in more APBs per cell (Osterwald *et al.*, 2012). Induction of stress-associated APBs by methionine starvation is specific to ALT cells (Jiang *et al.*, 2005). *De novo* formation of APBs by recruitment of shelterin compounds or recombination factors to telomeres induced telomere lengthening (Chung *et al.*, 2011). Furthermore, it has been hypothesized that APBs provide an environment required for telomere recombination, because factors like MMS21, SMC5, SMC6, and MUS81 are not only required for APB formation but also for telomeric recombination (Nabetani *et al.*, 2004; Potts & Yu, 2007; Zeng *et al.*, 2009). Artificially enlarged PML-NBs in ALT cells have been shown to accumulate chromosomal telomeres and facilitate telomere clustering only in APB-positive cells (Draskovic *et al.*, 2009). In summary, APBs can be used as markers for the ALT mechanism, but it is not clear if APBs have a functional role in the induction of the ALT pathway.

5 Scope of the thesis

The only known recurrent mutation that is strongly correlated with ALT in cancer is the loss of function mutation in *ATRX* and, to a lesser degree, mutations in *H3F3A*, encoding histone variant H3.3, and *DAXX* (Heaphy *et al.*, 2011a; Schwartzentruber *et al.*, 2012; Sturm *et al.*, 2014; Barthel *et al.*, 2017). However, numerous proteins have been reported to have a role in telomere maintenance (TM), and ALT can also emerge in the absence of mutations in *ATRX* and *DAXX* (Chudasama *et al.*, 2018). Accordingly, it would be expected that multiple genes are differentially expressed in dependence of ALT activity. While a number of putative gene expression signatures were proposed for patient stratification into ALT-positive and ALT-negative by RNA-seq, these do not reliably differentiate between ALT-positive and ALT-negative tumors (Lafferty-Whyte *et al.*, 2009; Doyle *et al.*, 2012; Barthel *et al.*, 2017). One explanation for that might be that tissue cell type specific effects can scarcely be separated from TM associated deregulation of genes. On the other hand, the localization of PML to telomeres in APBs is a characteristic hallmark of ALT-positive cells and frequently used as reliable and robust biomarker for ALT (Henson & Reddel, 2010; Chung *et al.*, 2012). However, neither recurrent mutations in PML nor a deregulation at the gene expression level have been observed in ALT cells (Lovejoy *et al.*, 2012; Deeg *et al.*, 2017). Thus, the formation of APBs must be driven by other currently unknown factors. While a functional contribution of APBs to the process of telomere elongation in ALT cells has been reported previously (Chung *et al.*, 2011), the underlying mechanism remains elusive. Thus, there is a currently unmet need to develop new strategies for the identification of novel candidate genes and to elucidate the function of ALT biomarkers like APBs.

With this thesis, I addressed these issues in three areas. (i) A compilation and annotation of known TM genes was conducted. (ii) Strategies were developed and applied to identify novel candidate genes from ALT induction and suppression. (iii) The functional role of PML during ALT development was dissected. The results obtained in this thesis, provide new insights into the role of APBs as an ALT driver and provide a basis for patient stratification into ALT-positive and ALT-negative groups. The latter has a direct impact on the clinical setting because of a high incidence of ALT-positive tumors in cancer entities like leiomyosarcoma (53-78%) or pediatric glioblastoma (44%), where TMMs are correlated with patient outcome and overall survival (Heaphy *et al.*, 2011b; Sturm *et al.*, 2014; Chudasama *et al.*, 2018).

Materials and Methods

1 Materials

1.1 Buffers

Table 3. Buffer composition.

buffer	composition
1× CSK buffer	100 mM NaCl, 300 mM sucrose, 3 mM MgCl2, 10 mM PIPES pH 6.8, 0.5 % Triton X 100
1× FACS binding buffer	10 mM HEPES, 2.5 mM $CaCl_2$, 140 mM NaCl
1× FISH hybridization buffer	75% formamide, 20 mM NaCl, 20 mM Tris, 0.1% BSA
1× PBS	2.7 mM KCl, 1.7 mM KH_2PO_4, 137 mM NaCl 10 mM Na_2HPO_4 pH 7.4
1× RIPA buffer	150 mM NaCl, 1 % NP40, 0.5 % Na-desoxy-cholate, 0.1 % SDS, 50 mM Tris pH 8.0, 1× complete protease inhibitor cocktail (Roche, Germany)
1× TBS	25 mM Tris, 0.15 M NaCl, pH 7.5
1× TBST	25 mM Tris, 0.15 M NaCl, pH 7.5, 0,1% Tween20
1× transfer buffer	25 mM Tris, 192 mM glycine, 0.5 % (w/v) SDS; freshly added: 200 mL MeOH to 800 mL transfer buffer
10× SDS running buffer	250 mM Tris,1920 mM glycine, 1% (w/v) SDS, pH 8.3
20× SSC	3 M NaCl, 0.3 M $C_6H_8O_7Na_3$, pH 7
50× TAE	40 mM Tris, 20 mM acetic acid, 1 mM EDTA
6× Laemmli buffer	375 mM Tris pH 6.8, 300 mM DTT, 12% SDS, 60% Glycerol, 0.06% bromphenol blue
AE buffer	50 mM sodium acetate pH 5.3, 10 mM EDTA

1.2 Kits and reagents

Table 4. Kits and reagents.

kit/ reagent	company
Bioanalyzer chip, high sensitivity DNA	Agilent Technologies, USA
Biozym gold agarose	Biozym, Germany
clarity Western ECL substrate	Bio-Rad, Germany
complete protease inhibitor cocktail	Roche, Germany
NEBNext adapters, #E7337A	New England Biolabs, USA
NEBNext Multiplex Oligos for Illumina	New England Biolabs, USA

kit/ reagent	company
NEBNext ultra directional RNA library prep kit	New England Biolabs, USA
NEBNext ultraII directional RNA library prep kit	New England Biolabs, USA
nitrocellulose membrane	Bio-Rad, Germany
ProLong gold antifade with DAPI	ThermoFisher Scientific, USA
Puregene core Kit	ThermoFisher Scientific, USA
Qubit dsDNA HS assay Kit	ThermoFisher Scientific, USA
Qubit RNA HS assay Kit	ThermoFisher Scientific, USA
Ribo-Zero gold rRNA removal kit (human/ mouse/ rat)	Illumina, USA
Ribo-Zero magnetic gold kit (yeast)	Epicentre Biotechnologies, USA
RiboLock RNase inhibitor	Thermofisher Scientific, USA
RNeasy cleanup kit	Qiagen, Netherlands
Roti-Free stripping buffer	Carl Roth, Germany
ScreenTapes, D1000	Agilent Technologies, USA
TeloTAGGG telomere length assay	Roche, Germany

1.3 Instruments

Table 5. Instruments.

instrument	company
Bioanalyzer	Agilent Technologies, USA
Bio-Dot Apparatus	Bio-Rad, Germany
ChemiDoc MP System	Bio-Rad, Germany
FACS Canto II	BD Biosciences, USA
HiSeq 2000	Illumina, USA
HiSeq 4000	Illumina, USA
Leica TCS SP5 (DMI6000)	Leica Microsystems, Germany
Luna automated cell counter	Logos Biosystems, South Korea
MACSQuant VYB	Miltenyi Biotec, Germany
Qubit 2.0 Fluorometer	ThermoFisher Scientific, USA
Spectrophotometer NanoDrop	ThermoFisher Scientific, USA
T100 Thermo Cycler	Bio-Rad, Germany
TapeStation	Agilent Technologies, USA

1.4 Software

Table 6. Software.

software	version	source
Adobe Illustrator	15.0.2	Adobe systems, USA
bedtools	v2.17.0	(Quinlan & Hall, 2010)
cell segmentation 3D	1.12.1	(Wörz *et al.*, 2010; Osterwald *et al.*, 2012)
FIJI	ImageJ 1.48g	(Schindelin *et al.*, 2012)
Filemaker Pro 13 Advanced	13.0v9	Filemaker, USA

software	version	source
Filemaker server	version 15	Filemaker, USA
Image Lab	5.2.1	Bio-Rad, Germany
Integrative Genomics Viewer	2.3.91	(Robinson *et al.*, 2011)
KaleidaGraph	4.5.0	Synergy Software, USA
LAS AF		Leica Microsystems, Germany
Leica matrix screener		Leica Microsystems, Germany
RStudio	Version 1.0.153	RStudio, USA
samtools	0.1.18	(Li *et al.*, 2009)
Serial Cloner	2-6-1	Franck Perez, Serial Basics
STAR	020201	(Dobin *et al.*, 2013)
Weasel	2.7.4	Frank Battye – flow cytometry consulting, Australia

2 Cloning

All primers (**Table 7**) were designed using SerialCloner 2-6-1 (Franck Perez, Serial Basics) and ordered from Eurofins MWG Operon, Germany. PCR amplifications were carried out using Q5 High-Fidelity DNA Polymerase (New England Biolabs, USA). PCR fragments were purified and ligated to the respective backbone vector with T4 DNA Ligase (ThermoFisher Scientific, USA) within 4 h. Transformations were carried out in the XL10-Gold cells (Agilent Technologies, USA). Plasmid DNA was purified using the NucleoSpin plasmid purification kit (Macherey-Nagel, Germany) according to manufacturer's protocol and eluted in 30 µL H_2O.

All plasmids and backbone vectors are summarized in **Table 8**. The pEGFP-N1-TRF1 plasmid was constructed by insertion of TRF1 cDNA, amplified from pDEST53-GFP-TRF1 and digested with NheI/ SacI. Subsequently, PMLIII cDNA, amplified from pEGFP-C1-PMLIII and cut by BamHI/ AgeI was inserted. The resulting pEGFP-N1-TRF1-PMLIII (TPG) plasmid was then digested with NheI/ AgeI, NheI/ BamHI and BamHI/ AgeI and the 5' overhang was filled up using Klenow fragment in 1× Klenow buffer (both Fermentas/ ThermoFisher Scientific, USA) for 10 min at 37 °C. Blunt end ligation was performed for 2 h at 37 °C to receive pEGFP-N1 (G), pEGFP-N1-TRF1 (TG) and pEGFP-N1-PMLIII (PG).

Table 7. Primers.

primer	sequence (5'-3')	application	reference
TRF1 fwd	gctagcGTTCCGGACCGGAGTTagctagcGTTCCGGACCGGA	amplified from pDEST53-GFP-TRF1 Cloning	this thesis
TRF1 rev	gagctcGTCTTCGCTGTCTGAGGGCCCgagctcGTCTTCGCTGTCTGAGG		this thesis
PML fwd	ACAGggatccaTCTAAACCGAGAATCGAAACTAA	amplified from pEGFP-C1-PMLIII	this thesis
PML rev	ACGAaccggtaaGCGGGCTGGTGGGGAGG		this thesis

Table 8. Plasmids.

plasmid	construct	backbone vector	cloning/ cutting site	reference
pCMV_TET3G	transactivator 3G			Clontech, USA
pEGFP-N1	GFP			Clontech, USA
pDEST53-GFP-TRF1	GFP-TRF1			(Chung *et al.*, 2011)
pEGFP-C1-PMLIII	GFP-PMLIII			(Jegou *et al.*, 2009)
pEGFP-N1-TRF1	TRF1-GFP	pEGFP-N1	NheI/ SacI	this thesis
pEGFP-N1-TRF1-PMLIII (TPG)	TRF1-PMLIII-GFP	pEGFP-N1-TRF1	BamHI/ AgeI	this thesis
pEGFP-N1 (G)	GFP	pEGFP-N1-TRF1-PMLIII (TPG)	NheI/ AgeI	this thesis
pEGFP-N1-TRF1 (TG)	TRF1-GFP	pEGFP-N1-TRF1-PMLIII (TPG)	BamHI/ AgeI	this thesis
pEGFP-N1-PMLIII (PG)	PML-GFP	pEGFP-N1-TRF1-PMLIII (TPG)	NheI/ BamHI	This thesis

Table 9. Materials used for cloning experiments.

material	company
FastDigest AgeI	ThermoFisher Scientific, USA
FastDigest BamHI	ThermoFisher Scientific, USA
FastDigest NheI	ThermoFisher Scientific, USA
FastDigest SacI	ThermoFisher Scientific, USA
Klenow fragment, Klenow buffer	Fermentas/ ThermoFisher Scientific, USA
NucleoSpin Plasmid Kit	Macherey-Nagel, Germany
Q5 High-Fidelity DNA Polymerase	New England Biolabs, USA
T4 DNA ligase	ThermoFisher Scientific, USA
XL10-Gold cells	Agilent Technologies, USA

3 Cell culture and transfection

Cell lines and cell culture materials used within this thesis are listed in **Table 10** and **Table 11**, respectively. U2OS and HeLa cells were obtained from the German Collection of Microorganisms and Cell Cultures (DSMZ, Braunschweig, Germany). U2OS cells were maintained in low glucose DMEM (1.0 g/L) without phenol red (ThermoFisher Scientific, USA) and supplemented with 10% FBS (PAN Biotech GmbH, Germany), 2 mM L-glutamine (PAN Biotech GmbH, Germany), 100 µg/mL penicillin/ streptomycin (PAN Biotech GmbH, Germany). HeLa cells were cultured in RPMI without phenol red (ThermoFisher Scientific, USA) with the same supplements.

For transient transfection of U2OS and HeLa cells, Effectene (Qiagen, Germany), Lipofectamin 3000 (ThermoFisher Scientific, USA), or XtremeGene9 (Roche, Germany) were used according to manufacturer's protocol, respectively.

Table 10. Cell lines.

cell line	growth medium	reference
U2OS	low glucose DMEM, 10% FBS, 2 mM L-glutamine, 100 µg/mL penicillin/ streptomycin	DSMZ (Braunschweig, Germany)
U2OS Tet-On 3G	low glucose DMEM, 10% tet-free FBS, 2 mM L-glutamine, 100 µg/mL penicillin/ streptomycin, 1 mg/mL geniticin	Katharina Deeg (Prof. Karsten Rippe, DKFZ)
$U2OS^{G}$, $U2OS^{PG}$, $U2OS^{TG}$, $U2OS^{TPG}$ Tet-On 3G	low glucose DMEM, 10% tet-free FBS, 2 mM L-glutamine, 100 µg/mL penicillin/ streptomycin, 0.2 µg/mL geniticin 0.5 µg/mL puromycin	this thesis
HeLa	RPMI, 10% FBS, 2 mM L-glutamine, 100 µg/mL penicillin/ streptomycin	DSMZ (Braunschweig, Germany)
HeLa Tet-On 3G	RPMI, 10% FBS, 2 mM L-glutamine, 100 µg/mL penicillin/ streptomycin, 1 mg/mL geniticin	Dominik Niopek (Prof. Roland Eils, DKFZ)
$HeLa^{G}$, $HeLa^{PG}$, $HeLa^{TG}$, $HeLa^{TPG}$ Tet-On 3G	RPMI10% FBS, 2 mM L-glutamine, 100 µg/mL penicillin/ streptomycin, 0.1 µg/mL geniticin, 0.5 µg/mL puromycin	this thesis
SJ-G2 (also known as SJ-02, ICGC_GBM41)	high glucose DMEM, 10% FBS, 2 mM L-glutamine, 100 µg/mL penicillin/ streptomycin 1 mM sodium pyruvate	Prof. Stefan Pfister, DKFZ
MGBM1 (also known as 10-801, ICGC_GBM39)		
SF188 (ICGC_GBM40)		
KNS42 (ICGC_GBM73)		
HeLa ST		(O'Sullivan *et al.*, 2014)
HeLa LT		

Table 11. Cell culture material.

medium/ supplement	company
DMEM medium, low (1.0 g/L) or high (4.5 g/L) glucose without phenol red	ThermoFisher Scientific, USA
doxycycline	Sigma-Aldrich, Germany
fetal bovine serum (FBS)	PAN Biotech GmbH, Germany
FBS tet-free	PAN Biotech GmbH, Germany
geneticin (G418 sulfate)	ThermoFisher Scientific, USA
L-glutamine	PAN Biotech GmbH, Germany
OptiMEM I Reduced Serum Medium	ThermoFisher Scientific, USA
penicillin/ streptomycin	PAN Biotech GmbH, Germany
puromycin	Sigma-Aldrich, Germany
RPMI without phenol red	ThermoFisher Scientific, USA
sodium pyruvate	ThermoFisher Scientific, USA

For generation of stable inducible cell lines, the doxycycline inducible Tet-On 3G system (**Figure 5**, Clontech, USA) was used according to the manufacturer's protocol. U2OS Tet-On 3G cells were generated by stable transfection of the geniticin-resistant pCMV_TET3G plasmid by Katharina Deeg (Prof. Karsten Rippe, DKFZ) under the same culturing conditions as U2OS with additional 1 mg/mL G-418 (ThermoFisher Scientific, USA) in order to select for plasmid carrying cells. $U2OS^{G}$, $U2OS^{PG}$, $U2OS^{TG}$, $U2OS^{TPG}$ Tet-On 3G were generated by stable transfection with puromycin-resistant plasmids

pEGFP-N1 (G), pEGFP-N1-PMLIII (PG), pEGFP-N1-TRF1 (TG), or pEGFP-N1-TRF1-PMLIII (TPG), and maintained with the same supplements except for only 0.2 µg/mL geniticin (ThermoFisher Scientific, USA) and additional 0.5 µg/mL puromycin (Sigma-Aldrich, Germany). To induce stable expression of GFP, PML-GFP, TRF1-GFP or TRF1-PML-GFP, the respective cell line was treated with 50 ng/mL doxycycline (Sigma-Aldrich, Germany).

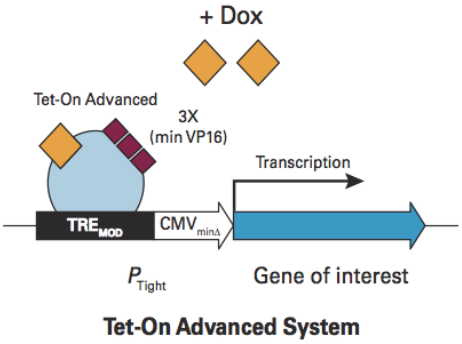

Figure 5. Tet-On 3G system for the generation of stable inducible cell lines.

Strategy for inducible gene expression. The 3G transactivator protein can only bind to the TRE promotor when doxycycline is added. Image taken from User manual for Tet-On® Advanced Inducible Gene Expression Systems User Manual (Clontech, USA).

HeLa Tet-On 3G cells were kindly provided by Dominik Niopek (Prof. Roland Eils, DKFZ) and were cultured in RPMI without phenol red (ThermoFisher Scientific, USA) with the same supplements as U2OS Tet-On 3G cells. HeLa^{G}, HeLa^{PG}, HeLa^{TG}, HeLa^{TPG} Tet-On 3G were generated as described for stable U2OS cells and maintained with the same supplements except for only 0.1 µg/mL geniticin (ThermoFisher Scientific, USA). To induce expression of GFP, PML-GFP, TRF1-GFP or TRF1-PML-GFP in the respective cell line, 100 ng/mL doxycycline (Sigma-Aldrich, Germany) was added. HeLa ST and HeLa LT, described previously (O'Sullivan *et al.*, 2014), were kindly provided by Jan Karlseder (Salk Institute, USA) and cultured in high glucose DMEM (ThermoFisher Scientific, USA) and supplemented as described for U2OS and HeLa cells above with additional 1 mM sodium pyruvate solution (ThermoFisher Scientific, USA). Pediatric glioblastoma cell lines SJ-G2, MGBM1, SF188 and KNS42 were kindly provided by Prof. Stefan Pfister (DKFZ, Germany) and were maintained as described for HeLa ST and LT cells. All cells were cultured at 37 °C and 5% CO2. Every 2-3 days, cells were split 1:3 by briefly washing with PBS (1×), and thereafter treating with trypsin/ EDTA (0.05/ 0.02% in 1× PBS) and incubated for in 3-5 min at 37 °C.

3.1 siRNA transfections

HeLa ST and HeLa LT cells were transfected with siASF1A and B as described previously (O'Sullivan et al 2014). Briefly, cells were seeded in 15-cm dishes and after 24 h transfected with a final concentration of 50 nM On-Target Plus SMARTpool siRNA, which was dissolved in 1× siRNA buffer, and Dharmafect (Dharmacon, USA), and previously incubated for 20 min in OptiMEM (ThermoFisher Scientific). After 24 h, transfection medium was exchanged with complete growth medium and cells were harvested ~72 h after transfection.

Table 12. siRNAs used for ASF1 knockdown.

siRNA	target Sequences (5'-3')	company
ON-TARGETplus SMARTpool: ASF1A siRNA	1) CGAUCAAGUUUUAGACUCU 2) CAUUAGACCAGGUUGUAAA 3) AGCCAUAUGAUGCAGGUUA 4) GGCAUAUGUUUGUAUUUCA	Dharmacon, USA
ON-TARGETplus SMARTpool: ASF1B siRNA	1) GCAGGGAGACACAUGUUUG 2) CGGACGACCUGGAGUGGAA 3) GACAGGAGUUCAUCCGAGU 4) GCACUCCUAUCAAGGGCUU	Dharmacon, USA
ON-TARGETplus Non- targeting control pool	1) UGGUUUACAUGUCGACUAA 2) UGGUUUACAUGUUGUGUGA 3) UGGUUUACAUGUUUUCUGA 4) UGGUUUACAUGUUUUCCUA	Dharmacon, USA

3.2 Small molecule inhibitors

The histone deacetylase inhibitor, suberoylanilide hydroxamic acid (SAHA, Millipore, Germany) was dissolved in absolute ethanol. For the treatment, fresh drug was added anew every 24 h to complete growth medium of treated cells, since the *in vitro* half-live of SAHA is 75 min in human plasma (Konsoula & Jung, 2008), and is therefore assumed to be degraded after 24 h in aqueous solution. For combined ASF1 knockdown (kd) and SAHA treatment, the SAHA was added in 10 µL absolute ethanol, so that a final concentration of 0, 0.5 µM or 2 µM was achieved. SAHA was added first after 3-4 h of transfection, and then every 24 h, without changing the medium. The ATRi, VE-821 (Selleckchem, USA), was solved in DMSO. 3×10^5 cells were either treated with 3 µM VE-821 or with the same volume of DMSO for the control samples for 6 days, as described before (Flynn *et al.*, 2015).

4 Fluorescence activated cell sorting (FACS)

For FACS, cells were harvested with trypsin/ EDTA as described above (**methods section 3**). Both cells in washing buffer and trypsinated cells were merged and cells were counted on a Luna automated cell counter (Logos Biosystems, South Korea). Cells were resuspended to a final concentration of 2×10^6 cells in FACS binding buffer (1×) and filtrated. Single stained and unstained samples were prepared for each cell line. For this, cells were stained with a final concentration of 20 µM Vybrant Dyecycle Violet (ThermoFisher Scientific, USA), 5 µL annexin V-FITC (Lot#177338, BioLegend, USA) for 15 min at room temperature and immediately before the measurement, 1 µL propidium iodide (1 mg/mL, Invitrogen/ ThermoFisher Scientific, USA) to a final concentration of 2.5 µg/mL was added. Samples were then analyzed by flow cytometry on a FACS Canto II (BD Biosciences, USA) at the DKFZ flow cytometry core facility or on a MACSQuant VYB (Miltenyi Biotec, Germany) kindly provided by Andres Florez (Prof. Thomas Höfer, DKFZ). Per sample 10'000 total cells were counted using a middle flow rate of ~60 cells/s.

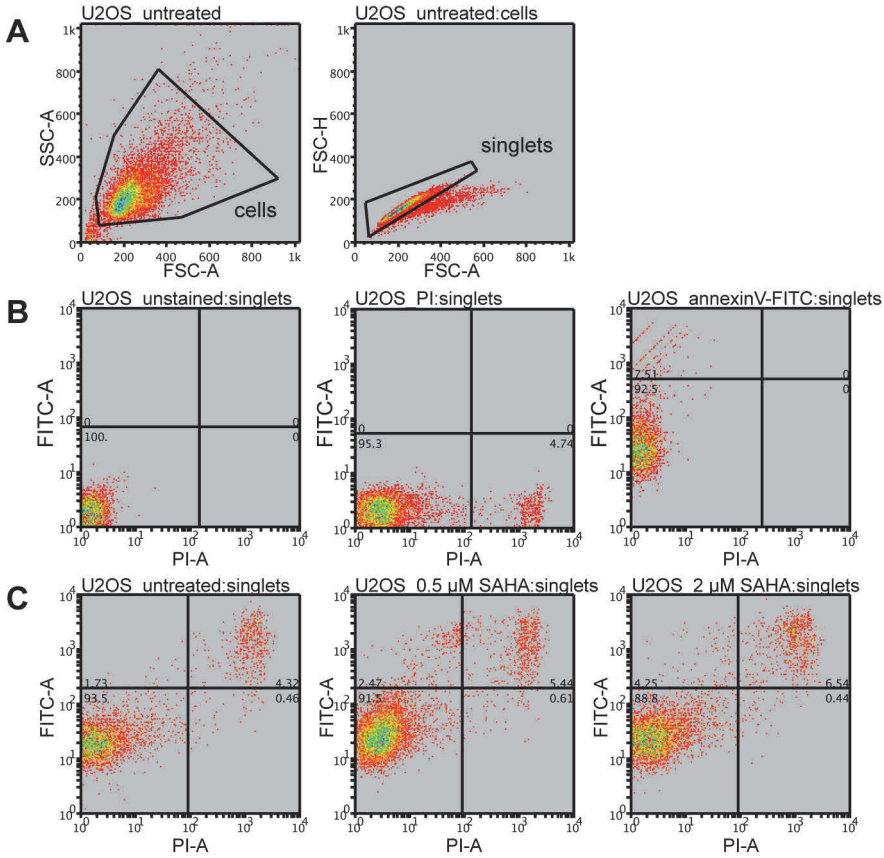

Figure 6. FACS gating and compensation.

U2OC cells were analyzed by FACS. **(A)** Gating was done for side scatter vs forward scatter to exclude small artifacts and large cell aggregates (gate was termed "cells"). Height vs area of the forward scatter was used to gate out duplets (gate was called "singlets"). **(B)** + **(C)** Annexin V vs propidium iodide signal are shown for **(B)** unstained and single-stained cells, and **(C)** untreated and SAHA-treated cells. Unstained cells were used as a negative control and single stained cells were used for compensation of spill-over from green to red channel. Statistic markers were set to separate living (lower left) from apoptotic (upper left) and dead (upper right) cell clusters.

4.1 Analysis of induced apoptosis

For FACS analysis the Weasel software (Frank Battye – flow cytometry Consulting, Australia) was used. After compensation of both FITC and propidium iodide (PI), cells were gated to remove small artifacts and duplets (examples are shown in **Figure 6**). Cells positive for PI were specified as dead cells, whereas cells only positive for annexin V-FITC were labeled as apoptotic. Cells negative for both signals were the fraction of viable cells. Induced apoptosis a_{ind} was calculated as in (Deeg *et al.*, 2016):

$$\mathbf{a}_{ind} = \frac{\mathbf{\%\ of\ apoptotic\ cells - \%\ of\ apoptotic\ cells\ (ctrl)}}{\mathbf{viable\ cells\ (ctrl)}}$$

4.2 Cell cycle analysis

Weasel was also used for visualization and fitting of cell cycle phases. Histograms of FACS-analyzed cells that incorporated membrane-permeant Vybrant Dyecycle Violet dye were plotted. A curve fit for cell cycle curves was performed, to obtain the percentages of subG0, G0, S, G2/M and super G2 phases.

5 Western blot

For protein extraction, 5×10^5 cells were harvested and washed with ice-cold PBS (1×). Cell pellets were then resuspended in ice-cold RIPA buffer and lysed for 60 min at 4 °C. After centrifugation for 30 min at full speed and 4 °C, lysates (25 µL aliquots) were stored at -20 °C. For Western blotting, 6 µL Laemmli buffer (6×, see **Table 3**) was added to 24 µL lysate and the sample was denatured at 95 °C for 5 min. Denatured proteins were loaded onto a stain-free acrylamide gel (4-20%, Bio-Rad Laboratories, USA) and separated for 45 min at 160 V. Separated proteins were then transferred to a nitrocellulose membrane (Bio-Rad Laboratories, USA) by semi-dry Western blotting in 1× transfer buffer at room temperature and 200 mA for 60 min. After transfer, the membrane was blocked with 5% skim milk powder (Lot# 040216, Gerbu, Germany) in TBST (1×, see **Table 3**) for 60 min at room temperature. Primary antibodies were diluted as indicated (**Table 13**) in 5% bovine serum albumin (BSA) in TBST (1×) and incubated overnight at 4 °C. After the incubation, the membrane was washed three times with TBST (1×) and then incubated with the secondary antibody, conjugated to horseradish peroxidase (HRP) and diluted as indicated (**Table 14**) with 5% milk in TBST (1×), for 60 min at room temperature.

Table 13. Primary antibodies used for Western blot.

antigen	host	dilution	Lot, company
ASF1A	rabbit	1:500	#2990, Cell Signaling, USA
ASF1B	rabbit	1:500	#2902, Cell Signaling, USA
GAPDH	mouse	1:3000	AM4300, Ambion/ Thermofisher Scientific, USA

Table 14. Secondary antibodies used for Western blot.

antigen	host	dilution	company
HRP-linked anti-rabbit IgG	goat	1:2000	Cell Signaling, USA
HRP-linked anti-mouse IgG	goat	1:2000	Cell Signaling, USA

For developing the membrane, Clarity Western ECL (Bio-Rad Laboratories, USA) was used according to manufacturer's protocol. For subsequent detection of the chemiluminescence signal, the ChemiDoc MP System (Bio-Rad, Germany) was used and the analysis was done with the corresponding Image Lab 4.1 software (Bio-Rad, Germany).

6 C-circle assay

The C-circle assay was performed as previously described (Henson *et al.*, 2009; Henson *et al.*, 2017). Briefly, DNA was extracted from 1×10^6 cells using the Puregene core Kit (Qiagen, Germany) according to the manufacturer's protocol. Genomic DNA (gDNA) was eluted with 100 µL 10 mmol Tris pH 7.5 and quantified using Qubit (ThermoFisher Scientific, USA). Subsequently, gDNA was diluted in triplicates to 20 ng in 10 µL. For the rolling circle amplification (**Figure 7**), 0.2 mg/mL BSA, 0.1% (v/v) Tween 20, 1 mM each dATP, dGTP and dTTP (ThermoFisher Scientific, USA), Φ29 Buffer (1×) and 7.5 U Φ29 DNA polymerase (both New England Biolabs, USA) were added to gDNA in a final volume of 20 µL.

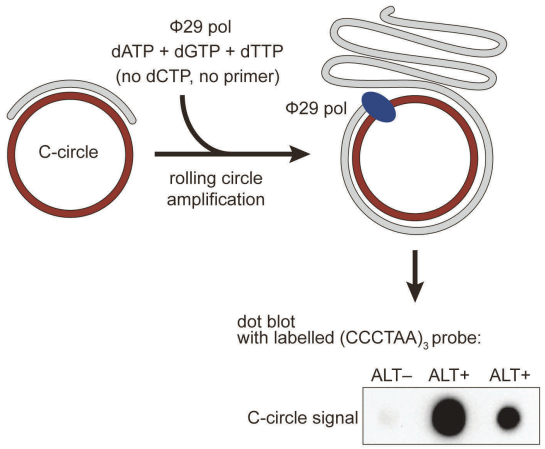

Figure 7. C-circle assay principle.

C-rich telomeric circles (red) that are partly double-stranded with G-rich (grey) telomere repeats are submitted to a rolling circle amplification. The G-rich fragment can serve as a primer and to specifically synthesize the G-rich telomeric DNA dATP, dGTP, dTTP but no dCTP is added. Φ29 polymerase amplifies telomere repeats. These are subsequently blotted and detected on a nylon membrane subsequently. Image adapted from (Henson *et al.*, 2017).

For every sample, a "no polymerase" control was used, and for every sample set an ALT-positive U2OS as well as an ALT-negative HeLa wild-type (wt) sample were used as a standard reference controls for each blot. The mixtures were first incubated for 8 h at 30 °C and then for 20 min at 65 °C. After the amplification step, the samples were mixed with 40 µl SSC (2×) and utilizing a Bio-Dot Apparatus (Bio-Rad, Germany) blotted onto a Roti Nylon plus membrane with a pore size 0.45 µm (Carl Roth, Germany), which was previously soaked in SSC (2×). The membrane was baked for 20 min at 120 °C and subsequently hybridized and developed using the TeloTAGGG Telomere Length Assay Kit (Roche, Germany) following the manufacturer's protocol. Roughly 60 min after the detection step, chemiluminescence signal was visualized using the high sensitivity program of the ChemiDoc MP System (Bio-Rad, Germany). In the accumulation modes, a series of images was taken. The image with maximum signal but no oversaturation was used for analysis with Image Lab 4.1 (Bio-Rad, Germany). The signals were first background-corrected and then the signal for "no polymerase" control subtracted from the "+ polymerase" signal. Finally, the signals for C-circle levels were normalized to a U2OS wt control (ALT-positive reference cell line).

7 Fluorescence microscopy

7.1 Fixation and permeabilization

For fluorescent microscopy cells were seeded on slides and fixed with PFA as described previously (Chung *et al.*, 2011). Briefly, cells were seeded on 24mm glass slides and treated as indicated in the respective results sections. After washing with PBS (1×), cells were fixed in 4% PFA in PBS (1×) for 12 min and subsequently washed with PBS (1×). Then cells were permeabilized with ice-cold 0.2% Triton X-100 in PBS (1×) for 5 min and again washed with PBS (1×).

7.2 Telomere PNA FISH

Telomere PNA FISH of cells was performed as described previously (Chung *et al.*, 2011). Briefly, cells were grown on coverslips and fixed and permeabilized cells as described above (**methods section 7.1**). After dehydration in a series of ethanol dilutions in water (70%, 85% and 100%), coverslips were allowed to air-dry and placed on a drop of 0.1 µM Cy3-labeled $(CCCTAA)_3$ PNA probe (Panagene, Korea) in hybridization buffer (75% formamide, 20 mM NaCl, 20 mM Tris, 0.1% BSA) on a coverslip. Coverslips were sealed with fixogum and let dry in the dark. After a denaturing step for 3 min at 80 °C, hybridization was performed overnight at 30 °C. Subsequently, coverslips were washed consecutively in 70% formamide (in 10 mM Tris-HCl, pH 7.4), 2× SSC, 0.1× SSC at 55 °C and 0.05% (v/v) Tween-20 in 2× SSC. Finally, coverslips were washed thrice in PBS (1×). Following PNA FISH either immunofluorescence against PML was performed as described in **methods section 7.3** starting with the blocking step, or DAPI staining was performed as described in **methods section 7.4**. As denaturation step of the PNA FISH procedure destroys GFP signal of tagged proteins, an antibody against GFP was used for immunofluorescence, to enhance the GFP signal. Alternatively, an APB staining was performed with anti-TRF2-ms-A568 and anti-PML-rb-ATTO633.

7.3 Immunofluorescence

Immunostaining was performed as described previously (Chung *et al.*, 2011). Briefly, fixed and permeabilized cells (from **methods section 7.1 or 7.2**) were blocked for 60 min with 10% goat serum in PBS (1×). After blocking, slides were incubated with primary and secondary antibodies, diluted as indicated (**Table 15**, **Table 16**) in blocking solution, for 60 min at room temperature or overnight at 4 °C. Between primary and secondary antibody incubations, slides were washed thrice with 0.002% NP40 in PBS (1×). Finally, slides were washed thrice in PBS (1×) and DAPI staining performed as described in **methods section 7.4**.

Table 15. Primary antibodies used for immunofluorescence.

antigen	host	dilution	Lot, company
TRF2	rabbit	1:250	NB110-57130, Novus Biologicals
PML	mouse	1:100	sc-966, Santa Cruz, USA
GFP	rabbit	1:500	ab290, Abcam, UK

Table 16. Secondary antibodies used for immunofluorescence.

antigen	conjugate	host	dilution	company
anti-rabbit IgG	Alexa 568	goat	1:300	Life Technologies/ ThermoFisher Scientific, USA
anti-rabbit IgG	Alexa 633	goat	1:200	Life Technologies/ ThermoFisher Scientific, USA
anti-mouse IgG	Alexa 568	goat	1:300	Life Technologies/ ThermoFisher Scientific, USA
anti-rabbit IgG	Alexa 488	goat	1:300	Life Technologies/ ThermoFisher Scientific, USA

7.4 DAPI staining

After fixed and permeabilized cells were stained with telomere FISH (**methods section 7.2**) and/ or immunofluorescence (**methods section 7.3)**, slides were subsequently washed. After another PBS wash, the coverslips were mounted with Prolong Gold antifade reagent (ThermoFisher Scientific, USA) containing DAPI.

7.5 Manual and automatic confocal image acquisition

For confocal image acquisition, a motorized inverted DMI6000 Leica TCS SP5 confocal laser scanning microscope (Leica Microsystems, Germany) with an oil immersion objective (63×/ 1.40 PL APO) was used. Four laser sources were used for excitation with wavelengths of 405 nm (UV diode), 488 nm, 561 nm and 633 nm (all three from a multiline argon laser). Microscope parameters were set in the LAS AF software (Leica Microsystems, Germany) for manual and automatic image acquisition (scan speed

400 Hz, resolution of 512 × 512 pixel, 3× zoom, pinhole: 1 airy, 8-bit depth, sequential mode, switch between stacks). The general procedure for screening a high number of cells is depicted in (**Figure 8A**). For automated image acquisition, the Leica MatrixScreener software (Leica Microsystems, Germany) was used as described previously (Osterwald *et al.*, 2012). First, a predictive focus map was generated and used for the noise-based autofocus job to determine the central z-position of the cells. Then, 50 images with a spacing of 1 µm were taken around the z-position of the predictive focus map with a scan speed of 600 Hz and a resolution of 64 × 64 pixel in the DAPI channel. After the autofocus job, the screening job was started automatically with z-positions from -5 µM to 5 µM around the specified position of the autofocus job.

7.6 Automatic image analysis

For manually acquired images, FIJI/ Image J (Schindelin *et al.*, 2012) was used to generate maximum image projections. To analyze telomere and PML spots in manually or automatic acquired images, the cell segmentation 3D software was used (Wörz *et al.*, 2010; Osterwald *et al.*, 2012) (**Figure 8B**). Briefly, raw images were converted into 3D image stacks using the Stack Builder Plugin (https://imagej.nih.gov/ij/plugins/builder.html, Nicolas Roggli and Wayne Rasband). For 3D segmentation of nuclei, a standard deviation of σ=1.2 for Gaussian smoothing was used. Telomeres and PML nuclear bodies were detected in a 2-pass system for larger and smaller spots with a standard deviation of σ=1.1 for Gaussian smoothing. Border cells with more than 300 voxels on the image margins were excluded from the analysis. Parameters for clipping and the region size for local maxima search of telomere and PML spots were set to detect all visually detectable telomeres in untransfected or GFP transfected cells. The output file contained information on number, volume and integrated intensities of detected spots, as well as overall integrated intensities of all channels in the segmented nuclei. The results files were loaded into R to extract and visualize these data for all spots and cells.

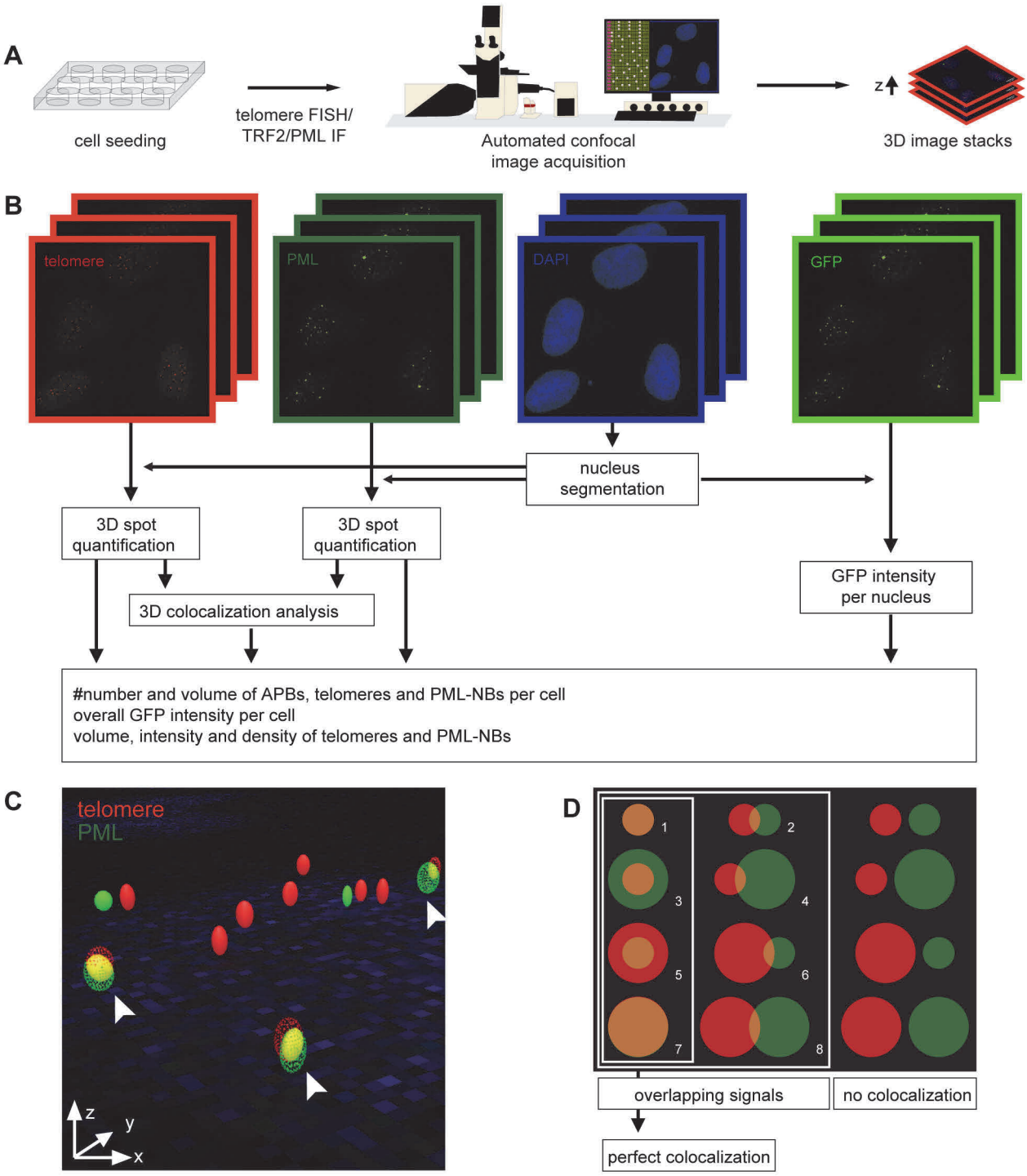

Figure 8. Automatic 3D confocal fluorescence microscopy platform.

(**A**) Confocal image acquisition of fixed cells. After cell seeding and treatment, cells were fixed and stained via immunfluorescence or telomere FISH. Images were acquired automatically using the Leica matrix screener software (Leica Microsystems, Germany). (**B**) Automated 3D image analysis of confocal stacks in four channels. First, the nucleus segmentation was done in the DAPI channel. Next, spots in the red (telomere) and green (PML) channel were detected and quantified to perform a 3D colocalization analysis. For all spots number, volume and integrated intensity was calculated. Overall, the total intensity was summarized for four channels in the segmented area. **(C)** Visualization of colocalizing telomere (red) and PML (green) signals. White arrows indicate colocalizing signals. **(D)** The 12 categories for the assembly of two spots are shown. The white squares mark all possible colocalizations, however only the first, third, fifth and seventhes mark highest overlapping cases.

8 RNA isolation for RNA-seq

Human

1×10^7 cells were harvested and RNA was isolated using the NucleoSpin RNA plus kit (Macherey Nagel, USA). First, cell pellets were lysed in LBP buffer and stored at -80 °C until all lysates of a sample set were collected. RNA was extracted according to the manufacturer's protocol. Finally, only long RNA was eluted twice in 2× 25 µL RNase-free H_2O with 1 µL ribolock (ThermoFisher Scientific, USA). RNA concentration was measured by Qubit (RNA high sensitivity, ThermoFisher Scientific, USA). For complete removal of genomic DNA, 1 U/µg RQ1 DNase (Promega, USA) and 1 µL ribolock (ThermoFisher Scientific, USA) were added for 30 min at 37 °C in RNase-free RQ1 DNase reaction buffer (1×, Promega, USA). Depleted RNA was precipitated by adding sodium acetate to a final volume of 200 mM, 0.5 mg/mL glycoblue and 3 volumes of ethanol. The mixture was incubated for 60 min at -20 °C and subsequently pelleted by centrifugation at full speed and 4 °C. The air-dried RNA pellet was then resuspended in 30 µL RNase-free H_2O with 1 µL ribolock (ThermoFisher Scientific, USA).

Budding yeast

*S. cerevisiae est2*Δ cells were derived from meiotic products of a heterozygous diploid budding yeast strain 281 (*est2 sir2 exo1*) (Balk *et al.*, 2013). Cell pellets were prepared in two replicates on days 2, 6 and 10 of the survivor formation (start, crisis, survivor). RNA was isolated by phenol/ chloroform extraction as described previously (Schmitt *et al.*, 1990). Briefly, cells pellets were resuspended in 400 µL AE buffer and mixed with 40 µL 10% SDS. The mixture was incubated with an equal volume of phenol for 4 min at 65 °C. After quickly cooling the emulsion to form phenol crystals, a centrifugation step at maximum speed and 2 min separated the aqueous and the organic phases. The aqueous phase was extracted with phenol/ chloroform for 5 min at room temperature. RNA was precipitated by adding sodium acetate to a final volume of 300 mM and 2.5 volumes of absolute ethanol. Total RNA was eluted in 20 µL RNase-free water and stored at -80 °C. To remove genomic DNA, RNA samples were DNase treated for 35 min at 37 °C. Subsequent RNA purification was done with RNeasy Cleanup Kit (Qiagen, Netherlands).

9 RNA library preparation

Human

Preparation of libraries for the second replicate was performed independent of the first replicate. First, RNA concentrations were determined by NanoDrop (ThermoFisher Scientific, USA) and RNA integrity was measured for 100-500 ng RNA on the TapeStation (RNA ScreenTapes, Agilent Technologies, USA), following the manufacturer's protocol.

For rRNA removal in 2.5 µg input RNA, the Ribo-Zero Gold rRNA removal Kit (human/ mouse/ rat) (Illumina, USA) was used according to the manufacturer's protocol. Depleted RNA was purified using the Agencourt RNAClean XP beads Kit (Beckman Coulter, USA) and eluted in 15 µL H_2O. RNA concentrations were measured by Qubit (RNA high sensitivity, ThermoFisher Scientific, USA).

For the RNA library preparation of 6-11 ng RNA, the NEBNext Ultra II directional RNA library Prep Kit for Illumina (#E7760, New England Biolabs, USA) was used according to the manufacturer's protocol. According to the amount of input RNA, NEBNext adapters (#E7337A) were diluted 5 or 25-fold. NEBNext primers i501-i508 were uniquely combined with i701-i708 primers from dual index primers set 1 (NEBNext Multiplex Oligos for Illumina, New England Biolabs, USA).

PCR enrichment was performed in 10-13 PCR cycles. Libraries were eluted in 20 µL of 10 mM Tris pH 7.5 and concentrations were measured by Qubit (DNA high sensitivity, ThermoFisher Scientific, USA). Subsequently, size and quality of the libraries were determined on the TapeStation (D1000 ScreenTapes, Agilent Technologies, USA). Finally, 7-8 libraries were pooled to one multiplexed library.

Each multiplexed library was sequenced on a separate lane on a HiSeq 4000 (Illumina, USA) as single-read 50 bp and subsequently demultiplexed by the DKFZ sequencing core facility.

Budding yeast

All budding yeast libraries of replicates were prepared at the same time. First, RNA concentrations were measured by NanoDrop (ThermoFisher Scientific, USA). To determine RNA integrity, 200 ng RNA were mixed with an equal volume formamide to a final volume of 20 µL. After incubation for 5 min at 65 °C, samples were stored on ice and loaded onto a 2% E-gel EX (ThermoFisher Scientific, USA) and run for 10 min (program 7).

To remove rRNA, the Ribo-Zero Magnetic Gold Kit (Yeast) (Epicentre Biotechnologies, USA) was used according to the manufacturer's protocol. Depleted RNA was precipitated by adding sodium acetate to a final volume of 300 mM, 0.1 mg/mL Glycoblue and 3 volumes of absolute ethanol. The mixture was incubated for 60 min at -20 °C and subsequently pelleted by centrifugation at full speed and 4 °C. The air-dried RNA pellet was then resuspended in 10 µL RNase-free H_2O with 0.3 µL ribolock

(ThermoFisher Scientific, USA). RNA concentration was measured by Qubit (RNA high sensitivity, ThermoFisher Scientific, USA).

For the RNA library preparation of ~100 ng RNA, the NEBNext Ultra Directional RNA Library Prep Kit for Illumina #E7420, New England Biolabs, USA) was used according to the manufacturer's protocol for use with purified or ribosome depleted RNA. NEBNext adapters (#E7337A, New England Biolabs, USA) were diluted 3-fold.

PCR library enrichment was performed in 13 PCR cycles with NEBNext primers #1, #3, #8, #9, #10 and #11 from Index Primers Set 1, NEBNext Multiplex Oligos for Illumina (New England Biolabs, USA). The library was then eluted in 20 µL of RNase-free H_2O and concentrations were measured by Qubit (DNA high sensitivity, ThermoFisher Scientific, USA). Finally, size and quality of the libraries were determined on a bioanalyzer chip (High sensitivity DNA, Agilent Technologies, USA).

Libraries were pooled, sequenced on a HiSeq 2000 (Illumina, USA) as single-read 50 bp and subsequently demultiplexed by the DKFZ sequencing core facility.

10 RNA-seq data analysis

10.1 Mapping

First, the human genome sequence (GRCh38/ hg38) were downloaded from UCSC (http://hgdownload.cse.ucsc.edu/goldenPath/hg38/bigZips/hg38.fa.zip). The budding yeast genome sequence (SacCer_Apr2011/ sacCer3) was downloaded as single files per chromosome from UCSC (http://hgdownload.soe.ucsc.edu/goldenPath/sacCer3/chromosomes/) and merged to one file for all chromosomes (sacCer3.fa). The budding yeast annotation file was taken from UCSC table browser (gtf and bed (per whole gene), http://genome.ucsc.edu/cgi-bin/hgTables) (**Table 17**).

All budding yeast or human reads from unprocessed files (fastq) were uniquely mapped to the sacCer3 or hg38 assembly of the reference genome, respectively, without allowing mismatches using the spliced read aligner STAR (Dobin *et al.*, 2013). The sorted output bam files "Aligned.sortedByCoord.out.bam" were indexed using samtools (Li *et al.*, 2009).

Table 17. Settings for annotation files downloaded from the UCSC table browser.

	human	budding yeast
clade	mammal	other
genome	human	*S. cerevisiae*
assembly	Dec. 2013 (GRCh38/ hg38)	Apr. 2011 (SacCer_Apr2011/ sacCer3)
group	genes and gene predictions	genes and gene predictions
track	NCBI RefSeq	SGD Genes
table	RefSeq all (ncbi RefSeq)	sgdGene
region	genome	genome

10.2 Integrative genomics viewer (IGV)

For visualizing gene expression profiles in the IGV (Robinson *et al.*, 2011), bedgraph files were generated by bedtools (Quinlan & Hall, 2010) with the following line:

```
bedtools genomecov –ibam $i –bga –split –scale $factor > $i".bedgraph"
```

With $i being the name of the *.bam files and $factor being the per million scaling factor of each sample, that was calculated to normalize for sequencing depth (all mapped reads divided by 1,000,000). Bedgraph files were then loaded into IGV and an auto group scale was set. Human hg38 was used as reference genome.

10.3 Differential gene expression and GO pathway analysis

For the generation of a count table, multiBamCov (samtools) (Li *et al.*, 2009) with the same genome annotation (hg38/ sacCer3) as for mapping was used. Differential expression analysis was done in R using the DESeq2 package (Love *et al.*, 2014). The count table was loaded and all Isoforms or genes with zero read counts in all conditions were eliminated. For the human count table, containing all isoforms, the data set was reduced to one isoform per gene, selecting the longest isoform of the gene. DESeq analysis was performed according to the provided manual. The pheatmap package (https://CRAN.R-project.org/package=pheatmap) was used for generating all heatmaps. To access the similarities of samples, the DESeqDataSet was submitted to variance stabilizing transformation (vst) that selects a representative subset of 1000 genes. The sample distances were calculated (dist) and plotted using pheatmap. For further analysis, the DESeqDataSet was regularized–logarithm transformed (rlog). A result table was extracted for pairs of samples that were compared on the expression level. A histogram plot for the distribution of log2 fold changes was fitted with a centered Gaussian curve. At the points of convergence, the cut-off for the log2 fold change for deregulation was set. The adjusted p-value (FDR) was set to 0.05. For the gene ontology pathway analysis, the functional

annotation chart tool from DAVID based on biological process terms was used (Dennis *et al.*, 2003). Only enriched pathways with a p-value <0.05 were listed.

In order to take potential cell-cycle effects due to the perturbations into account, a study investigating the dependence of gene expression on the cell cycle was consulted (Grant *et al.*, 2013). The lists provided for U2OS and HeLa cells are partly overlapping with the *TelNet* genes (271 of 1813 for U2OS). Furthermore, the expression or localization of some known TMM genes are also dependent on the cell cycle, e.g. TRF1, MRE11, POT1, ATM, and NBS1 (Zhu *et al.*, 2000) (Verdun *et al.*, 2005). Therefore, genes from the Grant *et al.* lists were marked with a °circle but were not excluded from the analysis.

TMM pathway analysis was performed using the *TelNet* database. At all occurrences in the text and in the tables, *TelNet* genes were marked in bold.

11 Implementation of the *TelNet* database

For the implementation of the database, Filemaker Pro Advanced (Filemaker, USA) was used. The database is distributed via Filemaker server and access is provided via the Filmaker webdirect software at http://www.cancertelsys.org/TelNet. Currently, no password is necessary and the database is free to use via the guest account.

Databases in Filemaker consist of tables that have a number of different fields (**Table 18**). In *TelNet*, each organism has a separate table that covers all fields described in **Table 19** and **Table 20**. Another set of tables, i.e. “organism”, “TM significance”, “cellular function”, “TM function” and “TMM annotations”, were generated to contain value lists for some of the fields in the human or budding yeast table. Additional tables were set up with records to provide value lists for fields in the organism table or for background calculations, such as “statistics”, “start” and “virtual”. The table “info buttons” serves as help page. Value lists for the tables “organism”, “TM significance”, “cellular function” and “TM function” as well as all TMM annotations can be found in **Table 19** and **Table 20**.

The info buttons table contains help terms and an appropriate description of each field. The start page serves as front page and is used for processing search requests. The statistics table does only contain one record for display and temporarily saves ID lists for visual display. The “virtual” table is needed for all background calculations as well as temporary storage required for the statistics page. In summary, Filemaker served as implementation platform for setting up the *TelNet* database.

Table 18. FileMaker tables.

table	records	Fields
TelNet_human	human genes/ proteins	see table (Table 19 and Table 20)
TelNet_budding yeast	budding yeast genes/ proteins	
organism	designation of organisms	-
TM significance	predicted, screened, validated	-
cellular function	list of cellular functions (Table 19)	-
TM function	list of TM functions (Table 20)	-
human TMM annotation	list of respective TMM annotations and activity (Table 20)	TMM annotations, regulation activity
budding yeast TMM annotation		
info buttons	list of help terms	help term and description
start	every new list search generates a new record	search and selection fields
statistics	-	ID lists for export
virtual	only for background calculations	calculation storage for statistics page

Results

1 *TelNet* database

Telomere maintenance comprises complex processes from reverse transcription to homologous recombination with the help of a variety of different proteins. However, a systematic approach that integrates annotations with regard to TMMs is desirable. Therefore, the *TelNet* database as a comprehensive compilation of genes with a role in telomere maintenance (TM) has been developed. Furthermore, besides providing a comprehensive collection of TM genes, *TelNet* resulted in a helpful tool that enables identification of TM networks.

1.1 Screening studies provide an initial source of TM genes

To establish a solid foundation for the *TelNet* database, at first gene lists from screening studies or reviews that address TM in human and budding yeast have been selected (**Figure 9**). By applying proteomics of isolated chromatin segments (PICh) in ALT-positive Wi38-VA13 and telomerase-positive HeLa 1.2.11 cells Déjardin and Kingston identified proteins that bind to a telomere probe and 296 records were included into the database (Dejardin & Kingston, 2009). Grolimund *et al.* determined the telomere protein composition of HeLa cells with different telomeric states by quantitative telomeric chromatin isolation protocol (QTIP) and identified 34 proteins (Grolimund *et al.*, 2013). Among the 34 identified proteins they found a number of factors that have not been characterized at telomeres before. In another work, over 200 proteins were found in the protein network surrounding telomere repeat binding factors, TRF1, TRF2, and POT1 using dual-tag affinity purification in combination with multidimensional protein identification technology liquid chromatography-tandem mass spectrometry (MudPIT LC-MS/ MS) (Giannone *et al.*, 2010). In a broad interaction screen of telomeric core proteins with a vast amount of human proteins by protein complementation assay (PCA/ bimolecular fluorescent complementation (BiFC)) Lee *et al.* found over 300 proteins that occur in proximity to shelterin compounds (Lee *et al.*, 2011). They also confirmed their results by a secondary analysis with a GST-pulldown of FLAG-tagged candidate genes and subsequent dot blotting of respective telomeric proteins. Notably, their approach also captures transient, infrequent and low affinity interactions. Lovejoy *et al.* comprised a gene set of 297 genes with potential relevance to telomeres and the ALT pathway assigned with functional annotations (Lovejoy *et al.*, 2012). The RNA interference screen of Osterwald *et al.*

directly measured the effect of protein knockdown by two independent siRNAs on the number of APBs (Osterwald *et al.*, 2015). Another TM study dealt with the effect of telomere attrition caused by the telomerase inhibitor GRN163 (Geron) (Uziel *et al.*, 2015). Proteomic analyses identified 99 proteins that were deregulated in the process of telomere shortening.

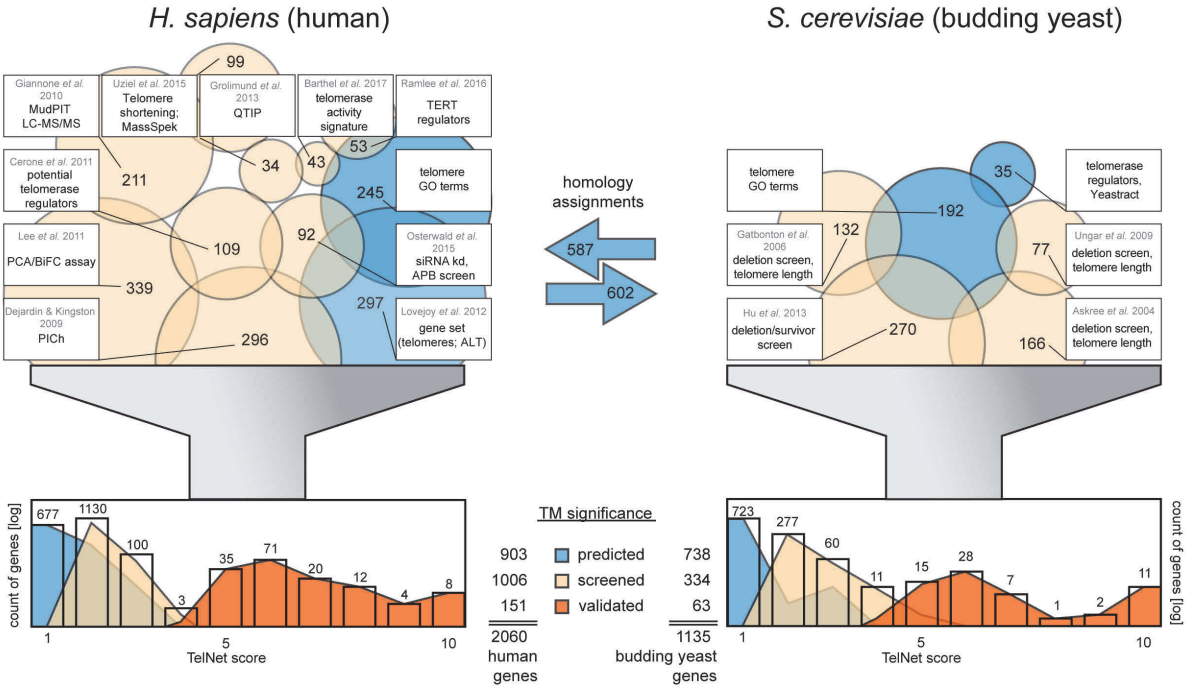

Figure 9. Sources for identification of genes associated to TM.

Gene lists from human and budding yeast screens or reviews and from GO (term "telo") are shown as circles. The color scheme indicates the TM significance, based on the source of the genes: blue, predicted; orange, screened or reviewed; red, validated by approved experimental research. Histograms display the distribution of the *TelNet* scores of all included genes and proteins per species. Overall, more than 2,000 human genes, and over 1,000 genes were included and manually curated for the *TelNet* database. Figure adapted from (Braun *et al.*, 2018).

Over 100 potential regulators of telomerase from a library screen of kinases were determined by quantitative TRAP assay (QTRAP) (Cerone *et al.*, 2011). Another set of telomerase regulators that act on the transcriptional level was reviewed recently (Ramlee *et al.*, 2016). Comparison of different published telomerase activity signatures resulted in 43 genes that can reliably predict telomerase activity from gene expression data (Barthel *et al.*, 2017). In budding yeast, it is possible to perform deletion screens and monitor alterations for instance in telomere length, and work from such screens has provided 326 genes to *TelNet* (Askree *et al.*, 2004; Gatbonton *et al.*, 2006; Ungar *et al.*, 2009). Another 270 genes from Hu *et al.*, who knocked out the RNA component of telomerase and subsequently investigated telomere structures of post-senescent survivors, were also implemented (Hu *et al.*, 2013). According to the type of study the gene was found or investigated we assigned a TM significance. (i) Genes with a suggested role in TM but lacking experimentally validation were ranked as "predicted". (ii) Genes collected from screening or review sources were classified as "screened". (iii) Proteins with detailed experimental evidence for a connection to TM were assigned as "validated". The proteins collected from the prior mentioned literature were mostly classified as "screened'. In addition, genes were included in

the database by homology assignment, if the orthologues' TM significance is categorized as "screened" or "validated'. For instance, even if no analysis comparable to budding yeast deletion screens exists in human, a human orthologue to a hit from such a screen was still included according to this procedure. As another source for *TelNet*, GO annotations of human and budding yeast genes were searched containing the term "telo" for subsequent inclusion in the database. Currently, additional 170 studies on human and 45 articles on budding yeast proteins that specifically characterized and validated the TM phenotype for example for ASF1, a and b, were taken into account (O'Sullivan *et al.*, 2014). Thus, screening studies, reviews, homology assignments and the GO database provided the basic compilation of proteins involved in TM, which was further extended by studies of single TM proteins.

1.2 General gene annotations are gained from external databases

In order to provide some standard information on each entry, external databases were consulted for names, descriptions and commonly used identifiers (**Figure 10** and **Table 19**). The ID conversion tool from the database for annotation, visualization and integrated discovery (DAVID, https://david.ncifcrf.gov) was accessed to unitize extracted identifier from the literature to a common set (Huang da *et al.*, 2008).

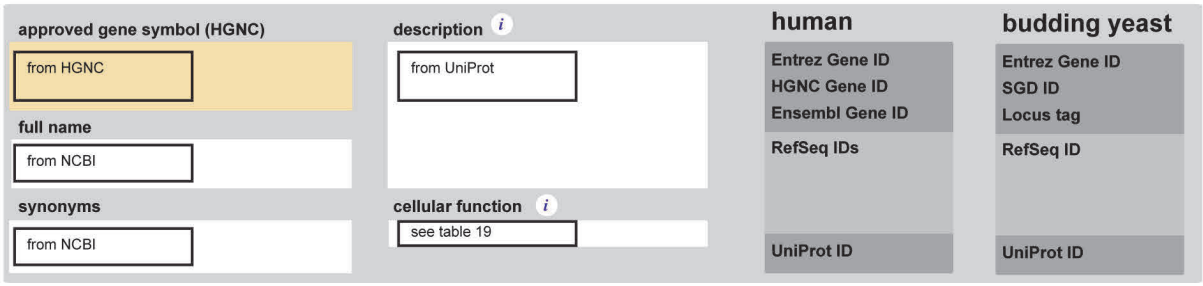

Figure 10. General part of a gene card.

The general part of the gene card view contains information from various external databases. Available terms for the annotation of a cellular function are listed.

The general part of each gene card consists of the full name, synonyms, Entrez Gene ID and RefSeq IDs (NCBI, www.ncbi.nlm.nih.gov) (Coordinators, 2017), HGNC Gene ID (HGNC, www.genenames.org) (Yates *et al.*, 2017), Ensembl Gene ID (Ensembl, www.ensembl.org) (Aken *et al.*, 2016; Aken *et al.*, 2017), Uniprot ID and functional description (UniProt, www.uniprot.org) (The UniProt, 2017) and for budding yeast, SGD ID and the Locus tag (SGD, www.yeastgenome.org) (Cherry, 2015). YeastMine (Balakrishnan *et al.*, 2012) from the saccharomyces genome database (SGD, www.yeastgenome.org) (Cherry *et al.*, 2012) was used to retrieve orthologues.

Table 19. General gene annotations.

Fields		Type	Comment
organism		entry field	*H. sapiens* or *S. cerevisiae*
approved symbol		entry field	official gene symbol
full name		entry field	full name as specified in external databases
synonyms		entry field	synonyms and aliases specified in external databases
description		entry field	general gene information
cellular function		entry field, value list	cell cycle; cell death; cell differentiation, cell membrane/ wall; cellular structure; chromatin organization; DNA replication and repair; metabolism; mitochondria; nuclear organization; nucleocytoplasmic transport; protein modification; protein synthesis and degradation; protein transport; RNA transcription and processing; signaling; telomere biology
gene ID		entry field	gene identifiers
human	HGNC ID	entry field	
	ensembl gene ID	entry field	
budding yeast	SGD ID	entry field	
	locus tag	entry field	
RefSeq ID		entry field	transcript identifiers
isoforms		entry field	
Uniprot		entry field	protein identifiers
orthologues		entry field	orthologues of the respective other organisms are entered and linked
source		entry fields	references categorized into three groups: “validated by”; “screened by”; “predicted by”
DOI		entry fields	DOI of the respective journal articles

Based on the functional annotations from gene ontology (GO, www.geneontology.org) and in line with biocuration guidelines, a list with concise terms annotating the cellular function was generated similar to curation procedures at SGD (**Table 19**). Every gene was manually annotated with the respective term that is most representative for its cellular function. Orthologous genes are listed and for those included in the database, an internal database link was integrated. In addition, literature information was referenced in the categories “predicted by”, “screened by” and “validated by” according to the TM significance. Web links are available for all external databases and literature articles. In summary, external databases served as source for composing the general part of each gene card.

1.3 Genes are annotated with TM information

In order to annotate each gene and protein with TM relevant information, peer-reviewed literature, such as above-mentioned screening and review papers, were exploited. The TM part of a gene card consists of text fields containing TM annotations (**Figure 11**, **Table 20**). A free-text summary of detailed information from experimental results can be found in the TM comment field.

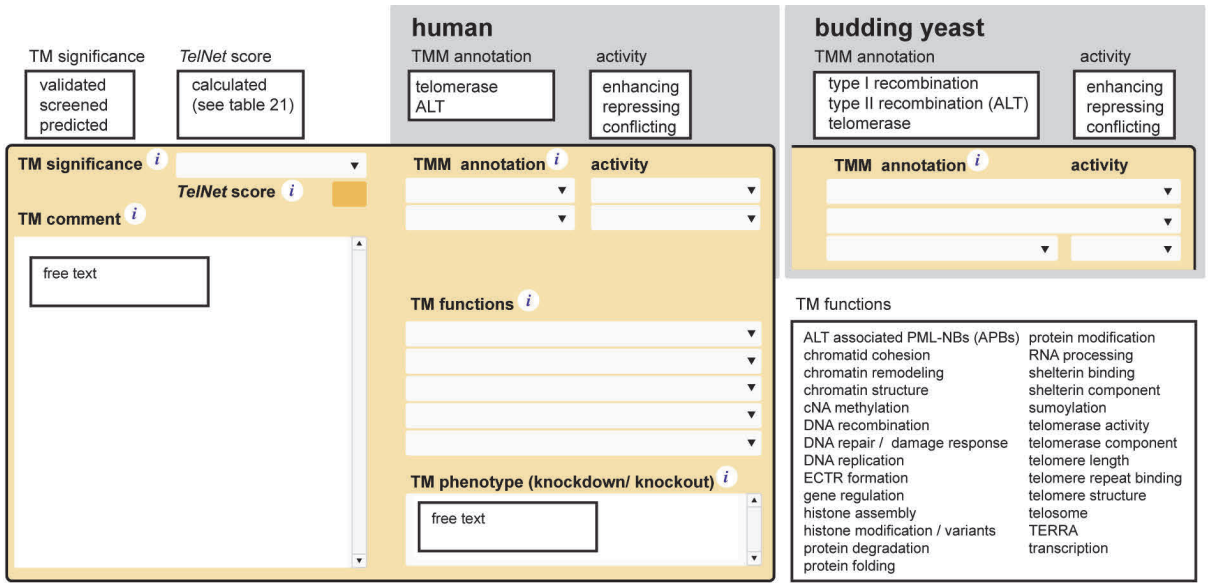

Figure 11. TM part of a gene card.

The TM part of the gene card contains information extracted from the literature. The descriptions of specific fields can be found in the text. Figure adapted from (Braun *et al.*, 2018).

Each protein can be assigned with up to five TM functions, such as molecular processes and functions as well as cellular structures associated with TM (**Figure 11**, **Table 20**). Furthermore, an effect resulting from knockout or knockdown that is linked to telomere length, telomerase activity or ALT hallmarks were documented in the field "TM phenotype". For distinguishing whether the wild-type (wt) gene is associated with telomerase-mediated TM mechanism (TMM) or the ALT pathway, the "TMM annotation" is provided.

Table 20. Fields of the TM part of a gene card.

fields		type	comment
TM significance		entry field, value list	"predicted", "screened" or "validated" (reflecting the experimental evidence on the association with TM)
TelNet score		calculation field	see **Table 21**
TM comment		entry field	all telomere-relevant information of a factor is summarized here.
human	TMM annotation	entry fields	telomerase-mediated or ALT
budding yeast			type I/II recombination or telomerase-mediated
TMM regulation activity		entry field, value list	repressing, enhancing or ambiguous
TM function [1-5]		entry field, value list	ALT associated PML-NBs (APBs); chromatid cohesion; chromatin remodelling; chromatin structure; DNA methylation; DNA recombination; DNA repair/ damage response; DNA replication; extrachromosomal telomeric repeat formation; gene regulation; histone assembly; histone modification, or variant; protein degradation; protein folding; protein modification; RNA processing; shelterin binding; shelterin component; SUMOylation; telosome; telomerase activity; telomerase component; telomerase localization; telomere length; telomere repeat binding; telomere structure; telosome; TERRA; transcription
TM phenotype		entry field	phenotype observed upon knock-down or knock-out related to TM features such as alterations in telomere length, increased or decreased ALT hallmarks, or effects on telomerase of the gene is given here.

For budding yeast genes, it can be additionally differentiated between type I and II survivors, with the latter having common features with the human ALT mechanism. Details of the regulation on each TMM as extracted from the literature were given in the enclosed activity field. Here, the options are an "enhancing", "repressing', or "ambiguous" regulation activity. The annotation "ambiguous" is selected for genes with opposing information from the literature or a lack of regulation description.

Table 21. Calculation of the *TelNet* score.

condition	score
if the TM significance is "predicted", the gene yields 5% of the orthologue's *TelNet* score	0-1
if the protein was identified in a TM related screen (added up if present in multiple screens)	1
if the TM significance is "validated"	3
if the cellular function contains the term "telomere'	1.5
if a TM function is assigned (added up for multiple functions)	0.5
extra score, if a TM function is "shelterin", "telosome" or "telomerase" (added up for multiple functions)	0.5

The *TelNet* score is calculated as a sum of information that was entered into the *TelNet* database. The maximum *TelNet* score is 10. Table adapted from (Braun *et al.*, 2018).

As outlined above (**results section 1.1**) the TM significance indicates experimental evidence of a genes connection to TM. The TM significance directly influences the *TelNet* score, that was established in this work to rank a gene according to several relevant parameters. It quantifies the TM significance and additionally takes the cellular function and TM functions into account (**Table 21**). The *TelNet* score is calculated as a sum of information that was entered into the *TelNet* database. The maximum *TelNet* score is 10. Thus, peer-reviewed literature was exploited for functional categorizing TM information, compositing of a comprehensive gene card for each entry, validating its TM significance and transferring it into a quantifiable score.

1.4 *TelNet* offers different search modes

For a convenient user interface, a decent front layout was designed that requires the selection of an organism (**Figure 12**). In order to cover all sorts of search requests, the *TelNet* database offers three search modes, "quick search", "list search", and "advanced card search". By pressing the button "show all" after selecting an organism, the user can explore all included genes of an organism.

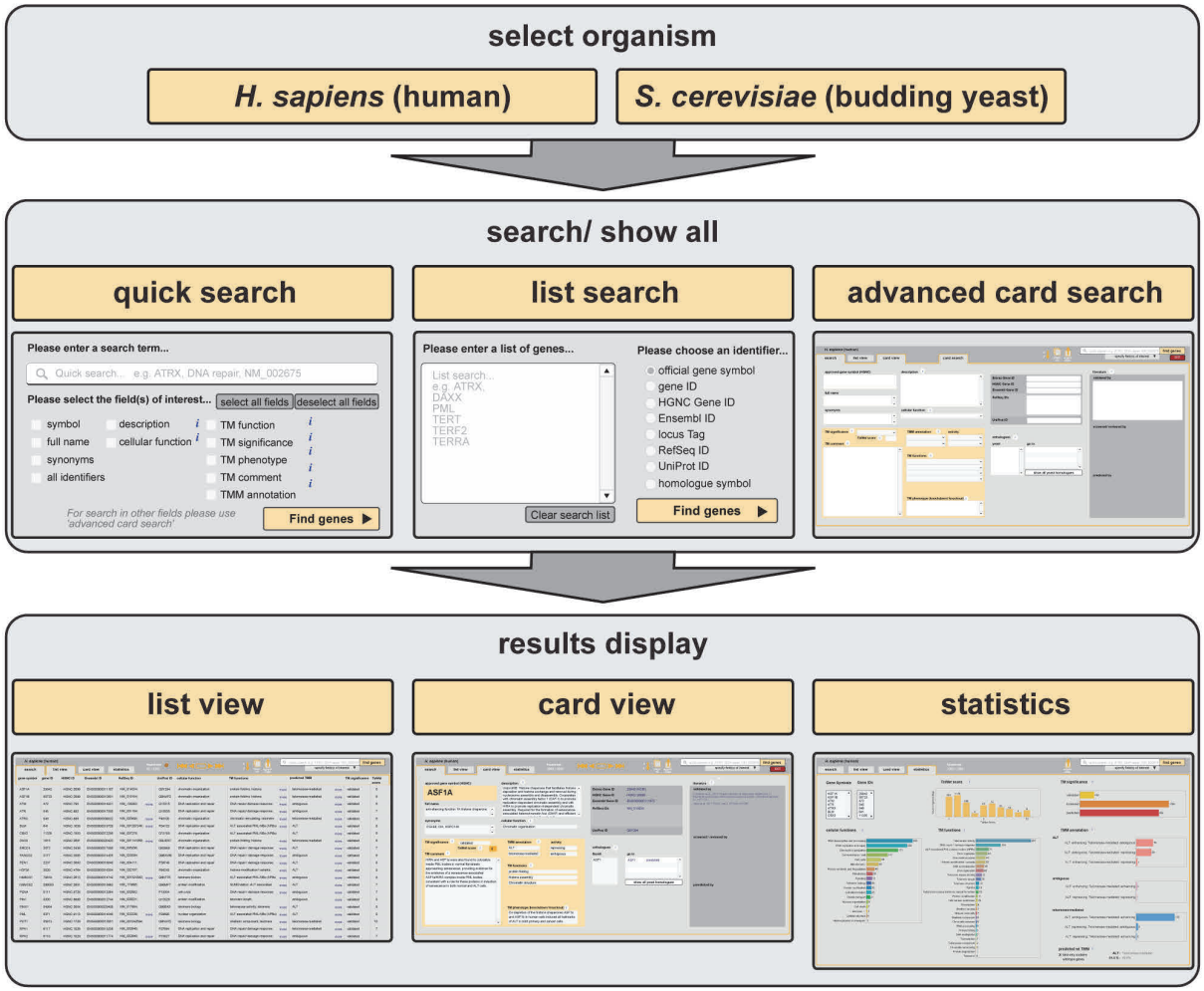

Figure 12. Usage chart for the *TelNet* database.

The navigation options and search modes of the *TelNet* database are depicted as flow chart. First the user has to select an organism. Next, either all entries can be selected or one of the three search modes can be applied. The resulting set of genes can be explored on list or card view. Finally, a statistics page displays a graphical overview over the different annotations. Figure adapted from (Braun *et al.*, 2018).

Alternatively, the user can perform a search request to find a set of interesting genes. A set of genes or proteins can be studied in the scrollable list view. From here, data export enables further bioinformatic analysis. The navigation menu on top allows a switch from list to gene card view for inspecting a single protein or gene of interest. The info buttons give a brief explanation of each field on the gene card. Thus, the *TelNet* database offers a user-friendly navigation and a comprehensive help page. To provide a thorough overview of annotations, a statistics page for a set of genes generated by a specific search was developed (**Figure 12**). Whole lists of genes can be directly copied from two fields containing the names and respective identifiers. Furthermore, a log-scaled histogram of the *TelNet* score is provided. Other annotations, such as TM significance, cellular and TM functions were charted as counts. Hence, the functional annotations enable a pathway analysis tailored for TM specific questions.

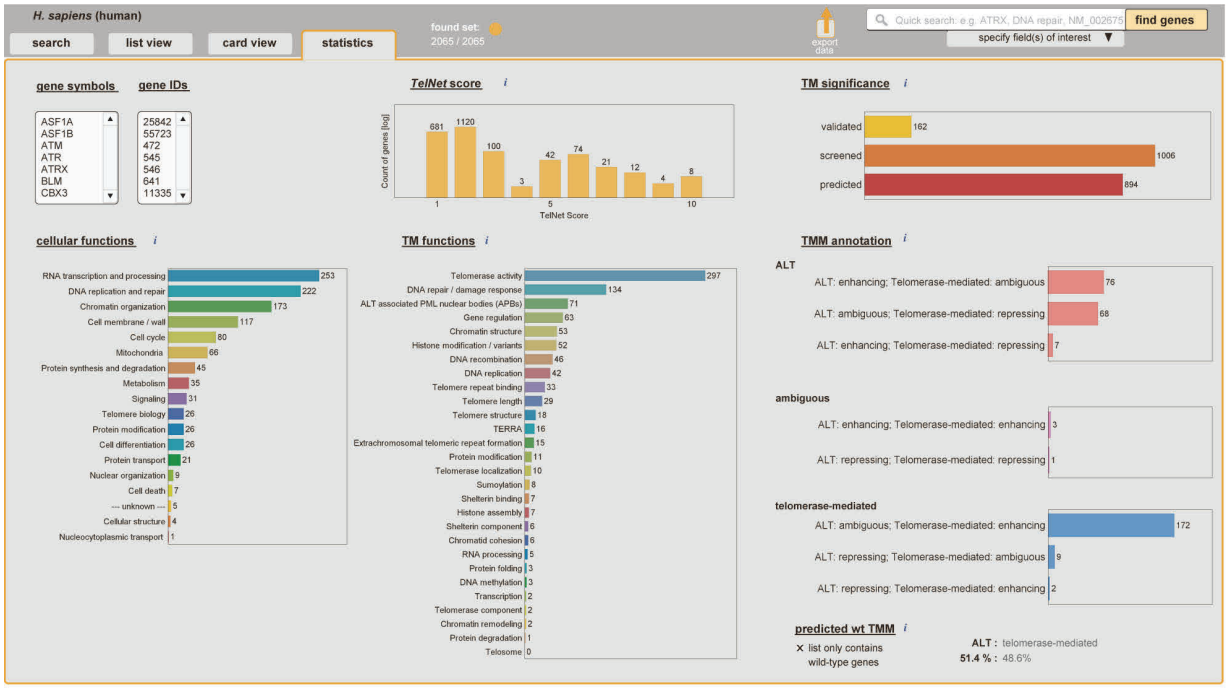

Figure 13. *TelNet* statistics page of all human genes.

A screen shot of the *TelNet* statistics page is displayed for all human genes. Gene symbols and IDs are stored in text fields for direct copying. The *TelNet* score, TM significance, cellular and TM functions, as well as TMM annotations are counted over all entries.

For the further analysis of the wt TMM annotation, the genes are grouped into three categories, “ALT”, “telomerase-mediated” and “ambiguous”. Proteins that drive the ALT mechanism and/ or repress telomerase fall into the category “ALT’. Those proteins repressing ALT and/ or promote telomerase activity fall into the category telomerase-mediated. For those that have no annotation or are indeterminate, the category ambiguous is chosen. For the predicted wt TMM, the user has to tick the respective field before the result is shown. Here, the *TelNet* score for each gene gives weight to the count of each category to calculate a probability for the proposed active TM mechanism. Thus, the *TelNet* statistics page is tailored for TM pathway analysis and for indication of the probable active TMM.

1.5 *TelNet* is a versatile tool for the identification of TM genes

For the “quick search’, the user can enter any search term and select the fields of interest. (for example: telomerase regulation, PML-NBs, serine/ threonine kinases). To identify gene candidates that are associated to TM from a gene list, the list search is the most appropriate search mode. The *TelNet* list search has a main application in bioinformatics data analysis pipeline as part of a TMM analysis, for which two examples are given in the following.

Sieverling *et al.* used the *TelNet* database for correlation of a gene list retrieved from a bioinformatics analysis pipeline (Sieverling *et al.*, 2018). In the ICGC pan-cancer project, whole-genome

sequencing (WGS) data of 2,594 matched tumor-control samples from 35 different tumor types have been analyzed. A systematic search discovered 2,759 somatic integrations of telomeric sequences into non-telomeric DNA. These telomere insertions were distributed across the genome and strongly correlated with increased telomere content, genomic breakpoint frequency and ALT-associated mutations. A list of genes that were found to harbor telomere insertions or mutations that correlated with telomere length was generated. Genes with telomere insertions and mutated genes were then passed into the *TelNet* list search to identify TM-associated genes. This procedure revealed a number of genes known to be associated with TM. Notably, among them were two genes, *PLCB2* (phospholipase C beta 2) and *ABCC8* (ATP binding cassette subfamily C member 8), that have been implemented in *TelNet* because their budding yeast homologues have been found to control telomere length. Based on the link provided by the *TelNet* database, it can be assumed that a functional association with telomeres also exists in humans, which has to be validated in further experiments.

In another example, a correlation was performed with data from the TCGA data set. In the TCGA pan-cancer project, Barthel *et al.* used the gene expression data of an "extended set" of 8953 tumor samples (Barthel *et al.*, 2017). The group estimated telomere lengths of matching samples by TelSeq (Ding *et al.*, 2014), a tool that counts telomere repeats from WGS data. As compared to Barthel *et al.*, the data set for the present analysis was reduced to a final patient set (n=281), within which matching normal control samples for each tumor sample were available. The ratio of tumor over normal was calculated for either telomere lengths as well as log2 of gene expression data. Next, the data was correlated using the spearman method, resulting in 1022 genes that significantly ($p<0.01$) (anti-)correlated with telomere length changes or that were differentially expressed (**Figure 14**). In order to filter for those genes that are related to TM, the *TelNet* database was used. Consequently, the list with gene candidates was passed into the *TelNet* "List search', which resulted in a set of 132 genes (12.9%) (**Suppl. table S2**). The 1,022 genes were also submitted to the HumanMine database that includes a GO enrichment analysis (Smith *et al.*, 2012). None of the enriched GO terms or pathways returned were related to telomeres. When simply searching for GO terms "telomere maintenance", "telomere organization" or "regulation of telomerase activity" only 13 genes (*RAD51*, *CCNE1*, *BRCA2*, *HIST1H4H*, *RECQL4*, *RFC4*, *FEN1*, *EXO1*, *BLM* and *HIST2H4A, PPARG*, *KLF4* and *PARM1*) were found. In contrast, *TelNet* found 132 genes associated with TM (including the 13 genes found with HumanMine). *TelNet* finds more genes, because it includes homology assignments in both directions and genes that do not have a GO term related to telomeres despite reported telomere related activities. In this analysis, no significantly upregulated genes ($l2fc>0.852$) that also significantly correlated ($Rho>0.186$) with telomere length changes were found. Also, none of the significantly downregulated *TelNet* genes ($l2fc<-0.782$) showed a significant anti-correlation ($Rho<0.184$) of gene expression and changes in telomere length. Furthermore, expression of *ARL4D* (ADP ribosylation factor like GTPase 4D) correlated with telomere length changes ($Rho=0.22$) and the gene was downregulated in tumors, indicating a role in telomere trimming. The gene was included in *TelNet* because telomeres get longer upon deletion of the budding

yeast homologue (Gatbonton *et al.*, 2006; Hu *et al.*, 2013). For the human genes, validation of a role in regulating telomere length awaits experimental testing.

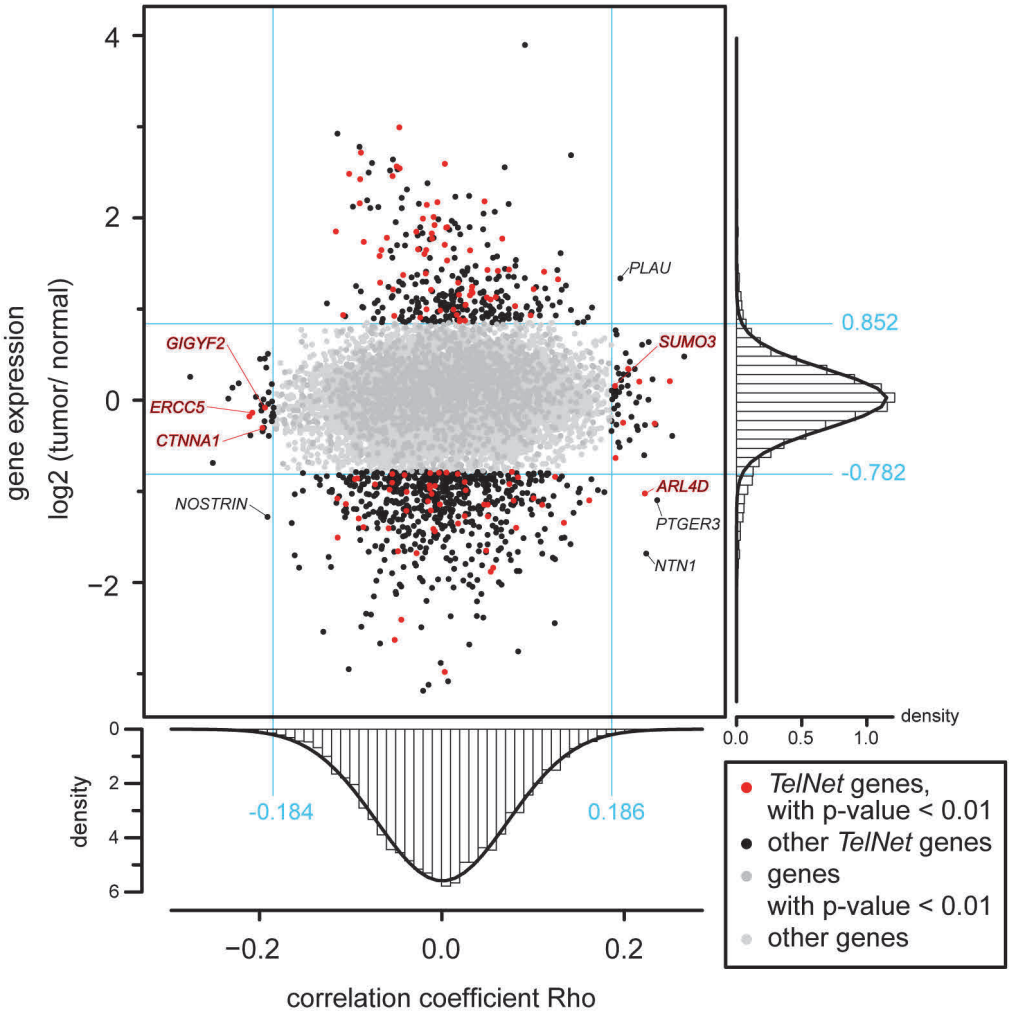

Figure 14. Correlation of gene expression data with telomere lengths.

Gene expression data from TCGA was correlated with telomere length values that were estimated by (Barthel *et al.*, 2017) using spearman correlation. The log2 fold change tumor over normal was plotted against the resulting correlation coefficients Rho. For gene expression as well as Rho values, histograms were plotted and fitted with a Gaussian fit. The 1% tails of both histograms were marked in light blue. Black dots reflect genes that are above at least one threshold, red dots are additionally included in the *TelNet* data base. Light grey dots miss both thresholds, dark grey spots are included in the *TelNet* database but miss both thresholds. Figure taken from (Braun *et al.*, 2018).

These examples show that *TelNet* is able to identify TM candidate genes for further validation in knockdown or overexpression experiments. Thus, the *TelNet* list search serves as helpful tool for the identification of TM networks. Overall, the TelNet database proves as a versatile resource that can be used for the identification of genes associated with TM from bioinformatic analysis pipelines.

2 ALT suppression and induction

Only few recurrent mutations are known to correlate with ALT and for instance in pediatric high-grade gliomas, with a high incidence of ALT, altered histone and DNA methylation have been observed (Bender *et al.*, 2013). Therefore, also epigenetic changes might induce or suppress ALT. In this part of the thesis, multiple ways of perturbing TMM were investigated by differential gene expression analysis. (i) Suppression of the ALT pathway by the HDACi SAHA, (ii) rapid ALT induction by ASF1 depletion in HeLa cells with long but not short telomeres, (iii) suppression of ALT induction by simultaneous treatment of ASF1 depleted cells with SAHA and (iv) ALT induction in survivors formed after *EST2* deletion in budding yeast.

2.1 Histone deacetylase inhibitor SAHA reduces ALT markers

SAHA (Vorinostat) is a pan inhibitor for HDACs of class I and II with an IC50 of 21 nM (HDAC1), 37 nM (HDAC3), 25 nM (HDAC6), and 1.2 µM (HDAC8) (Beckers *et al.*, 2007). Among other proteins, histones thus become hyperacetylated and the chromatin more open. Recently, it has been demonstrated that in ALT-positive U2OS cells, treatment with 2 µM SAHA significantly reduced the number of APBs (mean±SEM, -49.4±6.9%, $p<0.001$, **Figure 15A +B**) and C-circle levels (-45.3±10.3%, $p<0.001$) (Osterwald *et al.*, 2015). However, a concentration of 2 µM SAHA lies above the IC50 for cytotoxicity of 1.5 µM for HeLa cells after 72 h of treatment (Beckers *et al.*, 2007). Therefore, these results were revisited in this work using lower amounts of SAHA.

2.1.1 SAHA reduces ALT markers already at low concentration

In order to investigate which SAHA dose has minimal toxicity, yet can affect the ALT mechanism, SAHA concentration was titrated with respect to a decrease in the number of APBs as well as C-circle levels. Treatment of U2OS cells with SAHA resulted in a significant reduction in the number of APBs for 0.1 µM (-15.2±3.1%, $p<0.001$) over 0.25 µM (-40.1±3.0%, $p<0.001$) to 0.5 µM SAHA (-38.2±3.1%, $p<0.001$). Furthermore, a general trend towards reduction of C-circle levels was observed for 0.5 µM SAHA (-29.6±9.6, $p=0.08$, **Figure 15C**). Thus, a concentration of 0.5 µM SAHA was found to also significantly reduce the number of APBs and decrease C-circle levels after 24 h.

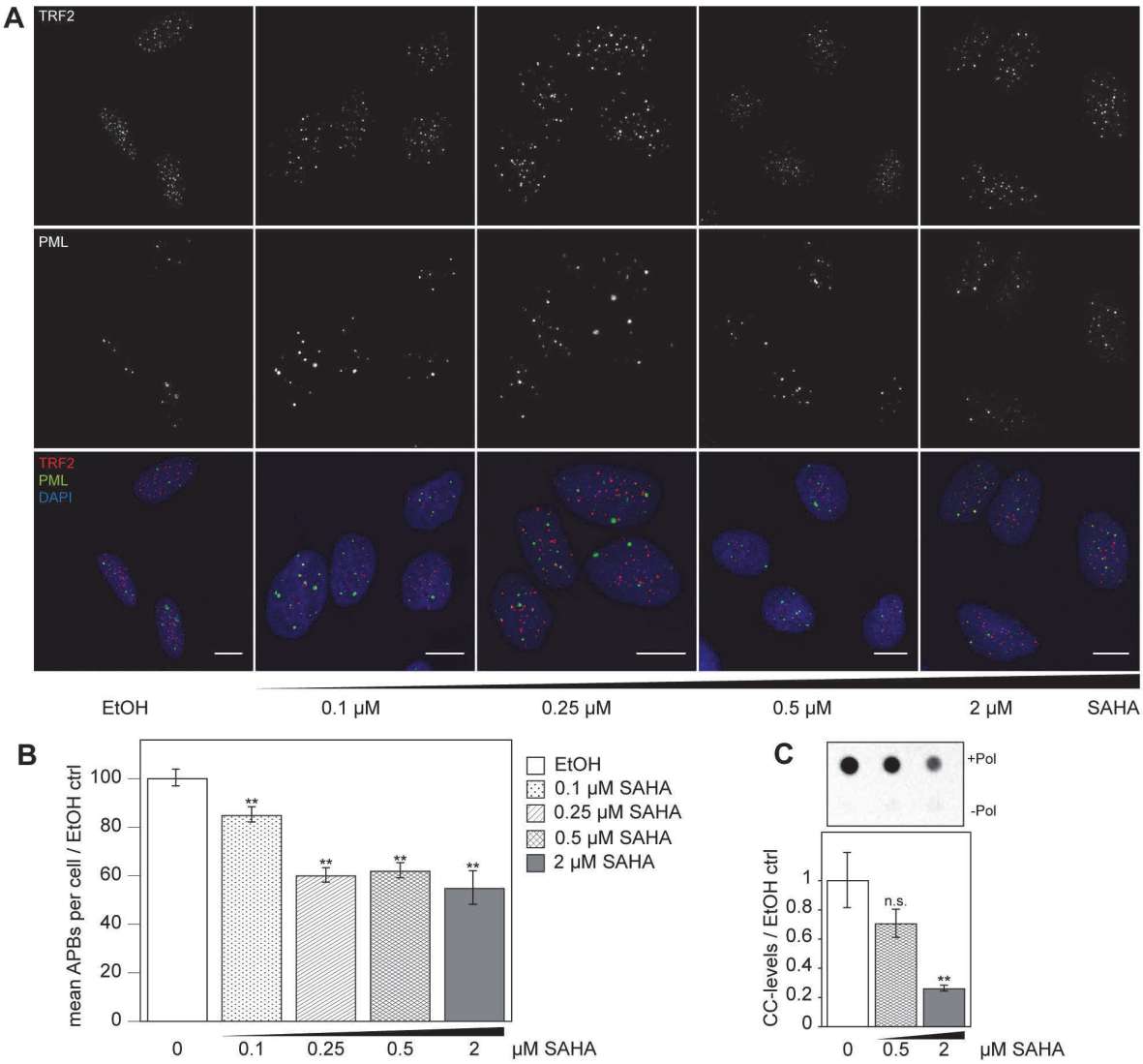

Figure 15. SAHA treated U2OS cells show decreased number of APBs and C-circle levels.

(A) Microscopy images of cells that were treated with solvent, 0.1, 0.25, 0.5 or 2 µM SAHA for 24h. Cells were stained with anti-TRF2-ms-A568, anti-PML-rb-A488 and DAPI. Scale bars are 10 µM. **(B)** Bar plot showing quantification of microscopy images of (A). PML and telomere foci were detected and colocalizations were calculated using Cell Segmentation 3D software. Resulting colocalizations were plotted as box plots. More than 2,400 cells were imaged per condition. **(C)** C-circle assay of U2OS cells treated with 0.5 or 2 µM SAHA for three days. Above the bar plots, exemplary dot blots of the C-circle assay are depicted. The upper row contains samples after amplification with polymerase addition, and the lower row shows the control without polymerase. Genomic DNA from two independent replicates was extracted for the C-circle assay that was performed in triplicates. Significance is indicated with asterisks, **p<0.001. Error bars represent the standard error of the mean (SEM). C-circle assay was performed by Caroline Bauer (Prof. Karsten Rippe, DKFZ, Heidelberg)

2.1.2 SAHA does not specifically induce apoptosis in ALT cells

In order to analyze the link of apoptosis induction by SAHA with TMM, different ALT-positive and ALT-negative cell lines were subjected to SAHA treatment followed by apoptosis staining and FACS analysis. ALT-positive U2OS and -negative HeLa cells served as well-studied reference cell lines. In addition, a panel of four pediatric glioblastoma (pedGBM) cell lines that was recently characterized in respect to their ALT status, was tested (Deeg *et al.*, 2017). FACS of annexin V and propidium iodide (PI) stained cells was used to quantify apoptotic cells treated with SAHA (**Figure 16A** and **B**).

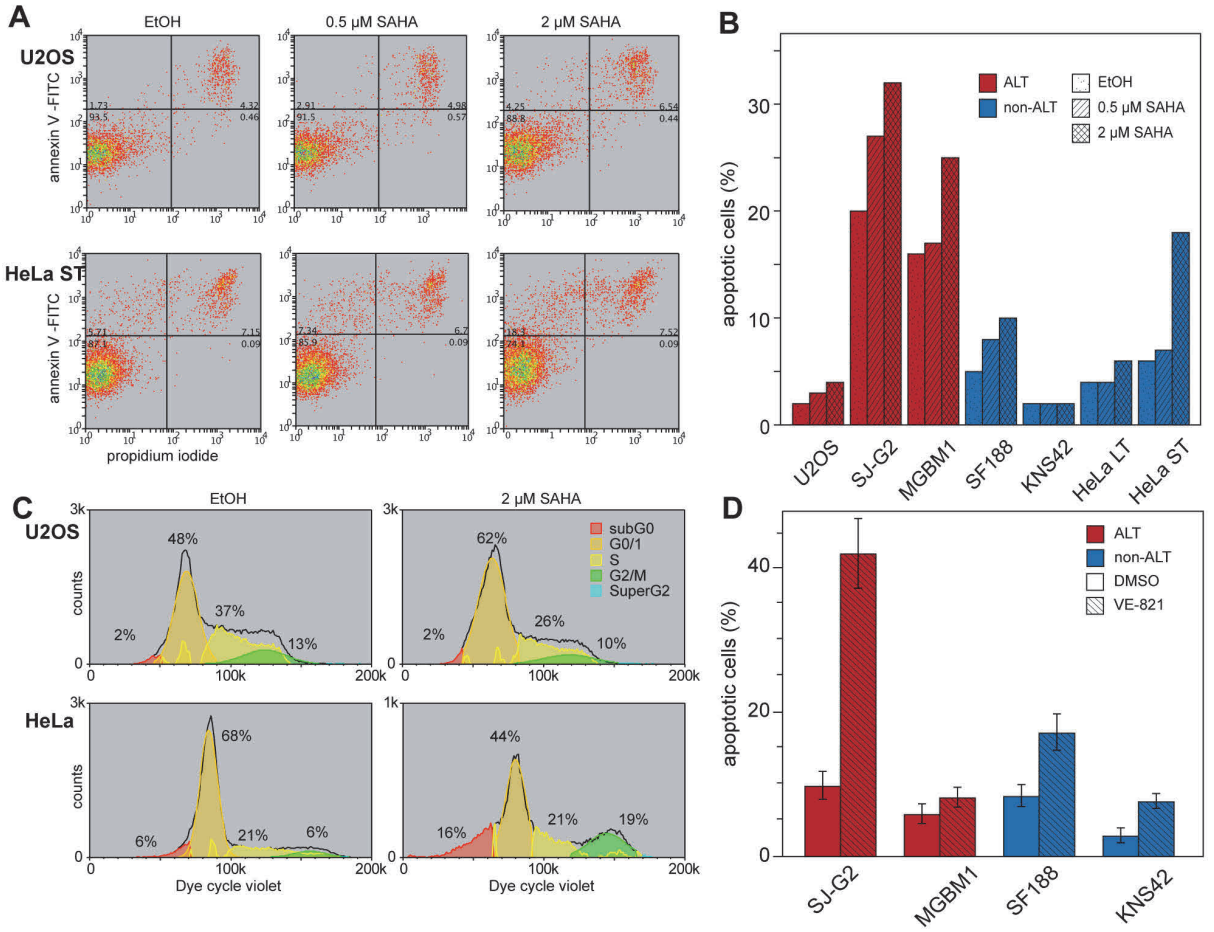

Figure 16. FACS analysis of cells treated with SAHA or ATRi VE-821.

(A) Exemplary cell death analysis of U2OS and HeLa ST cells (ST for short telomeres, average of 9 kb). Cells were treated with solvent, 0.5 or 2 µM SAHA for 24 h. Cells were stained with propidium iodide and annexin V-FITC and analyzed on a FACS Canto II. Subsequent data analysis was done with Weasel. **(B)** Quantification of apoptotic cells. Cells positive for annexin V, but negative for PI were classified as apoptotic and quantified in a bar plot. U2OS (ALT-positive reference cell line), SJ-G2 and MGBM1 (ALT-positive pedGBM cell lines), SF188 and KNS42 (telomerase-positive pedGBM cell lines), HeLa LT (LT for long telomeres, average of 20 kb) and HeLa ST (telomerase-positive reference cell line) **(C)** Cell cycle analysis of U2OS and HeLa cells treated with 2 µM SAHA or solvent. Estimation of cell cycle phase proportions was done using Weasel. **(D)** Quantification of apoptotic cells after treatment with 3 µM ATRi VE-821 or solvent. Cells positive for annexin V, but negative for PI were classified as apoptotic and quantified in a bar plot. Error bars represent the standard error of the mean from three independent experiments with two technical replicates each.

Cells were gated to exclude small artefacts and large cell aggregates (detailed description in **methods section 4**). For calculation of induced apoptosis, apoptotic cells were quantified as annexin V-positive

but PI-negative cells and translated via the formula of induced apoptosis (**methods section 4.1**). As depicted in **Figure 16B**, the range of induced apoptosis by 2 µM SAHA in ALT-positive cells reached from 2.7% in U2OS to 24.3% in SJ-G2. In the panel of ALT-negative cells, KNS42 cells did not show any response, whereas in 2.6% of HeLa LT cells (LT for long telomeres, average of 20 kb) and in 14.5% of HeLa ST cells (ST for short telomeres, average of 9 kb) apoptosis was induced. Therefore, no correlation of induced apoptosis with the active TMM was observed. HDACi have been shown to increase the acetylation of p53 and therefore lead to upregulated p21 levels resulting in apoptosis (Richon *et al.*, 2000). However, no correlation with the p53 mutational status was observed since all pedGBM cell lines have mutated *TP53* and only U2OS and HeLa cells are wild-type (Deeg, 2015). Thus, ALT-positive pedGBM cells are not specifically hypersensitive to apoptosis due to SAHA treatment.

Furthermore, cells treated with a lower SAHA concentration of 0.5 µM were analyzed with the same method. The percentage of cells with induced apoptosis was lower than the percentage detected for 2 µM SAHA. The greatest difference in sensitivity was observed in MGMB1, where only in 0.9% of cells were apoptotic. In comparison, in 14.8% of SJ-G2 cells apoptosis was induced. In ALT-negative cells the percentage of cells with induced apoptosis ranged from non-responding KNS42 cells, over 0.1% in HeLa LT and 1.9% of HeLa ST cells to 2.8% in SF188 cells. Thus, a concentration of 0.5 µM SAHA only led to a low percentage of apoptotic cells after 24 h.

To investigate cell cycle effects due to treatment with SAHA, simultaneous staining of live cells with cell membrane-permeant Vybrant Dyecycle Violet was performed (**Figure 16C**). In ALT-positive U2OS cells treated with 2 µM SAHA, an increase of 14% more cells in G0/1 and a decrease of 3% in G2 were detected, and the percentage of S-phase was reduced by 11%. However, in ALT-negative HeLa cells, SAHA treatment lead to 13.3% more cells in G2 and 23.9% fewer cells in G0/1-phase, whereas the percentage of cells in S-phase did not change. Thus, in cells treated with 2 µM for 24 h, SAHA appears to induce cell cycle arrest in a cell-type specific manner. In summary, SAHA did not selectively induce apoptosis in ALT-positive or -negative cell lines, but variations in the responses rather originated from other parameters in the different cell lines.

2.1.3 ALT-positive cells are not hypersensitive to ATR inhibitor (ATRi)

As the shelterin complex blocks telomeres from DNA damage response proteins and accidental recognition as DNA double-strand breaks, the ATR kinase, a major component of the DNA damage repair machinery, appears as a promising therapeutic target to treat ALT-positive tumors. It has been reported that treatment of ALT cells with ATRi VE-821 was able to decrease ALT hallmarks (O'Sullivan *et al.*, 2014; Flynn *et al.*, 2015). In order to evelaute these findings, the same panel of pediatric ALT-positive and -negative cell lines as described above were treated with 3 µM VE-821 for 6 days

(**Figure 16D**). Subsequently, the cells were stained with PI and annexin V to investigate induced apoptosis by FACS. No correlation of TMM and induced apoptosis was observed. In the ALT-positive SJ-G2 cell line, 40±12% of cells responded by induction of apoptosis, whereas in the other ALT-positive cell line MGBM1 only 3±1% of cells were sensitive to the treatment (**Figure 16D**). Additionally, among the ALT-negative cell lines SF188 had a stronger apoptotic response of 17±4% compared to 5±1% KNS42 cells with induced apoptosis. Thus, ALT-positive cell lines are not *per se* hypersensitive to apoptosis due to ATRi.

2.1.4 Inflammatory and immune response genes were deregulated upon SAHA

It is known that HDACi have effects on different pathways such as autophagy, cell cycle and cellular signaling pathways. However, only little work has been done to investigate the impact on TM, especially the ALT pathway. To dissect gene expression changes and find pathways and genes related to TM that are affected by SAHA treatment, RNA-sequencing (RNA-seq) data from U2OS cells treated with SAHA in different concentrations was generated and analyzed. U2OS cells were cultured with medium containing 0, 0.5 and 2 µM SAHA, with medium changed every 24 h. After three days, RNA was extracted and libraries for sequencing were prepared. Sequencing data was generated and analyzed as described in **methods sections 9 + 10**. For quality control of the two replicates per condition, sample distances for a representative subset of genes were calculated using the DESeq2 package (Love *et al.*, 2014) (**Figure 17A**). The similarity between replicates was higher between different conditions.

U2OS wt cells showed a high similarity to solvent-treated control (ctrl) cells (data not shown) and only one significantly ($p<0.05$) downregulated gene (log2 fold change (l2fc) =-1.62, $p<0.0001$), *GDF15* (growth differentiation factor 15), a cell cycle regulated gene (Grant *et al.*, 2013), was identified. As this was the only deregulated gene, solvent effects were minor. Since the amount of ethanol was the same for all samples, the ethanol treated cells were used as control cells in the further analysis. To evaluate gene expression changes upon SAHA treatment, results were called for the two concentrations over solvent control cells. Frequencies of l2fc were plotted as histograms and fitted with a centered gauss curve to set thresholds at the points of convergence (**Figure 17B**). Differentially expressed genes (n=1,269) with a l2fc<-2.5 or >2.5 for 2 µM SAHA over EtOH ctrl cells and an adjusted p-value (padj)<0.05 were identified, while gene expression did not change significantly (padj>0.05) or in the same direction (up or down) in the 0.5 µM SAHA over EtOH ctrl cells. 1,016 genes were significantly upregulated by 2 µM SAHA treatment for 3 days in U2OS cells and 253 genes were downregulated with statistical significance (padj<0.05). The gene signature of 1,269 deregulated genes was able to hierarchically cluster the samples according to the C-circle levels (**Figure 17C**).

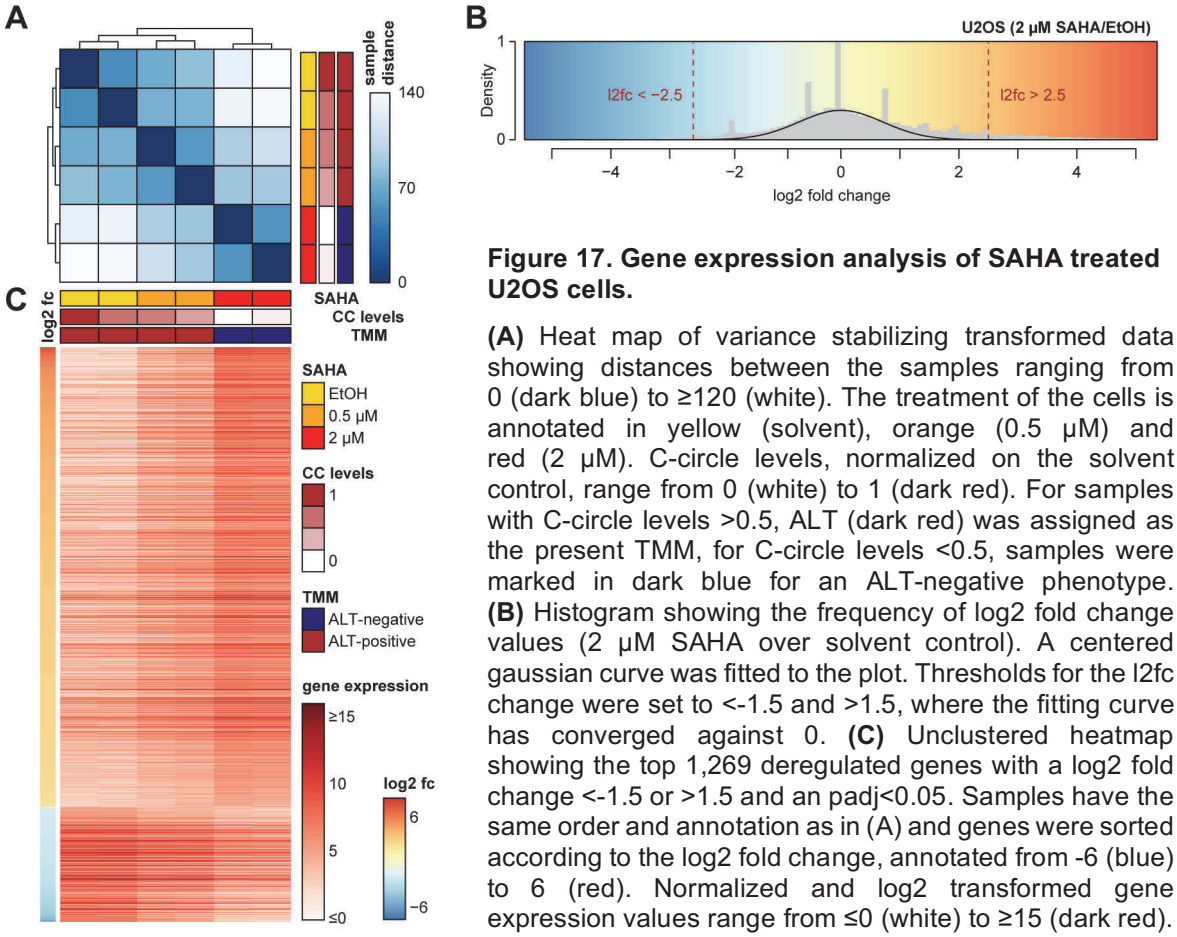

Figure 17. Gene expression analysis of SAHA treated U2OS cells.

(A) Heat map of variance stabilizing transformed data showing distances between the samples ranging from 0 (dark blue) to ≥120 (white). The treatment of the cells is annotated in yellow (solvent), orange (0.5 µM) and red (2 µM). C-circle levels, normalized on the solvent control, range from 0 (white) to 1 (dark red). For samples with C-circle levels >0.5, ALT (dark red) was assigned as the present TMM, for C-circle levels <0.5, samples were marked in dark blue for an ALT-negative phenotype. **(B)** Histogram showing the frequency of log2 fold change values (2 µM SAHA over solvent control). A centered gaussian curve was fitted to the plot. Thresholds for the l2fc change were set to <-1.5 and >1.5, where the fitting curve has converged against 0. **(C)** Unclustered heatmap showing the top 1,269 deregulated genes with a log2 fold change <-1.5 or >1.5 and an padj<0.05. Samples have the same order and annotation as in (A) and genes were sorted according to the log2 fold change, annotated from -6 (blue) to 6 (red). Normalized and log2 transformed gene expression values range from ≤0 (white) to ≥15 (dark red).

For all differentially expressed genes, RPKM (reads per kilobase of exon per million mapped reads) values were calculated to normalize raw counts for sequencing depth and gene length. Notably, many genes had a low coverage. Therefore, the gene set was further reduced by excluding all genes with an RPKM <1 in the highest expressed sample. This filtering step resulted in 318 up and 183 downregulated genes, listed in **Suppl. table S3.** Functional annotation analysis revealed a number of genes involved in the GO pathway "immune response", "signal transduction" and "cellular response to interleukin-1" (**Table 22**).

Table 22. Pathway analysis of genes upregulated in SAHA treated U2OS cells.

category	GO term	# genes
GO:0007269	neurotransmitter secretion**	6
GO:0019882	antigen processing and presentation*	5
GO:0006955	immune response*	11
GO:0006928	movement of cell or subcellular component*	5
GO:0046847	filopodium assembly	3
GO:0002504	antigen processing and presentation of peptide or polysaccharide antigen via MHC class II	3
GO:0007165	signal transduction	20
GO:0043547	positive regulation of GTPase activity	12
GO:0042361	menaquinone catabolic process	2
GO:0042377	vitamin K catabolic process	2
GO:0071805	potassium ion transmembrane transport	5
GO:0042376	phylloquinone catabolic process	2
GO:0071347	cellular response to interleukin-1	4

category	GO term	# genes
GO:0007267	cell-cell signaling	7
GO:0031295	T cell costimulation	4
GO:2001013	epithelial cell proliferation involved in renal tubule morphogenesis	2
GO:0006813	potassium ion transport	4
GO:0002503	peptide antigen assembly with MHC class II protein complex	2

From the 318 upregulated genes in U2OS upon SAHA treatment 56 genes were included in the functional annotation chart with biological processes using DAVID. Pathways that were enriched with statistical significance were marked with asterisks (*p<0.01, **p<0.001).

Since no TM pathway emerged from the analysis, TM pathway analysis was performed using the *TelNet* database. At all appearances in the text and in the tables throughout this thesis, *TelNet* genes were marked in bold. The link between the genes or encoding proteins and TM and respective genes were listed in (**Table 23**). Previous work by Grant *et al.* identified 1,813 cell-cycle-regulated genes in U2OS and 615 genes in HeLa, including some histone coding genes (Grant *et al.*, 2013). Furthermore, other histone coding genes might also be cell cycle-dependent. In order to take potential cell cycle effects into account, genes that were identified to be expressed periodically in dependence of cell cycle phase were marked with a °circle.

Table 23. *TelNet* genes, upregulated in U2OS treated with 2 µM SAHA.

TM comment	gene symbols
Genes were included in a gene set with potential relevance to telomeres and the ALT pathway and is annotated with the term “repair” or “APB’. (Lovejoy *et al.*, 2012)	***EID3, SP110***
Proteins were found in close proximity to a shelterin compound. (Lee *et al.*, 2011)	***CRYM, MT1X***
Telomeres get longer upon deletion of the budding yeast homolog. (Askree *et al.*, 2004), (Gatbonton *et al.*, 2006) or (Ungar *et al.*, 2009)	***SP140, SP110, DAW1, ARL14°***
telomerase repressor (Lafferty-Whyte *et al.*, 2010)	***TCEAL7°***

The table shows the results of *TelNet* analysis. Columns reflecting the *TelNet* TM comment, providing information that linked the gene or encoded protein to TM and gene symbols of upregulated genes. Genes reported to be cell cycle-regulated in HeLa cells (Grant *et al.*, 2013) were marked with a °circle.

In disagreement with ALT repression by SAHA, ***EID3*** was upregulated, which is part of the SMC5-SMC6 complex (Taylor *et al.*, 2008) that was shown to be involved in homologous recombination in ALT cells (Potts, 2009). A possible explanation might be an unknown functional role of **EID3**. Another reason could be the partly repression of ALT, only affecting some of the ALT characteristics. Since homologous recombination was not directly measured, further investigations are needed to complete the comprehensiveness of ALT suppression. Genes encoding the PML-NB components **SP110** and **SP140** showed a higher expression in SAHA treated cells. A result of this upregulation might be the sequestering of APB compounds away from telomeres, as it has been observed for overexpression of SP100 (Jiang *et al.*, 2005). Furthermore, ***TCEAL7°*** encoding for a known telomerase repressor (Lafferty-Whyte *et al.*, 2010) was upregulated upon SAHA treatment.

GO pathway enrichment analysis for downregulated genes was summarized in **Table 24**. Notably, genes encoding canonical histones were enriched among downregulated genes and therefore annotated GO pathways such as “nucleosome assembly”, “chromatin silencing”, but also “telomere organization/ capping”. Furthermore, also “inflammatory response” (*CCL24, TNFRSF11B, RARRES2, NMI, CCL2,*

SERPINA3, TRIL, BMPR1B, CD180) and "JAK-STAT cascade" (*NMI, CCL2, STAT5A*) were among enriched GO terms. The GO terms "positive regulation of gene expression/ transcription" included genes of the WNT-signaling pathway (*WNT11, WNT3A*) that were enriched without statistical significance. For the *TelNet* gene ***RARRES2*** (retinoic acid receptor responder 2) a tumor suppressive role by inhibiting the p38 MAP kinase pathway has been reported (Liu-Chittenden *et al.*, 2017). The transcription factor ***KLF17*** (Krüppel-like factor 17), included in *TelNet*, has been observed to be involved in potentiating TGFβ/ SMAD signaling (Ali *et al.*, 2015).

Table 24. Pathway analysis of genes downregulated in SAHA treated U2OS cells.

GO identifier	GO term	# genes
GO:0006342	chromatin silencing***	9
GO:0006334	nucleosome assembly***	12
GO:0045814	negative regulation of gene expression, epigenetic***	6
GO:0032200	telomere organization***	5
GO:0006335	DNA replication-dependent nucleosome assembly***	5
GO:0000183	chromatin silencing at rDNA **	5
GO:0051290	protein heterotetramerization**	5
GO:0030198	extracellular matrix organization**	8
GO:0045815	positive regulation of gene expression, epigenetic*	5
GO:0006954	inflammatory response*	9
GO:0045653	negative regulation of megakaryocyte differentiation*	3
GO:0031047	gene silencing by RNA*	5
GO:0044267	cellular protein metabolic process	5
GO:0016233	telomere capping	3
GO:0006935	chemotaxis	5
GO:0032972	regulation of muscle filament sliding speed	2
GO:0002227	innate immune response in mucosa	3
GO:0006366	transcription from RNA polymerase ii promoter	10
GO:0071300	cellular response to retinoic acid	4
GO:0006336	dna replication-independent nucleosome assembly	3
GO:0051301	cell division	8
GO:0001654	eye development	3
GO:0048706	embryonic skeletal system development	3
GO:0010332	response to gamma radiation	3
GO:0007259	JAK-STAT cascade	3
GO:0006352	DNA -templated transcription, initiation	3
GO:0048839	inner ear development	3
GO:0045893	positive regulation of transcription, DNA -templated	9
GO:0034080	cenp-a containing nucleosome assembly	3
GO:1904837	beta-catenin-TCF complex assembly	3
GO:0000082	G1/S transition of mitotic cell cycle	4
GO:0007062	sister chromatid cohesion	4
GO:0019731	antibacterial humoral response	3
GO:0001649	osteoblast differentiation	4
GO:0007187	G-protein coupled receptor signaling pathway, coupled to cyclic nucleotide second messenger	3
GO:0010628	positive regulation of gene expression	6
GO:0051726	regulation of cell cycle	4
GO:0060044	negative regulation of cardiac muscle cell proliferation	2
GO:0019221	cytokine-mediated signaling pathway	4

From the 183 downregulated genes in U2OS upon SAHA treatment 75 genes were included in the functional annotation chart with biological processes using DAVID. Pathways that are enriched with statistical significance were marked with asterisks (*p<0.01, **p<0.001, ***p<0.0001).

In order to identify genes that are related to TM, the *TelNet* database was used (**Table 25**). Most of the downregulated histone coding genes were also listed in the *TelNet* database because of telomere capping (Dejardin & Kingston, 2009). Both, telomerase repressors and activators have been identified as TMM-related from the downregulated genes. In summary, SAHA treatment leads to chromatin silencing and therefore, negative regulation of gene expression and in addition to deregulated immune and inflammatory response pathways. However, no clear correlation with previously reported functions regarding TMM as extracted from the *TelNet* database was found.

Table 25. *TelNet* genes, downregulated in SAHA treated U2OS cells.

TM comment	Gene symbols
Genes were included in a gene set with potential relevance to telomeres and the ALT pathway and is annotated with the term "replication" or "repair" (Lovejoy *et al.*, 2012).	***FANCD2, MCM5°, RAD51AP1***
Protein negatively affects APB formation (Osterwald *et al.*, 2012).	***FANCD2***
Proteins were found bound to telomeres (Dejardin & Kingston, 2009) or in close proximity to a shelterin compound (Giannone *et al.*, 2010; Lee *et al.*, 2011).	***H2AFY2, HIST1H4H, MCM5°, HIST1H4A, HIST1H3B°, HIST1H3D, HIST1H4I, KCTD15, CRYBB1, ANXA8L1***
Genes are members of telomerase activity signature (Barthel *et al.*, 2017).	***RAD51AP1, RARRES2, TRIM22, ALPL***
positive regulator of telomerase (Mac *et al.*, 2000), (Cerone *et al.*, 2011), or (Ramlee *et al.*, 2016)	***STAT5A, EDN2, MYCN***
negative regulator of telomerase (Racek *et al.*, 2005; Toh *et al.*, 2005; Beitzinger *et al.*, 2006)	***TP73°***
Gene was downregulated upon telomere shortening caused by the telomerase inhibitor GRN163 (Geron) in SK-N-MC cells (Uziel *et al.*, 2015).	***SERPINH1°***
The budding yeast homologue NAM7 is required for Type II survivor formation (Hu *et al.*, 2013) and telomeres get shorter upon budding yeast homologue NAM7 deletion (Askree *et al.*, 2004; Gatbonton *et al.*, 2006).	***MOV10L1***
Telomeres get longer upon budding yeast homologue deletion (Askree *et al.*, 2004; Ungar *et al.*, 2009; Hu *et al.*, 2013).	***TNNC1, FOXM1, PLCH1***
Yeast homologues are potential transcription factors of telomerase (from Yeastract) (Teixeira *et al.*, 2014).	***KLF17, FOXM1***

See legend of **Table 23**.

2.2 Knockdown of histone chaperone ASF1 induces ALT

To investigate gene expression changes upon induction of ALT, knockdown (kd) of histone chaperone ASF1 was performed. ASF1 kd in HeLa cells with long telomeres (HeLa LT) is the only system described up to date, in which ALT is rapidly induced in an ALT-negative cell line (O'Sullivan *et al.*, 2014). In other HeLa cells with shorter telomeres (HeLa ST), ALT was not induced. HeLa ST and HeLa LT originate from the same parental cell line (HeLa 1.2.11) and differ in telomere length being 9 kb and 20 kb in average, respectively (O'Sullivan *et al.*, 2014).

2.2.1 HeLa LT cells differ in several pathways and show low levels of *PDK4*

In order to answer the question, what makes telomeres longer in HeLa LT and predisposed for ALT induction, gene expression levels in both wt cell lines were compared using RNA-sequencing. Raw

reads were mapped to GRCh38/ hg38 by STAR (Dobin *et al.*, 2013) and analyzed with the DESEq2 package (Love *et al.*, 2014). For quality control, RNA-seq data was accessed by a sample distance matrix of a representative subset of genes (**Figure 20A**) showing that replicates were highly similar. Differential gene expression analysis of the two cell lines revealed 229 upregulated genes with respect to a log2 fold change (l2fc) >4 and an adjusted p-value (padj) <0.05 and 74 downregulated genes, with a l2fc <-4 and padj <0.05, listed in the appendix (**Suppl. table S4**). Gene expression level analysis of telomerase compounds TERT and TERC resulted in unchanged RPKM values for TERT and significantly higher expression of TERC (l2fc=1.33, padj=0.00045) in HeLa LT.

Next, a GO pathway enrichment analysis was performed. HeLa LT and ST cells differed in some genes that were annotated with a biological process. From the 229 higher expressed genes in HeLa LT, 158 were annotated with a biological process that was included in the functional annotation analysis (**Table 26)**. GO pathway analysis of the 55 lower genes with a biological process annotation resulted in a number of enriched GO terms. (**Table 27**). None of the deregulated pathways that were identified by GO pathway analysis was related to TM, neither was any biological process annotation of the differentially expressed genes.

Table 26. Pathway enrichment analysis of genes, higher expressed in HeLa LT versus ST.

GO identifier	GO term	# genes
GO:1901700	response to oxygen-containing compound*	36
GO:0009605	response to external stimulus*	43
GO:0072359	circulatory system development*	26
GO:0032101	regulation of response to external stimulus	21
GO:0033993	response to lipid	24
GO:0048585	negative regulation of response to stimulus	32
GO:0072358	cardiovascular system development	19
GO:0001944	vasculature development	19
GO:0051270	regulation of cellular component movement	22
GO:0001568	blood vessel development	18
GO:0042221	response to chemical	64
GO:0044767	single-organism developmental process	81
GO:0010033	response to organic substance	49
GO:2000145	regulation of cell motility	20
GO:0009887	animal organ morphogenesis	24
GO:0032502	developmental process	82
GO:0071230	cellular response to amino acid stimulus	6
GO:0030728	ovulation	4
GO:0032496	response to lipopolysaccharide	12
GO:0007275	multicellular organism development	72
GO:0048731	system development	66
GO:0048856	anatomical structure development	77
GO:0044707	single-multicellular organism process	83
GO:0009719	response to endogenous stimulus	30
GO:0009968	negative regulation of signal transduction	26
GO:0061383	trabecula morphogenesis	5
GO:0040012	regulation of locomotion	20
GO:0002237	response to molecule of bacterial origin	12
GO:0043062	extracellular structure organization	12
GO:0061098	positive regulation of protein tyrosine kinase activity	5
GO:0070887	cellular response to chemical stimulus	46

GO identifier	GO term	# genes
GO:0030198	extracellular matrix organization	12
GO:0060384	innervation	4
GO:0048514	blood vessel morphogenesis	15
GO:0010648	negative regulation of cell communication	27
GO:0009653	anatomical structure morphogenesis	42
GO:0048661	positive regulation of smooth muscle cell proliferation	6
GO:0032501	multicellular organismal process	92
GO:0023057	negative regulation of signaling	27
GO:0060343	trabecula formation	4
GO:0010575	positive regulation of vascular endothelial growth factor production	4
GO:0031663	lipopolysaccharide-mediated signaling pathway	5

From the 229 higher expressed genes in HeLa LT over HeLa ST 158 genes were included in the functional annotation chart with biological processes using DAVID. *stands for significantly enriched pathway ($p<0.01$).

Table 27. Pathway enrichment analysis of genes, lower expressed in HeLa LT versus ST.

GO identifier	GO term	# genes
GO:0052696	flavonoid glucuronidation***	7
GO:0052697	xenobiotic glucuronidation***	7
GO:0009812	flavonoid metabolic process***	7
GO:0052695	cellular glucuronidation***	7
GO:0006063	uronic acid metabolic process***	7
GO:0019585	glucuronate metabolic process***	7
GO:0006805	xenobiotic metabolic process***	7
GO:0071466	cellular response to xenobiotic stimulus**	7
GO:0009410	response to xenobiotic stimulus**	7
GO:0005996	monosaccharide metabolic process**	9
GO:0051552	flavone metabolic process**	3
GO:0042573	retinoic acid metabolic process*	4
GO:0044723	single-organism carbohydrate metabolic process*	10
GO:0032787	monocarboxylic acid metabolic process*	11
GO:0019752	carboxylic acid metabolic process*	14
GO:0006720	isoprenoid metabolic process*	6
GO:0043436	oxoacid metabolic process*	14
GO:0006789	bilirubin conjugation*	2
GO:0006082	organic acid metabolic process*	14
GO:0005975	carbohydrate metabolic process	10
GO:0001523	retinoid metabolic process	5
GO:0016101	diterpenoid metabolic process	5
GO:0006721	terpenoid metabolic process	5
GO:0002175	protein localization to paranode region of axon	2
GO:0042440	pigment metabolic process	4

From the 74 lower expressed in HeLa LT over HeLa ST 55 genes were included in the functional annotation chart with biological processes using DAVID. GO terms that were significantly enriched were marked with asterisks (*$p<0.01$, **$p<0.001$, ***$p<0.0001$).

In order to further explore whether the identified genes were involved in TM, the *TelNet* database was used. Notably, for 9 higher expressed and 2 lower expressed genes, a connection to TM was retrieved from *TelNet* (**Table 28** + **Table 29**). For ***ETV1*** a role as a *TERT* activator has been reported and the mouse homologue of human ***ZNF32*** has been shown to increase *mTERT* expression (Goueli & Janknecht, 2004; Gao *et al.*, 2014). Furthermore, **UCHL1** was found at telomeres of ALT cells (Dejardin & Kingston, 2009) and in close proximity to the shelterin complex (Lee *et al.*, 2011), as well as **RYR2** (Giannone *et al.*, 2010), **JSPRP1** and **HNMT** (Lee *et al.*, 2011).

Table 28. *TelNet* genes that are higher expressed in HeLa LT versus ST.

TM comment	Gene symbols
Protein was bound to telomeres of ALT cells (Dejardin & Kingston, 2009).	***UCHL1***
Proteins were found in close proximity to a shelterin compound (Giannone *et al.*, 2010) or (Lee *et al.*, 2011).	***RYR2, JSRP1, UCHL1, HNMT***
Genes are members of telomerase activity signature. (Barthel *et al.*, 2017)	***RARRES2, COCH***
Overexpression of mouse homologue increased mTERT expression (Gao *et al.*, 2014).	***ZNF32***
telomerase activator (Goueli & Janknecht, 2004)	***ETV1***
Telomeres get longer upon deletion of budding yeast homologue (Ungar *et al.*, 2009).	***TNNC1***

The table shows the results of *TelNet* list search with the first column reflecting the TM comment, providing the experimental information that linked the gene or encoded protein to TM. In the second column gene symbols were listed.

It will be interesting to clarify the role of **UCHL1**, since it is upregulated in HeLa LT and localized at telomeres of ALT-positive cells both cell lines harboring long telomeres. The budding yeast homologue deletion phenotypes indicate a role in telomere length regulation for **TNNC1** and **PDK4**. For ***CMD1***, the budding yeast homologue of ***TNNC1***, the deletion has been reported to result in longer telomeres (Ungar *et al.*, 2009), however, ***TNNC1*** was higher expressed in HeLa cells with long telomeres. On the other hand, deletion of ***PKP1***, the budding yeast homologue of ***PDK4***, has been shown to shorten telomeres (Askree *et al.*, 2004), and ***PDK4*** expression was strongly reduced in the HeLa cells with long telomeres. This might indicate an ongoing process of telomere shortening in HeLa LT cells, despite long telomeres. Also, telomerase activity, measured by the TRAP assay, has been shown to be slightly higher in HeLa ST cells (O'Sullivan *et al.*, 2014). It will be interesting to monitor telomere length in HeLa LT over a longer period to determine if telomeres get shorter.

Table 29. *TelNet* genes that are lower expressed in HeLa LT versus ST.

TM comment	gene symbols
Telomeres get shorter upon deletion of the budding yeast homologue PKP1 (Askree *et al.*, 2004).	***PDK4***
Genes is a member of telomerase activity signature (Barthel *et al.*, 2017).	***ST6GAL1***

The table shows the results of *TelNet* list search with the first column reflecting the TM comment, providing the experimental information that linked the gene or encoded protein to TM. In the second column gene symbols were listed.

A possible explanation for the long telomeres in HeLa LT might be that a telomere elongation process has happened in the past that was then re-balanced. In this scenario, the current state of TM might only compensate for telomere attrition at short telomeres, without a gain of additional telomere length. For a complete picture, differences in HeLa LT and ST have to be further investigated to identify e.g. genomic rearrangements or copy number variations. This is important to decide if HeLa LT and ST are essentially isogenic and only differ in telomere length. In summary, HeLa LT cells showed a similar telomerase expression as HeLa ST but had a strongly reduced in *PDK4* expression.

2.2.2 ASF1 depletion induces ALT in HeLa LT but not HeLa ST cells

For the siRNA mediated kd, the same materials were used as described in the original paper (O'Sullivan *et al.*, 2014). HeLa cells with long (LT) and short telomeres (ST) were treated with siRNA against ASF1A and ASF1B or a scrambled control siRNA (siCtrl). The kd efficiency of the siRNA pool targeting both ASF1A and ASF1B was confirmed by Western blot (**Figure 18A**).

Quantification of protein levels in HeLa LT revealed a reduction to 24% for ASF1A ($p<0.0001$) and 11% for ASF1B ($p<0.0001$) (**Figure 18B**) as demonstrated previously (Deeg, 2015). In order to address the kd efficiency on the transcript level, gene expression values in RPKM for ASF1A and ASF1B were calculated from RNA-sequencing data. RPKM values were reduced to 12±1% ($P<0.0001$) for ASF1A and 23±0.8% ($P<0.0001$) for ASF1B in HeLa LT upon the respective knockdown (**Figure 18C**).

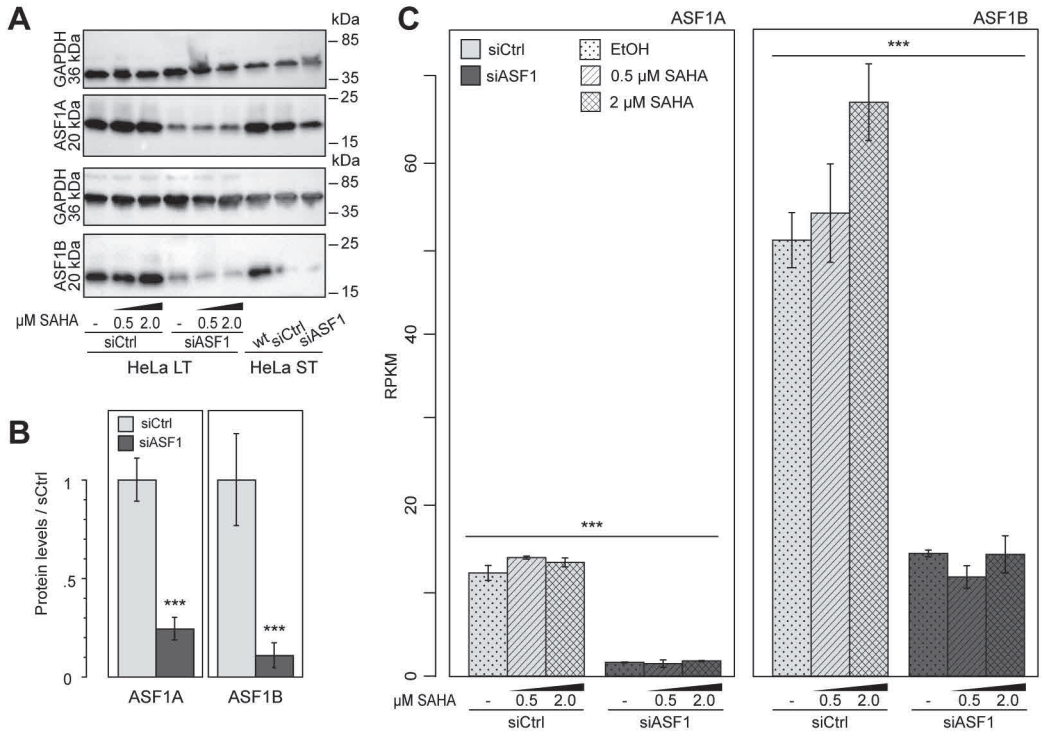

Figure 18. Reduction of ASF1 protein and transcript levels upon siRNA kd.

(A) Western blots showing ASF1A, ASF1B and GAPDH bands. HeLa cells with long and short telomeres (LT and ST) were transfected with or siRNA targeted against ASF1A and ASF1B or scrambled control (siCtrl) and treated with 0, 0.5 µM or 2 µM SAHA. **(B)** Bar plot showing protein levels of ASF1 A and B, quantified from Western blots (WB) after siASF1 kd (dark grey) or siCtrl (light grey). Error bars represent the SEM. Experiment was performed in two independent replicates. **(C)** RPKM values from RNA-seq analysis. Raw counts were normalized to sequencing depth and on gene lengths. SAHA treatment was performed in concentrations of 0 (dotted), 0.5 µM (diagonal) or 2 µM SAHA (crossed). Significance is indicated with asterisks, ***$p<0.0001$. Experimental parts of the WB were conducted by Caroline Bauer (Prof. Karsten Rippe, DKFZ, Heidelberg).

Next, to determine the effect of the kd on the induction of ALT, extrachromosomal telomeric repeats were measured by C-circle assay. C-circle levels were normalized to U2OS wt cells, which serve as a

ALT-positive reference cell line (**Figure 19**). The C-circle signal of HeLa LT transfected with siRNA targeted against ASF1 was increased 6-fold over the scrambled control (+84±3%, p=0.003).

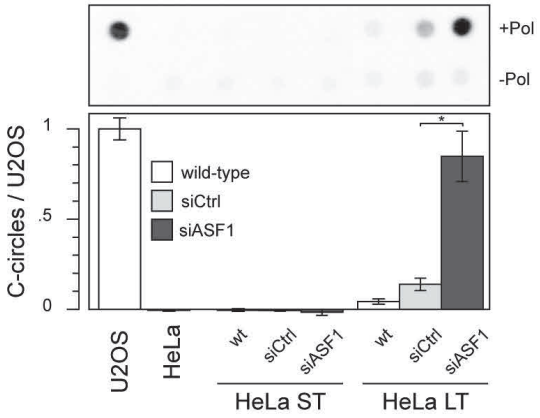

Figure 19. Circle levels after ASF1 kd.

Dot blot and quantification of the C-circle assay of HeLa LT and ST wt (white) cells and cells transfected with siRNA against ASF1 A and B (dark grey) or scrambled control (light grey). Above the bar plots, exemplary dot blots of the C-circle assay are depicted. The upper row contains samples after amplification with polymerase addition, and the lower row shows the control without polymerase. U2OS and HeLa wt cells were used positive and negative reference cell lines. The experiments were performed in two independent replicates, the C-circle assay in technical triplicates. Significance is indicated with an asterisk, *p<0.01. Experimental parts of the C-circle assays were conducted by Caroline Bauer (Prof. Karsten Rippe, DKFZ, Heidelberg)

With C-circle levels of 85±14%, ASF1 depleted cells (HeLa LT) were in the range of U2OS wt cells (100±15%) confirming previous results (O'Sullivan *et al.*, 2014; Deeg, 2015). As reported before, no ALT induction was observed in HeLa ST cells. Thus, induction of ALT by ASF1 kd in HeLa with long, but not short, telomeres was verified.

2.2.3 HeLa LT and ST cells respond differentially to ASF1 depletion

To investigate gene expression changes upon ASF1 depletion, RNA-seq libraries were prepared for HeLa LT and ST cells that were transfected with siRNA against ASF1. Sequencing data was processed as described above (**results sections 2.1.4 + 2.2.1**) and in **methods sections 9 + 10**. A sample distance matrix was calculated for all replicates and samples within HeLa LT and ST clustered well together (**Figure 20A**). Within the HeLa LT samples, the solvent-treated and the 0.5 µM SAHA treated cells were more similar than the 2 µM SAHA treated cells. The distributions of log2 fold changes were plotted as histograms and fitted with a centered Gaussian function (**Figure 20B**). Thresholds for significance ($p<0.05$) and l2fc were set for HeLa LT (l2fc <-1.6 or >1.6) and for HeLa ST (l2fc <-1.2 or >1.2). Deregulated genes in HeLa LT and ST were partly overlapping, visualized with VENN diagrams (**Figure 20B**). ASF1A and B and the H4 histone family, member M HIST1H4I were the only genes that were significantly downregulated in both cell lines. A subset of 139 genes was upregulated in both cell lines. The GO terms “multicellular organismal process” and “regulation of hormone levels”, were the only significantly enriched pathways from the overlapping genes. As siRNA kd might have an effect on cell cycle progression, and especially ASF1 kd leads to a G2/M arrest (O'Sullivan *et al.*, 2014), deregulated genes were checked for cell cycle-regulated genes. Therefore, a list of 615 of cell cycle-dependent genes identified in HeLa cells has been used (Grant *et al.*, 2013) to identify cell-cycle

regulated genes, which were marked with a °circle at all appearances in the text or in tables. HeLa LT and ST samples transfected with siRNA against ASF1 or scrambled control were submitted to hierarchical clustering by the gene signature from exclusively differentially expressed genes in HeLa LT siASF1 over siCtrl (n=522, l2fc <-1.6 or >1.6, padj <0.05) and not in HeLa ST siASF1 over siCtrl (**Figure 20C**).

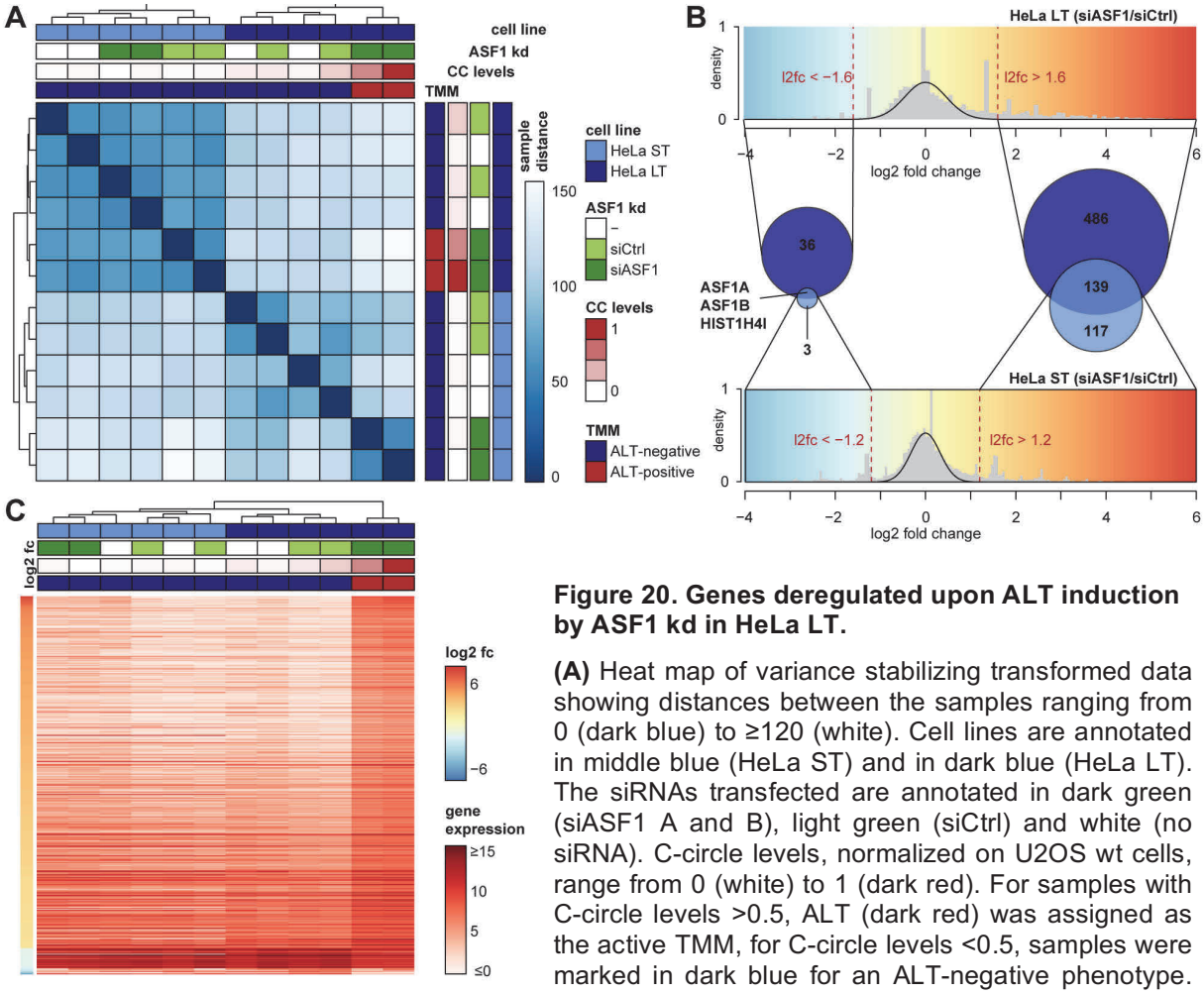

Figure 20. Genes deregulated upon ALT induction by ASF1 kd in HeLa LT.

(A) Heat map of variance stabilizing transformed data showing distances between the samples ranging from 0 (dark blue) to ≥120 (white). Cell lines are annotated in middle blue (HeLa ST) and in dark blue (HeLa LT). The siRNAs transfected are annotated in dark green (siASF1 A and B), light green (siCtrl) and white (no siRNA). C-circle levels, normalized on U2OS wt cells, range from 0 (white) to 1 (dark red). For samples with C-circle levels >0.5, ALT (dark red) was assigned as the active TMM, for C-circle levels <0.5, samples were marked in dark blue for an ALT-negative phenotype. **(B)** Histograms showing the frequency of log2 fold change values (siASF1 over siCtrl) in HeLa LT (upper histogram) and HeLa ST (lower histogram). Centered gaussian curve was fitted to the plots. Thresholds for the log2 fold change were set to <-1.6 and >1.6 (HeLa LT) and l2fc <1.2 and >1.2 (HeLa ST), where the fitting curve has converged against 0. VENN-diagrams in the middle showing overlaps of downregulated genes (left) and upregulated genes (right) according to the log2 fold change thresholds and with an adjusted p-value <0.05. **(C)** Unclustered heatmap showing the top 522 genes that are significantly deregulated in HeLa LT siASF1 over siCtrl with log2 fold change <-1.5 or >1.5 and no significant expression change in HeLa ST. Samples have the same annotation as in (A) and genes were sorted according to the log2 fold change, annotated from -6 (blue) to 6 (red). Normalized and log2 transformed gene expression values range from ≤ 0 (white) to ≥ 15 (dark red).

Interestingly, HeLa LT cells without siRNA or siCtrl clustered together with the HeLa ST samples, thus all ALT-negative samples clustered together. RPKM values were calculated for the differentially expressed genes as described above and all genes with an RPKM <1 in the highest expressed sample were excluded from the analysis. This filtering step resulted in 1 down- and 71 upregulated genes for

HeLa ST and 36 down- as well as 284 upregulated genes for HeLa LT, listed **Suppl. table S5** and **Suppl. table S6**. Thus, gene expression changed in dependence of the HeLa cell line that harbor different telomere length.

2.2.4 HeLa ST cells respond with immune response and virus defense to ASF1 kd

Pathway enrichment analysis for upregulated genes in ASF1 depleted HeLa ST revealed significant enrichment of the pathways "response to virus" (*DDX58, IFIT3, IFIT2, IFIT1, OASL, IFI44, OAS2, CCL5, DHX58*), "defense response to virus" (*IFIT3, IFIT2, IFIT1, IL6, OASL, ISG15, OAS2, DHX58*), "type I interferon signaling pathway" (*IFIT3, IFIT2, IFIT1, OASL, ISG15, OAS2*), "immune response" (*IL6, CCR4, SUSD2, TNFSF15, OAS2, CCL5, IL7R*) and "MAPK cascade" (*EPGN, PPM1L, CCL5, SCG2*) (**Table 30**).

Table 30. Pathway analysis of genes, upregulated in ASF1 depleted HeLa ST cells.

GO identifier	GO term	# genes
GO:0009615	response to virus***	9
GO:0051607	defense response to virus***	8
GO:0060337	type I interferon signaling pathway***	6
GO:0045071	negative regulation of viral genome replication***	5
GO:0006955	immune response*	7
GO:0007159	leukocyte cell-cell adhesion*	3
GO:0035987	endodermal cell differentiation*	3
GO:0030198	extracellular matrix organization*	5
GO:0032480	negative regulation of type I interferon production*	3
GO:0045429	positive regulation of nitric oxide biosynthetic process*	3
GO:0016049	cell growth	3
GO:0050679	positive regulation of epithelial cell proliferation	3
GO:0006508	proteolysis	6
GO:0035457	cellular response to interferon-alpha	2
GO:0048245	eosinophil chemotaxis	2
GO:0008544	epidermis development	3
GO:0006954	inflammatory response	5
GO:0031581	hemidesmosome assembly	2
GO:0001525	angiogenesis	4
GO:0048872	homeostasis of number of cells	2
GO:0007229	integrin-mediated signaling pathway	3
GO:0000165	MAPK cascade	4
GO:0010628	positive regulation of gene expression	4
GO:0050900	leukocyte migration	3
GO:0007155	cell adhesion	5
GO:0046427	positive regulation of JAK-STAT cascade	2
GO:0048870	cell motility	2
GO:0045070	positive regulation of viral genome replication	2
GO:0043542	endothelial cell migration	2

From the 74 upregulated genes in ASF1 depleted HeLa ST cells 37 genes were included in the functional annotation chart with biological processes using DAVID. Pathways that are significantly enriched were marked with asterisks (*p<0.01, **p<0.001, ***p<0.0001).

Also, inflammatory response genes were upregulated as well as genes involved in the positive regulation of JAK-STAT signaling. From the upregulated genes, only ***ISG15*** and ***SNCG*** were included in the *TelNet* database. ISG15 (Ubiquitin-like protein ISG15) was found at ALT telomere repeats (Dejardin &

Kingston, 2009) and SNCG (gamma-synuclein) in close proximity to TRF1 (Lee *et al.*, 2011). Furthermore, expression of ***ISG15*** has been reported to be regulated by telomere length (Lou *et al.*, 2009; Robin *et al.*, 2014; Hirashima & Seimiya, 2015). The only downregulated gene was *TNFAIP6*, coding for TNFα-induced protein 6, a suppressor of inflammatory response. The deregulated genes in HeLa ST are neither enriched in *TelNet* nor in cell cycle-regulated genes. Thus, HeLa ST cells show an upregulation of immune response and virus defense pathways upon ASF1 kd.

2.2.5 ALT induction correlates with expression of TGFβ and WNT signaling genes

Next, differentially expressed genes upon ASF1 depletion and concomitant ALT induction in HeLa LT cells were submitted to the pathway enrichment analysis (**Table 31**). From the 284 upregulated genes, 160 were annotated with a biological process. Pathway enrichment was obtained for extracellular matrix organization, positive regulation of cell migration, inflammatory response, immune response, and cell differentiation pathways. Genes encoding proteins that are involved in these signaling pathways were upregulated upon ASF1 depletion and are explained in more detail in the following.

Table 31. Pathway analysis of genes, upregulated in ASF1 depleted HeLa LT cells.

GO identifier	GO term	# genes
GO:0006954	inflammatory response***	17
GO:0030198	extracellular matrix organization***	12
GO:0030335	positive regulation of cell migration***	10
GO:0010596	negative regulation of endothelial cell migration**	4
GO:0007267	cell-cell signaling**	10
GO:0045766	positive regulation of angiogenesis**	7
GO:0001649	osteoblast differentiation**	6
GO:0030574	collagen catabolic process*	5
GO:0071526	semaphorin-plexin signaling pathway*	4
GO:0001525	angiogenesis*	8
GO:0010951	negative regulation of endopeptidase activity*	6
GO:0050900	leukocyte migration*	6
GO:0070374	positive regulation of ERK1 and ERK2 cascade*	7
GO:0006955	immune response*	11
GO:0030194	positive regulation of blood coagulation*	3
GO:0048011	neurotrophin TRK receptor signaling pathway*	3
GO:0007155	cell adhesion	11
GO:0030336	negative regulation of cell migration	5
GO:0038178	complement component C5a signaling pathway	2
GO:0045669	positive regulation of osteoblast differentiation	4
GO:0071356	cellular response to tumor necrosis factor	5
GO:0002040	sprouting angiogenesis	3
GO:0007219	notch signaling pathway	5
GO:0007200	phospholipase C-activating G-protein coupled receptor signaling pathway	4
GO:0001958	endochondral ossification	3
GO:0048843	negative regulation of axon extension involved in axon guidance	3
GO:0001938	positive regulation of endothelial cell proliferation	4
GO:2000726	negative regulation of cardiac muscle cell differentiation	2
GO:1903588	negative regulation of blood vessel endothelial cell proliferation involved in sprouting angiogenesis	2
GO:0045746	negative regulation of Notch signaling pathway	3
GO:0030449	regulation of complement activation	3

GO identifier	GO term	# genes
GO:0060325	face morphogenesis	3
GO:0071773	cellular response to BMP stimulus	3
GO:0008285	negative regulation of cell proliferation	9
GO:0070830	bicellular tight junction assembly	3
GO:0043524	negative regulation of neuron apoptotic process	5
GO:0007204	positive regulation of cytosolic calcium ion concentration	5
GO:0010718	positive regulation of epithelial to mesenchymal transition	3
GO:0050919	negative chemotaxis	3
GO:0001837	epithelial to mesenchymal transition	3
GO:0030282	bone mineralization	3
GO:0000122	negative regulation of transcription from RNA polymerase II promoter	13
GO:0007611	learning or memory	3
GO:0051897	positive regulation of protein kinase B signaling	4
GO:0007166	cell surface receptor signaling pathway	7
GO:0010757	negative regulation of plasminogen activation	2
GO:0030823	regulation of cGMP metabolic process	2
GO:0007162	negative regulation of cell adhesion	3
GO:0001822	kidney development	4
GO:0007565	female pregnancy	4
GO:0045668	negative regulation of osteoblast differentiation	3
GO:0030199	collagen fibril organization	3
GO:0006824	cobalt ion transport	2
GO:0030182	neuron differentiation	4
GO:0007169	transmembrane receptor protein tyrosine kinase signaling pathway	4
GO:0051549	positive regulation of keratinocyte migration	2
GO:0003209	cardiac atrium morphogenesis	2
GO:0090090	negative regulation of canonical WNT signaling pathway	5
GO:0042493	response to drug	7
GO:0045165	cell fate commitment	3
GO:0045600	positive regulation of fat cell differentiation	3
GO:0060972	left/ right pattern formation	2
GO:0010954	positive regulation of protein processing	2
GO:0015889	cobalamin transport	2
GO:0008284	positive regulation of cell proliferation	9
GO:0010862	positive regulation of pathway-restricted SMAD protein phosphorylation	3
GO:0016477	cell migration	5
GO:0000187	activation of MAPK activity	4
GO:0002544	chronic inflammatory response	2
GO:0010469	regulation of receptor activity	2
GO:0061314	notch signaling involved in heart development	2
GO:0060586	multicellular organismal iron ion homeostasis	2
GO:0007165	signal transduction	17
GO:0043547	positive regulation of GTPase activity	10
GO:0051918	negative regulation of fibrinolysis	2
GO:0060548	negative regulation of cell death	3
GO:2000178	negative regulation of neural precursor cell proliferation	2
GO:0048711	positive regulation of astrocyte differentiation	2
GO:0010759	positive regulation of macrophage chemotaxis	2

From the 284 upregulated genes in ASF1 depleted HeLa LT cells 101 genes were included in the functional annotation chart with biological processes using DAVID. Pathways that are significantly enriched were marked with asterisks (*p<0.01, **p<0.001, ***p<0.0001).

For S100A9 a repressive role in regulation of NFκB expression has been demonstrated (Wu *et al.*, 2017). IRF7 has been shown to have a role in transcriptional regulation of genes involved in the IFNβ pathway (Honda *et al.*, 2005). *NGFR,* highly expressed in a fraction of human gliomas, has been shown to have a role in p53 inactivation, thus preventing cells from activating apoptosis (Zhou *et al.*, 2016). WNT11, a member of the WNT signaling pathway, has been reported to be highly expressed in squamous cell

carcinoma and has therefore been suggested as prognostic marker for cervical carcinoma (Wei *et al.*, 2014). *THBS1* (aka *TSP1*) expression has been reported to be inducible by TNFα, mediated by p38 MAP kinase signaling (Fairaq *et al.*, 2015). Furthermore, a role for THBS1 in the positive regulation of TGFβ signaling has been shown (Rojas *et al.*, 2008). The IL10 cytokine IL24 has been demonstrated to induce apoptosis in a variety of cancers for example gliomas (Su *et al.*, 2003). *BMP2* and *BMP6* belong to a subfamily of TGFβ signaling factors. BMP2 has been demonstrated to form a heterodimer with BMP6, which can activate of SMADs and the MAP kinase signaling pathways (Valera *et al.*, 2010). Furthermore, a tumor suppressor role has been proposed for *BMP2* based on its capability to induce *p21* expression, thus inducing cell cycle arrest (Mitsui *et al.*, 2015). In addition, ***KLF17*** has been reported to be involved in TGFβ/ SMAD signaling (Ali *et al.*, 2015).

Table 32. *TelNet* genes, upregulated in ASF1 depleted HeLa LT cells.

TM comment	gene symbols
The proteins were found in close proximity or bound to telomeres or a shelterin compound (Dejardin & Kingston, 2009) or a shelterin compound (Lee *et al.*, 2011) or (Cerone *et al.*, 2011).	***HIST1H2AA, HIST1H2BA, TUBB2A°, GFPT2, TUBB3, NTRK1, HIST3H3***
Telomeres get longer upon budding yeast homologue deletion (Askree *et al.*, 2004; Ungar *et al.*, 2009).	***TNNC1, FOXJ1***
telomerase repressor (Kumar *et al.*, 2013; Yoo *et al.*, 2015)	***CEBPA, SNAI1***
Yeast homologues are potentially transcription factors of telomerase (from Yeastract) (Teixeira *et al.*, 2014).	***KLF17, FOXJ1***
Telomeres get shorter upon budding yeast homologue deletion (Askree *et al.*, 2004; Ungar *et al.*, 2009).	***TUBB2A°, TUBB3, PCSK9***

The table shows the results of *TelNet* list search with the first column reflecting the TM comment, providing the experimental information that linked the gene or encoded protein to TM. In the second column gene symbols were listed. Genes reported to be cell cycle-regulated in HeLa cells (Grant *et al.*, 2013) were marked with a °circle.

However, no TM related pathway was found to be enriched among the upregulated genes. Therefore, the *TelNet* list search was consulted to select for genes that have previously been connected to telomeres. From 182 upregulated genes, 13 were implemented in the *TelNet* database (**Table 32**). Most of them were histone coding genes coding for proteins that have been found near the telosome (Dejardin & Kingston, 2009; Cerone *et al.*, 2011; Lee *et al.*, 2011). Furthermore, ***CEBPA*** (CCAAT/ enhancer binding protein alpha) and ***SNAI1*** (snail family transcriptional repressor 1) have been reported to exhibit telomerase repressive features (Kumar *et al.*, 2013; Yoo *et al.*, 2015). ***SWI5***, a budding yeast homologue of ***KLF17*** (Krüppel-like factor 17) has been listed as a telomerase inhibitor in the Yeastract database.

All downregulated genes with a biological process annotation were genes encoding canonical histones. GO pathway enrichment analysis resulted in “nucleosome assembly” and “chromatin silencing” terms (**Table 33**).

Table 33. Pathway analysis of genes, downregulated in ASF1 depleted HeLa LT cells.

GO identifier	GO term	# genes
GO:0006334	nucleosome assembly***	14
GO:0000183	chromatin silencing at rDNA***	8
GO:0045814	negative regulation of gene expression, epigenetic***	8

GO identifier	GO term	# genes
GO:0032200	telomere organization***	7
GO:0045815	positive regulation of gene expression, epigenetic***	8
GO:0006335	DNA replication-dependent nucleosome assembly***	7
GO:0051290	protein heterotetramerization***	7
GO:0006342	chromatin silencing***	7
GO:0031047	gene silencing by RNA***	8
GO:0044267	cellular protein metabolic process***	8
GO:0060968	regulation of gene silencing***	4
GO:0034080	CENP-A containing nucleosome assembly***	4
GO:0007596	blood coagulation**	5
GO:0045653	negative regulation of megakaryocyte differentiation**	3
GO:0016233	telomere capping**	3
GO:0006336	DNA replication-independent nucleosome assembly**	3
GO:0006352	DNA-templated transcription, initiation*	3
GO:1904837	beta-catenin-TCF complex assembly*	3
GO:0006303	double-strand break repair via nonhomologous end joining*	3
GO:0098609	cell-cell adhesion*	4

From the 36 downregulated genes in ASF1 depleted HeLa LT cells 22 genes were included in the functional annotation chart with biological processes using DAVID. Pathways that are significantly enriched were marked with asterisks (*p<0.01, **p<0.001, ***p<0.0001).

TelNet genes were significantly enriched among downregulated genes (11 out of 35, p<0.0001) (**Table 34**). For example, histone H3 and H4 coding genes, were included in the *TelNet* database, because histones have been identified in direct proximity or bound to telomere repeats (Dejardin & Kingston, 2009; Lee *et al.*, 2011).

Table 34. *TelNet* genes, downregulated in ASF1 depleted HeLa LT cells.

TM comment	Gene symbols
Yeast homologue *KAE1* is required for Type II survivor formation (Hu *et al.*, 2013) and a suppressor of *CDC13* (Downey *et al.*, 2006).	***OSGEPL1***
The proteins were found in close proximity or bound to telomeres or a shelterin compound (Dejardin & Kingston, 2009) or a shelterin compound (Lee *et al.*, 2011).	***HIST1H4B°, HIST4H4, HSIT1H2AL, HIST1H3D, HIST1H3F, HIST1H3G, HIST1H3H, HIST1H4K***
Telomeres get longer upon budding yeast homologue *GLO4* deletion (Gatbonton *et al.*, 2006).	***HAGHL***
The gene is a member of telomerase activity signature (Barthel *et al.*, 2017).	***RARRES2***

The table shows the results of *TelNet* list search. For details please see table legend of **Table 32**.

To summarize, genes upregulated upon ASF1 kd in HeLa LT cells were mainly involved in TGFβ and WNT signaling pathways, whereas mostly canonical histone coding genes were downregulated.

2.3 HDAC inhibitor SAHA suppresses ALT induction

2.3.1 SAHA reduces ALT induction capacity of ASF1 depletion in HeLa LT cells

In order to investigate the effect of SAHA on the ALT induction capacity of siRNA-mediated kd of ASF1, HeLa LT cells were simultaneously treated with siRNA against ASF1 and with the HDACi SAHA in different concentrations. As a proof-of-concept, C-circle levels were measured as a representative ALT hallmark (**Figure 21**).

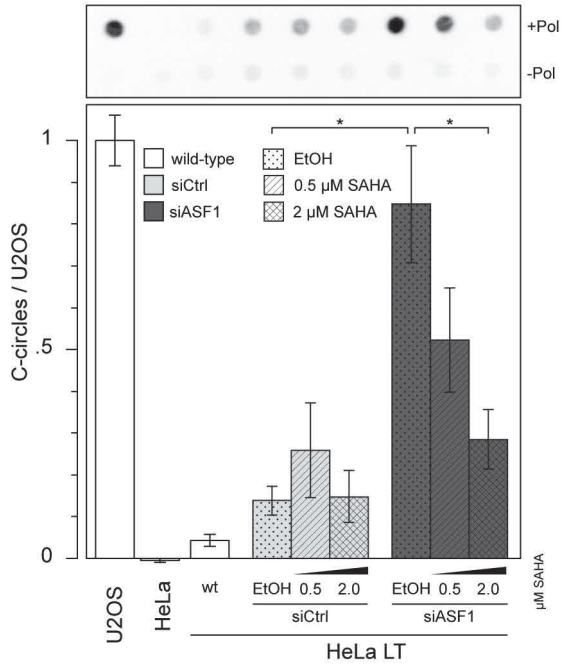

Figure 21. Circle levels of SAHA treated ASF1 kd cells.

Dot blot and quantification of the C-circle assay of HeLa LT wild-type (white) cells and cells transfected with siRNA against ASF1 A and B (dark grey) or scrambled control (light grey) and treated with solvent (dotted), 0.5 µM (diagonal) or 2 µM SAHA (crossed). Above the bar plots, exemplary dot blots of the C-circle assay are depicted. The upper row contains samples after amplification with polymerase addition, and the lower row shows the control without polymerase. U2OS and HeLa wild-type cells were used positive and negative reference cell lines. The experiments were performed in two independent replicates, the C-circle assay in technical triplicates. Significance is indicated with an asterisk, *p<0.01. Experimental parts of the C-circle assays were conducted by Caroline Bauer (Prof. Karsten Rippe, DKFZ, Heidelberg)

SAHA was added to the growth medium 4 h after transfection of siRNA to result in a final concentration of 0, 0.5 or 2 µM. In contrast, to EtOH ctrl cells, 2 µM SAHA treated cells showed a decrease of -66± 13% (p=0.008) of C-circle levels (**Figure 21**). Therefore, cells transfected with siASF1 and treated with 2 µM SAHA were in the range of HeLa LT cells transfected with siCtrl. Furthermore, also administration of only 0.5 µM SAHA reduced C-circle levels, although not significantly. In summary, treatment of SAHA reduced the ALT induction capacity of ASF1 depletion in HeLa LT cells.

2.3.2 Inhibitors of WNT signaling are up- and virus response genes are downregulated upon SAHA-mediated suppression of ALT induction

To better understand the mechanism behind changes in gene expression levels of ASF1 depleted HeLa LT cells treated with SAHA in different concentrations, RNA-seq was performed. Sequencing data was processed as described above (**results sections 2.1.4 + 2.2.1**) and in **methods sections 9 and 10**. To first assess the quality of replicates, raw counts were vst transformed and sample distances were calculated for a representative set of genes (**Figure 22A**). Replicates clustered closely together and the distance between 2 µM SAHA and the 0.5 µM samples was higher than the distance to the ethanol control samples.

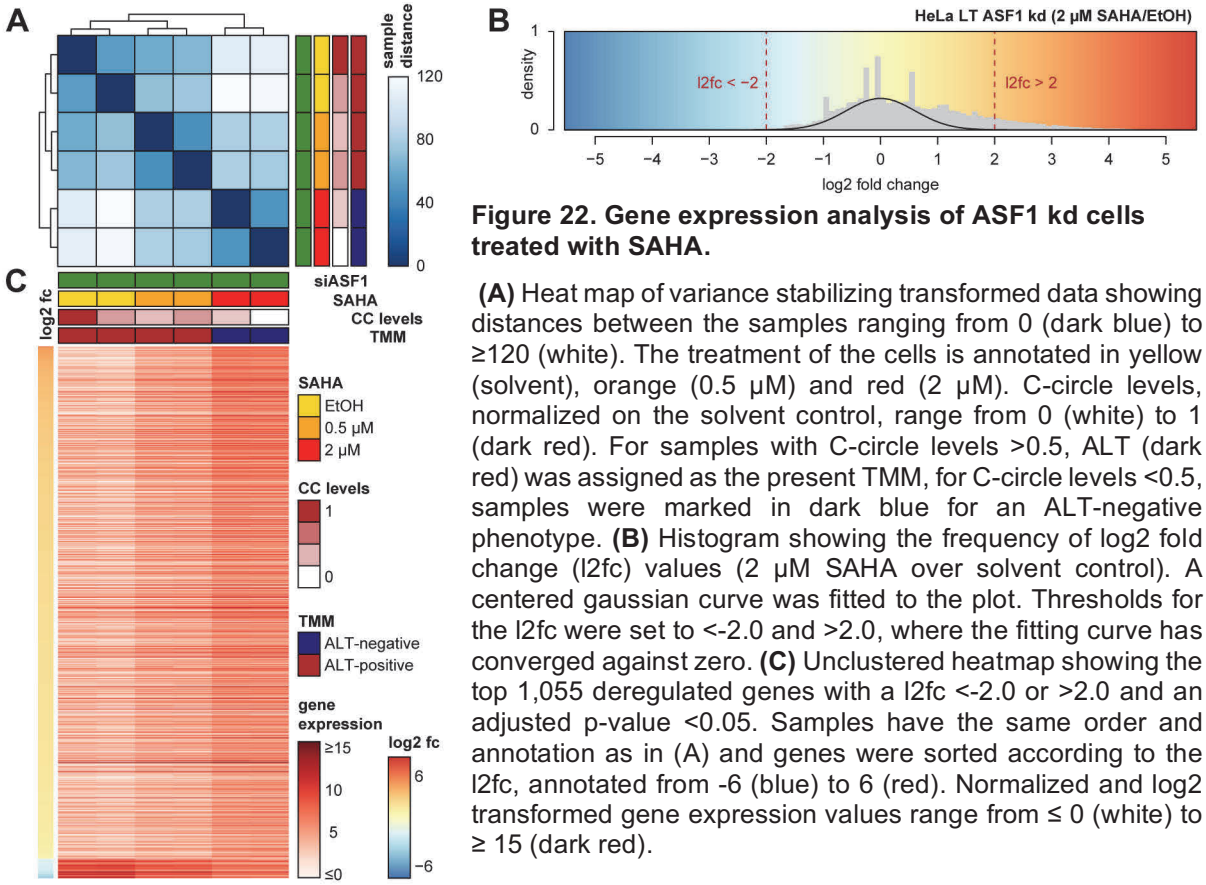

Figure 22. Gene expression analysis of ASF1 kd cells treated with SAHA.

(A) Heat map of variance stabilizing transformed data showing distances between the samples ranging from 0 (dark blue) to ≥120 (white). The treatment of the cells is annotated in yellow (solvent), orange (0.5 µM) and red (2 µM). C-circle levels, normalized on the solvent control, range from 0 (white) to 1 (dark red). For samples with C-circle levels >0.5, ALT (dark red) was assigned as the present TMM, for C-circle levels <0.5, samples were marked in dark blue for an ALT-negative phenotype. **(B)** Histogram showing the frequency of log2 fold change (l2fc) values (2 µM SAHA over solvent control). A centered gaussian curve was fitted to the plot. Thresholds for the l2fc were set to <-2.0 and >2.0, where the fitting curve has converged against zero. **(C)** Unclustered heatmap showing the top 1,055 deregulated genes with a l2fc <-2.0 or >2.0 and an adjusted p-value <0.05. Samples have the same order and annotation as in (A) and genes were sorted according to the l2fc, annotated from -6 (blue) to 6 (red). Normalized and log2 transformed gene expression values range from ≤ 0 (white) to ≥ 15 (dark red).

For the further analysis, raw counts were normalized and rlog transformed. Log2 fold changes of 2 µM SAHA over ethanol control were calculated and plotted as histogram (**Figure 22B**). After fitting the curve with a centered Gaussian function, the cut-offs for the log2 fold change were set to l2fc <-2.0 or >2.0, where the Gaussian function converged against zero. The filtering resulted in a list of 1,015 up- and 40 downregulated genes with an adjusted p-value <0.05 that was used for hierarchical clustering of the SAHA treated cells. The gene signature was suited to distinguish samples according to the delivered SAHA concentration. To remove low abundant genes, genes with an RPKM <1 in the sample with the highest expression were excluded for the functional pathways analysis. With that, the final list contained 501 up- and 35 downregulated genes (**Suppl. table S7**). From the 501 upregulated genes, only 137 were

annotated with biological processes. Functional pathway enrichment analysis of this subset resulted in enrichment of several pathways enriched with statistical significance (**Table 35**).

Table 35. GO analysis of upregulated genes, in ASF1 depleted HeLa LT, treated with SAHA.

GO identifier	GO term	# genes
GO:0035584	calcium-mediated signaling using intracellular calcium source**	5
GO:0007155	cell adhesion*	19
GO:0030178	negative regulation of WNT signaling pathway*	6
GO:0007399	nervous system development*	14
GO:0032331	negative regulation of chondrocyte differentiation*	4
GO:0086091	regulation of heart rate by cardiac conduction*	5
GO:0035556	intracellular signal transduction*	16
GO:0061337	cardiac conduction	5
GO:0043547	positive regulation of GTPase activity	20
GO:0001578	microtubule bundle formation	4
GO:0031175	neuron projection development	7
GO:0001778	plasma membrane repair	3
GO:0007157	heterophilic cell-cell adhesion via plasma membrane cell adhesion molecules	5
GO:0046785	microtubule polymerization	3
GO:0019882	antigen processing and presentation	5
GO:0007165	signal transduction	33
GO:0006887	exocytosis	6
GO:0007612	learning	5
GO:0007565	female pregnancy	6
GO:0007160	cell-matrix adhesion	6
GO:0009967	positive regulation of signal transduction	5
GO:0007411	axon guidance	8
GO:2000310	regulation of N-methyl-D-aspartate selective glutamate receptor activity	3
GO:0034332	adherens junction organization	4
GO:0030574	collagen catabolic process	5
GO:0007220	notch receptor processing	3
GO:0045956	positive regulation of calcium ion-dependent exocytosis	3
GO:0086002	cardiac muscle cell action potential involved in contraction	3
GO:0045668	negative regulation of osteoblast differentiation	4
GO:0019221	cytokine-mediated signaling pathway	7
GO:0046426	negative regulation of JAK-STAT cascade	4
GO:0009749	response to glucose	5
GO:0000226	microtubule cytoskeleton organization	5
GO:0001501	skeletal system development	7
GO:0034220	ion transmembrane transport	9
GO:0030155	regulation of cell adhesion	4
GO:1904659	glucose transmembrane transport	3
GO:0007267	cell-cell signaling	10
GO:0086047	membrane depolarization during Purkinje myocyte cell action potential	2
GO:0031652	positive regulation of heat generation	2
GO:0007507	heart development	8
GO:0035249	synaptic transmission, glutamatergic	3
GO:0090103	cochlea morphogenesis	3
GO:0007254	JNK cascade	4
GO:0007269	neurotransmitter secretion	4
GO:0016080	synaptic vesicle targeting	2
GO:0043276	anoikis	2
GO:0032386	regulation of intracellular transport	2
GO:0006655	phosphatidylglycerol biosynthetic process	2
GO:0051938	L-glutamate import	2
GO:0045671	negative regulation of osteoclast differentiation	3
GO:0035235	ionotropic glutamate receptor signaling pathway	3
GO:0030198	extracellular matrix organization	8

GO identifier	GO term	# genes
GO:0071805	potassium ion transmembrane transport	6
GO:0006656	phosphatidylcholine biosynthetic process	3
GO:0051491	positive regulation of filopodium assembly	3
GO:0032148	activation of protein kinase B activity	3
GO:0017157	regulation of exocytosis	3
GO:0006836	neurotransmitter transport	3
GO:0010976	positive regulation of neuron projection development	5
GO:0032496	response to lipopolysaccharide	7
GO:0021696	cerebellar cortex morphogenesis	2
GO:0086045	membrane depolarization during AV node cell action potential	2
GO:0086011	membrane repolarization during action potential	2
GO:0031032	actomyosin structure organization	3
GO:0035987	endodermal cell differentiation	3
GO:0007264	small GTPase mediated signal transduction	9
GO:0060079	excitatory postsynaptic potential	3
GO:0086010	membrane depolarization during action potential	3
GO:0043406	positive regulation of MAP kinase activity	4

From the 501 upregulated genes in ASF1 depleted HeLa LT cells upon SAHA treatment 192 genes were included in the functional annotation chart with biological processes using DAVID. Pathways that are significantly enriched were marked with asterisks (*p<0.01, **p<0.001).

"Negative regulators of WNT signaling" (*DKK3, LRP1, NXN, DACT3,* ***HMGA2****, CITED1*) were upregulated. From genes involved in signal transduction, *PTK7* has been shown to inhibit WNT signaling (Peradziryi *et al.*, 2011). Furthermore, "negative regulators of JAK-STAT cascade" (*RTN4RL1, RTN4RL2, DCN,* ***HMGA2***), "cytokine-mediated signaling pathway" (*STAT4, RTN4RL1, RTN4RL2, DCN, EDA, IL17RD, IL1A), and* "positive regulators of MAP kinase activity" (*DIRAS1, TENM1, PDE5A, CD40*) were upregulated.

Several of the upregulated genes were implemented in the *TelNet* database, thus are involved in TM (**Table 36**). For ***GLI2***, ***HMGA***, ***PRKAR2B***, ***TNIK***, ***MAST1****,* and the budding yeast homologue of ***CREB5*** a role in telomerase activation has been reported (Reimand *et al.*, 2010; Cerone *et al.*, 2011; Li *et al.*, 2011; Mazumdar *et al.*, 2013).

Table 36. *TelNet* genes, upregulated in ASF1 depleted HeLa LT, treated with SAHA.

TM comment	gene symbols
telomerase activator (Mazumdar *et al.*, 2013) or (Li *et al.*, 2011)	***GLI2, HMGA2***
potential telomerase activator (Cerone *et al.*, 2011)	***PRKAR2B, TNIK, MAST1***
Yeast homologue is a telomerase activator (Reimand *et al.*, 2010).	***CREB5***
Telomeres get shorter upon budding yeast homologue deletion (Askree *et al.*, 2004), (Ungar *et al.*, 2009) or (Gatbonton *et al.*, 2006).	***DAW1, ELOVL7, PRKD1***
Telomeres get longer upon budding yeast homologue deletion (Askree *et al.*, 2004) or (Hu *et al.*, 2013).	***ARHGAP26, CREB5, PLCL1, CABP1***
Yeast homologue is a telomerase repressor (Reimand *et al.*, 2010).	***GATA5***
Gene was downregulated upon telomere shortening caused by the telomerase inhibitor GRN163 (Geron) in SK-N-MC cells (Uziel *et al.*, 2015).	***IGF2BG2***
Proteins have been found in close proximity or bound to telomeres or a shelterin compound (Dejardin & Kingston, 2009) or a shelterin compound (Giannone *et al.*, 2010).	***AZGP1, MYH10***
Gene was included in a gene set with potential relevance to telomeres and the ALT pathway and is annotated with the term "TUDOR" (Lovejoy *et al.*, 2012).	***TDRKH***

The table shows the results of *TelNet* list search. For details please see table legend of **Table 32**.

Downregulated genes were significantly enriched in the GO terms "response to virus" (*IFIT3, IFIT2, OASL, DDX60, IFI44*), "type I interferon signaling pathway" (*IFIT3, IFIT2, OASL, ISG15*), and "defense response to virus" (*IFIT3, IFIT2, OASL, **ISG15**, DDX60*) (**Table 37**). Furthermore, in "cellular response to INFα" (*IFIT3, IFIT2*) and "positive regulators of apoptotic process" (*IFIT2, NUPR1, GPER1*) were enriched without statistical significance.

Table 37. GO analysis of downregulated genes, in ASF1 depleted HeLa LT, treated with SAHA.

GO identifier	GO term	# genes
GO:0009615	response to virus***	5
GO:0060337	type I interferon signaling pathway**	4
GO:0051607	defense response to virus**	5
GO:0045071	negative regulation of viral genome replication*	3
GO:0035457	cellular response to interferon-alpha	2
GO:0015718	monocarboxylic acid transport	2
GO:0048147	negative regulation of fibroblast proliferation	2
GO:0051603	proteolysis involved in cellular protein catabolic process	2
GO:0016049	cell growth	2
GO:0043065	positive regulation of apoptotic process	3

From the 35 downregulated genes in ASF1 depleted HeLa LT cells upon SAHA treatment 14 genes were included in the functional annotation chart with biological processes using DAVID. Pathways that are significantly enriched were marked with asterisks (*p<0.01, **p<0.001, ***p<0.0001).

The downregulated genes ***ISG15*** and ***KCTD15*** were included in the *TelNet* database, because of the localization of the encoded protein was found at ALT telomere repeats (Dejardin & Kingston, 2009) or in close proximity to a shelterin compound (Giannone *et al.*, 2010) (**Table 38**).

Table 38. *TelNet* genes, downregulated in ASF1 depleted HeLa LT, treated with SAHA.

TM comment	Gene symbols
Found in close proximity or bound to telomeres or a shelterin compound (Dejardin & Kingston, 2009) or a shelterin compound (Giannone *et al.*, 2010).	***KCTD15***, ***ISG15***

The table shows the results of *TelNet* list search. For details please see table legend of **Table 32**.

Thus, SAHA treatment of HeLa LT cells, in which ALT was induced by ASF1 kd resulted in downregulation genes involved in response to virus pathways as well as upregulation of WNT signaling inhibitors and telomerase activators.

2.4 Yeast survivor formation marginally changes gene expression

Deletion of the budding yeast homologue of telomerase *EST2* leads to survivor type II formation after 5-6 days in the absence of mutations (Makovets *et al.*, 2008). These survivors show ALT features like telomere lengthening in the absence of telomerase and RAD50-dependent recombination resulting in heterogeneous telomere length Lendvay (Lendvay *et al.*, 1996; Makovets *et al.*, 2008). To analyze changes in RNA expression that accompany ALT induction in budding yeast, the telomerase gene *EST2* was deleted to generate type II survivors (Balk *et al.*, 2013) and RNA was isolated at representative time points for RNA-sequencing (**Figure 23A**).

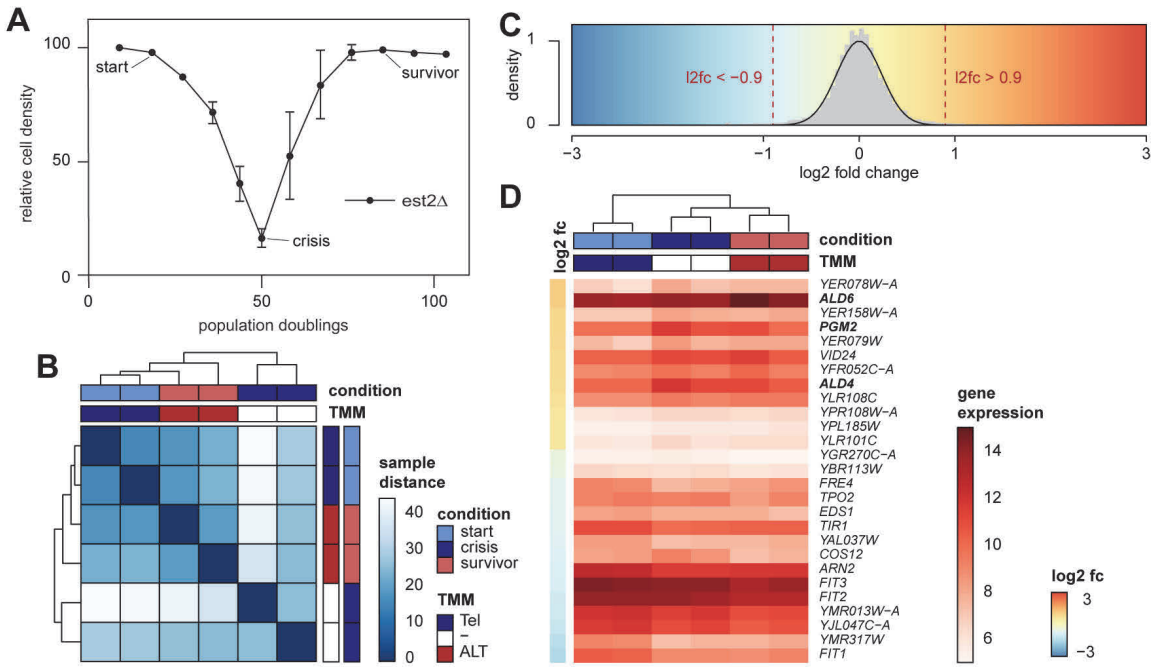

Figure 23. Differential gene expression analysis of budding yeast type II survivors.

(A) Relative cell density showing the growth of *est2*Δ cells. Yeast survivor formation and RNA extraction on days 2, 6 and 10 were performed by Bettina Balk, AG Luke, IBM Mainz. Image adapted from (Balk *et al.*, 2013). **(B)** Sample distance heat map of start (blue), crisis (dark blue) and survivor (red) samples. The TMM is annotated in dark blue (telomerase-positive), white (no TMM) and red (survivor type II, ALT) **(C)** Histogram of log2 fold change with a centered Gaussian fit and dashed lines showing the l2fc cut-offs >0.9 or <-0.9. **(D)** Hierarchical clustering of start, crisis and survivor samples by differentially expressed genes.

RNA-seq libraries were prepared in duplicates for every time point (start, crisis and survivor) and then sequenced as 50 bp single-end reads. Raw reads were mapped to the budding yeast genome using STAR (Dobin *et al.*, 2013) and resulting counts were analyzed with DESeq2 (Love *et al.*, 2014). To check the quality of replicates, a representative set of genes was vst transformed to generated a sample distance matrix (**Figure 23B**). Hierarchical clustering showed that gene expression in the crisis state differs strongly from start and survivor cells, whereas start and survivor samples appeared very similar. After rlog transformation, log2 fold changes (l2fc) of survivor over start samples were plotted as histogram and a centered Gaussian curve was fitted to the data. The significance cutoff was set to a l2fc<-0.9 or >0.9, where the centered Gaussian fit converged against zero and p<0.05 (**Figure 23 C**). As expected

upon deletion of the protein subunit of telomerase in budding yeast (*EST2*), cells went through crisis and formed survivors. Differential expression analysis revealed heavy expression changes during crisis, however less than 30 genes showed a relatively small, albeit statistically significant change in gene expression as compared to pre-senescent cells (**Figure 23D**). Only 4 of the 12 upregulated and 9 out of 15 downregulated genes were annotated with a biological process. ***ALD4***, ***ALD6*** and ***PGM2*** were identified to be involved in metabolic processes, such as acetate biosynthesis and the glucose 1-phosphate metabolic process. Furthermore, the gene set was enriched with 6 downregulated genes involved in ion transport namely, *FIT1, TPO2, ARN2, FRE4, FIT2*, and *FIT3* ($p<0.01$). Genes within the iron-regulon were overrepresented among downregulated genes, including *FIT1/ 2/ 3* (facilitator of iron transport 1/ 2/ 3), *ARN2* (AFT1 regulon protein 2), and *FRE4* (ferric reductase 4) indicating a stress response.

TelNet analysis was performed to identify genes involved in TM. Among the herewith-determined factors, ***ALD4*** (aldehyde dehydrogenase 4), ***ALD6*** (aldehyde dehydrogenase 6),, and ***PGM2*** (phosphoglucomutase) were identified as homologues of human genes that have been reported to be downregulated upon telomere shortening (Uziel *et al.*, 2015). The human phenotype therefore agrees with the result, because telomere lengths in survivors are likely to be elongated due to recombination events. ***COS12*** is located in the subtelomeric region of chromosome 7 (Jezek *et al.*, 2017).

Table 39. *TelNet* genes, upregulated in type II survivors.

TM comment	Gene symbols
Human homologues were downregulated after telomerase inhibition by GRN163 in SK-N-MC cells (Uziel *et al.*, 2015).	***ALD4***, ***ALD6***
Human homologues were found to be in close proximity of the shelterin compound TIN2 (Lee *et al.*, 2011).	***PGM2***
telomere proximal gene	***COS12***

The table shows the results of *TelNet* list search with the first column reflecting the TM comment, providing the experimental information that linked the gene or encoded protein to TM. In the second column gene symbols were listed.

In summary, budding yeast type II survivors formed after *EST2* deletion show only minor changes in gene expression as compared to pre-senescent cells. The results show that post-senescence survivors are very similar to pre-senescent cells with regard to their expression profiles. Since no genomic changes have been reported in the past, the protein pool that is needed for alternative lengthening of telomeres is already expressed in pre-senescent cells. The underlying mechanism of ALT induction therefore might lie elsewhere, probably in a de-localization of specific proteins or a change in posttranslational modifications.

3 ALT induction by recruiting PML to telomeres

The role of PML in the ALT pathway is only partly understood and further validation of its function is needed. To investigate the functional role of PML in the ALT pathway, we asked, whether a fusion of PMLIII to the shelterin compound TRF1 is able to induce artificial APBs in previous ALT-negative cells. To this end, the recruiting construct TRF1-PML and single control proteins were cloned into a pEGFP backbone (**Figure 24**).

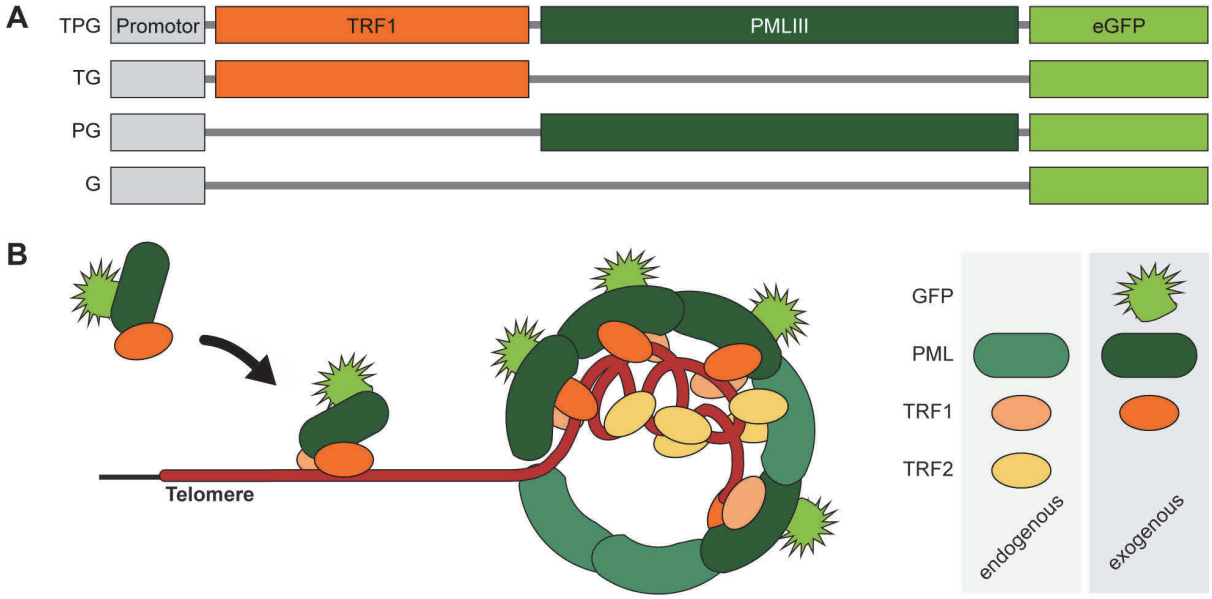

Figure 24. Recruiting PML to telomeres.

(A) Cloned constructs GFP, PML-GFP, TRF1-GFP and TRF1-PML-GFP. **(B)** Strategy: fusion protein TRF1-PML-GFP binds to telomere repeats and subsequent protein assembly forms a PML-NB around telomere (red). GFP (light green), PML (dark green), ectopic (orange) and endogenous (faint orange) TRF1 and endogenous TRF2 (yellow) are depicted.

GFP (green fluorescent protein) was used as a fluorescent tag to visualize the recruited protein. To account for any effects upon PML or TRF1 overexpression, TRF1-GFP and PML-GFP were used as controls. A GFP-only construct served as transfection control. Furthermore, the GFP protein can be used to recruit other proteins, fused to a GFP-binder protein. This will be useful for future studies of the effects upon recruitment of ALT candidate genes to telomeres (Rothbauer *et al.*, 2006; Zolghadr *et al.*, 2008; Chung *et al.*, 2011).

3.1 PML-TRF1 fusion protein leads to artificial APBs at the majority of telomeres

To validate the localization of cloned constructs within the nucleus, ALT-positive U2OS and ALT-negative HeLa cells were transiently transfected with the plasmids containing GFP (G), PML-GFP (PG), TRF1-GFP (TG) and PML-TRF1-GFP (TPG). Immunostaining of TRF2 and PML was used to visualize telomeres and colocalizations with PML-NBs.

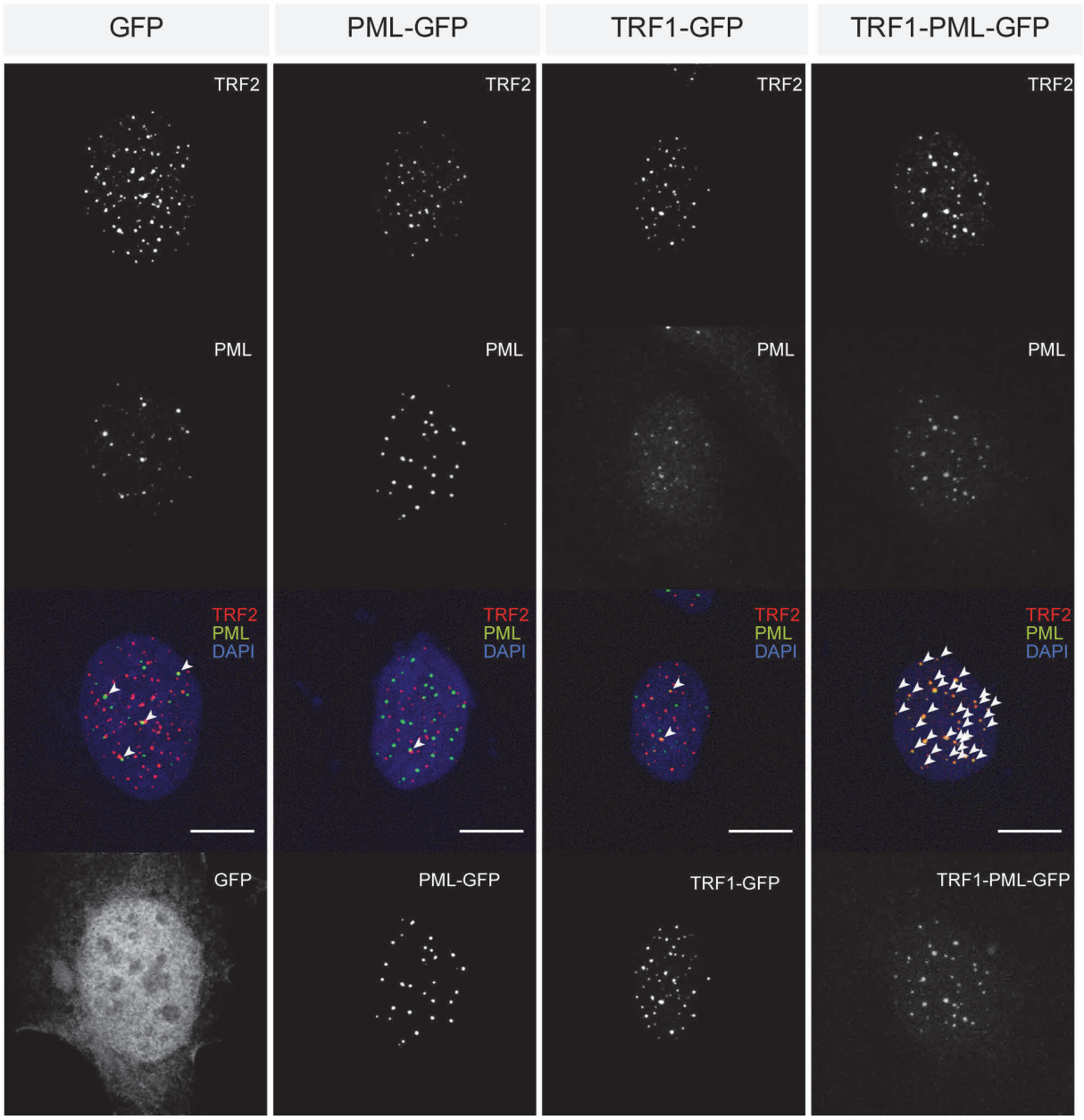

Figure 25. Recruitment of PML to majority of telomeres in ALT-positive U2OS cells.

Microcopy images of transiently transfected U2OS cells. U2OS cells were transfected with GFP (G), PML-GFP (PG), TRF1-GFP (TG) and TRF1-PML-GFP (TPG) encoding plasmids. After 24 h, cells were fixed and stained with αTRF2-rb-A568 and αPML-ms-ATTO633. Colocalizations of TRF2 (representative for telomeres) and PML are marked with white arrows. Scale bars are 10 µm.

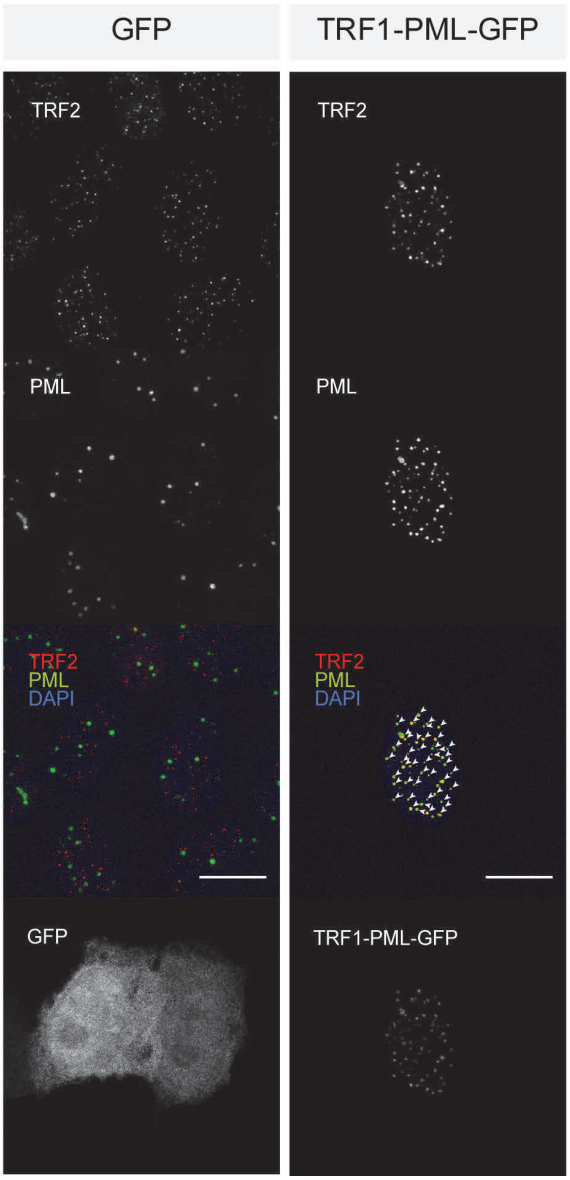

Figure 26. Recruitment of PML to the majority of telomeres in ALT-negative HeLa cells

Microcopy images of transiently transfected HeLa cells. HeLa cells were transfected with GFP (G) and TRF1-PML-GFP (TPG). After 24 h, cells were fixed and stained with αTRF2-rb-A568 and αPML-ms-ATTO633. Colocalizations of TRF2 (representative for telomeres) and PML are marked with white arrows. Scale bars are 10 µm.

GFP was distributed throughout the whole cell, whereas transfection of PG led to a higher number of PML-NBs, not attached to telomeres of both U2OS and HeLa cells. TRF1-GFP did colocalized with telomeres but not with endogenous PML. Upon transfection of TPG A strikingly high number of colocalizations between PML and telomeres was detected in both U2OS (**Figure 25**) and HeLa cells (**Figure 26**) transfected with TPG. Thus, exogenous expression of a PML-TRF1 fusion construct recruited PML to the majority of telomeres in cells independent of their ALT background.

3.2 PML at telomeres induces telomere clustering

Spot properties of signals derived from telomere and PML staining were in the acquired images were quantified using cell segmentation 3D (Wörz *et al.*, 2010; Osterwald *et al.*, 2012). For the present analysis, the detection spots in the telomere channel were changed to a 2-Pass segmentation, as already described for the PML channel, because telomere foci varied from very faint to very large dots (implemented by Stefan Wörz, Prof. Karl Rohr, Heidelberg). The DAPI staining was used for nucleus segmentation that was passed on to the next analysis step within the software to analyze the spots in the other three channels for telomeres, PML and GFP-construct. Parameters for the cell segmentation 3D software were calibrated to detect all visually detectable telomeric and PML spots in untransfected or GFP-transfected cells. For convenience, TRF2/ PML colocalizations are referred to as APBs in the following. However, it needs to be verified if recruited PML fulfills functional requirements of endogenous APBs.

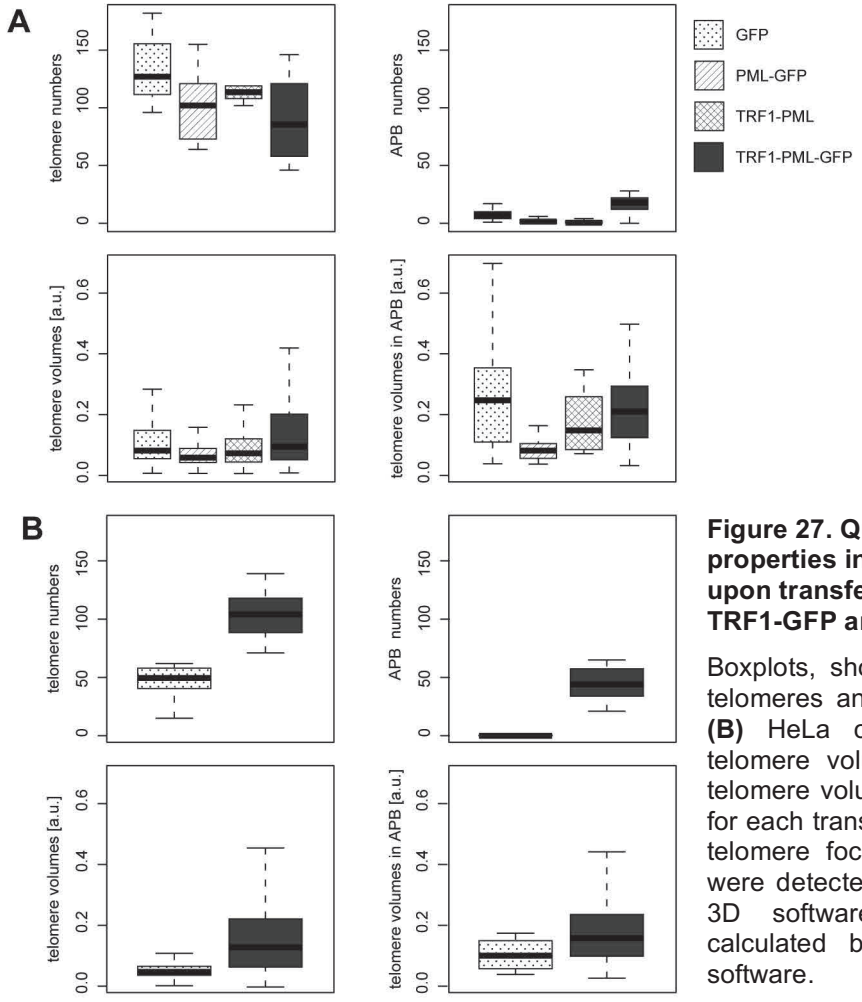

Figure 27. Quantification of telomere properties in U2OS and HeLa cells upon transfection of GFP, PML-GFP, TRF1-GFP and TRF1-PML-GFP.

Boxplots, showing the quantification of telomeres and APBs in **(A)** U2OS and **(B)** HeLa cells. Telomere numbers, telomere volumes, APB numbers and telomere volumes in APBs were plotted for each transfected construct. PML and telomere foci and their colocalizations were detected using Cell segmentation 3D software. Volumes were also calculated by Cell segmentation 3D software.

With this method the number of telomeres and APBs was determined as well as volumes of telomeres overall and in APBs in U2OS and HeLa cells after transfection of G, PG, TG and TPG (**Figure 27** and (**Table 40** and **Table 41**). U2OS wt cells have a diverging set of chromosomes with 77 chromosomes

with 144 telomeres (Jegou *et al.*, 2009). Since some chromosomes have signal-free ends, the obtained number of 129.6±9.1 for U2OS^{G} is in the expected range. In U2OS^{TPG} cells, the detected telomere number is lower than in all controls, and significantly reduced compared with the GFP-transfected control (33%, p = 0.0076). For calculating the number of colocalizations of TRF2 and PML spots, only the best colocalizations (1,3,5,7) were taken into account (see **methods section 7.6**).

The number of TRF2/ PML colocalizations was unexpectedly high in the GFP control U2OS cells and the number of telomeres was not significantly different between control transfections (p >0.05). Therefore, only TG- and PG-transfected cells served as controls. The number of detectable TRF2/ PML colocalizations in U2OS^{TPG} cells was significantly increased 8-fold over U2OS^{PG} cells (p = 1.1e-3) and 14-fold over U2OS^{TG} cells (p = 0.00079). However, the automatically detected number did not reflecting the strikingly high number from visual inspection.

Table 40. Quantification of telomere and APB properties in transiently transfected U2OS cells.

	Telomere number	APB number	Telomere volume	Telomere volume in APBs
GFP	129.6±9.1	6.8±1.5	0.14±0.006	0.41±0.052
TRF1-GFP	116.5±3.7	1.1±0.4	0.11±0.006	0.31±0.152
PML-GFP	103.9±10.1	1.9±0.7	0.09±0.005	0.08±0.008
TRF1-PML-GFP	87.0±10.9	15.6±3.0	0.18±0.010	0.27±0.024

The table shows the quantification of detected telomere spots in HeLa cells transfected with GFP, PML-GFP, TRF1-GFP or TRF1-PML-GFP. The columns reflect the telomere numbers, APB numbers, as well as telomere volumes and volumes of telomeres in APBs.

In all but U2OS^{PG} cells, telomeres in APBs had a higher volume as the mean of all telomeres confirming previous observations (Osterwald *et al.*, 2015). In U2OS^{PG} cells, the volume is similar, however, the volume range also included higher volumes for telomeres in APBs. The telomere volume in APBs in U2OS^{TPG} cells was not increased compared to U2OS^{G} and U2OS^{TG} cells.

Table 41. Quantification of telomere and APB properties in transiently transfected HeLa cells.

	telomere number	APB number	telomere volume	telomere volume in APBs
GFP	46.8±3.3	0.3±0.1	0.07±0.004	0.11±0.029
TRF1-PML-GFP	103.6±6.8	44.3±4.7	0.21±0.027	0.19±0.006

The table shows the quantification of detected telomere spots in HeLa cells transfected with GFP or TRF1-PML-GFP. The columns reflect the telomere numbers, APB numbers, as well as telomere volumes and volumes of telomeres in APBs.

In HeLa cells the number of telomeres in the GFP control cells was lower as expected. Since telomeres in HeLa cells are short, our method might not be suited to detect all telomeres. However, in HeLa^{TPG} cells, the number of telomeres is higher than in HeLa^{G} cells. Also, the percentage of telomeres colocalizing with PML was determined as 42%. The number of TRF2/ PML colocalizations was significantly (p=2.7e-06) increased from 0.3 in HeLa^{G} to 44.3 in HeLa^{TPG} cells. The mean volume of

telomeres in APBs was not different from the average volume of all telomeres. However, in HeLa^{TPG} cells the telomeres not colocalizing with PML had a significantly higher volume as compared to HeLa^{G} cells (p=8.0e-07). In summary, a telomere-repeat foci increased in volume while their absolute number was reduced indicating enhanced telomere clustering.

3.3 PML recruitment to telomeres increases C-circle levels

Experiments conducted with transiently transfected cells are limited because of low transfection efficiencies, variances in expression levels, and short time of overexpression. The generation of stable cell lines was required for further experiments to overcome these issues.

To enable long-term and bulk population experiments stable inducible U2OS and HeLa cell lines were generated using the Tet-On pTRE3G system. Different strategies for generating stable and inducible cell lines were taken into consideration. (a) The FlpIn-TRex system allows locus-specific integration, however it is restricted to commercially available cell lines. The (b) The PiggyBac system is a flexible system, which can be integrated into numerous cell lines, although the integration is not locus-specific. Furthermore, in our labaoratory up to now integration of a construct different from one encoding GFP was not successful. For the (c) TetOn pTRE3G system, U2OS and HeLa Tet-On cell lines already existed that were used for generating DOX inducible stable cell lines (see **methods Figure 5**). Thus, inducible U2OS and HeLa cells were generated utilizing the Tet-On 3G system. Therefore, the full construct (TRF1-PML-GFP) as well as control constructs (GFP, PML-GFP and TRF1-GFP) were cloned into a pTRE3G vector. U2OS and HeLa Tet-On cells were then transfected under puromycin selection. Parts of the generation of the stable cell lines were done by Caroline Bauer (Prof. Karsten Rippe, DKFZ, Heidelberg). Stable clones with an overall high expression but low variance in Doxycyclin (dox) inducible expression were selected for each construct and cell line. Various amounts of doxycycline were tested and the optimal concentration was determined to be 50 ng for U2OS and 100 ng for HeLa cells. Thus, stable cell lines inducible for GFP, PML-GFP, TRF1-GFP and TRF1-PML-GFP were generated using the TetOn pTRE3G system.

Next, it was addressed if artificial APBs as measured above have an effect on ALT activity by measuring C-circle levels after recruitment of PML to telomeres. C-circles are a robust marker for ongoing ALT activity (Henson *et al.*, 2017). In both U2OS cells and HeLa cells, no elevated levels of C-Circle levels were observed after 24 h upon transient transfection (data not shown). Next, stable expression of TRF1-PML-GFP was induced for 14 days in U2OS and HeLa cells and C-circle levels determined on day 0, 4, 7 and day 14 (**Figure 28A**). C-circle levels were normalized to a U2OS wt sample that serves as an ALT-positive reference cell line. Prior induction, C-circle levels were similar between the various expressed constructs. After four days of stable expression, C-circle levels were increased in U2OS^{TPG}

cells, however also U2OS^{G} cells showed elevated C-circle levels. C-circle levels in U2OS^{PG} and U2OS^{TG} cells did not change significantly. After 7 days of induction, a further increase in C-circle levels for U2OS^{TPG} was observed that was >4-fold over pre-induced U2OS^{TPG} cells. In addition, after 7 days C-circle levels were significantly higher in U2OS^{TPG} as compared to all controls ($p \leq 0.0085$). For U2OS^{PG} and U2OS^{TG}, no change in C-circle levels upon stable expression was observed. After 14 days of continuous induction of expression, C-circle levels of all stable cell lines were back at levels of pre-induced cells. Notably, also the percentage of positive cells for the construct as indicated by the fraction of GFP-positive cells decreased over induction time and was ~50% for U2OS^{TPG} and ~30% for U2OS^{TG} after 7 days of continuous doxycyclin delivery. For all pre-induced HeLa cells, only C-circle levels below 1% of U2OS wt were measured (**Figure 28B**).

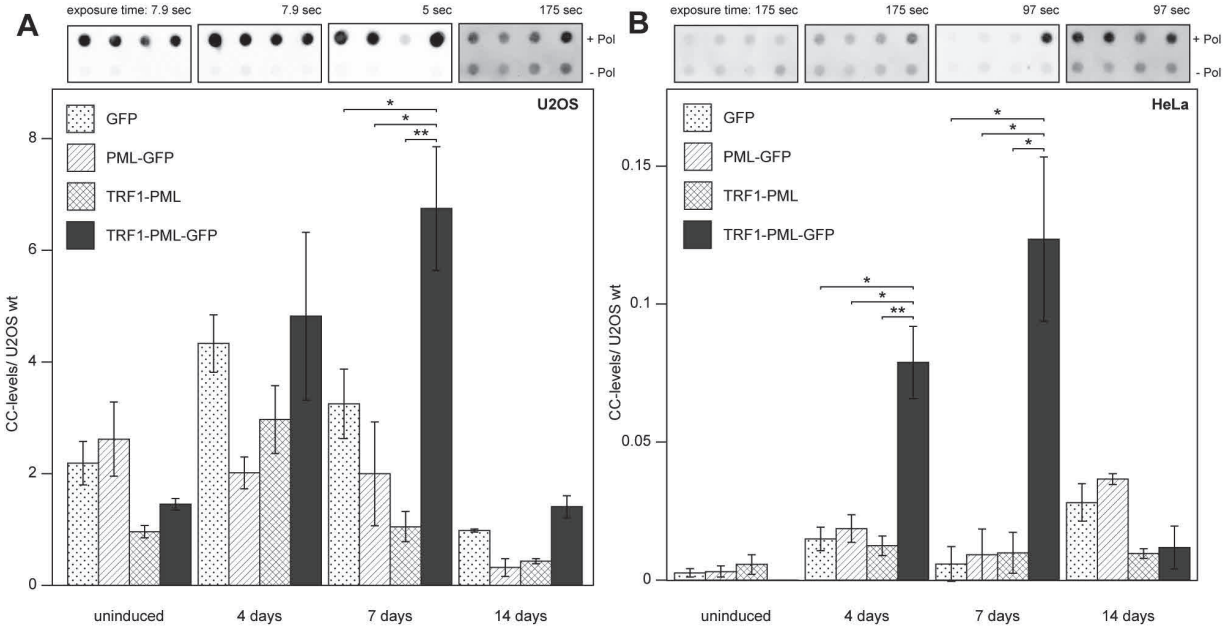

Figure 28. C-circle levels in U2OS and HeLa cells after induction of expression of GFP, PML-GFP, TRF1-PML, or TRF1-PML-GFP.

C-circle assay of **(A)** U2OS and **(B)** HeLa cells with induced expression of GFP, PML-GFP, TRF1-GFP and TRF1-PML-GFP after 4, 7 and 14 days. Above the bar plots, exemplary dot blots of the C-circle assay are depicted. The upper row contains samples after amplification with polymerase addition, and the lower row shows the control without polymerase. Error bars represent the SEM. Significance is indicated with asterisks, *p<0.01, and **p<0.001.Experiments were performed in two independent replicates, each in technical triplicates.

Already after 4 days, a striking increase in C-circle levels for HeLa^{TPG} to ~8% of U2OS levels was observed. None of the control constructs did show any significant change in C-circle levels. After 7 days of stable expression of TRF-PML-GFP, the C-circle levels did further increase to ~12% of U2OS wt cells. C-circle levels of all control cells stayed at the same levels as pre-induced and 4-days-induced cells. Thus, C-circle levels were significantly increased over controls after 4 ($p \leq 0.0013$), and 7 days ($p \leq 0.0024$) of stable expression of TRF1-PML-GFP in HeLa cells.

As for the U2OS cell lines, the number of positive cells also decreased with ongoing induction of expression in the HeLa cell lines. After 7 days of continuous induction, only 55% HeLa^{TPG}, 33% HeLa^{G}

and 1-2% HeLa^{PG} were positive for the construct, as determined microscopically. Continuous overexpression of any of the construct might be cytotoxic and potential effects of the remaining positive cells might not be detectable above noise. Furthermore, almost all HeLa^{TG} were non-viable after 7 days. Also, the generation of non-inducible stable overexpression of TRF1 failed in ALT-negative cells (HeLa, MCF-7) as all attempts resulted in cell death. Thus, TRF1 overexpression was toxic for HeLa cells and further validation and optimization of induction conditions have to be done. In summary, the recruitment of PML to telomeres via the telomere binding protein TRF1, was shown to increase C-circle levels after stable expression for 4-7 days indicating activation of the ALT mechanism even in an ALT-negative cell line.

Discussion

Maintenance of telomeres is one of the hallmarks of cancer and also plays a central role in other diseases like syndromes associated with premature aging. Furthermore, dissecting the TM is becoming increasingly important in the field of cancer research based on deep-sequencing approaches (Barthel *et al.*, 2017; Chudasama *et al.*, 2018; Sieverling *et al.*, 2018). Alternative lengthening of telomeres (ALT) is a mechanism used by cancer cells for recombination-mediated telomere elongation in the absence of telomerase. In this thesis, the *TelNet* database was developed as a TM pathway analysis tool that helped to identify novel ALT candidate genes detected from RNA-seq experiments from several cellular systems with perturbed TMM. Furthermore, a method to recruit any protein of interest to telomeres was established in telomerase-positive cells that can be applied for testing the effect of ALT candidate genes on ALT induction. With the *TelNet* database, identification of putative novel ALT enhancer genes, and establishment of a telomere recruitment method, this thesis lays the foundation for future investigations in the field of telomere maintenance (TM).

1 Annotation of known TM genes

With existing tools like HumanMine (Smith *et al.*, 2012) it is difficult to retrieve TM information on a given set of genes, because detailed TMM annotations are currently missing. Beyond HumanMine and other general gene databases, currently only the Telomerase database (Podlevsky *et al.*, 2008) and the MiCroKiTS database (Huang *et al.*, 2015) offer some telomere specific information. However, no information on TM phenotype upon knockdown or overexpression, or details on the active TMM are given. This current gap is filled with the *TelNet* database as a dedicated and useful resource for research in TM in cancer and other diseases like premature aging. The *TelNet* database addresses an unmet need of the corresponding research communities and provides an open-ended platform to compile existing knowledge on human and budding yeast genes involved in TM, especially the ALT pathway. Genes were collected from existing literature and annotated with TM information such as (i) TM mechanism and activity of regulation, (ii) TM functions, (iii) knockdown/ overexpression phenotype, (iv) a TM significance score, (v) TM summary/ comments, (vi) reference links, and (vii) orthologous genes. Different search and view modes can be used to explore the database, e.g. for results lists from bioinformatics pipelines. This is necessary and will become even more important because “omics” studies and screening experiments are on the advance. The most powerful tool is the *TelNet* list search,

enabling the fast identification of TMM genes from large gene lists derived from such analysis, e.g. genomic and transcriptomic data (Barthel *et al.*, 2017; Chudasama *et al.*, 2018; Sieverling *et al.*, 2018).

With the *TelNet* database, the user can retrieve detailed TM information on particular genes without any prior knowledge as compared to other databases. To demonstrate the advantages of TelNet, the transcription factors of the budding yeast telomerase protein subunit *EST2* that are listed as "documented" in the Yeastract database (Teixeira *et al.*, 2014), were submitted to the Saccharomyces genome database (SGD)/ YeastMine (Balakrishnan *et al.*, 2012). All regulators were indeed recognized as transcription factors in general, however, no hint was found towards telomerase or TM, because GO annotations did not contain TM information. In contrast, the complete list was included in the *TelNet* database as budding yeast telomerase regulators. A clear limitation of the GO pathway analysis is the lack of annotations for the majority of known genes, since only 33 % of all genes hold at least one GO biological process. Thus, the effective domain size was small in comparison to the total number of genes. All enrichment scores are therefore only first approximations and also enrichments without reaching a significance levels were also considered. Genes without a GO term with regard to telomeres, despite a reported role in TMM, were included in the *TelNet* database. With this, the effective domain size regarding TM annotations was substantially increased and by using the *TelNet* database more potential candidate genes can be found, by using the *TelNet* database.

The database certainly requires continuous maintenance which has to be assured over a long period of time. With the support of the telomere community, *TelNet* information will constantly be improved and extended by the latest research. For this process telomere researchers are encouraged to communicate their feedback via telnet@dkfz.de in order to constantly improve the database and keep the information relevant and up to date. The integration of new information requires manual curation, accordingly most of the fields are easy-to-fill with terms from a drop-down list. Furthermore, information from the general part can be copied from external databases, such as identifiers, synonyms and description. Since the database was designed in a way that easily enables addition of more organisms, the extension with data from *M musculus* and *S. pombe* and respective human and budding yeast orthologues will further strengthen the advantages of homology assignments in the future.

Recurrent TMM-associated mutations in *ATRX, DAXX* and the *TERT* promoter have been found in a variety of cancers and are well known. However, in many tumor samples these mutations are lacking, suggesting the contribution of other factors to the active TM. This view is supported by a recent integrative genome and transcriptome analysis of leiomyosarcoma, which applied *TelNet* for the TMM analysis and identified recurrent mutations in *RBL2* and *SP100* as linked to ALT (Chudasama *et al.*, 2018). Accordingly, it is anticipated that *TelNet* will help to reveal this type of novel correlations between deregulated cellular features and active TM networks in different tumor entities.

2 ALT suppression and induction

In budding yeast, it is feasible to perform deletion screen experiments, which is challenging in human cell lines. Therefore, other strategies have to be applied to study the activation and repression mechanisms of ALT. Investigating the suppression of ALT has been challenging because specific molecular targets other than ATRX are missing. Furthermore, depletion or overexpression of an ALT related protein or pathway only reduces some ALT hallmarks, not all of them. Especially interesting are small molecule drugs that might have the potential in reducing ALT activity in cancer cells potentially reducing their viability as a consequence. The ATRi VE-821 and the HDACi SAHA have been shown to reduce some ALT features. Upon treatment with ATRi a decrease in C-circle levels, T-SCE, and APB-positive cells as well as more telomere-free chromosomes, but unchanged TERRA levels and localization have been observed (Flynn *et al.*, 2015). Similarly, SAHA treatment has been demonstrated to reduce the number of APBs and C-circle levels (Osterwald *et al.*, 2015).

For detailed investigations on the mechanism underlying ALT, the defined induction of ALT is desired. So far, induction of ALT has been reported for (i) normal cells that went through crisis or were transformed to cancer cells (Yeager *et al.*, 1999), (ii) telomerase-positive cells that underwent telomere shortening because of telomerase depletion and evaded senescence by activating ALT (Min *et al.*, 2017), (iii) by combined depletion of ATRX and DAXX, inhibition of telomerase as well as DNA damage induction at telomeres (Hu *et al.*, 2016) and (iv) rapid ALT induction by ASF1 kd in telomerase-positive cells with long telomeres (HeLa LT) (O'Sullivan *et al.*, 2014). The first two processes are time-consuming and survivor formation is rare. The third treatment is very labor-intensive and accompanied by severe perturbations. In contrast, the ALT induction phenotype of ASF1 depletion can be reversed after recovery of ASF1 and requires single siRNA transfection without generating stable cell lines (O'Sullivan *et al.*, 2014). Thus, siRNA mediated-depletion of ASF1 is currently the only way to rapidly induce ALT in ALT-negative human cell lines, and thus the method was exploited in the present work.

In this thesis, strategies to induce or suppress the ALT pathway in human and budding yeast were applied to identify novel ALT driver or suppressor candidates via a differential gene expression analysis. ALT-positive cells were treated with HDACi SAHA to repress ALT and ASF1 was depleted in telomerase-positive cells followed by ALT induction. In addition, the budding yeast type II survivors were studied that form upon *EST2* deletion. The integrative analysis of deregulated pathways resulted in common and distinct signaling pathways as outlined below.

First, the treatment conditions for SAHA were optimized in order to to find a low and effective concentration that still leads to reduced C-circle levels as an established marker for ALT activity. The reduction of APBs and C-circle levels was in agreement with previous findings (Osterwald *et al.*, 2015). It is noted that SAHA treatment did not selectively induce apoptosis in ALT cells. Rather it appears that

drug sensitivity with respect to cell viability might be cell-type specific. This is similar to previous reports investigating the effects of ATRi VE-821 (Deeg *et al.*, 2016). Next, it was confirmed that ALT is induced by ASF1 depletion in HeLa LT cells with long telomeres. In previous reports, it has been shown that the number of APBs, events of telomere recombination as well as TERRA levels were elevated with this approach (O'Sullivan *et al.*, 2014; Deeg, 2015). Furthermore, a decrease in TERT expression, detected by qPCR, and telomerase activity was reported (O'Sullivan *et al.*, 2014). In contrast, determining TERT expression levels from the RNA-seq data acquired here did not show a change upon ASF1 depletion in HeLa LT or ST cells. A possible explanation is the low abundance of transcript reads for the TERT gene that are difficult to quantify. For the lowly expressed TERT mRNA, qPCR appears to be better suited than RNA-seq to measure its expression.

As shown in this thesis, ALT suppression in ALT-positive cells with SAHA also reduced the ALT induction capacity of ASF1 depletion in HeLa LT cells. The combination of ASF1 kd with drugs targeting DDR signaling pathways or cytostatica has been performed previously and indicated a role of replication stress sensing and ATR signaling for ALT induction (O'Sullivan *et al.*, 2014).

In the present thesis, differential gene expression analysis was applied to gain insight into the mechanism of ALT suppression and induction mechanisms. To identify genes that recurrently correlated or anti-correlated with the ALT status in the present thesis, lists from the different induction and suppression experiments were checked for overlapping genes and pathways. Genes that were downregulated upon SAHA treatment are discussed as ALT enhancing and upregulated genes are referred to as potentially ALT repressing. Since, ASF1 depletion induced a number of ALT features in ALT-negative HeLa LT cells, upregulated genes upon ASF1 kd were considered as ALT enhancing genes and downregulated factors as ALT repressing. In line with previous findings, HeLa ST was incapable of ALT induction by depletion of ASF1. The difference between HeLa LT and ST cells could not be deduced to different expression levels of TERT. The response of HeLa ST to ASF1 depletion was only marginally investigated previously (O'Sullivan *et al.*, 2014). Comparison of gene expression changes after ASF1 kd in HeLa ST with those in HeLa LT allowed for the identification of genes and pathways that protect from ALT induction in HeLa cells with short telomeres. In the present analysis only genes exclusively deregulated in one of the cell lines (LT or ST) were further analyzed, in order to identify reasons for the different responses. Genes that were deregulated upon SAHA treatment of ASF1 depleted HeLa LT cells were referred to as ALT suppressor candidates for up- and ALT enhancer candidates for downregulated genes, respectively.

Matching of deregulated genes from suppression and induction experiments resulted in 28 potential ALT suppressors (**Figure 29**) and 13 ALT enhancer candidates (**Figure 30**). ALT enhancer candidate ***KCTD15*** was downregulated upon suppression of ALT maintenance as well as ALT induction. The protein has been found in close proximity of shelterin and was therefore included in the *TelNet* database. The zebrafish homologue (*Kctd15*) of the human *KCTD1*, a close family member of ***KCTD15***, has been

demonstrated inhibit canonical WNT signaling and interacts with transcription factors of the AP-2 family (Zarelli & Dawid, 2013; Li *et al.*, 2014). Furthermore, AP-2 transcription factors have been reported to activate human *TERT* (Doloff *et al.*, 2008). Thus, it can be speculated that, ***KCTD15*** might be involved in repressing *TERT* activators. A second interesting ALT enhancer candidate is ***TNNC1***, that was upregulated upon ALT induction and in agreement downregulated upon ALT suppression, thus correlating with the presence of ALT markers. The gene was included into the *TelNet* database because of the budding yeast homologues *CMD1* phenotype of telomere elongation after deletion. Further investigations are suggested to confirm their role as ALT enhancers.

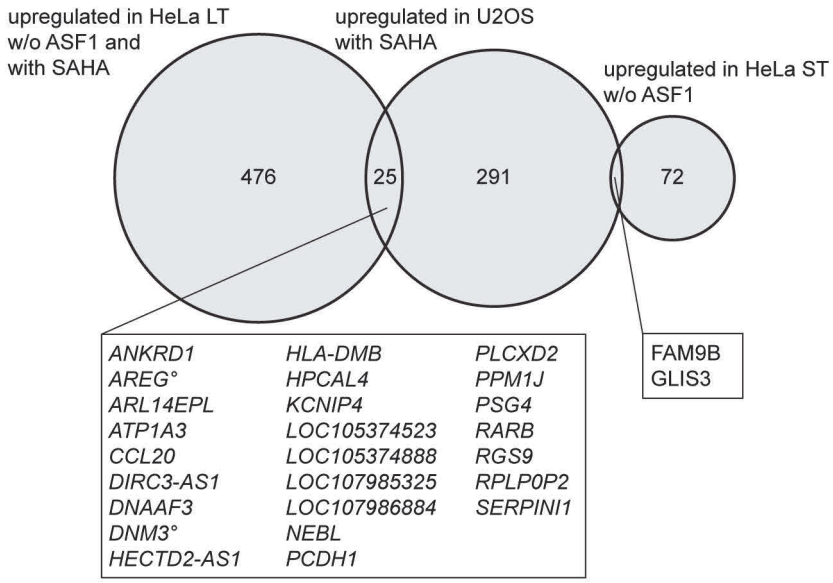

Figure 29. ALT suppressor candidate genes.

Merged lists of ALT suppressor candidate genes from different DESeq results of perturbed cell lines. Genes reported to be cell cycle-regulated in U2OS or HeLa cells (Grant *et al.*, 2013) are marked with a °circle.

Furthermore, also results from the functional annotation clustering and pathway enrichment analyses were checked for overlapping pathways. Global gene expression levels of ASF1 depleted HeLa LT cells were previously analyzed by microarray (O'Sullivan *et al.*, 2014). From this only selected enriched pathways have been shown, namely upregulation of genes involved in TNFα, IL-10, NFκB and TGFβ signaling pathways and downregulated genes were associated with the HIF-1 and AP-1 transcription factor network. With the here-performed RNA-seq method, the transcriptome was analyzed in an unbiased manner, e.g. also taking pseudogenes into account. None of the in the previous study mentioned genes (*IL1A*, *IL1B*, *IL6*, *CXCL8* (aka *IL8*), *IKBKG* or *NFKB2* (aka *p100*) have been identified as upregulated in ASF1 depleted HeLa LT cells. However, other genes involved in inflammatory and/ or immune response were upregulated in ASF1 depleted HeLa LT cells but not in HeLa ST. It is noted, that the detection of short RNAs, for example microRNAs, is beyond the range of the analysis because a size selection step was used to retrieve only transcripts longer than 200 kb.

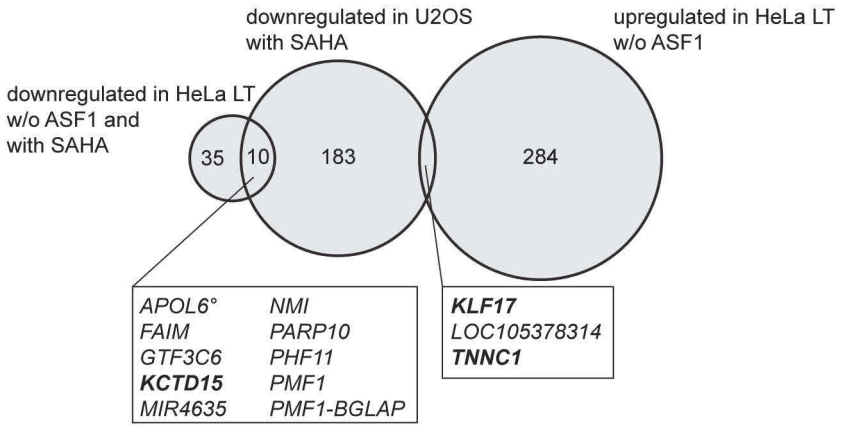

Figure 30. ALT enhancer candidate genes.

Merged lists of ALT enhancer candidate genes from different DESeq results of perturbed cell lines. Those genes implemented in the *TelNet* database are marked in bold. For details please see legend of **Figure 29**.

In terms of changes in signaling pathways, the findings from this study are consistent with the microarray analysis with identifying the upregulation of TNFα signaling (*THBS1*), the IL-10 cytokine *IL24*, and TGFβ signaling (*BMP2*, *BMP6*, *KLF17*) in ASF1 depleted HeLa LT cells the results are consistent with the microarray analysis. However, *IL24°* was also upregulated upon SAHA treatment of U2OS cells, which suppressed ALT markers. In U2OS cells, a cell-cycle dependent expression has been observed (Grant *et al.*, 2013), indicating a secondary effect leading to upregulation of *IL24°*, independent of the ALT status. The downregulation of the TGFβ signaling factor ***KLF17*** upon SAHA treatment in U2OS cells is in agreement with the upregulation of ***KLF17*** upon ALT induction. From this, it can be reasoned that TGFβ signaling has a positive correlation with ALT. Proteins of TGFβ signaling have been shown to repress telomerase (Li *et al.*, 2006; Cassar *et al.*, 2017). Thus, it can be speculated that one aspect of ALT induction in ASF1 depleted HeLa LT cells is the TGFβ mediated telomerase repression.

SAHA treatment of U2OS cells induced ALT suppression and the downregulation of WNT signaling (*WNT11*, *WNT3A*, *WNT5B*). This is consistent with the upregulation of WNT signaling inhibitors (*DKK3, LRP1, NXN, DACT3,* ***HMGA2*** *CITED1*, and PTK7) in ASF1 depleted HeLa LT treated with SAHA associated with suppression of ALT induction. Thus, suppression of ALT is correlated with the inhibition of WNT signaling. This is consistent with activated WNT signaling (*WNT11*), upon ALT induction in ASF1 depleted HeLa LT cells. Thus, WNT signaling correlates with the presence of an active ALT mechanism. Downregulation of canonical WNT signaling has been reported in mice deficient of telomerase RNA component TERC and harboring shortened telomeres (Yang *et al.*, 2017). Activation of WNT signaling in these mice was shown to result in re-established telomere capping. Also, the telomerase catalytic subunit TERT has been reported to have a transcriptional modulator role in the WNT signaling pathway (Park *et al.*, 2009; Hoffmeyer *et al.*, 2012; Zhang *et al.*, 2012).

Moreover, ALT repressor SAHA mediated the upregulation of TNF/ NFκB signaling (*TRAF1*, *CXCL8*, *IQGAP2*, *TNFSF9, and CCL20*), and decreased the expression of p38 MAP kinase pathway inhibitor ***RARRES2***. In agreement with an ALT repressive role for TNF/ NFκB/ p38 MAP kinase signaling, SAHA induced the upregulation of p38 MAP kinase signaling genes (PTK7) in ASF1 depleted HeLa LT cells. ALT induction in ASF1 depleted HeLa LT cells was associated with the upregulation of NFκB repressor *S100A9*. Together, TNF/ NFκB/ p38 MAP kinase signaling anti-correlates with the occurrence of ALT. The link between signaling pathways such as TNF or NFκB has been discussed in the literature. TNFα treatment has been shown to induce telomere shortening (Maekawa *et al.*, 2018). A model for the interaction of TERT with WNT and NFκB signaling pathways has been proposed (Li & Tergaonkar, 2014).

Interestingly, ASF1 depleted HeLa ST cells that did not display ALT induction, showed upregulation of IL6 and other genes involved in defense virus response (*IL6, IFIT3, IFIT2, IFIT1°, OASL,* ***ISG15****, OAS2, DHX58),* inflammatory response (*IL6, CCR4, ITGB2, CCL5, SCG2*) or immune response (*IL6, CCR4, SUSD2, TNFSF15, OAS2, CCL5, IL7R*). A portion of these genes overlap with factors of type I interferon signaling pathway (*IFIT3*, *IFIT2*, *IFIT1°*, *OASL*, *ISG15*). Furthermore, *TNFAIP6*, repressing inflammatory response was downregulated, which is in agreement with the upregulation of immune response on the other hand. For *IFIT3*, *IFIT2*, *OASL* and ***ISG15***, basal expression levels were already higher in untreated HeLa LT than ST cells. Upon ASF1 depletion in HeLa LT cells, expression levels of *IFIT3*, *IFIT2*, *OASL* and ***ISG15*** were then further increased without reaching the level of significance and thus not showing up in the results list. Upon SAHA treatment and associated with suppression of ALT induction, the type I interferon signaling genes *IFIT3, IFIT2, OASL*, and ***ISG15***, were downregulated. Activation of type I IFN signaling has been observed for cytosolic sensing of extra-chromosomal telomeric repeats (Tao *et al.*, 2016). ALT cells that lack functional ATRX on the other hand have been shown to be defective in cytosolic DNA sensing, because this requires intact ATRX (Chen *et al.*, 2017). A possible explanation of the results might be that ASF1 depletion generates ECTRs that diffuse into the cytosol, activate the cGAS-STING pathway and lead to induction type I INF signaling. In the case of HeLa ST, cells activate an unknown downstream mechanism that protects from ALT induction. In contrast, HeLa LT cells lack this mechanism and develop ALT despite an intact cGAS-STING mediated sensing of ECTRs. Since SAHA reduced C-circles, sensing of cytosolic DNA and therefore type I IFN signaling might be reduced. Downregulation of *IFIT3, IFIT2, OASL*, and ***ISG15*** upon SAHA might therefore be the result of dispersed C-circles.

Overall it can be speculated that WNT and TGFβ pathways have enhancing roles in the ALT mechanism, and NFκB and p38 MAP kinase signaling in turn comprise ALT repressive pathways. Despite the dramatic changes in multiple signaling pathways of cancer cells, the role of the above-mentioned pathways should be further investigated in the context of TMM. Investigations of ALT suppressor genes and pathways by their overexpression in ALT cells should help elucidate the negative

effect on ALT hallmarks. The identification of ALT repressors will help understanding the mechanisms of ALT. Equally, the role for ALT enhancing genes and pathways in the ALT mechanism remains to be demonstrated in validation experiments. It will be interesting to see, if single depletion experiments might reveal a requirement for APB formation or ECTR generation. This novel list of potential ALT genes offers great potential for targeting the ALT mechanism.

It will be interesting to further investigate the role of SAHA in the process of ALT suppression. Assessment of other ALT features other than C-circles may significantly improve the results as well as confirming the effects in other ALT cell lines. Further experiments with other pan HDACi such as panobinostat or TSA and specific depletion of single HDACs should help determine the role of HDAC inhibition on ALT suppression. It will be interesting to see, how SAHA performs in a currently recruiting clinical I/II trial, where the pan HDACi is applied to children with solid tumors, lymphoma or leukemia that did not respond to the standard therapy (Witt *et al.*, 2012). Further analysis of the data generated in this study may reveal a relation between TMM status and response to SAHA therapy.

3 Functional role of PML during ALT induction

In ALT-positive tumors, PML is neither recurrently mutated nor has deregulated gene expression (Lafferty-Whyte *et al.*, 2009; Doyle *et al.*, 2012; Lovejoy *et al.*, 2012; Deeg *et al.*, 2017). Nevertheless, the delocalization of PML to telomeres is specific for ALT cells. Thus, this process is driven by the deregulation of other factors as investigated previously (Osterwald *et al.*, 2015). Therefore, artificially recruiting PML to telomeres perfectly mimics this kind of alteration.

For recruiting PML to telomeres in U2OS and HeLa cells, a fusion construct consisting of TRF1 and PML was used. In transiently transfected cells, PML recruitment to almost all telomeres induced telomere clustering, as concluded from the confocal image analysis of telomere number and volume. Stable cell lines were generated that can be used to induce telomeric PML recruitment, enabling long-term bulk cell population experiments. The levels of extrachromosomal telomeric repeats, accessed by the C-circle assay, were increased in both cell lines, only between 4-7 days after induction.

With the strategy developed here it is possible to recruit PML to all telomeres in a given cell type that carries the PML-TRF1 construct. In contrast to the *lacO*-system described previously, which only allows for ectopic APB formation in an ALT-positive U2OS cell line (Jegou *et al.*, 2009; Chung *et al.*, 2011), the strategy can be applied to any cell line of interest as the fusion protein is encoded on a transfectable plasmid. By using somatic cells or ALT-positive cells with weak levels of ALT hallmarks, the functional role of PML in the induction of ALT could be further investigated. Moreover, the method can be

extended by transfecting another protein of interest fused to a GFP-binder domain (Rothbauer *et al.*, 2006; Zolghadr *et al.*, 2008; Chung *et al.*, 2011). After transient transfection and induction of TRF1-PML-GFP expression the GFP-binder fusion construct will be recruited to the artificial APBs. Subsequent analysis of an increase in ALT features will help confirming the ALT enhancing role for a protein of interest.

For ectopic expression of PML it is relevant, which isoform is used, because phenotypes upon depletion or overexpression can vary. Since especially isoform IV interacts with TRF1 (Yu *et al.*, 2010), overexpression results in an increase of APBs (Osterwald *et al.*, 2012; Yong *et al.*, 2012). In contrast, overexpression of PML isoforms III, V and VI slightly decreased the number of APBs (Osterwald *et al.*, 2012) and it has been suggested that regulation of the other isoforms is affected by changing the expression of one isoform (Chung *et al.*, 2011). In this thesis, PML III was used for overexpression and recruitment experiments since, if overexpressed at low levels, it induces a relatively low perturbation of endogenous PML concentrations and APB formation. Also, the selection of a telomeric binding part of the fusion construct is important, since its overexpression alone should not lead to a severe phenotype. Overexpression of TRF2 resulted in elevated levels of apoptotic cells (Osterwald *et al.*, 2012), probably because of replication fork stalling (Nera *et al.*, 2015). Overexpression of TRF1 was observed previously to increase homologous recombination (Munoz *et al.*, 2009). Furthermore, exogenous TRF1 protein might compete with TRF2 at telomeres, which in the most extreme scenario could lead to telomere fusions, observed for TRF2 depleted cells (van Steensel *et al.*, 1998). Considering these observations, in the present thesis cells with relatively low expression of the constructs were either manually selected from a transiently transfected cell pool or induced with a low doxycycline concentration in the stable cell lines. Under these conditions overexpression of TRF1 or PML alone in U2OS cells did not alter the apparent number of telomeres, localization of PML or C-circle levels. Likewise, C-circles were not induced in HeLa cells if only TRF1 or PML constructs were present. Telomere clustering after 24 h and increased C-circle levels after 4 days in HeLa cells point to the activation of ALT upon PML recruitment. However, telomere clustering has been also suggested to be a result of senescence (Chung *et al.*, 2012) and APB induction has been observed upon starvation triggered by methionine restriction (Jiang *et al.*, 2009). Indeed, cells were not viable for more than 7 days of stable expression of PML or TRF1. However, the cells stably expressing the fusion construct TRF1-PML were still viable on day 7 with 50% of the culture being positive for the construct. In future experiments, it would be interesting to investigate telomere clustering in a more direct manner, for example by high resolution microscopy. Further experiments involving automatic screening of stable cell lines will help confirm the results after optimization of induction conditions for the stable cell lines. For screening and subsequent analysis, quantification of the GFP signal yields an estimate of protein expression level in the nucleus. Thus, the degree of clustering can be calculated in dependence of the fusion protein concentration.

In addition to telomere clustering, also C-circles increased after 4 days in HeLa cells. A possible explanation might be ongoing homologous recombination in artificial APBs, since C-circles might be originating as a byproduct of homologous recombination (Pickett *et al.*, 2009). The results obtained in this thesis already indicate the induction of ALT in a previous ALT-negative cell line due to PML recruitment to telomeres. To further corroborate this finding, the activity of these artificial APBs in comparison to endogenous APBs needs to be further characterized. It will be important to show that factors indicating active DNA repair and recombination at telomeres, e.g. pATM or γH2A.X or essential APB compounds are indeed present at artificial APBs as has been shown for artificial APBs in ALT-positive U2OS cells.

The stable cell lines are especially useful for studying long-term and bulk effects. In addition, the inducible system allows for the investigation of the same cell population before and after the initiation of the recruitment. In these cell lines, variation in telomere length can be monitored over a long induction time. The induction of ALT by recruitment of PML to telomeres implicates a fundamental role for PML in ALT (**Figure 31**).

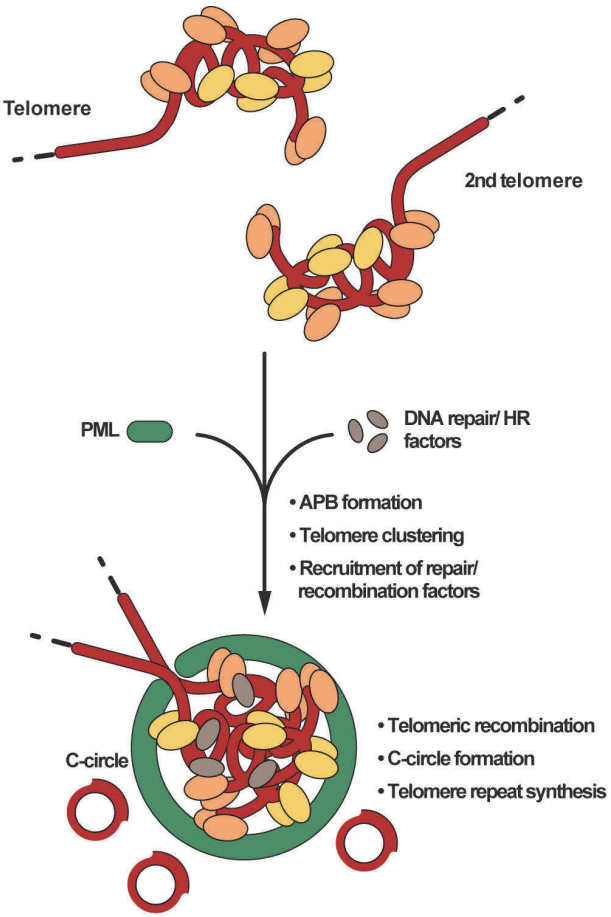

Figure 31. Model for ALT by homologous recombination in APBs.

The scheme shows a model for alternative lengthening of telomeres (ALT) by homologous recombination. PML forms APBs around telomeres leading to telomere clustering. Recruitment of factors involved in DNA repair and homologous recombination (HR) enables telomeric recombination resulting in the generation of C-circles and telomere elongation.

APBs might therefore not only be a characteristic hallmark of ALT-positive cells, but indeed essential for the organization of an environment that facilitates telomeric clustering and recombination. From quantification of the telomere repeat signal, it is not possible to asses if extrachromosomal telomeric

repeats accumulate in APBs and thus lead to an increase of the signal in addition to telomere clustering. However, it appears more likely that more than one telomere cluster together in APBs and that ECTRs, e.g. C-circles, join the ensemble. Since C-circle levels increased only 4 days after induction and telomere clustering was already observed after 24 h, generation of C-circles can be considered as a subsequent event, taking place after the formation of APBs and telomere clustering (**Figure 31**). One can imagine that C-circles are as well amplified by homologous recombination as chromosomal telomeres are, or that they result from trimming events, contributing to heterogeneous telomere length. In summary, these results show that PML recruitment to telomeres is sufficient to establish a setting that enables telomere clustering and subsequent generation of extrachromosomal telomeric repeats, and thus contribute to the understanding of ALT induction mechanisms.

In future experiments, it will be exciting to see if the combination with other factors will have an effect on ALT induction, even when its single perturbation did not show a change in TMM. Different scenarios can be imagined: (i) Overexpression of an ALT repressor in ALT-positive U2OS cells, e.g. ATRX. Since, *ATRX* is a recurrently mutated gene in ALT-positive tumors and most ALT cell lines lack ATRX, it is considered as an ALT repressor. In normal or telomerase-positive cells, ATRX has been observed to localize at PML-NBs, however the connection between APBs and ATRX remains elusive. The PML recruitment system could be combined with a re-activation of ATRX in ATRX-negative U2OS cells, already available in our group Deeg, 2015), to explore the effect on telomere lengthening. (ii) Depletion of an ALT repressor in telomerase-positive HeLa cells, e.g. ATRX or ASF1. ASF1 kd in HeLa cells with long telomeres results in rapid ALT induction, however if telomeres are short, no effect is observed. Therefore, it might be interesting to investigate the combination of PML recruitment with ASF1 kd in HeLa cells with short telomeres. (iii) Overexpression or co-recruitment of an ALT enhancer, e.g. BLM or WRN in telomerase-positive cells. Depletion of both BLM and WRN has been reported to block ALT induction by ASF1 kd in HeLa cells. Therefore, these proteins are considered as ALT enhancers and might facilitate ALT induction when overexpressed or recruited.

4 Conclusions

In this thesis, the approach depicted in **Figure 32** was advanced and applied, which consists of four major steps: (i) perturbation of TMM, (ii) bioinformatics analysis, including *TelNet*, (iii) prediction of factors and pathways that (anti-)correlate with the presence of ALT, and (iv) functional validation of predicted candidate genes. In the first step, ALT was perturbed in different cellular model systems to identify candidate genes with a potential role in the mechanisms of ALT induction or suppression (**Figure 32**). This was achieved by (i) treatment with the HDACi SAHA to suppress ALT, (ii) ALT induction by ASF1 depletion, and (iii) deletion of *EST2* in budding yeast cells to induce formation of ALT-like survivors. The next step comprised a differential gene expression analysis of perturbed vs unperturbed conditions that identified deregulated genes. To identify those deregulated genes linked to TM, the *TelNet* database developed in this thesis was applied. *TelNet* retrieves human and budding yeast genes with a reported role in TM via its list search tool (**Figure 32**). In addition, a conventional GO pathway analysis of the sets of deregulated genes associates them with pathways. From combined analysis novel ALT candidate genes and (anti-)correlated pathways are predicted, e.g. ***KCTD15*** and ***TNNC1*** as potential ALT enhancer genes that were upregulated upon ALT induction and/ or downregulated due to ALT suppression. In addition, an ALT enhancing role for proteins of the WNT family as well as TGFβ signaling was suggested as well as an ALT repressive role for NFκB/ p38 MAP kinase signaling (**Figure 32**). The final part of the workflow involves the further evaluation and validation of the novel genes and signaling pathways identified in this manner with respect to their ALT enhancing or repressive features. Knockdown of potential ALT enhancing proteins in combination with ASF1 kd might be suited to reveal a requirement of the protein for ALT induction. In addition, kd experiments in ALT-positive cell lines might result in the decrease of ALT markers. Another option is the protein overexpression in ALT-negative cell lines that might induce ALT features, but could also require the combination with another ALT enhancing factor, e.g. TERT inhibition or ASF1 depletion. A third option is the recruitment of the protein of interest to telomeres of telomerase-positive cells in order to measure ongoing ALT activity. This was demonstrated here for the essential APB component PML. Upon PML recruitment, telomeres clustered and subsequently extrachromosomal telomere repeats were generated, indicating the induction of ALT. This method can be combined with transient transfection of a protein of interest, tagged with a GFP-binder protein that is recruited to artificial APBs upon induction of TRF1-PML-GFP expression or to telomeres upon induction of TRF1-GFP (**Figure 32**). Follow-up experiments measuring ALT activity might confirm ALT enhancing features of candidate genes.

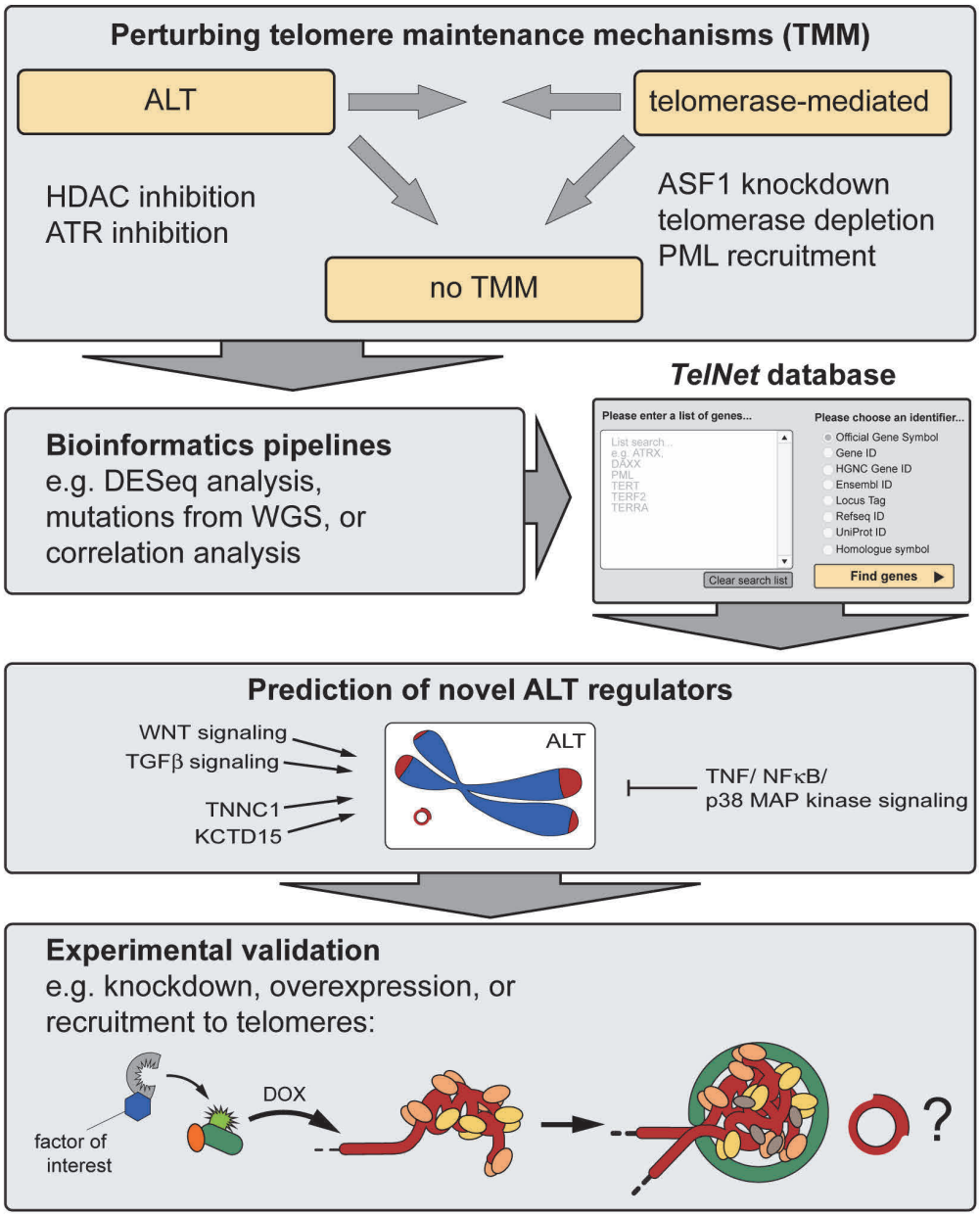

Figure 32. Workflow of strategies to investigate TMMs.

The workflow shows strategies to study ALT by perturbing TMMs. Comparing the original state with the perturbed state by bioinformatics pipelines generate gene lists reflecting e.g. differences in expression. The *TelNet* database can be used to identify known TMM genes. Next, a model for ALT can be developed that requires further validation experiments involving protein knockdown, overexpression, or recruitment to telomeres. A factor of interest tagged with a GFP-binder protein can be recruited to TRF1-PML-GFP, expressed upon DOX induction, and in turn to telomeres. Subsequent validation of induced ALT features will enable confirmation of an ALT enhancing phenotype.

Thus, the results obtained in this thesis provide new insight into gene networks that drive or suppress ALT. Identified candidate genes could represent putative novel drug targets specific for ALT tumor cells. Furthermore, it contributes to developing prognostic expression profiles for patient stratification into ALT-positive and ALT-negative groups. The latter is particularly relevant for several many tumor entities with a high incidence of ALT, e.g., leiomyosarcoma (53-78%) or pediatric glioblastoma (44%) that are often incurable or show a poor clinical outcome (Heaphy *et al.*, 2011b; Sturm *et al.*, 2014; Chudasama *et al.*, 2018; De Vitis *et al.*, 2018).

References

Aken BL, Ayling S, Barrell D, Clarke L, Curwen V, Fairley S, Fernandez Banet J, Billis K, Garcia Giron C, Hourlier T, Howe K, Kahari A, Kokocinski F, Martin FJ, Murphy DN, Nag R, Ruffier M, Schuster M, Tang YA, Vogel JH, White S, Zadissa A, Flicek P, and Searle SM (2016). The Ensembl gene annotation system. *Database (Oxford)* **2016**(baw093): 1-19.

Aken BL, Achuthan P, Akanni W, Amode MR, Bernsdorff F, Bhai J, Billis K, Carvalho-Silva D, Cummins C, Clapham P, Gil L, Giron CG, Gordon L, Hourlier T, Hunt SE, Janacek SH, Juettemann T, Keenan S, Laird MR, Lavidas I, Maurel T, McLaren W, Moore B, Murphy DN, Nag R, Newman V, Nuhn M, Ong CK, Parker A, Patricio M*, et al.* (2017). Ensembl 2017. *Nucleic Acids Res* **45**(D1): D635-D642.

Ali A, Zhang P, Liangfang Y, Wenshe S, Wang H, Lin X, Dai Y, Feng XH, Moses R, Wang D, Li X, and Xiao J (2015). KLF17 empowers TGF-beta/Smad signaling by targeting Smad3-dependent pathway to suppress tumor growth and metastasis during cancer progression. *Cell Death Dis* **6**(e1681): 1-13.

Arnoult N, Van Beneden A, and Decottignies A (2012). Telomere length regulates TERRA levels through increased trimethylation of telomeric H3K9 and HP1alpha. *Nat Struct Mol Biol* **19**(9): 948-56.

Askree SH, Yehuda T, Smolikov S, Gurevich R, Hawk J, Coker C, Krauskopf A, Kupiec M, and McEachern MJ (2004). A genome-wide screen for Saccharomyces cerevisiae deletion mutants that affect telomere length. *Proceedings of the National Academy of Sciences of the United States of America* **101**(23): 8658-63.

Aubert G, Hills M, and Lansdorp PM (2012). Telomere length measurement-Caveats and a critical assessment of the available technologies and tools. *Mutation Research/Fundamental and Molecular Mechanisms of Mutagenesis* **730**(1-2): 59-67.

Azzalin CM, Reichenbach P, Khoriauli L, Giulotto E, and Lingner J (2007). Telomeric repeat containing RNA and RNA surveillance factors at mammalian chromosome ends. *Science* **318**(5851): 798-801.

Bailey SM, Williams ES, Cornforth MN, and Goodwin EH (2010). Chromosome Orientation fluorescence in situ hybridization or strand-specific FISH. *Methods Mol Biol* **659** 173-83.

Balakrishnan R, Park J, Karra K, Hitz BC, Binkley G, Hong EL, Sullivan J, Micklem G, and Cherry JM (2012). YeastMine--an integrated data warehouse for Saccharomyces cerevisiae data as a multipurpose tool-kit. *Database (Oxford)* **2012**(bar062): 1-8.

Balk B, Maicher A, Dees M, Klermund J, Luke-Glaser S, Bender K, and Luke B (2013). Telomeric RNA-DNA hybrids affect telomere-length dynamics and senescence. *Nat Struct Mol Biol* **20**(10): 1199-205.

Barthel FP, Wei W, Tang M, Martinez-Ledesma E, Hu X, Amin SB, Akdemir KC, Seth S, Song X, Wang Q, Lichtenberg T, Hu J, Zhang J, Zheng S, and Verhaak RG (2017). Systematic analysis of telomere length and somatic alterations in 31 cancer types. *Nat Genet* **49**(3): 349-357.

Bechter OE, Zou Y, Walker W, Wright WE, and Shay JW (2004). Telomeric recombination in mismatch repair deficient human colon cancer cells after telomerase inhibition. *Cancer Res* **64**(10): 3444-51.

Beckers T, Burkhardt C, Wieland H, Gimmnich P, Ciossek T, Maier T, and Sanders K (2007). Distinct pharmacological properties of second generation HDAC inhibitors with the benzamide or hydroxamate head group. *Int J Cancer* **121**(5): 1138-48.

Beitzinger M, Oswald C, Beinoraviciute-Kellner R, and Stiewe T (2006). Regulation of telomerase activity by the p53 family member p73. *Oncogene* **25**(6): 813-26.

Bender S, Tang Y, Lindroth AM, Hovestadt V, Jones DT, Kool M, Zapatka M, Northcott PA, Sturm D, Wang W, Radlwimmer B, Hojfeldt JW, Truffaux N, Castel D, Schubert S, Ryzhova M, Seker-Cin H, Gronych J, Johann PD, Stark S, Meyer J, Milde T, Schuhmann M, Ebinger M, Monoranu CM, Ponnuswami A, Chen S, Jones C, Witt O, Collins VP*, et al.* (2013). Reduced H3K27me3 and DNA hypomethylation are major drivers of gene expression in K27M mutant pediatric high-grade gliomas. *Cancer Cell* **24**(5): 660-72.

Bhattacharyya S, Keirsey J, Russell B, Kavecansky J, Lillard-Wetherell K, Tahmaseb K, Turchi JJ, and Groden J (2009). Telomerase-associated protein 1, HSP90, and topoisomerase IIalpha associate directly with the BLM helicase in immortalized cells using ALT and modulate its helicase activity using telomeric DNA substrates. *Journal of Biological Chemistry* **284**(22): 14966-77.

Blackburn E (1991). Structure and function of telomeres. *Nature* **350** 569-573.

Blackburn EH (1984). The molecular structure of centromeres and telomeres. *Annu Rev Biochem* **53** 163-94.

Blackburn EH (1990). Telomeres: structure and synthesis. *Journal of Biological Chemistry* **265**(11): 5919-21.

Blasco MA (2007). The epigenetic regulation of mammalian telomeres. *Nat Rev Genet* **8**(4): 299-309.

Boisvert FM, Hendzel MJ, and Bazett-Jones DP (2000). Promyelocytic leukemia (PML) nuclear bodies are protein structures that do not accumulate RNA. *J Cell Biol* **148**(2): 283-292.

Brand P, Lenser T, and Hemmerich P (2010). Assembly dynamics of PML nuclear bodies in living cells. *PMC Biophys* **3**(3): 1-15.

Braun DM, Chung I, Kepper N, Deeg KI, and Rippe K (2018). TelNet – a database of human and yeast genes involved in telomere maintenance. *BMC Genetics* **19**(32): 1-10.

Bryan TM, Englezou A, Gupta J, Bacchetti S, and Reddel RR (1995). Telomere elongation in immortal human cells without detectable telomerase activity. *EMBO J* **14**(17): 4240-8.

Bryan TM, Englezou A, Dalla-Pozza L, Dunham MA, and Reddel RR (1997). Evidence for an alternative mechanism for maintaining telomere length in human tumors and tumor-derived cell lines. *Nat Med* **3**(11): 1271-4.

Bryan TM, and Reddel RR (1997). Telomere dynamics and telomerase activity in in vitro immortalised human cells. *Eur J Cancer* **33**(5): 767-73.

Cassar L, Nicholls C, Pinto AR, Chen R, Wang L, Li H, and Liu JP (2017). TGF-beta receptor mediated telomerase inhibition, telomere shortening and breast cancer cell senescence. *Protein Cell* **8**(1): 39-54.

Cerone MA, Londono-Vallejo JA, and Bacchetti S (2001). Telomere maintenance by telomerase and by recombination can coexist in human cells. *Hum Mol Genet* **10**(18): 1945-52.

Cerone MA, Autexier C, Londono-Vallejo JA, and Bacchetti S (2005). A human cell line that maintains telomeres in the absence of telomerase and of key markers of ALT. *Oncogene* **24**(53): 7893-901.

Cerone MA, Burgess DJ, Naceur-Lombardelli C, Lord CJ, and Ashworth A (2011). High-Throughput RNAi Screening Reveals Novel Regulators of Telomerase. *Cancer research* **71**(9): 3328-40.

Cesare AJ, Kaul Z, Cohen SB, Napier CE, Pickett HA, Neumann AA, and Reddel RR (2009). Spontaneous occurrence of telomeric DNA damage response in the absence of chromosome fusions. *Nat Struct Mol Biol* **16**(12): 1244-51.

Cesare AJ, and Reddel RR (2010). Alternative lengthening of telomeres: models, mechanisms and implications. *Nat Rev Genet* **11**(5): 319-30.

Cesare AJ, Hayashi MT, Crabbe L, and Karlseder J (2013). The telomere deprotection response is functionally distinct from the genomic DNA damage response. *Mol Cell* **51**(2): 141-55.

Chan SW, and Blackburn EH (2002). New ways not to make ends meet: telomerase, DNA damage proteins and heterochromatin. *Oncogene* **21**(4): 553-63.

Chang HR, Munkhjargal A, Kim MJ, Park SY, Jung E, Ryu JH, Yang Y, Lim JS, and Kim Y (2017). The functional roles of PML nuclear bodies in genome maintenance. *Mutat Res* **809** 99-107.

Chang S, Khoo CM, Naylor ML, Maser RS, and DePinho RA (2003). Telomere-based crisis: functional differences between telomerase activation and ALT in tumor progression. *Genes Dev* **17**(1): 88-100.

Chen Q, Ijpma A, and Greider CW (2001). Two survivor pathways that allow growth in the absence of telomerase are generated by distinct telomere recombination events. *Molecular and Cellular Biology* **21**(5): 1819-1827.

Chen W, Chen SM, Yu Y, Xiao BK, Huang ZW, and Tao ZZ (2010). Telomerase inhibition alters telomere maintenance mechanisms in laryngeal squamous carcinoma cells. *J Laryngol Otol* **124**(7): 778-83.

Chen YA, Shen YL, Hsia HY, Tiang YP, Sung TL, and Chen LY (2017). Extrachromosomal telomere repeat DNA is linked to ALT development via cGAS-STING DNA sensing pathway. *Nat Struct Mol Biol* **24**(12): 1124-1131.

Cherry JM, Hong EL, Amundsen C, Balakrishnan R, Binkley G, Chan ET, Christie KR, Costanzo MC, Dwight SS, Engel SR, Fisk DG, Hirschman JE, Hitz BC, Karra K, Krieger CJ, Miyasato SR, Nash RS, Park J, Skrzypek MS, Simison M, Weng S, and Wong ED (2012). Saccharomyces Genome Database: the genomics resource of budding yeast. *Nucleic Acids Res* **40**(Database issue): D700-5.

Cherry JM (2015). The Saccharomyces Genome Database: A Tool for Discovery. *Cold Spring Harb Protoc* **2015**(12): 1033-6.

Chiappori AA, Kolevska T, Spigel DR, Hager S, Rarick M, Gadgeel S, Blais N, Von Pawel J, Hart L, Reck M, Bassett E, Burington B, and Schiller JH (2015). A randomized phase II study of the telomerase inhibitor imetelstat as maintenance therapy for advanced non-small-cell lung cancer. *Ann Oncol* **26**(2): 354-62.

Chin L, Artandi SE, Shen Q, Tam A, Lee SL, Gottlieb GJ, Greider CW, and DePinho RA (1999). p53 deficiency rescues the adverse effects of telomere loss and cooperates with telomere dysfunction to accelerate carcinogenesis. *Cell* **97**(4): 527-38.

Cho NW, Dilley RL, Lampson MA, and Greenberg RA (2014). Interchromosomal Homology Searches Drive Directional ALT Telomere Movement and Synapsis. *Cell* **159**(1): 108-121.

Chudasama P, Mughal SS, Sanders MA, Hubschmann D, Chung I, Deeg KI, Wong SH, Rabe S, Hlevnjak M, Zapatka M, Ernst A, Kleinheinz K, Schlesner M, Sieverling L, Klink B, Schrock E, Hoogenboezem RM, Kasper B, Heilig CE, Egerer G, Wolf S, von Kalle C, Eils R, Stenzinger A, Weichert W, Glimm H, Groschel S, Kopp HG, Omlor G, Lehner B*, et al.* (2018). Integrative genomic and transcriptomic analysis of leiomyosarcoma. *Nat Commun* **9**(144): 1-15.

Chung I, Leonhardt H, and Rippe K (2011). De novo assembly of a PML nuclear subcompartment occurs through multiple pathways and induces telomere elongation. *J Cell Sci* **124**(Pt 21): 3603-18.

Chung I, Osterwald S, Deeg KI, and Rippe K (2012). PML body meets telomere: the beginning of an ALTernate ending? *Nucleus* **3**(3): 263-75.

Clynes D, Jelinska C, Xella B, Ayyub H, Scott C, Mitson M, Taylor S, Higgs DR, and Gibbons RJ (2015). Suppression of the alternative lengthening of telomere pathway by the chromatin remodelling factor ATRX. *Nat Commun* **6**(7538): 1-11.

Conomos D, Pickett HA, and Reddel RR (2013). Alternative lengthening of telomeres: remodeling the telomere architecture. *Frontiers in oncology* **3**(27): 1-7.

Coordinators NR (2017). Database Resources of the National Center for Biotechnology Information. *Nucleic Acids Res* **45**(D1): D12-D17.

Counter CM, Hahn WC, Wei W, Caddle SD, Beijersbergen RL, Lansdorp PM, Sedivy JM, and Weinberg RA (1998). Dissociation among in vitro telomerase activity, telomere maintenance, and cellular immortalization. *Proc Natl Acad Sci U S A* **95**(25): 14723-8.

Cusanelli E, and Chartrand P (2015). Telomeric repeat-containing RNA TERRA: a noncoding RNA connecting telomere biology to genome integrity. *Front Genet* **6**(143): 1-9.

d'Adda di Fagagna F, Reaper PM, Clay-Farrace L, Fiegler H, Carr P, Von Zglinicki T, Saretzki G, Carter NP, and Jackson SP (2003). A DNA damage checkpoint response in telomere-initiated senescence. *Nature* **426**(6963): 194-8.

Dagg RA, Pickett HA, Neumann AA, Napier CE, Henson JD, Teber ET, Arthur JW, Reynolds CP, Murray J, Haber M, Sobinoff AP, Lau LMS, and Reddel RR (2017). Extensive Proliferation of Human Cancer Cells with Ever-Shorter Telomeres. *Cell Rep* **19**(12): 2544-2556.

Dantzer F, Giraud-Panis MJ, Jaco I, Ame JC, Schultz I, Blasco M, Koering CE, Gilson E, Menissier-de Murcia J, de Murcia G, and Schreiber V (2004). Functional interaction between poly(ADP-Ribose) polymerase 2 (PARP-2) and TRF2: PARP activity negatively regulates TRF2. *Mol Cell Biol* **24**(4): 1595-607.

Danussi C, Bose P, Parthasarathy PT, Silberman PC, Van Arnam JS, Vitucci M, Tang OY, Heguy A, Wang Y, Chan TA, Riggins GJ, Sulman EP, Lang F, Creighton CJ, Deneen B, Miller CR, Picketts DJ, Kannan K, and Huse JT (2018). ATRX inactivation drives disease-defining phenotypes in glioma cells of origin through global epigenomic remodeling. *Nat Commun* **9**(1057): 1-15.

de Lange T (2004). T-loops and the origin of telomeres. *Nat Rev Mol Cell Biol* **5**(4): 323-9.

de Lange T (2005a). Telomere-related genome instability in cancer. *Cold Spring Harbor symposia on quantitative biology* **70** 197-204.

de Lange T (2005b). Shelterin: the protein complex that shapes and safeguards human telomeres. *Genes & Development* **19**(18): 2100-10.

De Vitis M, Berardinelli F, and Sgura A (2018). Telomere Length Maintenance in Cancer: At the Crossroad between Telomerase and Alternative Lengthening of Telomeres (ALT). *Int J Mol Sci* **19**(2): 1-15.

Deeg KI (2015). Identifying drivers and suppressors of the alternative lengthening of telomeres pathway. *PhD thesis* under the supervision of Prof. Dr. Karsten Rippe at the Ruperto-Carola University, Heidelberg.

Deeg KI, Chung I, Bauer C, and Rippe K (2016). Cancer Cells with Alternative Lengthening of Telomeres Do Not Display a General Hypersensitivity to ATR Inhibition. *Frontiers in oncology* **6**(186): 1-7.

Deeg KI, Chung I, Poos AM, Braun DM, Korshunov A, Oswald M, Kepper N, Bender S, Castel D, Lichter P, Grill J, Pfister SM, König R, Jones DTW, and Rippe K (2017). Dissecting telomere maintenance mechanisms in pediatric glioblastoma. Preprint: *bioRxiv* 129106. doi: 10.1101/129106.

Dejardin J, and Kingston RE (2009). Purification of proteins associated with specific genomic Loci. *Cell* **136**(1): 175-86.

Dellaire G, and Bazett-Jones DP (2004). PML nuclear bodies: dynamic sensors of DNA damage and cellular stress. *Bioessays* **26**(9): 963-77.

Denchi EL, and de Lange T (2007). Protection of telomeres through independent control of ATM and ATR by TRF2 and POT1. *Nature* **448**(7157): 1068-71.

Dennis G, Jr., Sherman BT, Hosack DA, Yang J, Gao W, Lane HC, and Lempicki RA (2003). DAVID: Database for Annotation, Visualization, and Integrated Discovery. *Genome Biol* **4**(5): P3.

Dikmen ZG, Gellert GC, Jackson S, Gryaznov S, Tressler R, Dogan P, Wright WE, and Shay JW (2005). In vivo inhibition of lung cancer by GRN163L: a novel human telomerase inhibitor. *Cancer Research* **65**(17): 7866-7873.

Dilley RL, and Greenberg RA (2015). ALTernative Telomere Maintenance and Cancer. *Trends Cancer* **1**(2): 145-156.

Ding Z, Mangino M, Aviv A, Spector T, Durbin R, and Consortium UK (2014). Estimating telomere length from whole genome sequence data. *Nucleic Acids Res* **42**(9): e75.

Dmitriev PV, Petrov AV, and Dontsova OA (2003). Yeast telosome complex: components and their functions. *Biochemistry (Mosc)* **68**(7): 718-34.

Dobin A, Davis CA, Schlesinger F, Drenkow J, Zaleski C, Jha S, Batut P, Chaisson M, and Gingeras TR (2013). STAR: ultrafast universal RNA-seq aligner. *Bioinformatics* **29**(1): 15-21.

Doksani Y, and de Lange T (2016). Telomere-Internal Double-Strand Breaks Are Repaired by Homologous Recombination and PARP1/Lig3-Dependent End-Joining. *Cell Rep* **17**(6): 1646-1656.

Doloff JC, Waxman DJ, and Jounaidi Y (2008). Human telomerase reverse transcriptase promoter-driven oncolytic adenovirus with E1B-19 kDa and E1B-55 kDa gene deletions. *Hum Gene Ther* **19**(12): 1383-400.

Downey M, Houlsworth R, Maringele L, Rollie A, Brehme M, Galicia S, Guillard S, Partington M, Zubko MK, Krogan NJ, Emili A, Greenblatt JF, Harrington L, Lydall D, and Durocher D (2006). A genome-wide screen identifies the evolutionarily conserved KEOPS complex as a telomere regulator. *Cell* **124**(6): 1155-68.

Doyle KR, Mitchell MA, Roberts CL, James S, Johnson JE, Zhou Y, von Mehren M, Lev D, Kipling D, and Broccoli D (2012). Validating a gene expression signature proposed to differentiate liposarcomas that use different telomere maintenance mechanisms. *Oncogene* **31**(2): 265-6.

Draskovic I, Arnoult N, Steiner V, Bacchetti S, Lomonte P, and Londono-Vallejo A (2009). Probing PML body function in ALT cells reveals spatiotemporal requirements for telomere recombination. *Proc Natl Acad Sci U S A* **106**(37): 15726-31.

Dunham MA, Neumann AA, Fasching CL, and Reddel RR (2000). Telomere maintenance by recombination in human cells. *Nat Genet* **26**(4): 447-50.

Eckschlager T, Plch J, Stiborova M, and Hrabeta J (2017). Histone Deacetylase Inhibitors as Anticancer Drugs. *Int J Mol Sci* **18**(7): 1-25.

Episkopou H, Draskovic I, Van Beneden A, Tilman G, Mattiussi M, Gobin M, Arnoult N, Londono-Vallejo A, and Decottignies A (2014). Alternative Lengthening of Telomeres is characterized by reduced compaction of telomeric chromatin. *Nucleic Acids Res* **42**(7): 4391-405.

Fagerberg L, Hallstrom BM, Oksvold P, Kampf C, Djureinovic D, Odeberg J, Habuka M, Tahmasebpoor S, Danielsson A, Edlund K, Asplund A, Sjostedt E, Lundberg E, Szigyarto CA, Skogs M, Takanen JO, Berling H, Tegel H, Mulder J, Nilsson P, Schwenk JM, Lindskog C, Danielsson F, Mardinoglu A, Sivertsson A, von Feilitzen K, Forsberg M, Zwahlen M, Olsson I, Navani S*, et al.* (2014). Analysis of the human tissue-specific expression by genome-wide integration of transcriptomics and antibody-based proteomics. *Mol Cell Proteomics* **13**(2): 397-406.

Fagioli M, Alcalay M, Pandolfi PP, Venturini L, Mencarelli A, Simeone A, Acampora D, Grignani F, and Pelicci PG (1992). Alternative splicing of PML transcripts predicts coexpression of several carboxy-terminally different protein isoforms. *Oncogene* **7**(6): 1083-91.

Fairaq A, Goc A, Artham S, Sabbineni H, and Somanath PR (2015). TNFalpha induces inflammatory stress response in microvascular endothelial cells via Akt- and P38 MAP kinase-mediated thrombospondin-1 expression. *Molecular and Cellular Biochemistry* **406**(1-2): 227-36.

Falconer E, Chavez E, Henderson A, and Lansdorp PM (2010). Chromosome orientation fluorescence in situ hybridization to study sister chromatid segregation in vivo. *Nat Protoc* **5**(7): 1362-77.

Fan Q, Zhang F, Barrett B, Ren K, and Andreassen PR (2009). A role for monoubiquitinated FANCD2 at telomeres in ALT cells. *Nucleic Acids Research* **37**(6): 1740-54.

Fasching CL, Bower K, and Reddel RR (2005). Telomerase-independent telomere length maintenance in the absence of alternative lengthening of telomeres-associated promyelocytic leukemia bodies. *Cancer Res* **65**(7): 2722-9.

Fasching CL, Neumann AA, Muntoni A, Yeager TR, and Reddel RR (2007). DNA damage induces alternative lengthening of telomeres (ALT) associated promyelocytic leukemia bodies that preferentially associate with linear telomeric DNA. *Cancer Res* **67**(15): 7072-7.

Flynn RL, Cox KE, Jeitany M, Wakimoto H, Bryll AR, Ganem NJ, Bersani F, Pineda JR, Suva ML, Benes CH, Haber DA, Boussin FD, and Zou L (2015). Alternative lengthening of telomeres renders cancer cells hypersensitive to ATR inhibitors. *Science* **347**(6219): 273-7.

Fogal V, Gostissa M, Sandy P, Zacchi P, Sternsdorf T, Jensen K, Pandolfi PP, Will H, Schneider C, and Del Sal G (2000). Regulation of p53 activity in nuclear bodies by a specific PML isoform. *EMBO J* **19**(22): 6185-95.

Ford LP, Zou Y, Pongracz K, Gryaznov SM, Shay JW, and Wright WE (2001). Telomerase can inhibit the recombination-based pathway of telomere maintenance in human cells. *Journal of Biological Chemistry* **276**(34): 32198-203.

Friedrich U, Griese E, Schwab M, Fritz P, Thon K, and Klotz U (2000). Telomere length in different tissues of elderly patients. *Mech Ageing Dev* **119**(3): 89-99.

Frink RE, Peyton M, Schiller JH, Gazdar AF, Shay JW, and Minna JD (2016). Telomerase inhibitor imetelstat has preclinical activity across the spectrum of non-small cell lung cancer oncogenotypes in a telomere length dependent manner. *Oncotarget* **7**(22): 31639-51.

Galati A, Magdinier F, Colasanti V, Bauwens S, Pinte S, Ricordy R, Giraud-Panis MJ, Pusch MC, Savino M, Cacchione S, and Gilson E (2012). TRF2 controls telomeric nucleosome organization in a cell cycle phase-dependent manner. *PLoS ONE* **7**(4): 1-10.

Galati A, Micheli E, Alicata C, Ingegnere T, Cicconi A, Pusch MC, Giraud-Panis MJ, Gilson E, and Cacchione S (2015). TRF1 and TRF2 binding to telomeres is modulated by nucleosomal organization. *Nucleic Acids Res* **43**(12): 5824-37.

Gao B, Li K, Wei YY, Zhang J, Li J, Zhang L, Gao JP, Li YY, Huang LG, Lin P, and Wei YQ (2014). Zinc finger protein 637 protects cells against oxidative stress-induced premature senescence by mTERT-mediated telomerase activity and telomere maintenance. *Cell Death Dis* **5**(e1334): 1-13.

Gao H, Cervantes RB, Mandell EK, Otero JH, and Lundblad V (2007). RPA-like proteins mediate yeast telomere function. *Nat Struct Mol Biol* **14**(3): 208-14.

Garcia-Cao M, O'Sullivan R, Peters AH, Jenuwein T, and Blasco MA (2004). Epigenetic regulation of telomere length in mammalian cells by the Suv39h1 and Suv39h2 histone methyltransferases. *Nat Genet* **36**(1): 94-9.

Garcia-Exposito L, Bournique E, Bergoglio V, Bose A, Barroso-Gonzalez J, Zhang S, Roncaioli JL, Lee M, Wallace CT, Watkins SC, Opresko PL, Hoffmann JS, and O'Sullivan RJ (2016). Proteomic Profiling Reveals a Specific Role for Translesion DNA Polymerase eta in the Alternative Lengthening of Telomeres. *Cell Rep* **17**(7): 1858-1871.

Gatbonton T, Imbesi M, Nelson M, Akey JM, Ruderfer DM, Kruglyak L, Simon JA, and Bedalov A (2006). Telomere length as a quantitative trait: genome-wide survey and genetic mapping of telomere length-control genes in yeast. *PLoS Genet* **2**(3): 304-15.

Gene Ontology C (2015). Gene Ontology Consortium: going forward. *Nucleic Acids Res* **43**(Database issue): D1049-56.

Giannone RJ, McDonald HW, Hurst GB, Shen RF, Wang Y, and Liu Y (2010). The protein network surrounding the human telomere repeat binding factors TRF1, TRF2, and POT1. *PLoS ONE* **5**(8): 1-10.

Giraud-Panis MJ, Teixeira MT, Geli V, and Gilson E (2010). CST meets shelterin to keep telomeres in check. *Mol Cell* **39**(5): 665-76.

Gocha AR, Acharya S, and Groden J (2014). WRN loss induces switching of telomerase-independent mechanisms of telomere elongation. *PLoS ONE* **9**(4): 1-16.

Goldblatt EM, Gentry ER, Fox MJ, Gryaznov SM, Shen C, and Herbert BS (2009). The telomerase template antagonist GRN163L alters MDA-MB-231 breast cancer cell morphology, inhibits growth, and augments the effects of paclitaxel. *Mol Cancer Ther* **8**(7): 2027-35.

Gonzalo S, Garcia-Cao M, Fraga MF, Schotta G, Peters AH, Cotter SE, Eguia R, Dean DC, Esteller M, Jenuwein T, and Blasco MA (2005). Role of the RB1 family in stabilizing histone methylation at constitutive heterochromatin. *Nat Cell Biol* **7**(4): 420-8.

Gonzalo S, Jaco I, Fraga MF, Chen T, Li E, Esteller M, and Blasco MA (2006). DNA methyltransferases control telomere length and telomere recombination in mammalian cells. *Nature cell biology* **8**(4): 416-24.

Gotta M, Laroche T, Formenton A, Maillet L, Scherthan H, and Gasser SM (1996). The clustering of telomeres and colocalization with Rap1, Sir3, and Sir4 proteins in wild-type Saccharomyces cerevisiae. *J Cell Biol* **134**(6): 1349-63.

Goueli BS, and Janknecht R (2004). Upregulation of the Catalytic Telomerase Subunit by the Transcription Factor ER81 and Oncogenic HER2/Neu, Ras, or Raf. *Mol Cell Biol* **24**(1): 25-35.

Grandin N, Damon C, and Charbonneau M (2001a). Cdc13 prevents telomere uncapping and Rad50-dependent homologous recombination. *EMBO J* **20**(21): 6127-39.

Grandin N, Damon C, and Charbonneau M (2001b). Ten1 functions in telomere end protection and length regulation in association with Stn1 and Cdc13. *EMBO J* **20**(5): 1173-83.

Grant GD, Brooks L, 3rd, Zhang X, Mahoney JM, Martyanov V, Wood TA, Sherlock G, Cheng C, and Whitfield ML (2013). Identification of cell cycle-regulated genes periodically expressed in U2OS cells and their regulation by FOXM1 and E2F transcription factors. *Mol Biol Cell* **24**(23): 3634-50.

Greider CW, and Blackburn EH (1985). Identification of a specific telomere terminal transferase activity in Tetrahymena extracts. *Cell* **43**(2 Pt 1): 405-13.

Greider CW (1993). Telomerase and telomere-length regulation: lessons from small eukaryotes to mammals. *Cold Spring Harb Symp Quant Biol* **58** 719-23.

Griffith JD, Comeau L, Rosenfield S, Stansel RM, Bianchi A, Moss H, and de Lange T (1999). Mammalian telomeres end in a large duplex loop. *Cell* **97**(4): 503-14.

Grobelny JV, Kulp-McEliece M, and Broccoli D (2001). Effects of reconstitution of telomerase activity on telomere maintenance by the alternative lengthening of telomeres (ALT) pathway. *Hum Mol Genet* **10**(18): 1953-61.

Grolimund L, Aeby E, Hamelin R, Armand F, Chiappe D, Moniatte M, and Lingner J (2013). A quantitative telomeric chromatin isolation protocol identifies different telomeric states. *Nat Commun* **4**(2848): 1-12.

Grudic A, Jul-Larsen A, Haring SJ, Wold MS, Lonning PE, Bjerkvig R, and Boe SO (2007). Replication protein A prevents accumulation of single-stranded telomeric DNA in cells that use alternative lengthening of telomeres. *Nucleic Acids Res* **35**(21): 7267-78.

Guan D, and Kao HY (2015). The function, regulation and therapeutic implications of the tumor suppressor protein, PML. *Cell Biosci* **5**(60): 1-14.

Guo A, Salomoni P, Luo J, Shih A, Zhong S, Gu W, and Pandolfi PP (2000). The function of PML in p53-dependent apoptosis. *Nat Cell Biol* **2**(10): 730-6.

Hanahan D, and Weinberg RA (2000). The hallmarks of cancer. *Cell* **100**(1): 57-70.

Hanahan D, and Weinberg RA (2011). Hallmarks of cancer: the next generation. *Cell* **144**(5): 646-74.

Harley CB, Futcher AB, and Greider CW (1990). Telomeres shorten during ageing of human fibroblasts. *Nature* **345**(6274): 458-60.

Hayflick L (1965). The Limited in Vitro Lifetime of Human Diploid Cell Strains. *Exp Cell Res* **37** 614-36.

Heaphy CM, de Wilde RF, Jiao Y, Klein AP, Edil BH, Shi C, Bettegowda C, Rodriguez FJ, Eberhart CG, Hebbar S, Offerhaus GJ, McLendon R, Rasheed BA, He Y, Yan H, Bigner DD, Oba-Shinjo SM, Marie SK, Riggins GJ, Kinzler KW, Vogelstein B, Hruban RH, Maitra A, Papadopoulos N, and Meeker AK (2011a). Altered telomeres in tumors with ATRX and DAXX mutations. *Science* **333**(6041): 425.

Heaphy CM, Subhawong AP, Hong SM, Goggins MG, Montgomery EA, Gabrielson E, Netto GJ, Epstein JI, Lotan TL, Westra WH, Shih Ie M, Iacobuzio-Donahue CA, Maitra A, Li QK, Eberhart CG, Taube JM, Rakheja D, Kurman RJ, Wu TC, Roden RB, Argani P, De Marzo AM, Terracciano L, Torbenson M, and Meeker AK (2011b). Prevalence of the alternative lengthening of telomeres telomere maintenance mechanism in human cancer subtypes. *Am J Pathol* **179**(4): 1608-15.

Hemann MT, Strong MA, Hao LY, and Greider CW (2001). The shortest telomere, not average telomere length, is critical for cell viability and chromosome stability. *Cell* **107**(1): 67-77.

Henson JD, Hannay JA, McCarthy SW, Royds JA, Yeager TR, Robinson RA, Wharton SB, Jellinek DA, Arbuckle SM, Yoo J, Robinson BG, Learoyd DL, Stalley PD, Bonar SF, Yu D, Pollock RE, and Reddel RR (2005). A robust assay for alternative lengthening of telomeres in tumors shows the significance of alternative lengthening of telomeres in sarcomas and astrocytomas. *Clin Cancer Res* **11**(1): 217-25.

Henson JD, Cao Y, Huschtscha LI, Chang AC, Au AY, Pickett HA, and Reddel RR (2009). DNA C-circles are specific and quantifiable markers of alternative-lengthening-of-telomeres activity. *Nat Biotechnol* **27**(12): 1181-5.

Henson JD, and Reddel RR (2010). Assaying and investigating Alternative Lengthening of Telomeres activity in human cells and cancers. *FEBS Lett* **584**(17): 3800-11.

Henson JD, Lau LM, Koch S, Martin La Rotta N, Dagg RA, and Reddel RR (2017). The C-Circle Assay for alternative-lengthening-of-telomeres activity. *Methods* **114** 74-84.

Hirashima K, and Seimiya H (2015). Telomeric repeat-containing RNA/G-quadruplex-forming sequences cause genome-wide alteration of gene expression in human cancer cells in vivo. *Nucleic Acids Research* **43**(3): 2022-32.

Hochreiter AE, Xiao H, Goldblatt EM, Gryaznov SM, Miller KD, Badve S, Sledge GW, and Herbert BS (2006). Telomerase template antagonist GRN163L disrupts telomere maintenance, tumor growth, and metastasis of breast cancer. *Clin Cancer Res* **12**(10): 3184-92.

Hockemeyer D, Sfeir AJ, Shay JW, Wright WE, and de Lange T (2005). POT1 protects telomeres from a transient DNA damage response and determines how human chromosomes end. *EMBO J* **24**(14): 2667-78.

Hockemeyer D, Palm W, Else T, Daniels JP, Takai KK, Ye JZ, Keegan CE, de Lange T, and Hammer GD (2007). Telomere protection by mammalian Pot1 requires interaction with Tpp1. *Nat Struct Mol Biol* **14**(8): 754-61.

Hoffmeyer K, Raggioli A, Rudloff S, Anton R, Hierholzer A, Del Valle I, Hein K, Vogt R, and Kemler R (2012). Wnt/β-Catenin Signaling Regulates Telomerase in Stem Cells and Cancer Cells. *Science (New York, NY)* **336**(6088): 1549-1554.

Honda K, Yanai H, Negishi H, Asagiri M, Sato M, Mizutani T, Shimada N, Ohba Y, Takaoka A, Yoshida N, and Taniguchi T (2005). IRF-7 is the master regulator of type-I interferon-dependent immune responses. *Nature* **434**(7034): 772-7.

Hsieh MH, Tsai CH, Lin CC, Li TK, Hung TW, Chang LT, Hsin LW, and Teng SC (2015). Topoisomerase II inhibition suppresses the proliferation of telomerase-negative cancers. *Cell Mol Life Sci* **72**(9): 1825-37.

Hu J, Hwang SS, Liesa M, Gan B, Sahin E, Jaskelioff M, Ding Z, Ying H, Boutin AT, Zhang H, Johnson S, Ivanova E, Kost-Alimova M, Protopopov A, Wang YA, Shirihai OS, Chin L, and DePinho RA (2012). Antitelomerase therapy provokes ALT and mitochondrial adaptive mechanisms in cancer. *Cell* **148**(4): 651-63.

Hu Y, Tang HB, Liu NN, Tong XJ, Dang W, Duan YM, Fu XH, Zhang Y, Peng J, Meng FL, and Zhou JQ (2013). Telomerase-null survivor screening identifies novel telomere recombination regulators. *PLoS Genet* **9**(1): 1-17.

Hu Y, Shi G, Zhang L, Li F, Jiang Y, Jiang S, Ma W, Zhao Y, Songyang Z, and Huang J (2016). Switch telomerase to ALT mechanism by inducing telomeric DNA damages and dysfunction of ATRX and DAXX. *Sci Rep* **6**(32280): 1-10.

Huang C, Jia P, Chastain M, Shiva O, and Chai W (2017). The human CTC1/STN1/TEN1 complex regulates telomere maintenance in ALT cancer cells. *Exp Cell Res* **355**(2): 95-104.

Huang da W, Sherman BT, Stephens R, Baseler MW, Lane HC, and Lempicki RA (2008). DAVID gene ID conversion tool. *Bioinformation* **2**(10): 428-30.

Huang Z, Ma L, Wang Y, Pan Z, Ren J, Liu Z, and Xue Y (2015). MiCroKiTS 4.0: a database of midbody, centrosome, kinetochore, telomere and spindle. *Nucleic Acids Res* **43**(Database issue): D328-34.

Imai S, Armstrong CM, Kaeberlein M, and Guarente L (2000). Transcriptional silencing and longevity protein Sir2 is an NAD-dependent histone deacetylase. *Nature* **403**(6771): 795-800.

Jager K, and Walter M (2016). Therapeutic Targeting of Telomerase. *Genes (Basel)* **7**(7): 1-24.

Jamiruddin MR, Kaitsuka T, Hakim F, Fujimura A, Wei FY, Saitoh H, and Tomizawa K (2016). HDAC9 regulates the alternative lengthening of telomere (ALT) pathway via the formation of ALT-associated PML bodies. *Biochemical and Biophysical Research Communications* **481**(1-2): 25-30.

Jegou T, Chung I, Heuvelman G, Wachsmuth M, Gorisch SM, Greulich-Bode KM, Boukamp P, Lichter P, and Rippe K (2009). Dynamics of telomeres and promyelocytic leukemia nuclear bodies in a telomerase-negative human cell line. *Mol Biol Cell* **20**(7): 2070-82.

Jeitany M, Bakhos-Douaihy D, Silvestre DC, Pineda JR, Ugolin N, Moussa A, Gauthier LR, Busso D, Junier MP, Chneiweiss H, Chevillard S, Desmaze C, and Boussin FD (2017). Opposite effects of GCN5 and PCAF knockdowns on the alternative mechanism of telomere maintenance. *Oncotarget* **8**(16): 26269-26280.

Jensen K, Shiels C, and Freemont PS (2001). PML protein isoforms and the RBCC/TRIM motif. *Oncogene* **20**(49): 7223-33.

Jezek M, Gast A, Choi G, Kulkarni R, Quijote J, Graham-Yooll A, Park D, and Green EM (2017). The histone methyltransferases Set5 and Set1 have overlapping functions in gene silencing and telomere maintenance. *Epigenetics* **12**(2): 93-104.

Jia X, Weinert T, and Lydall D (2004). Mec1 and Rad53 inhibit formation of single-stranded DNA at telomeres of Saccharomyces cerevisiae cdc13-1 mutants. *Genetics* **166**(2): 753-64.

Jiang WQ, Zhong ZH, Henson JD, Neumann AA, Chang AC, and Reddel RR (2005). Suppression of alternative lengthening of telomeres by Sp100-mediated sequestration of the MRE11/RAD50/NBS1 complex. *Mol Cell Biol* **25**(7): 2708-21.

Jiang WQ, Zhong ZH, Henson JD, and Reddel RR (2007). Identification of candidate alternative lengthening of telomeres genes by methionine restriction and RNA interference. *Oncogene* **26**(32): 4635-4647.

Jiang WQ, Zhong ZH, Nguyen A, Henson JD, Toouli CD, Braithwaite AW, and Reddel RR (2009). Induction of alternative lengthening of telomeres-associated PML bodies by p53/p21 requires HP1 proteins. *J Cell Biol* **185**(5): 797-810.

Jiang WQ, Nguyen A, Cao Y, Chang AC, and Reddel RR (2011). HP1-mediated formation of alternative lengthening of telomeres-associated PML bodies requires HIRA but not ASF1a. *PLoS ONE* **6**(2): 1-12.

Johnson FB, Marciniak RA, McVey M, Stewart SA, Hahn WC, and Guarente L (2001). The Saccharomyces cerevisiae WRN homolog Sgs1p participates in telomere maintenance in cells lacking telomerase. *EMBO J* **20**(4): 905-13.

Jurgendohmen R (2004). SUMO protein modification. *Biochimica et Biophysica Acta (BBA) - Molecular Cell Research* **1695**(1-3): 113-131.

Kamitani T, Kito K, Nguyen HP, Wada H, Fukuda-Kamitani T, and Yeh ET (1998). Identification of three major sentrinization sites in PML. *Journal of Biological Chemistry* **273**(41): 26675-82.

Kim NW, Piatyszek MA, Prowse KR, Harley CB, West MD, Ho PL, Coviello GM, Wright WE, Weinrich SL, and Shay JW (1994). Specific association of human telomerase activity with immortal cells and cancer. *Science* **266**(5193): 2011-5.

Kimura M, Stone RC, Hunt SC, Skurnick J, Lu X, Cao X, Harley CB, and Aviv A (2010). Measurement of telomere length by the Southern blot analysis of terminal restriction fragment lengths. *Nat Protoc* **5**(9): 1596-607.

Konsoula R, and Jung M (2008). In vitro plasma stability, permeability and solubility of mercaptoacetamide histone deacetylase inhibitors. *Int J Pharm* **361**(1-2): 19-25.

Kumar M, Witt B, Knippschild U, Koch S, Meena JK, Heinlein C, Weise JM, Krepulat F, Kuchenbauer F, Iben S, Rudolph KL, Deppert W, and Gunes C (2013). CEBP factors regulate telomerase reverse transcriptase promoter activity in whey acidic protein-T mice during mammary carcinogenesis. *Int J Cancer* **132**(9): 2032-43.

Kupiec M (2014). Biology of telomeres: lessons from budding yeast. *FEMS Microbiology Reviews* **38**(2): 144-171.

Lafferty-Whyte K, Cairney CJ, Will MB, Serakinci N, Daidone MG, Zaffaroni N, Bilsland A, and Keith WN (2009). A gene expression signature classifying telomerase and ALT immortalization reveals an hTERT regulatory network and suggests a mesenchymal stem cell origin for ALT. *Oncogene* **28**(43): 3765-74.

Lafferty-Whyte K, Bilsland A, Hoare SF, Burns S, Zaffaroni N, Cairney CJ, and Keith WN (2010). TCEAL7 inhibition of c-Myc activity in alternative lengthening of telomeres regulates hTERT expression. *Neoplasia* **12**(5): 405-14.

Lai TP, Wright WE, and Shay JW (2018). Comparison of telomere length measurement methods. *Philos Trans R Soc Lond B Biol Sci* **373**(1741):

Lallemand-Breitenbach V, and de The H (2010). PML nuclear bodies. *Cold Spring Harb Perspect Biol* **2**(5): 1-17.

Lallemand-Breitenbach V, and de The H (2018). PML nuclear bodies: from architecture to function. *Curr Opin Cell Biol* **52** 154-161.

Lang M, Jegou T, Chung I, Richter K, Munch S, Udvarhelyi A, Cremer C, Hemmerich P, Engelhardt J, Hell SW, and Rippe K (2010). Three-dimensional organization of promyelocytic leukemia nuclear bodies. *J Cell Sci* **123**(Pt 3): 392-400.

Le S, Moore JK, Haber JE, and Greider CW (1999). RAD50 and RAD51 define two pathways that collaborate to maintain telomeres in the absence of telomerase. *Genetics* **152**(1): 143-52.

Lee OH, Kim H, He Q, Baek HJ, Yang D, Chen LY, Liang J, Chae HK, Safari A, Liu D, and Songyang Z (2011). Genome-wide YFP fluorescence complementation screen identifies new regulators for telomere signaling in human cells. *Mol Cell Proteomics* **10**(2): 1-11.

Lendvay TS, Morris DK, Sah J, Balasubramanian B, and Lundblad V (1996). Senescence mutants of Saccharomyces cerevisiae with a defect in telomere replication identify three additional EST genes. *Genetics* **144**(4): 1399-412.

Levy MZ, Allsopp RC, Futcher AB, Greider CW, and Harley CB (1992). Telomere end-replication problem and cell aging. *J MOL BIOL* **225**(4): 951-60.

Li AY, Lin HH, Kuo CY, Shih HM, Wang CC, Yen Y, and Ann DK (2011). High-mobility group A2 protein modulates hTERT transcription to promote tumorigenesis. *Mol Cell Biol* **31**(13): 2605-17.

Li B, Oestreich S, and de Lange T (2000). Identification of human Rap1: implications for telomere evolution. *Cell* **101**(5): 471-83.

Li C, Peng Q, Wan X, Sun H, and Tang J (2017). C-terminal motifs in promyelocytic leukemia protein isoforms critically regulate PML nuclear body formation. *J Cell Sci* **130**(20): 3496-3506.

Li H, Xu D, Li J, Berndt MC, and Liu JP (2006). Transforming growth factor beta suppresses human telomerase reverse transcriptase (hTERT) by Smad3 interactions with c-Myc and the hTERT gene. *Journal of Biological Chemistry* **281**(35): 25588-600.

Li H, Handsaker B, Wysoker A, Fennell T, Ruan J, Homer N, Marth G, Abecasis G, Durbin R, and Genome Project Data Processing S (2009). The Sequence Alignment/Map format and SAMtools. *Bioinformatics* **25**(16): 2078-9.

Li X, Chen C, Wang F, Huang W, Liang Z, Xiao Y, Wei K, Wan Z, Hu X, Xiang S, Ding X, and Zhang J (2014). KCTD1 suppresses canonical Wnt signaling pathway by enhancing beta-catenin degradation. *PLoS ONE* **9**(4): 1-12.

Li Y, and Tergaonkar V (2014). Noncanonical functions of telomerase: implications in telomerase-targeted cancer therapies. *Cancer Res* **74**(6): 1639-44.

Liou GG, Tanny JC, Kruger RG, Walz T, and Moazed D (2005). Assembly of the SIR complex and its regulation by O-acetyl-ADP-ribose, a product of NAD-dependent histone deacetylation. *Cell* **121**(4): 515-27.

Lippuner AD, Julou T, and Barral Y (2014). Budding yeast as a model organism to study the effects of age. *FEMS Microbiology Reviews* **38**(2): 300-325.

Liu D, O'Connor MS, Qin J, and Songyang Z (2004). Telosome, a mammalian telomere-associated complex formed by multiple telomeric proteins. *Journal of Biological Chemistry* **279**(49): 51338-42.

Liu-Chittenden Y, Jain M, Gaskins K, Wang S, Merino MJ, Kotian S, Kumar Gara S, Davis S, Zhang L, and Kebebew E (2017). RARRES2 functions as a tumor suppressor by promoting beta-catenin phosphorylation/degradation and inhibiting p38 phosphorylation in adrenocortical carcinoma. *Oncogene* **36**(25): 3541-3552.

Lombard DB, and Guarente L (2000). Nijmegen breakage syndrome disease protein and MRE11 at PML nuclear bodies and meiotic telomeres. *Cancer Res* **60**(9): 2331-4.

Londono-Vallejo JA, Der-Sarkissian H, Cazes L, Bacchetti S, and Reddel RR (2004). Alternative lengthening of telomeres is characterized by high rates of telomeric exchange. *Cancer research* **64**(7): 2324-7.

Lou Z, Wei J, Riethman H, Baur JA, Voglauer R, Shay JW, and Wright WE (2009). Telomere length regulates ISG15 expression in human cells. *Aging (Albany NY)* **1**(7): 608-21.

Love MI, Huber W, and Anders S (2014). Moderated estimation of fold change and dispersion for RNA-seq data with DESeq2. *Genome Biol* **15**(12): 1-21.

Lovejoy CA, Li W, Reisenweber S, Thongthip S, Bruno J, de Lange T, De S, Petrini JH, Sung PA, Jasin M, Rosenbluh J, Zwang Y, Weir BA, Hatton C, Ivanova E, Macconaill L, Hanna M, Hahn WC, Lue NF, Reddel RR, Jiao Y, Kinzler K, Vogelstein B, Papadopoulos N, Meeker AK, and Consortium ALTSC (2012). Loss of ATRX, genome instability, and an altered DNA damage response are hallmarks of the alternative lengthening of telomeres pathway. *PLoS Genet* **8**(7): 1-16.

Lu Y, Day FR, Gustafsson S, Buchkovich ML, Na J, Bataille V, Cousminer DL, Dastani Z, Drong AW, Esko T, Evans DM, Falchi M, Feitosa MF, Ferreira T, Hedman AK, Haring R, Hysi PG, Iles MM, Justice AE, Kanoni S, Lagou V, Li R, Li X, Locke A, Lu C, Magi R, Perry JR, Pers TH, Qi Q, Sanna M*, et al.* (2016). New loci for body fat percentage reveal link between adiposity and cardiometabolic disease risk. *Nat Commun* **7**(10495): 1-15.

Luke B, Panza A, Redon S, Iglesias N, Li Z, and Lingner J (2008). The Rat1p 5' to 3' exonuclease degrades telomeric repeat-containing RNA and promotes telomere elongation in Saccharomyces cerevisiae. *Molecular cell* **32**(4): 465-77.

Luke-Glaser S, Poschke H, and Luke B (2012). Getting in (and out of) the loop: regulating higher order telomere structures. *Frontiers in oncology* **2**(180): 1-6.

Lundblad V, and Szostak JW (1989). A mutant with a defect in telomere elongation leads to senescence in yeast. *Cell* **57**(4): 633-43.

Lundblad V, and Blackburn EH (1993). An alternative pathway for yeast telomere maintenance rescues est1-senescence. *Cell* **73**(2): 347-60.

Lundblad V (2002). Telomere maintenance without telomerase. *Oncogene* **21**(4): 522-31.

Luo Z, Dai Z, Xie X, Feng X, Liu D, Songyang Z, and Xiong Y (2015). TeloPIN: a database of telomeric proteins interaction network in mammalian cells. *Database (Oxford)* **2015**(0): 1-9.

Mac SM, D'Cunha CA, and Farnham PJ (2000). Direct recruitment of N-myc to target gene promoters. *Mol Carcinog* **29**(2): 76-86.

Maciejowski J, and de Lange T (2017). Telomeres in cancer: tumour suppression and genome instability. *Nat Rev Mol Cell Biol* **18**(3): 175-186.

Maekawa T, Liu B, Nakai D, Yoshida K, Nakamura KI, Yasukawa M, Koike M, Takubo K, Chatton B, Ishikawa F, Masutomi K, and Ishii S (2018). ATF7 mediates TNF-alpha-induced telomere shortening. *Nucleic Acids Res* **46**(9): 4487-4504.

Makarov VL, Hirose Y, and Langmore JP (1997). Long G tails at both ends of human chromosomes suggest a C strand degradation mechanism for telomere shortening. *Cell* **88**(5): 657-66.

Makovets S, Williams TL, and Blackburn EH (2008). The telotype defines the telomere state in Saccharomyces cerevisiae and is inherited as a dominant non-Mendelian characteristic in cells lacking telomerase. *Genetics* **178**(1): 245-257.

Marchesini M, Matocci R, Tasselli L, Cambiaghi V, OrlethOrleth A, Furia L, Marinelli C, Lombardi S, Sammarelli G, Aversa F, Minucci S, Faretta M, Pelicci PG, and Grignani F (2015). PML is required for telomere stability in non-neoplastic human cells. *Oncogene* **35**(14): 1811-21.

Marciniak RA, Cavazos D, Montellano R, Chen Q, Guarente L, and Johnson FB (2005). A novel telomere structure in a human alternative lengthening of telomeres cell line. *Cancer Res* **65**(7): 2730-7.

Marian CO, Cho SK, McEllin BM, Maher EA, Hatanpaa KJ, Madden CJ, Mickey BE, Wright WE, Shay JW, and Bachoo RM (2010). The telomerase antagonist, imetelstat, efficiently targets glioblastoma tumor-initiating cells leading to decreased proliferation and tumor growth. *Clin Cancer Res* **16**(1): 154-63.

Marzec P, Armenise C, Perot G, Roumelioti FM, Basyuk E, Gagos S, Chibon F, and Dejardin J (2015). Nuclear-receptor-mediated telomere insertion leads to genome instability in ALT cancers. *Cell* **160**(5): 913-27.

Mazumdar T, Sandhu R, Qadan M, DeVecchio J, Magloire V, Agyeman A, Li B, and Houghton JA (2013). Hedgehog signaling regulates telomerase reverse transcriptase in human cancer cells. *PLoS ONE* **8**(9): 1-10.

McKay SJ, and Cooke H (1992). hnRNP A2/B1 binds specifically to single stranded vertebrate telomeric repeat TTAGGGn. *Nucleic Acids Res* **20**(24): 6461-4.

Mender I, and Shay JW (2015). Telomerase Repeated Amplification Protocol (TRAP). *Bio Protoc* **5**(22): 1-8.

Meyne J, and Goodwin EH (1994). Strand-specific fluorescence in situ hybridization for determining orientation and direction of DNA sequences. *Methods Mol Biol* **33** 141-5.

Meyne J, and Moyzis RK (1994). In situ hybridization using synthetic oligomers as probes for centromere and telomere repeats. *Methods Mol Biol* **33** 63-74.

Min J, Wright WE, and Shay JW (2017). Alternative lengthening of telomeres can be maintained by preferential elongation of lagging strands. *Nucleic Acids Res* **45**(5): 2615-2628.

Mitsui Y, Hirata H, Arichi N, Hiraki M, Yasumoto H, Chang I, Fukuhara S, Yamamura S, Shahryari V, Deng G, Saini S, Majid S, Dahiya R, Tanaka Y, and Shiina H (2015). Inactivation of bone morphogenetic protein 2 may predict clinical outcome and poor overall survival for renal cell carcinoma through epigenetic pathways. *Oncotarget* **6**(11): 9577-91.

Mondello C, Petropoulou C, Monti D, Gonos ES, Franceschi C, and Nuzzo F (1999). Telomere length in fibroblasts and blood cells from healthy centenarians. *Exp Cell Res* **248**(1): 234-42.

Montpetit AJ, Alhareeri AA, Montpetit M, Starkweather AR, Elmore LW, Filler K, Mohanraj L, Burton CW, Menzies VS, Lyon DE, and Jackson-Cook CK (2014). Telomere length: a review of methods for measurement. *Nurs Res* **63**(4): 289-99.

Moran-Jones K, Wayman L, Kennedy DD, Reddel RR, Sara S, Snee MJ, and Smith R (2005). hnRNP A2, a potential ssDNA/RNA molecular adapter at the telomere. *Nucleic Acids Res* **33**(2): 486-96.

Moretti P, Freeman K, Coodly L, and Shore D (1994). Evidence that a complex of SIR proteins interacts with the silencer and telomere-binding protein RAP1. *Genes Dev* **8**(19): 2257-69.

Morin GB (1989). The human telomere terminal transferase enzyme is a ribonucleoprotein that synthesizes TTAGGG repeats. *Cell* **59**(3): 521-9.

Moyzis RK, Buckingham JM, Cram LS, Dani M, Deaven LL, Jones MD, Meyne J, Ratliff RL, and Wu JR (1988). A highly conserved repetitive DNA sequence, (TTAGGG)n, present at the telomeres of human chromosomes. *Proc Natl Acad Sci U S A* **85**(18): 6622-6.

Muller S, Matunis MJ, and Dejean A (1998). Conjugation with the ubiquitin-related modifier SUMO-1 regulates the partitioning of PML within the nucleus. *Embo J* **17**(1): 61-70.

Munoz P, Blanco R, de Carcer G, Schoeftner S, Benetti R, Flores JM, Malumbres M, and Blasco MA (2009). TRF1 controls telomere length and mitotic fidelity in epithelial homeostasis. *Mol Cell Biol* **29**(6): 1608-25.

Nabetani A, Yokoyama O, and Ishikawa F (2004). Localization of hRad9, hHus1, hRad1, and hRad17 and caffeine-sensitive DNA replication at the alternative lengthening of telomeres-associated promyelocytic leukemia body. *Journal of Biological Chemistry* **279**(24): 25849-57.

Nabetani A, and Ishikawa F (2011). Alternative lengthening of telomeres pathway: recombination-mediated telomere maintenance mechanism in human cells. *J Biochem* **149**(1): 5-14.

Naderlinger E, and Holzmann K (2017). Epigenetic Regulation of Telomere Maintenance for Therapeutic Interventions in Gliomas. *Genes (Basel)* **8**(5): 1-22.

Napier CE, Huschtscha LI, Harvey A, Bower K, Noble JR, Hendrickson EA, and Reddel RR (2015). ATRX represses alternative lengthening of telomeres. *Oncotarget* **6**(18): 16543-58.

Nera B, Huang HS, Lai T, and Xu L (2015). Elevated levels of TRF2 induce telomeric ultrafine anaphase bridges and rapid telomere deletions. *Nat Commun* **6**(10132): 1-11.

Nisole S, Maroui MA, Mascle XH, Aubry M, and Chelbi-Alix MK (2013). Differential Roles of PML Isoforms. *Frontiers in oncology* **3** 1-17.

O'Sullivan RJ, and Almouzni G (2014). Assembly of telomeric chromatin to create ALTernative endings. *Trends Cell Biol* **24**(11): 675-685.

O'Sullivan RJ, Arnoult N, Lackner DH, Oganesian L, Haggblom C, Corpet A, Almouzni G, and Karlseder J (2014). Rapid induction of alternative lengthening of telomeres by depletion of the histone chaperone ASF1. *Nat Struct Mol Biol* **21**(2): 167-74.

Oh W, Ghim J, Lee EW, Yang MR, Kim ET, Ahn JH, and Song J (2009). PML-IV functions as a negative regulator of telomerase by interacting with TERT. *J Cell Sci* **122**(Pt 15): 2613-22.

Olovnikov AM (1973). A theory of marginotomy. The incomplete copying of template margin in enzymic synthesis of polynucleotides and biological significance of the phenomenon. *J Theor Biol* **41**(1): 181-90.

Osterwald S (2012). Dissecting the alternative lengthening of telomeres pathway in human cancer cells using a high-content confocal microscopy screening approach. *PhD thesis* under the supervision of Prof. Dr. Karsten Rippe at the Ruperto-Carola University, Heidelberg.

Osterwald S, Wörz S, Reymann J, Sieckmann F, Rohr K, Erfle H, and Rippe K (2012). A three-dimensional colocalization RNA interference screening platform to elucidate the alternative lengthening of telomeres pathway. *Biotechnol J* **7**(1): 103-16.

Osterwald S, Deeg KI, Chung I, Parisotto D, Wörz S, Rohr K, Erfle H, and Rippe K (2015). PML induces compaction, TRF2 depletion and DNA damage signaling at telomeres and promotes their alternative lengthening. *J Cell Sci* **128**(10): 1887-900.

Palm W, and de Lange T (2008). How shelterin protects mammalian telomeres. *Annu Rev Genet* **42** 301-34.

Park JI, Venteicher AS, Hong JY, Choi J, Jun S, Shkreli M, Chang W, Meng Z, Cheung P, Ji H, McLaughlin M, Veenstra TD, Nusse R, McCrea PD, and Artandi SE (2009). Telomerase modulates Wnt signalling by association with target gene chromatin. *Nature* **460**(7251): 66-72.

Pascolo E, Wenz C, Lingner J, Hauel N, Priepke H, Kauffmann I, Garin-Chesa P, Rettig WJ, Damm K, and Schnapp A (2002). Mechanism of human telomerase inhibition by BIBR1532, a synthetic, non-nucleosidic drug candidate. *Journal of Biological Chemistry* **277**(18): 15566-72.

Pearson M, Carbone R, Sebastiani C, Cioce M, Fagioli M, Saito S, Higashimoto Y, Appella E, Minucci S, Pandolfi PP, and Pelicci PG (2000). PML regulates p53 acetylation and premature senescence induced by oncogenic Ras. *Nature* **406**(6792): 207-10.

Peradziryi H, Kaplan NA, Podleschny M, Liu X, Wehner P, Borchers A, and Tolwinski NS (2011). PTK7/Otk interacts with Wnts and inhibits canonical Wnt signalling. *EMBO J* **30**(18): 3729-40.

Perrem K, Bryan TM, Englezou A, Hackl T, Moy EL, and Reddel RR (1999). Repression of an alternative mechanism for lengthening of telomeres in somatic cell hybrids. *Oncogene* **18**(22): 3383-90.

Perrem K, Colgin LM, Neumann AA, Yeager TR, and Reddel RR (2001). Coexistence of alternative lengthening of telomeres and telomerase in hTERT-transfected GM847 cells. *Mol Cell Biol* **21**(12): 3862-75.

Pickett HA, Cesare AJ, Johnston RL, Neumann AA, and Reddel RR (2009). Control of telomere length by a trimming mechanism that involves generation of t-circles. *EMBO J* **28**(7): 799-809.

Pickett HA, and Reddel RR (2015). Molecular mechanisms of activity and derepression of alternative lengthening of telomeres. *Nat Struct Mol Biol* **22**(11): 875-80.

Podlevsky JD, Bley CJ, Omana RV, Qi X, and Chen JJ (2008). The telomerase database. *Nucleic Acids Res* **36**(Database issue): D339-43.

Poon SS, Martens UM, Ward RK, and Lansdorp PM (1999). Telomere length measurements using digital fluorescence microscopy. *Cytometry* **36**(4): 267-78.

Poon SS, and Lansdorp PM (2001). Quantitative fluorescence in situ hybridization (Q-FISH). *Curr Protoc Cell Biol* **12**(1): 18.4.1-18.4.21.

Potts PR, and Yu H (2007). The SMC5/6 complex maintains telomere length in ALT cancer cells through SUMOylation of telomere-binding proteins. *Nat Struct Mol Biol* **14**(7): 581-90.

Potts PR (2009). The Yin and Yang of the MMS21-SMC5/6 SUMO ligase complex in homologous recombination. *DNA Repair (Amst)* **8**(4): 499-506.

Quinlan AR, and Hall IM (2010). BEDTools: a flexible suite of utilities for comparing genomic features. *Bioinformatics* **26**(6): 841-2.

Racek T, Mise N, Li Z, Stoll A, and Putzer BM (2005). C-terminal p73 isoforms repress transcriptional activity of the human telomerase reverse transcriptase (hTERT) promoter. *Journal of Biological Chemistry* **280**(49): 40402-5.

Rahman R, and Grundy R (2011). Histone deacetylase inhibition as an anticancer telomerase-targeting strategy. *Int J Cancer* **129**(12): 2765-74.

Ramlee MK, Wang J, Toh WX, and Li S (2016). Transcription Regulation of the Human Telomerase Reverse Transcriptase (hTERT) Gene. *Genes* **7**(8): 1-43.

Reimand J, Vaquerizas JM, Todd AE, Vilo J, and Luscombe NM (2010). Comprehensive reanalysis of transcription factor knockout expression data in Saccharomyces cerevisiae reveals many new targets. *Nucleic Acids Res* **38**(14): 4768-77.

Reineke EL, and Kao HY (2009). PML: An emerging tumor suppressor and a target with therapeutic potential. *Cancer Ther* **7**(A): 219-226.

Reymond A, Meroni G, Fantozzi A, Merla G, Cairo S, Luzi L, Riganelli D, Zanaria E, Messali S, Cainarca S, Guffanti A, Minucci S, Pelicci PG, and Ballabio A (2001). The tripartite motif family identifies cell compartments. *EMBO J* **20**(9): 2140-51.

Richon VM, Sandhoff TW, Rifkind RA, and Marks PA (2000). Histone deacetylase inhibitor selectively induces p21WAF1 expression and gene-associated histone acetylation. *Proceedings of the National Academy of Sciences of the USA* **97**(18): 10014-10019.

Rippe K, and Luke B (2015). TERRA and the state of the telomere. *Nat Struct Mol Biol* **22**(11): 853-8.

Robin JD, Ludlow AT, Batten K, Magdinier F, Stadler G, Wagner KR, Shay JW, and Wright WE (2014). Telomere position effect: regulation of gene expression with progressive telomere shortening over long distances. *Genes Dev* **28**(22): 2464-76.

Robinson JT, Thorvaldsdottir H, Winckler W, Guttman M, Lander ES, Getz G, and Mesirov JP (2011). Integrative genomics viewer. *Nat Biotechnol* **29**(1): 24-6.

Rojas A, Meherem S, Kim YH, Washington MK, Willis JE, Markowitz SD, and Grady WM (2008). The aberrant methylation of TSP1 suppresses TGF-beta1 activation in colorectal cancer. *Int J Cancer* **123**(1): 14-21.

Romaniuk A, Kopczynski P, Ksiazek K, and Rubis B (2014). Telomerase modulation in therapeutic approach. *Curr Pharm Des* **20**(41): 6438-51.

Root H, Larsen A, Komosa M, Al-Azri F, Li R, Bazett-Jones DP, and Stephen Meyn M (2016). FANCD2 limits BLM-dependent telomere instability in the alternative lengthening of telomeres pathway. *Hum Mol Genet* **25**(15): 3255-3268.

Roth A, Harley CB, and Baerlocher GM (2010). Imetelstat (GRN163L)--telomerase-based cancer therapy. *Recent Results Cancer Res* **184**(0080-0015 (Print)): 221-34.

Rothbauer U, Zolghadr K, Tillib S, Nowak D, Schermelleh L, Gahl A, Backmann N, Conrath K, Muyldermans S, Cardoso MC, and Leonhardt H (2006). Targeting and tracing antigens in live cells with fluorescent nanobodies. *Nature methods* **3**(11): 887-9.

Rousseau P, and Autexier C (2015). Telomere biology: Rationale for diagnostics and therapeutics in cancer. *RNA Biol* **12**(10): 1078-82.

Sahin U, Lallemand-Breitenbach V, and de The H (2014). PML nuclear bodies: regulation, function and therapeutic perspectives. *The Journal of pathology* **234**(3): 289-91.

Salloum R, Hummel TR, Kumar SS, Dorris K, Li S, Lin T, Daryani VM, Stewart CF, Miles L, Poussaint TY, Stevenson C, Goldman S, Dhall G, Packer R, Fisher P, Pollack IF, Fouladi M, Boyett J, and Drissi R (2016). A molecular biology and phase II study of imetelstat (GRN163L) in children with recurrent or refractory central nervous system malignancies: a pediatric brain tumor consortium study. *J Neurooncol* **129**(3): 443-451.

Saretzki G, and Von Zglinicki T (2002). Replicative aging, telomeres, and oxidative stress. *Ann N Y Acad Sci* **959** 24-9.

Schindelin J, Arganda-Carreras I, Frise E, Kaynig V, Longair M, Pietzsch T, Preibisch S, Rueden C, Saalfeld S, Schmid B, Tinevez JY, White DJ, Hartenstein V, Eliceiri K, Tomancak P, and Cardona A (2012). Fiji: an open-source platform for biological-image analysis. *Nat Methods* **9**(7): 676-82.

Schmitt ME, Brown TA, and Trumpower BL (1990). A rapid and simple method for preparation of RNA from Saccharomyces cerevisiae. *Nucleic Acids Res* **18**(10): 3091-2.

Schoeftner S, and Blasco MA (2008). Developmentally regulated transcription of mammalian telomeres by DNA-dependent RNA polymerase II. *Nat Cell Biol* **10**(2): 228-36.

Schwartzentruber J, Korshunov A, Liu XY, Jones DT, Pfaff E, Jacob K, Sturm D, Fontebasso AM, Quang DA, Tonjes M, Hovestadt V, Albrecht S, Kool M, Nantel A, Konermann C, Lindroth A, Jager N, Rausch T, Ryzhova M, Korbel JO, Hielscher T, Hauser P, Garami M, Klekner A, Bognar L, Ebinger M, Schuhmann MU, Scheurlen W, Pekrun A, Fruhwald MC, *et al.* (2012). Driver mutations in histone H3.3 and chromatin remodelling genes in paediatric glioblastoma. *Nature* **482**(7384): 226-31.

Shay JW, and Wright WE (1989). Quantitation of the frequency of immortalization of normal human diploid fibroblasts by SV40 large T-antigen. *Exp Cell Res* **184**(1): 109-18.

Shay JW, Reddel RR, and Wright WE (2012). Cancer. Cancer and telomeres--an ALTernative to telomerase. *Science* **336**(6087): 1388-90.

Shay JW (2016). Role of Telomeres and Telomerase in Aging and Cancer. *Cancer Discov* **6**(6): 584-93.

Shen TH, Lin HK, Scaglioni PP, Yung TM, and Pandolfi PP (2006). The mechanisms of PML-nuclear body formation. *Mol Cell* **24**(3): 331-9.

Shi T, Bunker RD, Mattarocci S, Ribeyre C, Faty M, Gut H, Scrima A, Rass U, Rubin SM, Shore D, and Thoma NH (2013). Rif1 and Rif2 shape telomere function and architecture through multivalent Rap1 interactions. *Cell* **153**(6): 1340-53.

Siddiqa A, Cavazos D, Chavez J, Long L, and Marciniak RA (2012). Modulation of telomeres in alternative lengthening of telomeres type I like human cells by the expression of werner protein and telomerase. *J Oncol* **2012** 806382.

Sieverling L, Hong C, Koser SD, Ginsbach P, Kleinheinz K, Hutter B, Braun DM, Cortes-Ciriano I, Xi R, Kabbe R, Park PJ, Eils R, Schlesner M, Rippe K, Jones DTW, Brors B, and Feuerbach L (2018). Genomic footprints of activated telomere maintenance mechanisms in cancer. *Nature communications, in press*. Preprint: *bioRxiv* 157560. doi: 10.1101/157560.

Silverman J, Takai H, Buonomo SB, Eisenhaber F, and de Lange T (2004). Human Rif1, ortholog of a yeast telomeric protein, is regulated by ATM and 53BP1 and functions in the S-phase checkpoint. *Genes Dev* **18**(17): 2108-19.

Smith RN, Aleksic J, Butano D, Carr A, Contrino S, Hu F, Lyne M, Lyne R, Kalderimis A, Rutherford K, Stepan R, Sullivan J, Wakeling M, Watkins X, and Micklem G (2012). InterMine: a flexible data warehouse system for the integration and analysis of heterogeneous biological data. *Bioinformatics* **28**(23): 3163-5.

Smith S, and de Lange T (1997). TRF1, a mammalian telomeric protein. *Trends Genet* **13**(1): 21-6.

Sobinoff AP, Allen JA, Neumann AA, Yang SF, Walsh ME, Henson JD, Reddel RR, and Pickett HA (2017). BLM and SLX4 play opposing roles in recombination-dependent replication at human telomeres. *EMBO J* **36**(19): 2907-2919.

Sobinoff AP, and Pickett HA (2017). Alternative Lengthening of Telomeres: DNA Repair Pathways Converge. *Trends Genet* **33**(12): 921-932.

Song J, Durrin LK, Wilkinson TA, Krontiris TG, and Chen Y (2004). Identification of a SUMO-binding motif that recognizes SUMO-modified proteins. *Proceedings of the National Academy of Sciences of the USA* **101**(40): 14373-8.

Spardy N, Duensing A, Hoskins EE, Wells SI, and Duensing S (2008). HPV-16 E7 reveals a link between DNA replication stress, fanconi anemia D2 protein, and alternative lengthening of telomere-associated promyelocytic leukemia bodies. *Cancer Res* **68**(23): 9954-63.

Stagno D'Alcontres M, Mendez-Bermudez A, Foxon JL, Royle NJ, and Salomoni P (2007). Lack of TRF2 in ALT cells causes PML-dependent p53 activation and loss of telomeric DNA. *J Cell Biol* **179**(5): 855-67.

Stavropoulos DJ, Bradshaw PS, Li X, Pasic I, Truong K, Ikura M, Ungrin M, and Meyn MS (2002). The Bloom syndrome helicase BLM interacts with TRF2 in ALT cells and promotes telomeric DNA synthesis. *Hum Mol Genet* **11**(25): 3135-44.

Strahl-Bolsinger S, Hecht A, Luo K, and Grunstein M (1997). SIR2 and SIR4 interactions differ in core and extended telomeric heterochromatin in yeast. *Genes Dev* **11**(1): 83-93.

Sturm D, Bender S, Jones DT, Lichter P, Grill J, Becher O, Hawkins C, Majewski J, Jones C, Costello JF, Iavarone A, Aldape K, Brennan CW, Jabado N, and Pfister SM (2014). Paediatric and adult glioblastoma: multiform (epi)genomic culprits emerge. *Nat Rev Cancer* **14**(2): 92-107.

Su ZZ, Lebedeva IV, Sarkar D, Gopalkrishnan RV, Sauane M, Sigmon C, Yacoub A, Valerie K, Dent P, and Fisher PB (2003). Melanoma differentiation associated gene-7, mda-7/IL-24, selectively induces growth suppression, apoptosis and radiosensitization in malignant gliomas in a p53-independent manner. *Oncogene* **22**(8): 1164-80.

Takai KK, Kibe T, Donigian JR, Frescas D, and de Lange T (2011). Telomere protection by TPP1/POT1 requires tethering to TIN2. *Mol Cell* **44**(4): 647-59.

Tao J, Zhou X, and Jiang Z (2016). cGAS-cGAMP-STING: The three musketeers of cytosolic DNA sensing and signaling. *IUBMB Life* **68**(11): 858-870.

Tarsounas M, Munoz P, Claas A, Smiraldo PG, Pittman DL, Blasco MA, and West SC (2004). Telomere maintenance requires the RAD51D recombination/repair protein. *Cell* **117**(3): 337-47.

Taylor EM, Copsey AC, Hudson JJ, Vidot S, and Lehmann AR (2008). Identification of the proteins, including MAGEG1, that make up the human SMC5-6 protein complex. *Mol Cell Biol* **28**(4): 1197-206.

Teixeira MC, Monteiro PT, Guerreiro JF, Goncalves JP, Mira NP, dos Santos SC, Cabrito TR, Palma M, Costa C, Francisco AP, Madeira SC, Oliveira AL, Freitas AT, and Sa-Correia I (2014). The YEASTRACT database: an upgraded information system for the analysis of gene and genomic transcription regulation in Saccharomyces cerevisiae. *Nucleic Acids Res* **42**(Database issue): D161-6.

Temime-Smaali N, Guittat L, Wenner T, Bayart E, Douarre C, Gomez D, Giraud-Panis MJ, Londono-Vallejo A, Gilson E, Amor-Gueret M, and Riou JF (2008). Topoisomerase IIIalpha is required for normal proliferation and telomere stability in alternative lengthening of telomeres. *EMBO J* **27**(10): 1513-24.

Teng SC, and Zakian VA (1999). Telomere-telomere recombination is an efficient bypass pathway for telomere maintenance in Saccharomyces cerevisiae. *Molecular and Cellular Biology* **19**(12): 8083-8093.

The UniProt C (2017). UniProt: the universal protein knowledgebase. *Nucleic Acids Res* **45**(D1): D158-D169.

Toh WH, Kyo S, and Sabapathy K (2005). Relief of p53-mediated telomerase suppression by p73. *Journal of Biological Chemistry* **280**(17): 17329-38.

Udugama M, FT MC, Chan FL, Tang MC, Pickett HA, JD RM, Mayne L, Collas P, Mann JR, and Wong LH (2015). Histone variant H3.3 provides the heterochromatic H3 lysine 9 tri-methylation mark at telomeres. *Nucleic Acids Res* **43**(21): 10227-37.

Uhlmann V, Prasad M, Silva I, Luettich K, Grande L, Alonso L, Thisted M, Pluzek KJ, Gorst J, Ring M, Sweeney M, Kenny C, Martin C, Russell J, Bermingham N, O'Donovan M, Sheils O, and O'Leary JJ (2000). Improved in situ detection method for telomeric tandem repeats in metaphase spreads and interphase nuclei. *Mol Pathol* **53**(1): 48-50.

Ungar L, Yosef N, Sela Y, Sharan R, Ruppin E, and Kupiec M (2009). A genome-wide screen for essential yeast genes that affect telomere length maintenance. *Nucleic Acids Research* **37**(12): 3840-9.

Uziel O, Yosef N, Sharan R, Ruppin E, Kupiec M, Kushnir M, Beery E, Cohen-Diker T, Nordenberg J, and Lahav M (2015). The effects of telomere shortening on cancer cells: a network model of proteomic and microRNA analysis. *Genomics* **105**(1): 5-16.

Valera E, Isaacs MJ, Kawakami Y, Izpisua Belmonte JC, and Choe S (2010). BMP-2/6 heterodimer is more effective than BMP-2 or BMP-6 homodimers as inductor of differentiation of human embryonic stem cells. *PLoS ONE* **5**(6): 1-14.

Van Damme E, Laukens K, Dang TH, and Van Ostade X (2010). A manually curated network of the PML nuclear body interactome reveals an important role for PML-NBs in SUMOylation dynamics. *Int J Biol Sci* **6**(1): 51-67.

van Steensel B, Smogorzewska A, and de Lange T (1998). TRF2 protects human telomeres from end-to-end fusions. *Cell* **92**(3): 401-13.

Verdun RE, Crabbe L, Haggblom C, and Karlseder J (2005). Functional human telomeres are recognized as DNA damage in G2 of the cell cycle. *Mol Cell* **20**(4): 551-61.

Voon HPJ, Collas P, and Wong LH (2016). Compromised Telomeric Heterochromatin Promotes ALTernative Lengthening of Telomeres. *Trends Cancer* **2**(3): 114-116.

Wei H, Wang N, Zhang Y, Wang S, Pang X, Zhang J, Luo Q, Su Y, and Zhang S (2014). Clinical significance of Wnt-11 and squamous cell carcinoma antigen expression in cervical cancer. *Med Oncol* **31**(933): 1-7.

Wellinger RJ, and Zakian VA (2012). Everything you ever wanted to know about Saccharomyces cerevisiae telomeres: beginning to end. *Genetics* **191**(4): 1073-105.

Wilson FR, Ho A, Walker JR, and Zhu XD (2016). Cdk-dependent phosphorylation regulates TRF1 recruitment to PML bodies and promotes C-circle production in ALT cells. *J Cell Sci* **129**(13): 2559-72.

Witt O, Milde T, Deubzer HE, Oehme I, Witt R, Kulozik A, Eisenmenger A, Abel U, and Karapanagiotou-Schenkel I (2012). Phase I/II intra-patient dose escalation study of vorinostat in children with relapsed solid tumor, lymphoma or leukemia. *Klin Padiatr* **224**(6): 398-403.

Wörz S, Sander P, Pfannmöller M, Rieker RJ, Joos S, Mechtersheimer G, Boukamp P, Lichter P, and Rohr K (2010). 3D Geometry-based quantification of colocalizations in multi-channel 3D microscopy images of human soft tissue tumors. *IEEE Trans on Medical Imaging* **29** 1474-1484.

Wright JH, Gottschling DE, and Zakian VA (1992). Saccharomyces telomeres assume a non-nucleosomal chromatin structure. *Genes Dev* **6**(2): 197-210.

Wright JH, and Zakian VA (1995). Protein-DNA interactions in soluble telosomes from Saccharomyces cerevisiae. *Nucleic Acids Res* **23**(9): 1454-60.

Wu G, Lee WH, and Chen PL (2000). NBS1 and TRF1 colocalize at promyelocytic leukemia bodies during late S/G2 phases in immortalized telomerase-negative cells. Implication of NBS1 in alternative lengthening of telomeres. *Journal of Biological Chemistry* **275**(39): 30618-22.

Wu G, Jiang X, Lee WH, and Chen PL (2003). Assembly of functional ALT-associated promyelocytic leukemia bodies requires Nijmegen Breakage Syndrome 1. *Cancer Res* **63**(10): 2589-95.

Wu P, Quan H, Kang J, He J, Luo S, Xie C, Xu J, Tang Y, and Zhao S (2017). Downregulation of Calcium-Binding Protein S100A9 Inhibits Hypopharyngeal Cancer Cell Proliferation and Invasion Ability Through Inactivation of NF-kappaB Signaling. *Oncol Res* **25**(9): 1479-1488.

Xi L, and Cech TR (2014). Inventory of telomerase components in human cells reveals multiple subpopulations of hTR and hTERT. *Nucleic Acids Res* **42**(13): 8565-77.

Xu Y, Wang X, Chen SM, Chen C, Wang Y, Xiao BK, and Tao ZZ (2016). Effect of silencing key proteins in telomerase mechanism and alternative lengthening of telomeres mechanism in laryngeal cancer cells. *Am J Otolaryngol* **37**(6): 552-558.

Xu Z, Duc KD, Holcman D, and Teixeira MT (2013). The length of the shortest telomere as the major determinant of the onset of replicative senescence. *Genetics* **194**(4): 847-57.

Yang TB, Chen Q, Deng JT, Jagannathan G, Tobias JW, Schultz DC, Wang S, Lengner CJ, Rustgi AK, Lynch JP, and Johnson FB (2017). Mutual reinforcement between telomere capping and canonical Wnt signalling in the intestinal stem cell niche. *Nat Commun* **8**(14766): 1-10.

Yankiwski V, Marciniak RA, Guarente L, and Neff NF (2000). Nuclear structure in normal and Bloom syndrome cells. *Proc Natl Acad Sci U S A* **97**(10): 5214-9.

Yates B, Braschi B, Gray KA, Seal RL, Tweedie S, and Bruford EA (2017). Genenames.org: the HGNC and VGNC resources in 2017. *Nucleic Acids Res* **45**(D1): D619-D625.

Ye JZ, Donigian JR, van Overbeek M, Loayza D, Luo Y, Krutchinsky AN, Chait BT, and de Lange T (2004). TIN2 binds TRF1 and TRF2 simultaneously and stabilizes the TRF2 complex on telomeres. *Journal of Biological Chemistry* **279**(45): 47264-71.

Yeager TR, Neumann AA, Englezou A, Huschtscha LI, Noble JR, and Reddel RR (1999). Telomerase-negative immortalized human cells contain a novel type of promyelocytic leukemia (PML) body. *Cancer Res* **59**(17): 4175-9.

Yong JW, Yeo X, Khan MM, Lee MB, and Hande MP (2012). Stable expression of promyelocytic leukaemia (PML) protein in telomerase positive MCF7 cells results in alternative lengthening of telomeres phenotype. *Genome Integr* **3**(5): 1-13.

Yoo YS, Park S, Gwak J, Ju BG, and Oh S (2015). Involvement of transcription repressor Snail in the regulation of human telomerase reverse transcriptase (hTERT) by transforming growth factor-beta. *Biochemical and Biophysical Research Communications* **465**(1): 131-6.

Yu J, Lan J, Wang C, Wu Q, Zhu Y, Lai X, Sun J, Jin C, and Huang H (2010). PML3 interacts with TRF1 and is essential for ALT-associated PML bodies assembly in U2OS cells. *Cancer Lett* **291**(2): 177-86.

Zarelli VE, and Dawid IB (2013). Inhibition of neural crest formation by Kctd15 involves regulation of transcription factor AP-2. *Proc Natl Acad Sci U S A* **110**(8): 2870-5.

Zeng S, Xiang T, Pandita TK, Gonzalez-Suarez I, Gonzalo S, Harris CC, and Yang Q (2009). Telomere recombination requires the MUS81 endonuclease. *Nat Cell Biol* **11**(5): 616-23.

Zhang Y, Cai L, Wei RX, Hu H, Jin W, and Zhu XB (2011). Different expression of alternative lengthening of telomere (ALT)-associated proteins/mRNAs in osteosarcoma cell lines. *Oncol Lett* **2**(6): 1327-1332.

Zhang Y, Toh L, Lau P, and Wang X (2012). Human telomerase reverse transcriptase (hTERT) is a novel target of the Wnt/beta-catenin pathway in human cancer. *Journal of Biological Chemistry* **287**(39): 32494-511.

Zhong S, Muller S, Ronchetti S, Freemont PS, Dejean A, and Pandolfi PP (2000). Role of SUMO-1-modified PML in nuclear body formation. *Blood* **95**(9): 2748-52.

Zhong ZH, Jiang WQ, Cesare AJ, Neumann AA, Wadhwa R, and Reddel RR (2007). Disruption of telomere maintenance by depletion of the MRE11/RAD50/NBS1 complex in cells that use alternative lengthening of telomeres. *Journal of Biological Chemistry* **282**(40): 29314-22.

Zhou X, Hao Q, Liao P, Luo S, Zhang M, Hu G, Liu H, Zhang Y, Cao B, Baddoo M, Flemington EK, Zeng SX, and Lu H (2016). Nerve growth factor receptor negates the tumor suppressor p53 as a feedback regulator. *eLife* **5**(e15099): 1-22.

Zhu J, Wang H, Bishop JM, and Blackburn EH (1999). Telomerase extends the lifespan of virus-transformed human cells without net telomere lengthening. *Proc Natl Acad Sci U S A* **96**(7): 3723-8.

Zhu XD, Kuster B, Mann M, Petrini JH, and de Lange T (2000). Cell-cycle-regulated association of RAD50/MRE11/NBS1 with TRF2 and human telomeres. *Nat Genet* **25**(3): 347-52.

Zhu XD, Niedernhofer L, Kuster B, Mann M, Hoeijmakers JH, and de Lange T (2003). ERCC1/XPF removes the 3' overhang from uncapped telomeres and represses formation of telomeric DNA-containing double minute chromosomes. *Mol Cell* **12**(6): 1489-98.

Zolghadr K, Mortusewicz O, Rothbauer U, Kleinhans R, Goehler H, Wanker EE, Cardoso MC, and Leonhardt H (2008). A fluorescent two-hybrid assay for direct visualization of protein interactions in living cells. *Mol Cell Proteomics* **7**(11): 2279-87.

Appendix

Suppl. table S1. Components of ALT-associated PML-NBs.

protein name (a)	localized at APBs in ALT-positive cells (b)	localized in PML-NBs (c)	localized at normal telomeres (d)	effect of APBs upon protein depletion/ knockdown (e)	effect of APBs upon overexpression/ recruitment (f)
ASF1A/ B				de novo APB formation (O'Sullivan *et al.*, 2014)	
ATM	yes (Stagno D'Alcontres *et al.*, 2007)	yes		no effect (Osterwald *et al.*, 2012; Flynn *et al.*, 2015; Osterwald *et al.*, 2015)	
ATR	yes (Fan *et al.*, 2009)	yes		no sign. effect (Osterwald *et al.*, 2015); decrease (Flynn *et al.*, 2015)	
BLM	yes (Yankiwski *et al.*, 2000; Stavropoulos *et al.*, 2002; Bhattacharyya *et al.*, 2009; O'Sullivan *et al.*, 2014; Osterwald *et al.*, 2015; Sobinoff *et al.*, 2017)	yes (Yankiwski *et al.*, 2000; Stavropoulos *et al.*, 2002)	no (Yankiwski *et al.*, 2000; Stavropoulos *et al.*, 2002)	decrease (Gocha *et al.*, 2014; Osterwald *et al.*, 2015)	overexpression leads to increase (Sobinoff *et al.*, 2017)
BRCA1	yes (Wu *et al.*, 2003; Gocha *et al.*, 2014)	no (Wu *et al.*, 2003)		no effect (Osterwald *et al.*, 2015)	
BRCA2 (aka FANCD1)	yes (Spardy *et al.*, 2008)				
CDK2	partly (Jiang *et al.*, 2009)			no effect (Osterwald *et al.*, 2015)	
CDKN1A (aka p21	partly (Jiang *et al.*, 2009)		no (Jiang *et al.*, 2009)	decrease (Osterwald *et al.*, 2015)	upregulation upon p53 activation leads to increase (Jiang *et al.*, 2009)
CTC1	yes (Huang *et al.*, 2017)		no (Huang *et al.*, 2017)	no effect (Huang *et al.*, 2017)	
DNA2				increase (O'Sullivan *et al.*, 2014)	
DNMT1				decrease (Osterwald *et al.*, 2015)	
ERCC1	yes (Nabetani *et al.*, 2004) (Zhu *et al.*, 2003)		yes (Zhu *et al.*, 2003)	no effect (Osterwald *et al.*, 2015)	
ERCC4 (aka XPF)	yes (Zhu *et al.*, 2003)		yes (Zhu *et al.*, 2003)	decrease (Osterwald *et al.*, 2015)	
EXO1				increase (O'Sullivan *et al.*, 2014)	
FANCA				no effect (Osterwald *et al.*, 2015)	
FANCD2	yes (Spardy *et al.*, 2008; Fan *et al.*, 2009; Root *et al.*, 2016)		no (Fan *et al.*, 2009)	increase (Osterwald *et al.*, 2015; Root *et al.*, 2016)	
FANCJ (aka BRIP1)	partly (Garcia-Exposito *et al.*, 2016)	no (Garcia-Exposito *et al.*, 2016)		no effect (Osterwald *et al.*, 2015)	
FANCL				increase (Osterwald *et al.*, 2015)	
FEN1				decrease (Osterwald *et al.*, 2015)	
HDAC7				decrease (Osterwald *et al.*, 2015)	
HDAC9				decrease (Jamiruddin *et al.*, 2016)	
HMGN5				increase (Osterwald *et al.*, 2015)	no *de novo* APB formation (telomeric sites) (Osterwald *et al.*, 2015)
hnRNP A2/B1	yes (Moran-Jones *et al.*, 2005)		yes (McKay & Cooke, 1992)		
HP1α (aka CBX1)	yes (Jiang *et al.*, 2009)	yes (Lang *et al.*, 2010)		no effect (Osterwald *et al.*, 2015); decrease (Jiang *et al.*, 2009)	

protein name (a)	localized at APBs in ALT-positive cells (b)	localized in PML-NBs (c)	localized at normal telomeres (d)	effect of APBs upon protein depletion/ knockdown (e)	effect of APBs upon overexpression/ recruitment (f)
HP1β (aka CBX3)	yes (Jiang *et al.*, 2009)			no effect (Osterwald *et al.*, 2015); decrease (Jiang *et al.*, 2009)	
HP1γ (aka CBX5)	yes (Jiang *et al.*, 2009)			decrease (Osterwald *et al.*, 2015); decrease (Jiang *et al.*, 2009)	*de novo* APB formation at telomeric sites (Osterwald *et al.*, 2015)
HSP90	yes (Bhattacharyya *et al.*, 2009)		no (Bhattacharyya *et al.*, 2009)		
HUS1	yes (Nabetani *et al.*, 2004)			no sign. effect (Osterwald *et al.*, 2015)	
KAT2A (aka GCN5)			yes (Jeitany *et al.*, 2017)	no effect (Jeitany *et al.*, 2017)	overexpression leads to decrease (Jeitany *et al.*, 2017)
KAT2B (aka PCAF)			no (Jeitany *et al.*, 2017)	decrease (Jeitany *et al.*, 2017)	
LSD1 (aka KDM1A)				decrease (Osterwald *et al.*, 2015)	
MDC1				no effect (Osterwald *et al.*, 2015)	
MORC3				decrease (Osterwald *et al.*, 2015)	
MRE11	yes (Zhu *et al.*, 2000; Spardy *et al.*, 2008; Cesare *et al.*, 2009)	yes (Lombard & Guarente, 2000)		decrease (Jiang *et al.*, 2007; Zhong *et al.*, 2007; O'Sullivan *et al.*, 2014); no sign. effect (Osterwald *et al.*, 2015)	
MUS81	yes (Spardy *et al.*, 2008; Zeng *et al.*, 2009)		no (Zeng *et al.*, 2009)	no effect (Osterwald *et al.*, 2015)	
NBS1 (aka NBN or p95)	yes (Wu *et al.*, 2000; Zhu *et al.*, 2000; Johnson *et al.*, 2001; Wu *et al.*, 2003; Cesare *et al.*, 2009; Wilson *et al.*, 2016)	no (Wu *et al.*, 2000)		decrease (Wu *et al.*, 2003; Jiang *et al.*, 2007; Zhong *et al.*, 2007); no effect (Osterwald *et al.*, 2015)	*de novo* APB(-like) formation at telomeric and pericentric sites (Chung *et al.*, 2011)
NR2C2	yes (Marzec *et al.*, 2015)			decrease (Osterwald *et al.*, 2015)	
NR2F1				no effect (Osterwald *et al.*, 2015)	
NR2F2	yes (Marzec *et al.*, 2015)			decrease (Osterwald *et al.*, 2015)	
NSMCE2 (aka MMS21)	yes (Potts & Yu, 2007; Chung *et al.*, 2011)	no (Potts & Yu, 2007)		decrease (Potts & Yu, 2007; Osterwald *et al.*, 2012; Osterwald *et al.*, 2015)	*de novo* APB(-like) formation at telomeric and pericentric sites (Chung *et al.*, 2011)
P300				decrease (Jeitany *et al.*, 2017)	
p53 (aka TP53)	partly (Stagno D'Alcontres *et al.*, 2007)			no effect (Osterwald *et al.*, 2015)	
PARP2	yes (Dantzer *et al.*, 2004)		no (Dantzer *et al.*, 2004)	decrease (Osterwald *et al.*, 2015)	
PCNA	yes (Jiang *et al.*, 2009)			no effect (Jiang *et al.*, 2009); increase (Osterwald *et al.*, 2015)	
PML	yes (Yeager *et al.*, 1999)	yes	no (Yeager *et al.*, 1999)	decrease (Jiang *et al.*, 2007; Osterwald *et al.*, 2012; O'Sullivan *et al.*, 2014; Osterwald *et al.*, 2015)	*de novo* APB(-like) formation at telomeric and pericentric sites (Chung *et al.*, 2011)
POLH (aka Pol η)	partly (Garcia-Exposito *et al.*, 2016)	no (Garcia-Exposito *et al.*, 2016)		increase (Garcia-Exposito *et al.*, 2016)	oe leads to decrease (Garcia-Exposito *et al.*, 2016)
POT1	yes (Temime-Smaali *et al.*, 2008)			increase (Osterwald *et al.*, 2015)	
RAD1	yes (Nabetani *et al.*, 2004)			no effect (Osterwald *et al.*, 2015)	
RAD17	yes (Nabetani *et al.*, 2004)	partly (Nabetani *et al.*, 2004)	no (Nabetani *et al.*, 2004)	no effect (Osterwald *et al.*, 2012; O'Sullivan *et al.*, 2014; Osterwald *et al.*, 2015)	no effect upon recruitment to telomeric or pericentric sites (Chung *et al.*, 2011)
RAD18	partly (Garcia-Exposito *et al.*, 2016)	no (Garcia-Exposito *et al.*, 2016)		increase (Garcia-Exposito *et al.*, 2016)	
RAD21	partly (Spardy *et al.*, 2008)				
RAD50	yes (Zhu *et al.*, 2000; Jiang *et al.*, 2007)			decrease (Jiang *et al.*, 2007) (Zhong *et al.*, 2007; Osterwald *et al.*, 2015)	

protein name (a)	localized at APBs in ALT-positive cells (b)	localized in PML-NBs (c)	localized at normal telomeres (d)	effect of APBs upon protein depletion/ knockdown (e)	effect of APBs upon overexpression/ recruitment (f)
RAD51	yes (Yeager *et al.*, 1999; Wu *et al.*, 2003; Tarsounas *et al.*, 2004)		yes (Tarsounas *et al.*, 2004)	no effect (Potts & Yu, 2007; Osterwald *et al.*, 2015); decrease (O'Sullivan *et al.*, 2014)	*de novo* APB formation at telomeric but not at sites) (Chung *et al.*, 2011)
RAD51D	yes (Tarsounas *et al.*, 2004)		yes (Tarsounas *et al.*, 2004)	no effect (Osterwald *et al.*, 2015)	
RAD52	yes (Yeager *et al.*, 1999)			no sign. effect (Osterwald *et al.*, 2015)	
RAD9	yes (Nabetani *et al.*, 2004)	no (Nabetani *et al.*, 2004)	no (Nabetani *et al.*, 2004)	no sign. effect (Osterwald *et al.*, 2015)	*de novo* APB formation at telomeric sites (Chung *et al.*, 2011)
RAP1	yes (Yeager *et al.*, 1999; Wu *et al.*, 2003; Cesare *et al.*, 2009; Wilson *et al.*, 2016)		yes	decrease (Jiang *et al.*, 2007)	
RBBP8 (aka CTIP)				decrease (O'Sullivan *et al.*, 2014)	
RIF1	yes (Silverman *et al.*, 2004)		no (Silverman *et al.*, 2004)	no effect (Osterwald *et al.*, 2015)	
RPA1	yes (Yeager *et al.*, 1999; Grudic *et al.*, 2007; Spardy *et al.*, 2008; Cesare *et al.*, 2009)	no (Yankiwski *et al.*, 2000; Grudic *et al.*, 2007)	no (Grudic *et al.*, 2007)	increase (Osterwald *et al.*, 2015)	
RPA2	yes (Yeager *et al.*, 1999; Grudic *et al.*, 2007; O'Sullivan *et al.*, 2014)	no (Yankiwski *et al.*, 2000; Grudic *et al.*, 2007)	no (Grudic *et al.*, 2007; O'Sullivan *et al.*, 2014)	increase (Osterwald *et al.*, 2015)	
SENP6				increase (Osterwald *et al.*, 2015)	
SLX4	yes (Sobinoff *et al.*, 2017)				overexpression leads to decrease (Sobinoff *et al.*, 2017)
SMC5	yes (Potts & Yu, 2007)	no (Potts & Yu, 2007)		decrease (Potts & Yu, 2007)	
SMC6	yes (Potts & Yu, 2007)	no (Potts & Yu, 2007)		decrease (Potts & Yu, 2007)	
SP100	yes (Chung *et al.*, 2011)	yes		no effect (Jiang *et al.*, 2007; Osterwald *et al.*, 2012; Osterwald *et al.*, 2015)	overexpression leads to a decrease in APBs (Jiang *et al.*, 2005)
STN1	yes (Huang *et al.*, 2017)		no (Huang *et al.*, 2017)	no effect (Osterwald *et al.*, 2015; Huang *et al.*, 2017)	
SUMO1	yes (Chung *et al.*, 2011)	yes (Muller *et al.*, 1998; Lang *et al.*, 2010)		decrease (Osterwald *et al.*, 2012; Osterwald *et al.*, 2015)	*de novo* APB formation at telomeric sites (Chung *et al.*, 2011)
SUMO2/3	yes (Chung *et al.*, 2011)	partly (Lang *et al.*, 2010)		decrease (Osterwald *et al.*, 2012; Osterwald *et al.*, 2015)	*de novo* APB formation at telomeric sites (Chung *et al.*, 2011)
SUV420H2				decrease (Osterwald *et al.*, 2015)	
TEP1	yes (Bhattacharyya *et al.*, 2009),		no (Bhattacharyya *et al.*, 2009)	no sign. effect (Osterwald *et al.*, 2015)	
TIN2	yes (Cesare *et al.*, 2009; Wilson *et al.*, 2016)		yes	decrease (Jiang *et al.*, 2007; Osterwald *et al.*, 2015)	
TOP2A	yes (Bhattacharyya *et al.*, 2009; Hsieh *et al.*, 2015)		no (Bhattacharyya *et al.*, 2009)	no effect (Osterwald *et al.*, 2015); decreased (Hsieh *et al.*, 2015)	
TOP2B	yes (Hsieh *et al.*, 2015)			decreased (Hsieh *et al.*, 2015)	
TOP3A	yes (Temime-Smaali *et al.*, 2008)			decrease (Osterwald *et al.*, 2015)	
TP53BP1 (aka 53BP1)	partly (Jiang *et al.*, 2007)			no effect (Jiang *et al.*, 2007) (Osterwald *et al.*, 2012; Osterwald *et al.*, 2015)	
TRF1	yes (Yeager *et al.*, 1999) (Zeng *et al.*, 2009; Wilson *et al.*, 2016)	no	yes	decrease (Jiang *et al.*, 2007); increase (Osterwald *et al.*, 2012; Osterwald *et al.*, 2015)	*de novo* APB(-like) formation at telomeric and pericentric sites (Chung *et al.*, 2011)
TRF2	yes (Yeager *et al.*, 1999; Cesare *et al.*, 2009; Zeng *et al.*, 2009; Osterwald *et al.*, 2012; O'Sullivan *et al.*, 2014; Wilson *et al.*, 2016)	no	yes	decrease (Jiang *et al.*, 2007; O'Sullivan *et al.*, 2014); no effect (Osterwald *et al.*, 2015)	*de novo* APB(-like) formation at telomeric and pericentric sites (Chung *et al.*, 2011)

protein name (a)	localized at APBs in ALT-positive cells (b)	localized in PML-NBs (c)	localized at normal telomeres (d)	effect of APBs upon protein depletion/ knockdown (e)	effect of APBs upon overexpression/ recruitment (f)
UBE2I (aka UBC9)				decrease (Osterwald *et al.*, 2012; Osterwald *et al.*, 2015)	
USP22	yes (Jeitany *et al.*, 2017)	yes (Jeitany *et al.*, 2017)	no (Jeitany *et al.*, 2017)	no effect (Jeitany *et al.*, 2017)	
WRN	yes (Johnson *et al.*, 2001)	no (Johnson *et al.*, 2001)		no effect (Osterwald *et al.*, 2015); decrease (Gocha *et al.*, 2014); increase (O'Sullivan *et al.*, 2014)	overexpression leads to increase
XRCC6				decrease (Osterwald *et al.*, 2015)	
γH_2AX	yes (Nabetani *et al.*, 2004) (Spardy *et al.*, 2008; Cesare *et al.*, 2009; Chung *et al.*, 2011)			no effect (Osterwald *et al.*, 2015)	

Suppl. table S1. Components of ALT-associated PML-NBs. The table shows a collection of proteins that have been reported in the literature in relation to APBs. (a) The first column contains the protein name and in some cases an alias. aka stands for also known as. (b) References confirming the localization to APBs are listed in the second column. (c) + (d) Some of the proteins also localize to PML-NBs or telomeres in ALT-negative cells, which is indicated in the third column, whenever information was available. (e) + (f) For those protein that have been investigating with regard to APB formation by depletion or overexpression, the phenotype is given in column 4 and 5.

Suppl. table S2. *TelNet* genes from TCGA data analysis.

gene symbol	gene ID	Rho	p-value (Rho)	log2 expression ratio (tumor/normal)	p-value (expr.)
PRPS2	5634	0.25	4.7E-04	0.21	4.4E-01
GATA3	2625	0.23	1.1E-03	-0.26	3.6E-01
ARL4D	379	0.22	1.8E-03	-1.02	8.6E-04
PDK3	5165	0.22	2.4E-03	0.21	4.5E-01
FAM58A	92002	0.20	4.2E-03	0.35	2.3E-01
MRPL34	64981	0.20	5.4E-03	-0.25	3.8E-01
TSPYL5	85453	0.19	7.6E-03	-0.63	3.5E-02
SUMO3	6612	0.19	7.8E-03	0.16	5.4E-01
RGMA	56963	0.16	2.3E-02	-1.10	3.5E-04
MT1X	4501	0.13	6.0E-02	-1.34	1.4E-05
FOXP3	50943	0.13	7.3E-02	1.33	1.8E-05
PPM1K	152926	0.12	8.1E-02	-0.84	5.9E-03
PAFAH1B3	5050	0.11	1.1E-01	1.41	5.2E-06
PDGFRA	5156	0.11	1.2E-01	-1.15	1.9E-04
SLC7A5	8140	0.10	1.6E-01	1.22	7.6E-05
TAGLN	6876	0.10	1.6E-01	-1.07	4.7E-04
PYCRL	65263	0.10	1.7E-01	0.93	2.3E-03
ARHGAP10	79658	0.08	2.4E-01	-0.84	5.5E-03
SNCG	6623	0.08	2.5E-01	-1.40	6.2E-06
CHEK1	1111	0.08	2.6E-01	1.03	7.6E-04
CSRP1	1465	0.08	2.7E-01	-1.10	3.4E-04
LPIN1	23175	0.08	2.8E-01	-0.78	9.8E-03
RARRES2	5919	0.07	2.9E-01	-0.92	2.6E-03
RMI2	116028	0.07	3.0E-01	1.43	3.6E-06
RECQL4	9401	0.07	3.5E-01	1.77	1.2E-08
CDC25A	993	0.06	3.8E-01	1.42	4.5E-06
ATAD2	29028	0.06	4.0E-01	1.13	2.3E-04
PHYHD1	254295	0.06	4.2E-01	-1.84	3.6E-09
USP2	9099	0.05	4.5E-01	-1.88	1.6E-09
CHAF1B	8208	0.05	4.5E-01	1.11	3.2E-04
EPHX2	2053	0.05	4.7E-01	-1.27	3.7E-05
HAAO	23498	0.05	4.7E-01	-1.14	2.0E-04
MCM2	4171	0.05	4.8E-01	1.43	3.8E-06
MCM4	4173	0.05	4.8E-01	1.13	2.5E-04
PRKAR2B	5577	0.05	4.9E-01	-1.65	1.1E-07
TUBB3	10381	0.05	5.0E-01	2.18	2.7E-12
PRKCB	5579	0.05	5.1E-01	-1.14	2.0E-04
HMGA1	3159	0.03	6.3E-01	1.18	1.3E-04
HMGB3	3149	0.03	6.3E-01	1.25	5.3E-05

gene symbol	gene ID	Rho	p-value (Rho)	log2 expression ratio (tumor/normal)	p-value (expr.)
RNASEH2A	10535	0.03	6.3E-01	1.18	1.3E-04
DSCC1	79075	0.03	6.4E-01	1.20	9.7E-05
CCNE1	898	0.03	6.6E-01	1.64	1.2E-07
POC1A	25886	0.03	6.6E-01	1.15	1.8E-04
PALM	5064	0.03	7.0E-01	-0.99	1.3E-03
FEN1	2237	0.03	7.1E-01	1.05	6.4E-04
RFC4	5984	0.03	7.1E-01	1.04	6.8E-04
HIST2H4A	8370	0.03	7.1E-01	0.87	4.1E-03
PDE1B	5153	0.03	7.1E-01	-1.27	3.9E-05
FOXO1	2308	0.03	7.2E-01	-0.90	3.3E-03
MCM7	4176	0.02	7.7E-01	0.88	3.7E-03
CHEK2	11200	0.02	7.7E-01	0.87	4.4E-03
TNFRSF6B	8771	0.02	7.8E-01	1.16	1.7E-04
KPNA2	3838	0.02	7.9E-01	1.29	2.9E-05
PRDM16	63976	0.02	7.9E-01	-1.35	1.2E-05
BDKRB2	624	0.02	8.0E-01	-0.81	7.8E-03
HIST1H4H	8365	0.02	8.1E-01	0.94	2.2E-03
H2AFX	3014	0.01	8.5E-01	0.99	1.2E-03
EME1	146956	0.01	9.2E-01	1.90	1.1E-09
NFE2L3	9603	0.01	9.2E-01	1.53	7.5E-07
FOXN3	1112	0.01	9.3E-01	-0.79	9.0E-03
CDK1	983	0.00	9.4E-01	1.89	1.2E-09
CDC20	991	0.00	9.5E-01	2.59	2.2E-16
PDK4	5166	0.00	9.5E-01	-2.98	<1.0E-17
CCNB1	891	0.00	9.5E-01	1.71	4.0E-08
SERPINH1	871	0.00	9.7E-01	0.99	1.3E-03
PARM1	25849	0.00	9.6E-01	-1.14	2.1E-04
HNMT	3176	0.00	9.5E-01	-0.80	8.8E-03
CDCA8	55143	0.00	9.3E-01	2.17	3.4E-12
NR2F1	7025	-0.01	9.0E-01	-0.94	2.1E-03
KLF9	687	-0.01	9.0E-01	-1.44	3.4E-06
ORC1	4998	-0.01	9.0E-01	1.92	6.8E-10
ORC6	23594	-0.01	8.9E-01	2.01	1.1E-10
EGR1	1958	-0.01	8.9E-01	-1.41	5.1E-06
XRCC2	7516	-0.01	8.7E-01	1.77	1.2E-08
AURKA	6790	-0.01	8.7E-01	1.83	4.1E-09
CKB	1152	-0.01	8.7E-01	-1.03	8.2E-04
RACGAP1	29127	-0.01	8.6E-01	1.21	8.5E-05
TXNIP	10628	-0.01	8.6E-01	-1.21	8.8E-05
PDLIM2	64236	-0.01	8.5E-01	-0.80	8.6E-03
ZEB2	9839	-0.01	8.4E-01	-0.97	1.5E-03
ALPL	249	-0.01	8.4E-01	-0.93	2.3E-03
PLCL2	23228	-0.02	8.2E-01	-1.11	3.2E-04
TRIP13	9319	-0.02	8.1E-01	2.14	6.3E-12
RCC2	55920	-0.02	8.0E-01	1.00	1.1E-03
ECT2	1894	-0.02	8.0E-01	1.65	1.1E-07
DNMT3B	1789	-0.02	7.9E-01	1.39	6.9E-06
BLM	641	-0.02	7.8E-01	1.61	2.3E-07
CCNA2	890	-0.02	7.6E-01	1.99	1.6E-10
DDX39A	10212	-0.02	7.3E-01	0.91	2.9E-03
RAD51AP1	10635	-0.03	7.0E-01	1.66	9.8E-08
ALDH1A1	216	-0.03	6.9E-01	-1.68	6.7E-08
RAD51	5888	-0.03	6.9E-01	1.85	2.8E-09
RAPGEF3	10411	-0.04	5.8E-01	-1.00	1.0E-03
PRX	57716	-0.04	5.8E-01	-1.21	8.4E-05
FOXO4	4303	-0.04	5.6E-01	-0.82	7.0E-03
LMNB1	4001	-0.04	5.4E-01	1.37	8.8E-06
FOSB	2354	-0.04	5.3E-01	-2.41	1.4E-14
FOXM1	2305	-0.05	5.1E-01	2.54	4.4E-16
KIF4A	24137	-0.05	5.1E-01	2.99	<1.0E-17
FOS	2353	-0.05	4.9E-01	-1.66	9.7E-08
EXO1	9156	-0.05	4.8E-01	2.57	2.2E-16
FHL1	2273	-0.05	4.6E-01	-2.63	<1.0E-17
FOXD2	2306	-0.05	4.6E-01	0.93	2.5E-03
FANCD2	2177	-0.05	4.5E-01	1.22	8.0E-05
PLK1	5347	-0.05	4.4E-01	2.46	3.6E-15
JUN	3725	-0.05	4.4E-01	-0.81	7.8E-03
MACROD2	140733	-0.05	4.4E-01	-0.90	3.1E-03
ARRB1	408	-0.06	4.2E-01	-0.98	1.4E-03
TAL1	6886	-0.06	4.1E-01	-1.40	5.7E-06
EZH2	2146	-0.06	3.9E-01	1.78	9.9E-09
E2F1	1869	-0.07	3.5E-01	1.65	1.1E-07
BRCA2	675	-0.07	3.4E-01	1.29	2.9E-05
FANCI	55215	-0.07	3.3E-01	1.58	3.3E-07
AHNAK	79026	-0.07	3.0E-01	-0.92	2.5E-03
FANCA	2175	-0.09	2.3E-01	1.74	2.3E-08

gene symbol	gene ID	Rho	p-value (Rho)	log2 expression ratio (tumor/normal)	p-value (expr.)
ALDH2	217	-0.09	2.3E-01	-1.39	6.8E-06
TOP2A	7153	-0.09	2.1E-01	2.72	<1.0E-17
CENPF	1063	-0.09	2.1E-01	2.43	8.4E-15
ASF1B	55723	-0.09	2.0E-01	2.16	4.4E-12
KLF4	9314	-0.09	2.0E-01	-1.30	2.7E-05
PLCE1	51196	-0.09	1.9E-01	-0.86	4.9E-03
KLF6	1316	-0.10	1.8E-01	-0.87	4.5E-03
MKI67	4288	-0.10	1.5E-01	2.48	2.0E-15
KLF2	10365	-0.11	1.4E-01	-1.14	2.2E-04
BRCA1	672	-0.11	1.3E-01	0.94	2.2E-03
PPARG	5468	-0.11	1.1E-01	-1.51	1.2E-06
EPAS1	2034	-0.11	1.1E-01	-1.08	4.5E-04
SLC7A11	23657	-0.12	1.0E-01	1.85	2.7E-09
GIGYF2	26058	-0.19	6.6E-03	-0.08	7.2E-01
PPM1D	8493	-0.20	5.9E-03	-0.30	2.9E-01
CTNNA1	1495	-0.21	3.6E-03	-0.14	5.9E-01
ERCC5	2073	-0.21	3.1E-03	-0.18	5.0E-01

Suppl. table S2. TelNet genes from TCGA data analysis. The table shows a list of *TelNet* genes that were extracted from TCGA data set because their expression either correlates or anti-correlates with telomere length changes, or the gene expression is significantly different in tumor over normal samples. The columns show the official gene symbol, Entrez gene ID, Correlation coefficient Rho from Pearson correlation (telomere length ratio vs log2 expression ratio), p-value of the correlation, log2 expression ratio (tumor/normal) and p-value of the expression data.

Suppl. table S3. DESeq results of SAHA treated U2OS cells.

gene symbol	RefSeq ID	2 µM SAHA/ EtOH		0.5 µM SAHA/ EtOH	
		log2 fold change	padj	log2 fold change	padj
LOC107985745	XR_001738282	9.67	2.72E-09	5.47	4.35E-03
LOC105369504	XR_948035	9.43	3.30E-09	5.96	1.23E-03
CYP4F2	NM_001082	8.95	1.80E-66	5.08	2.10E-20
LOC105373286	XR_938455	8.34	9.77E-07	6.23	1.32E-03
LL22NC03-75H12.2	NR_109967	7.94	3.73E-10	4.72	1.16E-03
LOC101929181	NR_104624	7.54	2.65E-56	3.40	1.07E-10
LOC105377520	XR_939419	7.48	8.82E-07	4.93	5.94E-03
LOC105378800	XR_947517	7.15	7.35E-10	3.63	1.11E-02
LOC102724895	XR_430113	7.14	8.99E-22	4.18	3.99E-07
CCL20	NM_001130046	7.09	2.50E-66	3.51	1.08E-15
LOC105374126	XR_924532	7.02	2.68E-13	3.81	6.77E-04
ARL14EPL	NM_001195581	6.95	1.79E-20	3.50	4.07E-05
LOC105374346	XR_925043	6.95	1.64E-04	5.52	1.07E-02
LOC107986608	XR_001744188	6.93	7.67E-27	4.16	3.87E-09
LOC101927421	NR_109882	6.83	8.85E-57	4.86	8.54E-28
FAM9B	NM_205849	6.42	4.22E-53	4.16	3.92E-21
LOC105374523	XR_001741614	6.36	1.80E-29	2.54	1.62E-04
LOC105373914	XR_001739905	6.34	1.53E-62	3.56	1.72E-18
LINC01214	NR_110186	6.05	9.93E-25	2.91	1.93E-05
LINC01608	NR_125416	5.64	7.89E-23	1.68	3.17E-02
LINC01517	NR_120652	5.56	5.72E-10	3.38	1.25E-03
LINC01091	NR_027105	5.54	1.83E-43	4.04	4.00E-22
LOC107986820	XR_001745270	5.41	2.02E-98	2.79	1.77E-24
TEX19°	NM_207459	5.39	6.31E-57	2.98	3.17E-16
LOC101929470	NR_125817	5.38	4.02E-29	2.87	8.91E-08
MYOZ2	NM_016599	5.25	6.63E-17	2.98	2.28E-05
HLA-DRA	NM_019111	5.22	4.21E-13	3.88	8.59E-07
LOC107987110	XR_001746873	5.21	4.72E-59	3.27	8.67E-22
MYCT1	NM_025107	5.21	6.26E-65	2.62	3.84E-15
IL21R	NM_021798	5.20	4.12E-61	2.72	1.61E-15
LOC105373186	XR_949035	5.06	3.39E-17	3.28	8.59E-07
ERICH1-AS1	NR_073397	5.05	6.09E-174	3.81	6.54E-96
LOC107986489	XR_001743018	5.04	1.38E-12	2.58	2.46E-03
SYP	NM_003179	5.02	1.60E-136	4.11	6.31E-90
LOC107986884	XR_001745703	5.01	3.32E-18	2.41	4.13E-04
CYLC1	NM_001271680	4.98	2.31E-04	3.75	2.02E-02
LOC105377721	XR_941213	4.98	1.02E-05	3.00	3.31E-02
NLRP10	NM_176821	4.96	6.18E-30	3.24	5.42E-12
STMN2	NM_001199214	4.95	1.37E-56	3.35	1.90E-24
SLC35F4	NM_001206920	4.85	1.40E-42	1.93	3.07E-06
SLN	NM_003063	4.82	3.80E-44	2.64	2.45E-12
EID3	NM_001008394	4.80	3.50E-43	3.47	3.02E-21
LOC105377087	XR_001740698	4.77	1.44E-14	2.43	1.03E-03

gene symbol	RefSeq ID	2 µM SAHA/ EtOH		0.5 µM SAHA/ EtOH	
		log2 fold change	padj	log2 fold change	padj
LOC105370731	XR_001751442	4.76	8.62E-78	1.99	1.76E-12
UBE2QL1	NM_001145161	4.75	2.96E-99	2.91	1.15E-35
PCDH1	NM_001278613	4.74	3.95E-113	3.01	1.94E-43
LOC105376639	XR_931213	4.71	5.76E-20	2.08	7.27E-04
LOC107986068	XR_001740619	4.71	6.88E-70	2.62	3.66E-20
LOC102467223	NR_104678	4.68	1.44E-11	3.50	4.63E-06
TEKT5	NM_144674	4.66	5.79E-49	2.69	3.03E-15
LOC105373682	XR_923467	4.60	8.43E-32	3.03	8.22E-13
LOC105372948	XR_001755437	4.58	2.12E-30	2.40	9.48E-08
LOC105372773	XR_937655	4.55	3.44E-13	2.44	7.02E-04
RAB3C	NM_001317915	4.54	2.46E-64	3.08	8.13E-28
LOC107986623	XR_001744259	4.52	5.12E-14	3.61	2.40E-08
LOC105370302	XR_001749950	4.52	4.03E-71	3.74	6.94E-47
HLA-DMB	NM_002118	4.52	1.24E-22	3.68	4.06E-14
BIRC3°	NM_001165	4.48	5.21E-270	1.61	1.18E-32
LOC339166	NR_040000	4.44	1.76E-60	1.72	2.36E-08
FGD2	NM_173558	4.42	1.80E-21	2.96	5.00E-09
KCNJ15	NM_001276435	4.41	2.08E-27	2.70	1.53E-09
LINC01317	NR_126403	4.40	2.00E-16	1.94	3.16E-03
SLC16A12	NM_213606	4.36	3.50E-67	2.72	1.78E-24
MAPK8IP2	NM_012324	4.36	4.83E-63	2.09	2.70E-13
XKR7	NM_001011718	4.36	2.66E-32	2.94	1.03E-13
CXCL8°	NM_000584	4.36	6.52E-25	2.38	2.76E-07
ETV7	NM_001207035	4.33	9.12E-60	1.09	1.10E-03
TRAF1°	NM_001190945	4.32	3.29E-69	2.29	2.33E-18
DAW1	NM_178821	4.29	7.92E-17	2.82	7.24E-07
JAKMIP1	NM_001099433	4.28	2.45E-22	2.74	1.32E-08
IL24°	NM_001185156	4.28	1.20E-13	2.27	6.42E-04
IQGAP2	NM_001285460	4.25	9.68E-123	1.64	4.28E-17
GABRA1	NM_000806	4.24	2.56E-43	2.14	3.48E-10
AREG°	NM_001657	4.22	4.66E-88	1.82	5.38E-15
NOL4	NM_001198546	4.21	1.06E-37	2.14	4.97E-09
KCNK9	NM_001282534	4.21	4.63E-34	2.68	7.39E-13
TMEM145	NM_173633	4.19	7.31E-14	2.71	1.88E-05
RGS4	NM_001102445	4.17	8.27E-63	2.46	2.28E-20
HTR3A	NM_000869	4.14	1.88E-35	2.49	7.86E-12
LOC105376987	XR_001740620	4.13	1.22E-15	1.75	6.78E-03
LOC105373627	XR_001739714	4.13	2.04E-14	3.31	1.20E-08
BCO2	NM_001037290	4.11	1.36E-41	1.39	1.51E-04
LOC105377865	XR_942710	4.10	4.52E-73	0.84	3.91E-03
LOC101928767	NR_110155	4.10	5.76E-88	1.06	1.61E-05
LOC105372666	XR_001754669	4.07	8.91E-121	2.43	3.13E-41
DNAJC12	NM_021800	4.05	1.49E-27	2.85	1.09E-12
SP140	NM_001005176	4.05	9.38E-106	2.60	1.16E-41
LOC101928277	XR_001744363	4.04	3.77E-50	1.27	1.25E-04
LOC105369832	XR_001749198	4.04	1.61E-09	1.85	3.24E-02
KRT34	NM_021013	4.03	5.57E-19	2.53	2.95E-07
LOC105379387	XR_001745881	4.00	4.73E-26	3.39	1.18E-17
LINC01615	NR_132622	4.00	5.56E-23	1.83	1.24E-04
LOC107985960	XR_001739773	3.98	1.49E-27	2.16	1.42E-07
CHODL	NM_001204174	3.97	1.01E-40	1.19	1.25E-03
PSG9	NM_001301707	3.96	3.80E-18	3.87	3.07E-16
LOC101928106	XR_241972	3.93	1.50E-31	1.54	1.19E-04
ARL14°	NM_025047	3.92	3.28E-23	1.88	4.72E-05
LOC107986429	XR_001742762	3.92	3.56E-68	2.24	5.67E-21
FILIP1	NM_001289987	3.88	3.09E-22	3.01	1.52E-12
SYT5	NM_001297774	3.88	5.78E-13	2.53	3.33E-05
PROSER2-AS1	NR_038222	3.87	7.02E-43	2.12	4.75E-12
INSL4	NM_002195	3.87	9.70E-04	2.97	3.60E-02
LIPH°	NM_139248	3.86	3.18E-28	2.09	1.02E-07
LCAL1	NR_130915	3.85	1.35E-59	2.61	4.33E-26
CYTH4	NM_001318024	3.81	2.24E-29	1.86	1.55E-06
LOC105374888	XR_926394	3.74	1.80E-11	2.46	9.66E-05
DES	NM_001927	3.74	2.54E-33	0.95	2.12E-02
COL26A1	NM_001278563	3.69	3.56E-40	0.82	2.92E-02
SLCO5A1	NM_001146008	3.67	7.41E-69	2.53	3.65E-31
LOC101926940	NR_104632	3.66	1.35E-32	3.27	1.25E-24
CHAT	NM_001142929	3.66	2.61E-37	2.02	1.29E-10
LINC00534	NR_051989	3.63	7.57E-05	3.20	1.94E-03
LINC01088	NR_038342	3.62	1.51E-38	1.46	6.80E-06
CFAP58-AS1	NR_108036	3.62	2.79E-10	1.94	5.54E-03
LOC101928477	XR_001748340	3.61	6.95E-33	1.05	6.54E-03
SPANXD	NM_032417	3.58	8.51E-09	1.37	1.14E-01
DEC1	NM_017418	3.57	3.36E-43	1.96	2.80E-12
LOC105379849	XR_001747342	3.56	6.43E-07	1.51	1.28E-01
LOC102724465	XR_001751744	3.56	1.56E-08	1.70	3.61E-02
LINC00189	NR_027072	3.55	3.19E-32	1.90	1.38E-08
SCEL	NM_001160706	3.55	5.30E-62	2.49	5.43E-29
NRG3	NM_001010848	3.53	5.13E-14	1.29	2.84E-02
CCL4	NM_002984	3.52	1.97E-16	2.48	1.27E-07
LOC107985543	XR_001755440	3.50	2.21E-13	1.85	1.12E-03

gene symbol	RefSeq ID	2 µM SAHA/ EtOH		0.5 µM SAHA/ EtOH	
		log2 fold change	padj	log2 fold change	padj
CTNNA2	NM_001164883	3.49	3.16E-78	2.99	1.90E-55
C10ORF113	NM_001010896	3.49	1.72E-07	1.52	9.02E-02
LINC00243	NR_130726	3.48	1.53E-10	2.55	2.72E-05
LOC107986046	XR_001740566	3.48	3.73E-17	2.83	1.23E-10
LINC01204	NR_104644	3.47	2.96E-17	1.87	7.31E-05
LIPK	NM_001080518	3.45	4.49E-05	3.26	4.57E-04
LOC101929294	NR_125808	3.43	7.15E-31	2.40	3.97E-14
HES7	NM_001165967	3.42	4.24E-10	2.87	1.49E-06
GLIS3	NM_001042413	3.42	1.57E-12	1.98	3.06E-04
LOC100507477	NR_121622	3.42	4.86E-18	1.14	2.80E-02
HECTD2-AS1	NR_024467	3.40	8.48E-27	0.86	4.96E-02
LOC100996643	XM_003846387	3.38	6.27E-22	2.12	3.57E-08
LOC285629	NR_027111	3.36	1.47E-121	2.97	1.42E-93
LGR5	NM_001277226	3.36	2.37E-35	2.32	7.13E-16
ADCY8	NM_001115	3.34	2.89E-40	1.46	2.77E-07
B3GALT1	NM_020981	3.33	1.48E-13	1.27	2.39E-02
PAEP°	NM_001018048	3.32	5.66E-07	1.41	1.22E-01
ACTBL2	NM_001017992	3.31	1.58E-80	1.58	4.28E-17
OTOGL	NM_173591	3.30	1.07E-38	2.60	8.60E-23
HIST1H1T	NM_005323	3.28	8.62E-10	0.85	3.19E-01
LOC107986098	XR_001740754	3.26	1.38E-07	2.82	3.37E-05
LOC105376567	XR_001748139	3.26	2.09E-09	3.32	6.41E-09
LOC107985072	XR_001752885	3.25	7.78E-08	2.04	4.32E-03
RPLP0P2	NR_002775	3.25	2.03E-59	1.92	2.12E-19
PTGS1	NM_000962	3.24	7.17E-27	1.83	5.01E-08
TMEM132C	NM_001136103	3.21	1.76E-33	1.72	5.53E-09
LOC105376387	XR_001747351	3.21	4.01E-08	1.90	6.71E-03
PMEL	NM_001200053	3.20	5.16E-15	1.66	5.26E-04
TMEM198	NM_001005209	3.19	7.52E-20	1.21	5.51E-03
LOC146795	NR_135222	3.18	1.65E-54	2.49	6.45E-32
KCNK15-AS1	NR_132377	3.17	1.46E-08	2.07	1.47E-03
LOC152225	NR_026934	3.17	7.51E-38	1.79	3.25E-11
LOC101927947	XR_001741892	3.16	2.52E-24	1.05	7.28E-03
ANKRD1	NM_014391	3.16	4.38E-176	1.00	3.95E-17
LOC105376440	XR_930720	3.15	1.98E-03	1.44	3.37E-01
HYDIN	NM_001198542	3.15	3.76E-44	1.78	3.80E-13
PI3	NM_002638	3.14	4.13E-05	1.55	1.36E-01
C1ORF54	NM_001301039	3.14	3.08E-07	2.70	6.50E-05
SYN1	NM_006950	3.14	3.47E-22	1.20	2.59E-03
RUNDC3A	NM_001144825	3.13	4.02E-22	1.98	2.47E-08
NRG2	NM_001184935	3.13	3.57E-19	1.79	5.34E-06
MTSS1	NM_001282971	3.12	3.68E-44	1.86	9.21E-15
DACH2	NM_001139514	3.11	3.29E-25	1.27	3.33E-04
LOC105375370	XR_001744960	3.11	3.49E-04	3.50	1.66E-04
SPANXC	NM_022661	3.10	2.93E-35	1.55	3.04E-08
SYN3	NM_001135774	3.10	4.66E-55	1.47	1.43E-11
FXYD1	NM_001278717	3.09	1.28E-08	1.90	3.14E-03
PAG1	NM_018440	3.09	7.05E-58	1.32	6.48E-10
LOC107986639	XR_001744317	3.07	2.79E-13	1.53	2.43E-03
CYP1A1°	NM_000499	3.07	2.70E-22	2.10	9.05E-10
GRAMD1C	NM_001172105	3.07	2.71E-109	1.18	4.10E-15
TNFRSF19	NM_001204458	3.06	2.42E-23	1.81	1.21E-07
CLUL1	NM_001289036	3.05	2.06E-12	1.63	1.49E-03
KCNIP4	NM_001035003	3.05	3.40E-09	1.52	1.46E-02
LOC107987059	XR_001746645	3.04	8.55E-03	2.65	5.45E-02
LOC105373954	XR_001739961	3.04	1.73E-14	2.27	1.59E-07
LOC105377955	XR_942893	3.03	1.78E-07	2.83	6.65E-06
LOC105378486	XR_946321	3.03	1.45E-19	1.76	2.74E-06
SFMBT2	NM_001018039	3.03	1.08E-66	1.10	1.60E-08
SERPINI1	NM_001122752	3.02	2.01E-22	1.71	8.74E-07
RAET1E	NM_001243325	3.01	1.69E-08	1.73	7.33E-03
LOC107985983	XR_001739876	3.01	1.14E-11	2.31	1.84E-06
ROBO2	NM_001128929	3.00	3.84E-48	2.52	2.00E-32
LOC100506922	XR_001739698	3.00	7.24E-49	1.78	3.07E-16
LOC105376235	XR_930270	3.00	1.04E-05	1.39	1.32E-01
ADAM28	NM_001304351	2.99	1.78E-25	2.35	9.47E-15
CD274	NM_001267706	2.97	1.82E-62	2.04	7.55E-28
ADGRF5	NM_001098518	2.97	1.28E-26	1.30	5.66E-05
SPANXN3	NM_001009609	2.97	2.30E-32	1.76	1.45E-10
ADAMTSL1	NM_001040272	2.97	1.78E-70	1.66	7.74E-21
NCKAP5	NM_207363	2.96	2.61E-18	2.93	7.62E-17
PPM1J	NM_005167	2.95	3.00E-37	1.82	2.88E-13
FGD6	NM_018351	2.95	3.69E-96	1.18	1.78E-14
LINC00595	NR_073447	2.95	3.62E-05	1.77	5.00E-02
PRUNE2	NM_001308047	2.95	1.09E-71	1.92	3.26E-29
LOC105376602	XR_931143	2.95	4.88E-25	1.78	1.30E-08
ENPP2	NM_001040092	2.95	2.77E-38	1.66	2.72E-11
DOCK4	NM_014705	2.95	3.09E-94	1.45	4.37E-22
LOC105370529	XR_943932	2.94	1.27E-08	1.35	4.29E-02
LOC107985366	XR_001738535	2.93	6.56E-11	0.93	1.44E-01
MYOM1	NM_003803	2.92	3.34E-60	0.81	1.58E-04

gene symbol	RefSeq ID	2 µM SAHA/ EtOH		0.5 µM SAHA/ EtOH	
		log2 fold change	padj	log2 fold change	padj
LINC01405	NR_036513	2.92	1.83E-25	1.91	3.92E-10
SLC18A3	NM_003055	2.92	4.41E-13	1.49	1.83E-03
TSPAN7	NM_004615	2.91	9.39E-38	1.96	6.29E-16
KCNA4	NM_002233	2.91	7.59E-15	2.40	2.03E-09
TET2-AS1	NR_126420	2.91	1.66E-13	0.96	7.31E-02
LOC105378813	XR_001738114	2.91	1.93E-80	0.66	3.76E-04
MTUS2	NM_001033602	2.91	2.89E-31	0.89	3.58E-03
RGS9	NM_001081955	2.91	2.59E-41	1.96	1.28E-17
LOC105376234	XR_930268	2.91	1.77E-03	2.33	3.65E-02
LOC105377732	XR_001743000	2.90	5.14E-20	1.70	1.75E-06
DNM3°	NM_001136127	2.90	5.24E-94	1.87	1.39E-37
HCG27	NR_026791	2.90	1.61E-22	0.71	8.67E-02
LINC01033	NR_126379	2.90	8.53E-08	1.30	6.72E-02
UBD	NM_006398	2.90	1.17E-04	2.17	1.55E-02
PAGE4°	NM_001318877	2.89	4.01E-07	2.34	2.49E-04
MIR3189	NR_036156	2.89	5.45E-06	0.60	6.08E-01
G0S2	NM_015714	2.89	2.46E-10	1.07	8.34E-02
NID2	NM_007361	2.88	2.58E-19	2.20	1.88E-10
LINC01456	NR_133641	2.86	1.07E-02	2.68	4.15E-02
RARB	NM_000965	2.86	6.73E-77	1.40	2.13E-17
LOC105372681	XR_936894	2.86	2.56E-04	4.27	6.72E-08
ERBB4	NM_001042599	2.86	7.17E-41	1.98	1.65E-18
LINC00693	NR_038840	2.86	1.35E-14	0.87	8.44E-02
LINC01449	NR_110832	2.85	1.00E-08	1.76	2.43E-03
LINC00589	NR_026765	2.84	9.57E-09	1.52	1.28E-02
TSSC2	NR_024248	2.83	2.38E-11	0.90	1.28E-01
IL1RAPL1	NM_014271	2.83	1.13E-38	1.17	2.29E-06
AGBL4-IT1	NR_046839	2.83	1.46E-03	1.49	2.30E-01
LINC00936	NR_028138	2.82	9.30E-21	1.16	1.48E-03
ENOX1	NM_001127615	2.81	4.93E-48	1.63	3.29E-15
ARHGAP22	NM_001256024	2.80	6.53E-28	1.59	1.73E-08
LOC105377199	XR_001755529	2.80	1.72E-14	1.50	4.33E-04
HPSE	NM_001098540	2.80	7.76E-74	1.35	2.55E-16
FAM19A3	NM_001004440	2.80	4.47E-07	1.31	7.19E-02
NECAB1	NM_022351	2.79	1.52E-13	2.42	1.90E-09
SPANXB1	NM_032461	2.79	4.04E-83	1.36	1.08E-18
KRTAP2-3	NM_001165252	2.78	2.05E-10	1.37	1.09E-02
LOC102723803	XR_001746597	2.77	1.84E-12	2.59	4.32E-10
LOC107986806	XR_001745227	2.77	3.75E-12	1.96	9.78E-06
ABCB1	NM_000927	2.76	4.54E-95	1.24	4.10E-18
CRYM	NM_001888	2.75	6.85E-24	1.84	4.83E-10
KCNH7	NM_033272	2.75	2.09E-66	1.42	1.02E-16
TCEAL7°	NM_152278	2.74	2.10E-08	2.03	2.41E-04
DIRAS2	NM_017594	2.73	3.01E-34	1.82	3.07E-14
TRIM9	NM_015163	2.73	1.23E-29	1.25	6.14E-06
NGFR	NM_002507	2.73	1.16E-31	1.81	4.07E-13
LOC102724904	XM_011518105	2.73	4.59E-05	0.89	3.98E-01
PSG5	NM_001130014	2.72	9.29E-07	2.00	1.66E-03
MEIKIN	NM_001303622	2.72	2.84E-20	2.00	2.89E-10
ABCD2	NM_005164	2.71	2.32E-18	1.89	2.26E-08
CD3D	NM_000732	2.71	3.16E-05	1.46	8.56E-02
ARHGDIB	NM_001175	2.71	3.29E-07	1.61	1.30E-02
LOC105377374	XR_939085	2.70	3.02E-22	1.83	1.50E-09
COL5A3	NM_015719	2.70	1.16E-29	1.05	1.96E-04
LINC01500	NR_110547	2.69	2.08E-09	0.54	4.89E-01
ESRRG	NM_001134285	2.69	4.14E-41	1.37	5.68E-10
LOC102724566	XR_001751649	2.68	3.46E-10	1.87	1.12E-04
LOC107985869	XR_001739409	2.68	4.66E-38	1.21	2.35E-07
HLA-DQB1	NM_001243961	2.68	2.80E-10	1.96	3.38E-05
ID4°	NM_001546	2.68	6.66E-29	0.45	2.24E-01
LOC105372572	XR_937384	2.67	2.82E-07	0.79	3.28E-01
KHDRBS2	NM_152688	2.67	3.97E-54	1.79	5.12E-23
LOC107984509	XR_001749000	2.66	2.84E-06	0.15	9.07E-01
LOC101929021	XR_428765	2.66	6.34E-04	1.90	4.72E-02
ZNF280A	NM_080740	2.65	2.57E-12	1.39	2.06E-03
GDF15°	NM_004864	2.65	4.73E-53	1.09	1.66E-08
SLC5A4	NM_014227	2.63	2.19E-11	0.96	6.93E-02
ME3	NM_001014811	2.63	9.41E-16	1.12	4.83E-03
KATNBL1	NM_024713	2.63	4.75E-86	0.42	1.45E-02
SYTL5	NM_001163334	2.63	1.65E-88	1.99	2.76E-49
BTG4	NM_017589	2.63	7.65E-16	0.91	3.48E-02
DIRC3-AS1	NR_133642	2.62	5.56E-46	1.48	7.20E-14
LOC107985677	XR_001755774	2.62	4.94E-10	2.13	3.67E-06
PSG4	NM_001276495	2.62	7.83E-36	1.95	1.36E-18
KCNA1°	NM_000217	2.62	2.21E-41	1.08	1.09E-06
ATP1A3	NM_001256213	2.62	2.46E-35	1.57	7.75E-12
CRLF2	NM_001012288	2.61	2.32E-17	2.03	7.49E-10
SP110	NM_001185015	2.61	3.22E-57	0.84	8.35E-06
XIRP2-AS1	NR_046665	2.61	2.15E-13	1.99	2.62E-07
MT1X	NM_005952	2.61	2.09E-67	0.79	5.56E-06
ADTRP	NM_001143948	2.60	3.71E-24	1.97	4.93E-13

gene symbol	RefSeq ID	2 µM SAHA/ EtOH		0.5 µM SAHA/ EtOH	
		log2 fold change	padj	log2 fold change	padj
ZMAT4	NM_001135731	2.60	2.07E-28	1.02	2.57E-04
LOC105378481	XR_946316	2.59	4.19E-15	1.49	9.00E-05
ADAMTS9	NM_001318781	2.59	2.75E-25	0.73	2.48E-02
GOLGA8IP	NR_024074	2.59	1.87E-06	1.98	1.33E-03
RND1	NM_014470	2.58	3.06E-07	1.82	1.80E-03
LOC107985325	XR_001754012	2.58	1.62E-08	1.39	1.41E-02
N4BP3	NM_015111	2.58	1.81E-32	1.42	3.07E-09
CDA	NM_001785	2.57	1.25E-18	0.93	1.23E-02
LOC107984782	XR_001751569	2.57	2.97E-04	1.28	1.95E-01
HPCAL4	NM_001282396	2.57	2.21E-48	1.70	5.70E-20
PAQR5	NM_001104554	2.57	3.60E-37	1.09	1.85E-06
LOC105369949	XR_001749294	2.56	4.07E-08	1.40	1.47E-02
TNFSF9	NM_003811	2.55	1.07E-74	0.72	8.86E-06
NEBL	NM_001173484	2.55	1.33E-56	1.07	1.73E-09
CYP4F11	NM_001128932	2.55	5.89E-23	1.36	3.08E-06
LOC101928046	XR_943988	2.55	2.94E-05	0.41	7.13E-01
PLCXD2	NM_001185106	2.54	2.25E-98	0.88	3.10E-11
MALAT1	XR_001748267	2.54	3.41E-08	0.35	6.71E-01
ROS1	NM_002944	2.54	1.78E-51	1.70	4.94E-22
OLAH	NM_001039702	2.54	1.67E-38	1.80	2.52E-18
GMFG	NM_001301008	2.53	2.02E-11	0.66	2.46E-01
XIRP1	NM_001198621	2.53	1.62E-27	0.64	4.13E-02
LOC101929541	NR_125982	2.53	2.06E-04	0.86	4.27E-01
RIMKLA	NM_173642	2.52	8.57E-39	1.26	3.12E-09
APBA1	NM_001163	2.51	8.00E-44	1.29	6.07E-11
LUM	NM_002345	2.51	2.62E-68	1.40	1.43E-20
EGOT	NR_004428	2.51	2.52E-09	1.58	1.21E-03
GPRIN3	NM_198281	2.51	4.35E-33	1.18	5.01E-07
DNAAF3	NM_001256714	2.50	9.37E-27	1.66	4.02E-11
DGKI	NM_001321708	2.50	1.67E-18	1.40	1.53E-05
LOC105378394	XR_946141	2.50	2.69E-14	2.87	1.29E-17
LOC101927653	NR_120452	2.50	2.99E-24	2.49	1.20E-22
KCTD15	NM_001129994	-2.51	1.48E-46	-1.10	1.35E-09
CCNB2°	NM_004701	-2.51	2.16E-71	-0.81	8.48E-08
PLK4°	NM_001190799	-2.52	1.11E-50	-0.57	3.22E-03
STAT5A	NM_001288718	-2.52	1.21E-16	-1.15	4.57E-04
ZWINT	NM_001005413	-2.52	1.64E-80	-0.34	4.97E-02
POU6F1	NM_002702	-2.53	2.04E-07	-1.17	3.92E-02
LOC105372707	XR_936965	-2.53	7.32E-10	-0.90	6.98E-02
FANCD2	NM_001018115	-2.54	1.29E-77	-0.60	7.34E-05
ZNF726	NM_001244038	-2.55	1.55E-11	-0.41	4.67E-01
LOC105374378	XM_011533215	-2.55	4.14E-29	-0.97	8.27E-05
LOC100507377	NR_038300	-2.55	1.04E-03	-1.29	1.84E-01
MCM5°	NM_006739	-2.55	2.97E-104	-0.77	8.66E-10
BMPR1B	NM_001203	-2.57	8.98E-30	-1.83	5.29E-15
HIST1H2AJ°	NM_021066	-2.57	7.35E-58	-0.32	1.44E-01
LOC102723591	XR_430558	-2.57	5.41E-11	-1.36	1.42E-03
TMPO-AS1	NR_027157	-2.58	4.72E-07	-0.69	3.24E-01
SOX2-OT	NR_004053	-2.58	1.06E-22	-1.97	3.80E-13
NAPA-AS1	NR_038452	-2.60	6.79E-08	-0.89	1.35E-01
HIST1H4I	NM_003495	-2.60	1.66E-72	-0.25	2.07E-01
LPCAT2	NM_017839	-2.61	5.60E-17	-0.27	5.83E-01
IL17RB	NM_018725	-2.61	1.15E-08	-1.61	1.13E-03
SYTL1	NM_001193308	-2.61	3.84E-09	-1.91	5.81E-05
PLCH1	NM_001130960	-2.62	1.33E-15	-1.63	2.26E-06
RBP4	NM_001323517	-2.63	2.92E-03	-2.73	6.53E-03
TUBA1B°	NM_006082	-2.63	2.10E-99	-0.59	2.94E-05
TNFRSF11B	NM_002546	-2.63	1.76E-60	-0.97	1.31E-08
HIST1H2BN	NM_003520	-2.64	1.54E-43	-0.60	5.37E-03
CYBRD1	NM_001127383	-2.64	2.01E-50	-1.06	1.36E-08
LOC105372652	XR_001754661	-2.64	4.24E-05	-2.09	3.36E-03
KIAA0101°	NM_001029989	-2.65	2.15E-85	-0.60	5.67E-05
RAD51AP1	NM_001130862	-2.66	1.07E-57	-0.65	5.06E-04
HIST1H2AI	NM_003509	-2.67	2.97E-51	-0.43	5.98E-02
TP73°	NM_001126240	-2.67	5.04E-16	-0.54	2.00E-01
MIAT	NR_003491	-2.67	8.12E-28	-1.04	1.20E-04
FLJ22447	NR_039985	-2.68	4.54E-63	-1.34	2.33E-16
CERS3-AS1	NR_120374	-2.68	2.05E-18	-0.83	1.72E-02
FAIM	NM_001033030	-2.68	2.98E-14	-1.15	2.66E-03
SPC25°	NM_020675	-2.69	1.10E-54	-0.44	3.48E-02
HIST1H2BL	NM_003519	-2.69	2.96E-52	-0.20	4.80E-01
EDN2	NM_001302269	-2.69	9.87E-17	-0.30	5.56E-01
MXD3	NM_001142935	-2.70	1.86E-54	-1.02	1.95E-08
FBXW4	NM_001323541	-2.71	8.02E-13	-1.47	2.50E-04
NMI	NM_004688	-2.71	2.10E-23	-1.34	2.25E-06
MFAP2	NM_001135247	-2.71	1.72E-74	-0.98	1.22E-10
MTMR9LP	NR_026850	-2.72	1.55E-10	-0.81	1.14E-01
TNNC1	NM_003280	-2.73	2.32E-55	-0.91	1.58E-06
CD34	NM_001025109	-2.73	3.80E-07	-1.86	1.34E-03
PMF1-BGLAP	NM_001199661	-2.75	2.89E-54	-1.23	8.18E-12
SELENOP°	NM_001085486	-2.76	1.48E-14	-1.74	3.71E-06

gene symbol	RefSeq ID	2 µM SAHA/ EtOH		0.5 µM SAHA/ EtOH	
		log2 fold change	padj	log2 fold change	padj
CDK3	NM_001258	-2.76	1.13E-13	-1.12	5.84E-03
CEBPD	NM_005195	-2.76	9.52E-13	-1.64	6.04E-05
SCARNA1	NR_002997	-2.76	1.26E-04	-0.80	4.13E-01
MIR4771-2	NR_039929	-2.76	1.55E-02	-0.75	6.70E-01
HIST1H2AH°	NM_080596	-2.76	7.27E-98	-0.41	1.17E-02
IQGAP3	NM_178229	-2.77	6.56E-111	-0.63	3.33E-06
HIST1H2BM	NM_003521	-2.77	2.88E-56	-0.23	3.88E-01
LINC01348	NR_027454	-2.77	2.70E-21	-0.16	7.48E-01
ABCB9	NM_001243013	-2.79	1.25E-61	-1.99	1.32E-31
TMEM42°	NM_144638	-2.80	4.47E-03	-0.57	7.09E-01
PMF1	NM_001199653	-2.81	3.98E-54	-1.25	8.47E-12
WNT3A	NM_033131	-2.81	7.88E-21	-0.99	2.18E-03
TRIL	NM_014817	-2.81	3.01E-14	-1.50	1.12E-04
ZNF428	NM_182498	-2.82	6.78E-52	-1.20	1.67E-10
HIST1H2BF	NM_003522	-2.82	2.72E-102	-0.52	5.85E-04
CYS1	NM_001037160	-2.83	2.37E-22	-0.96	2.43E-03
FOXM1	NM_001243088	-2.84	4.42E-95	-0.68	4.18E-06
COL16A1	NM_001856	-2.84	8.61E-121	-0.77	2.42E-09
HIST1H4H	NM_003543	-2.84	4.38E-127	-0.66	3.43E-07
AP1M2	NM_001300887	-2.84	8.97E-57	-1.12	2.44E-09
MYH16	NR_002147	-2.86	4.40E-05	-1.21	1.51E-01
PARP10	NM_001317895	-2.86	8.95E-56	-1.17	2.60E-10
FOXS1	NM_004118	-2.87	1.92E-22	-1.76	3.46E-09
GPR87	NM_023915	-2.88	1.77E-21	-0.95	3.78E-03
CRYBB1	NM_001887	-2.88	7.15E-04	-0.22	8.81E-01
HIST1H3D	NM_003530	-2.88	4.28E-104	-0.53	5.62E-04
EHF	NM_001206615	-2.89	1.62E-09	-3.19	6.58E-10
HAPLN1	NM_001884	-2.89	2.17E-88	-0.58	5.37E-04
APOL6°	NM_030641	-2.92	2.07E-41	-1.38	5.62E-10
HIST1H2AD°	NM_021065	-2.92	5.63E-88	-0.67	5.16E-05
CDHR1	NM_001171971	-2.92	1.96E-35	-1.70	6.50E-13
KLF17	NM_173484	-2.94	9.11E-10	-2.04	4.57E-05
LOC105371204	XR_942166	-2.95	6.31E-57	-0.98	6.08E-07
SERPINH1°	NM_001207014	-2.96	2.80E-98	-1.00	2.69E-11
LSP1	NM_001013253	-2.98	8.86E-16	-1.96	2.05E-07
LOC107984172	XR_001747287	-2.98	2.34E-03	-1.75	1.30E-01
JAM2	NM_001270407	-3.00	3.98E-24	-1.66	2.62E-08
HOXD11	NM_021192	-3.00	3.53E-05	-1.42	9.18E-02
GPR1	NM_001098199	-3.01	3.81E-16	-1.90	4.81E-07
MIR6875	NR_106935	-3.02	2.76E-03	-0.31	8.57E-01
HIST1H2BJ	NM_021058	-3.02	2.60E-142	-0.56	2.71E-05
GTF3C6	NM_138408	-3.02	6.66E-37	-1.42	4.38E-09
LOC101929504	NR_125863	-3.03	3.29E-11	-0.56	3.62E-01
LTBP2	NM_000428	-3.03	1.90E-130	-1.38	5.46E-28
HIST1H2AG	NM_021064	-3.04	1.54E-102	-0.52	1.93E-03
LCTL	NM_001278562	-3.04	2.49E-53	-1.72	7.75E-18
H2AFY2	NM_018649	-3.05	5.65E-67	-1.29	3.90E-13
MAP1LC3C	NM_001004343	-3.06	7.94E-07	-1.50	2.96E-02
LOC107984308	XR_001748118	-3.07	9.00E-04	-1.88	7.47E-02
LOC107985534	XR_001755607	-3.07	4.84E-23	-0.41	3.21E-01
MOV10L1	NM_001164104	-3.08	1.78E-18	-2.29	1.13E-10
HIST1H3B°	NM_003537	-3.08	6.45E-117	-0.67	1.01E-05
HIST1H2BC	NM_003526	-3.10	4.52E-121	-0.56	2.22E-04
LOXL1	NM_005576	-3.11	1.72E-100	-0.66	2.61E-05
TYMS	NM_001071	-3.12	2.38E-113	-0.93	9.93E-11
ALPL	NM_000478	-3.12	1.58E-11	-2.37	6.34E-07
JAK3	NM_000215	-3.16	1.47E-19	-1.56	1.32E-05
NXPH2	NM_007226	-3.18	2.33E-45	-1.38	7.51E-10
PHF11	NM_001040443	-3.19	5.13E-17	-1.37	4.30E-04
CST5	NM_001900	-3.20	7.80E-04	-2.22	3.62E-02
HIST2H2AB°	NM_175065	-3.21	1.11E-116	-0.82	5.49E-08
LOC105377390	XR_939106	-3.23	6.39E-08	-1.90	2.43E-03
PRSS2	NM_001303414	-3.23	1.03E-03	-2.69	1.42E-02
FAP	NM_001291807	-3.24	1.17E-18	-1.50	5.23E-05
HIST1H2AB	NM_003513	-3.25	2.20E-106	-0.73	8.35E-06
XKR5	NM_001289973	-3.26	4.74E-09	-1.23	4.72E-02
LOC105377067	XR_940804	-3.27	7.24E-09	-1.67	5.55E-03
EPCAM	NM_002354	-3.30	4.71E-13	-1.48	1.79E-03
GALNT15	NM_001319051	-3.31	8.63E-19	0.07	9.26E-01
FGF21°	NM_019113	-3.31	1.66E-10	-1.18	3.71E-02
LRRN4	NM_152611	-3.31	1.31E-10	-0.98	9.70E-02
SOX2°	NM_003106	-3.32	1.73E-28	-2.30	2.71E-14
MATN2	NM_001317748	-3.32	3.44E-70	-1.44	3.95E-15
LOC105378314	XR_001747454	-3.33	8.26E-18	-1.81	3.44E-06
LOC105378313	XR_001747453	-3.34	7.59E-05	-2.21	1.72E-02
LINC01173	NR_132376	-3.36	1.76E-07	-1.29	7.19E-02
LINC00452	NM_001278674	-3.38	6.74E-133	-0.54	4.86E-04
HIST1H2AK	NM_003510	-3.43	8.92E-68	-0.58	7.25E-03
LOC105372981	XR_938124	-3.49	5.55E-48	-1.39	2.56E-09
HIST1H4A	NM_003538	-3.53	5.34E-94	-0.50	1.41E-02
LINC00689°	NR_024394	-3.55	3.51E-10	-1.16	6.13E-02

gene symbol	RefSeq ID	2 µM SAHA/ EtOH		0.5 µM SAHA/ EtOH	
		log2 fold change	padj	log2 fold change	padj
ANXA8L1	NM_001098845	-3.56	1.14E-07	-2.31	7.56E-04
DMTN	NM_001114135	-3.58	8.31E-17	-1.27	3.82E-03
DENND2A	NM_001318052	-3.58	3.51E-40	-1.06	1.13E-04
MIR6799	NR_106857	-3.61	2.37E-11	-0.26	7.58E-01
SERPINA3	NM_001085	-3.63	9.38E-05	-2.58	9.35E-03
LOC102723594	XR_427017	-3.65	1.74E-04	-0.97	4.32E-01
LOC105373411	XR_001739274	-3.69	1.23E-31	-2.40	2.71E-15
MYCN	NM_001293228	-3.70	1.06E-20	-1.17	3.69E-03
CCL24	NM_002991	-3.70	1.19E-20	-2.01	1.52E-07
DRD1	NM_000794	-3.74	1.59E-50	-1.61	6.57E-11
MIR4635	NR_039778	-3.75	7.04E-05	-2.03	4.36E-02
CCL2	NM_002982	-3.77	6.07E-79	-1.23	1.36E-09
WNT5B	NM_030775	-3.78	1.68E-19	-2.74	2.04E-11
C5ORF46	NM_206966	-3.80	8.80E-62	-1.34	5.92E-09
SLC12A7	NM_006598	-3.81	1.69E-175	-1.73	3.68E-38
TRIM22	NM_001199573	-3.82	5.54E-64	-1.95	5.59E-19
PTP4A3	NM_007079	-3.85	5.37E-24	-1.56	3.04E-04
UBA7	NM_003335	-3.85	4.72E-12	-2.85	2.23E-07
LOC107984684	XR_001750691	-3.92	5.27E-07	-3.09	1.04E-04
KRT75	NM_004693	-4.00	2.60E-147	-0.90	2.13E-08
HRCT1	NM_001039792	-4.02	2.06E-08	-2.48	4.22E-04
KRT14	NM_000526	-4.09	3.02E-12	-2.82	6.32E-07
LOC107985005	XR_001752991	-4.13	6.63E-04	-1.75	1.81E-01
C6ORF15	NM_014070	-4.15	2.88E-89	-2.26	8.48E-30
LOC105369395	XR_950328	-4.17	2.71E-06	-2.83	1.96E-03
ZXDB	NM_007157	-4.19	2.46E-151	-0.98	3.11E-09
CACNG6	NM_031897	-4.23	6.88E-21	-2.99	1.78E-12
ZXDA	NM_007156	-4.25	6.76E-159	-0.81	5.58E-07
LINC01429	NR_110016	-4.27	1.93E-19	-2.43	2.40E-08
PALMD°	NM_017734	-4.32	1.40E-05	-2.97	2.75E-03
LOC105376672	XR_946890	-4.33	7.60E-10	-2.08	1.59E-03
SCX	NM_001080514	-4.41	2.88E-110	-1.05	1.53E-08
LOC107985401	XR_001754648	-4.46	1.10E-25	-1.72	4.00E-06
WNT11	NM_004626	-4.51	2.03E-10	-3.45	6.23E-06
PODNL1	NM_001146254	-4.53	3.13E-14	-2.65	1.40E-06
LOC105371401	XR_933873	-4.55	4.52E-62	-1.86	3.26E-15
SALL4	NM_001318031	-4.63	1.70E-32	-2.95	7.91E-18
LOC107985006	XR_001752992	-4.76	1.25E-05	-1.37	2.33E-01
C2ORF54	NM_001085437	-4.81	1.97E-05	-3.87	4.47E-04
TRIM17	NM_001024940	-4.82	4.19E-10	-2.52	2.07E-04
LOC105377978	XR_942935	-4.92	3.46E-06	-2.62	4.96E-03
LOC101928100	NR_120430	-4.99	1.16E-78	-1.84	1.99E-16
CCDC129	NM_001257967	-5.14	7.67E-47	-1.20	1.47E-05
CD180	NM_005582	-5.19	4.97E-04	-2.49	6.08E-02
RARRES2	NM_002889	-5.29	3.30E-12	-3.58	1.73E-08
LOC107986370	XR_001742490	-5.38	1.19E-14	-2.27	2.71E-03
LOC105379461	XR_001752103	-5.39	1.57E-06	-0.57	6.58E-01
LINC00639	NR_039982	-5.52	5.81E-21	-2.29	2.18E-07
LOC107985377	XR_001737789	-6.25	1.93E-06	-3.38	1.84E-04
TNNT2	NM_000364	-6.70	4.53E-31	-3.24	4.24E-21
SYT8	NM_001290332	-6.85	1.82E-08	-3.82	1.25E-07
SHISA3°	NM_001080505	-7.44	7.56E-06	-3.11	5.45E-04
CXCL14	NM_004887	-7.60	9.95E-35	-3.46	6.80E-08

Suppl. table S3. DESeq results of SAHA treated U2OS cells. 318 up- and 183 downregulated genes with a log2 fold change (l2fc) <-2.5 or >2.5 for 2 µM SAHA over EtOH ctrl while the l2fc of 0.5 µM SAHA over EtOH ctrl was either not statistical significant or in the same direction. The adjusted p-value was set to padj <0.05 and genes with an RPKM >1 in the highest expressed sample were selected for this table. Genes were sorted by l2fc (2 µM SAHA over EtOH ctrl). Those genes implemented in the *TelNet* database were marked in bold, genes reported to be cell cycle-regulated in U2OS cells (Grant *et al.*, 2013) were marked with a °circle.

Suppl. table S4. Differentially expressed genes in HeLa LT vs ST cells.

gene symbol	RefSeq ID	log2 fold change	padj
DPT	NM_001937	10.06	3.24E-104
CCL2	NM_002982	9.24	4.30E-09
LOC107985950	XR_001739738	9.15	3.85E-08
CDH19	NM_001271028	8.96	2.11E-20
SLC16A14	NM_152527	8.85	2.66E-35
LINC01234	NR_110025	8.67	2.01E-02
RARRES2	NM_002889	8.26	1.35E-35

gene symbol	RefSeq ID	log2 fold change	padj
SSTR2	NM_001050	8.24	3.65E-11
ATF7IP2	NM_001256160	8.20	2.78E-21
GREM2	NM_022469	8.17	1.90E-78
C14ORF132	NM_001252507	8.16	3.05E-36
PBDC1	NM_001300888	8.14	3.99E-06
LOC102723724	XR_001744390	7.99	4.66E-02
MIR3606	NR_037401	7.84	4.12E-07
ANXA3	NM_005139	7.82	5.29E-44
LOC107986438	XR_001742827	7.81	1.33E-17
SNTB1	NM_021021	7.74	1.18E-21
GBP1	NM_002053	7.61	4.26E-05
ARMCX1	NM_016608	7.56	7.29E-09
SLC1A3	NM_001166695	7.55	1.54E-33
COL3A1	NM_000090	7.49	4.56E-07
LOC107985951	XR_001739740	7.46	1.18E-08
NPY1R	NM_000909	7.44	2.23E-03
MIR1266	NR_031670	7.43	1.22E-03
M1AP	NM_001281295	7.43	2.48E-03
SLC12A7	NM_006598	7.42	9.15E-08
MPZL2	NM_005797	7.33	1.61E-04
EMB	NM_198449	7.28	2.61E-08
KCNG1	NM_002237	7.21	2.13E-14
MIR1245A	NR_031647	7.20	4.94E-02
LINC00517	NR_135286	7.20	3.96E-05
SMIM3	NM_032947	7.19	1.44E-11
TRIM6	NM_001003818	7.18	1.07E-04
TSTD1	NM_001113205	7.18	1.23E-11
CARD16	NM_001017534	7.11	3.13E-64
LOC105370057	XR_001749368	7.04	4.43E-03
GPR183	NM_004951	6.97	1.01E-41
LGALS8	NM_006499	6.95	5.00E-32
MIR3611	NR_037405	6.91	7.37E-03
DCP1B	NM_001319292	6.89	4.92E-07
LOC101060400	XR_934821	6.88	3.85E-04
TMEM47	NM_031442	6.84	4.49E-59
PLPPR4	NM_001166252	6.83	8.96E-04
DIO3	NM_001362	6.82	4.30E-04
LOC107986653	XR_001744391	6.81	1.14E-02
GYS2	NM_021957	6.77	1.68E-48
LOC440934	NR_136638	6.75	1.11E-06
LOC107985369	XR_001738560	6.71	7.22E-09
PCDHB12	NM_018932	6.70	1.54E-02
FUT4	NM_002033	6.63	1.97E-02
LOC107985638	XR_001755998	6.63	2.73E-06
MYOM3	NM_152372	6.62	6.88E-04
LOC728755	XR_943665	6.58	8.75E-14
EPHX4	NM_173567	6.56	4.52E-09
LUM	NM_002345	6.56	1.23E-50
LOC107986128	XR_001740894	6.55	2.62E-02
AGK	NM_018238	6.54	8.81E-55
LOC107984581	XR_001750003	6.49	2.87E-02
THBD	NM_000361	6.48	3.10E-02
ZC4H2	NM_001178032	6.48	1.80E-10
MIR4755	NR_039911	6.43	2.13E-03
LOC105374144	XR_001740944	6.41	3.70E-02
GSTM1	NM_000561	6.41	1.12E-10
KCNJ18	NM_001194958	6.41	3.84E-02
B3GNT5	NM_032047	6.39	4.04E-03
ZNF726	NM_001244038	6.38	3.26E-03
PLBD1	NM_024829	6.38	3.20E-03
RGS18	NM_130782	6.36	3.10E-02
SLC22A15	NM_018420	6.33	4.81E-08
DOK7	NM_001164673	6.32	7.89E-08
PARP8	NM_001178055	6.25	1.79E-32
MYO5C	NM_018728	6.24	3.68E-57
C22ORF34	NM_001289922	6.23	4.14E-03
CNNM1	NM_020348	6.23	1.65E-09
MIR4635	NR_039778	6.21	4.82E-02
LINC00960	NR_040004	6.16	8.87E-03
KCNE4	NM_080671	6.13	2.17E-09
LOC101929028	XR_001745817	6.04	6.91E-24
LBH	NM_030915	6.03	5.01E-22
NKD2	NM_001271082	6.01	1.16E-02
ZNF32	NM_001005368	6.00	6.83E-27
RORA	NM_002943	5.97	7.70E-24
DEFB1	NM_005218	5.93	8.78E-03
ADARB2	NM_018702	5.91	1.17E-03
MAN1A1	NM_005907	5.90	2.64E-03
HSD17B2	NM_002153	5.88	2.35E-19
HMX2	NM_005519	5.88	1.21E-02
CCDC152	NM_001134848	5.88	1.86E-11

gene symbol	RefSeq ID	log2 fold change	padj
LOC107985961	XR_001739793	5.82	1.18E-09
SYTL4	NM_001129896	5.82	2.14E-03
ETV1	NM_001163147	5.81	7.97E-32
TSPAN15	NM_012339	5.76	2.13E-07
FAM169A	NM_015566	5.75	2.38E-10
MCOLN2	NM_153259	5.74	1.73E-19
LOC101929494	XR_429962	5.74	1.30E-03
ATP6V0E2	NM_001100592	5.73	1.72E-18
LOC105373936	XR_923998	5.72	5.15E-04
PCDHB15	NM_018935	5.72	1.99E-03
MPPED2	NM_001145399	5.72	9.19E-04
PCDHB11	NM_018931	5.66	3.70E-02
CD70	NM_001252	5.64	6.08E-25
STARD5	NM_181900	5.63	4.22E-02
ECHDC2	NM_001198961	5.59	3.24E-16
ARSD	NM_001669	5.59	1.43E-06
CTSH	NM_001319137	5.58	2.04E-10
CHRM3	NM_000740	5.56	9.86E-19
GGT5	NM_001099781	5.55	1.06E-03
FAM155A-IT1	NR_046848	5.54	1.29E-03
CYP39A1	NM_001278738	5.52	1.13E-03
CARD6	NM_032587	5.47	1.40E-55
LINC00051	NR_024378	5.47	1.80E-03
ARHGAP22	NM_001256024	5.47	8.33E-09
COL6A1	NM_001848	5.47	4.92E-12
PDGFD	NM_025208	5.46	4.12E-10
PNMA2	NM_007257	5.45	1.28E-20
LINC00996	NR_034033	5.45	4.90E-02
STAP2	NM_001013841	5.44	1.06E-12
UCHL1	NM_004181	5.44	7.47E-08
KIAA1107	NM_015237	5.43	1.88E-10
MSR1	NM_002445	5.40	3.81E-02
SULF2	NM_001161841	5.39	8.25E-03
MCF2L2	NM_015078	5.38	2.65E-09
ISL1	NM_002202	5.37	4.81E-02
TNFRSF11B	NM_002546	5.36	1.44E-22
TARP	NM_001003799	5.35	4.72E-04
LOC107985702	XR_001755822	5.34	9.07E-03
TSNARE1	NM_001291931	5.34	4.31E-09
INTS6L	NM_182540	5.32	6.43E-07
SLC40A1	NM_014585	5.31	2.55E-03
PTGS1	NM_000962	5.28	1.05E-30
EGF	NM_001178130	5.25	3.51E-08
FAM43A	NM_153690	5.24	1.06E-26
CPEB1	NM_001079533	5.23	2.88E-06
ACTG2	NM_001199893	5.20	8.19E-11
LINC00623	NR_024510	5.18	2.28E-03
SEMA3A	NM_006080	5.17	1.55E-03
RIMS4	NM_001205317	5.14	5.52E-07
JSRP1	NM_144616	5.12	2.98E-06
TSPAN2	NM_001308315	5.11	1.79E-10
CACHD1	NM_001293274	5.11	2.84E-12
IGFBP1	NM_000596	5.08	7.87E-03
LOC100506691	NR_135044	5.07	1.62E-20
PTPRE	NM_001316676	5.06	9.42E-07
ATP6V0E2-AS1	NR_027040	5.04	9.78E-05
NRG1	NM_001159995	5.04	8.85E-27
SNPH	NM_001318234	5.01	1.59E-02
PLXDC2	NM_001282736	5.01	2.04E-07
NME8	NM_016616	5.01	4.87E-11
ADAM19	NM_033274	5.01	1.80E-02
RYR2	NM_001035	4.99	1.53E-32
HPGD	NM_000860	4.98	1.81E-11
CMTM8	NM_001320308	4.98	1.29E-06
LOC101927503	NM_001323425	4.96	9.78E-05
EREG	NM_001432	4.95	9.21E-04
GPX7	NM_015696	4.95	2.63E-02
FAM155A	NM_001080396	4.93	4.01E-13
LINC00942	NR_028415	4.89	7.41E-21
PCDHB2	NM_018936	4.89	1.77E-02
NKX3-1	NM_001256339	4.89	2.67E-14
MAGEA3	NM_005362	4.89	6.46E-30
SLITRK6	NM_032229	4.88	1.40E-06
CTSS	NM_001199739	4.87	1.89E-15
SLC25A27°	NM_001204051	4.87	1.01E-11
RANBP3L	NM_001161429	4.86	1.39E-03
SASH1	NM_015278	4.86	5.19E-10
PTGS2	NM_000963	4.85	3.27E-53
STK39	NM_013233	4.81	6.33E-32
MIR6724-3	NR_128716	4.78	3.62E-03
HYLS1	NM_001134793	4.78	5.26E-04

gene symbol	RefSeq ID	log2 fold change	padj
LOC105377794	XR_941373	4.73	3.80E-03
ANGPT1	NM_001146	4.70	3.61E-41
MMP7	NM_002423	4.68	3.64E-03
PRCD	NM_001077620	4.68	5.07E-07
PIEZO2	NM_022068	4.66	5.68E-18
FST	NM_006350	4.66	1.81E-18
ADGRG6°	NM_001032394	4.62	6.50E-08
MGLL	NM_001003794	4.61	1.13E-27
LOXL1	NM_005576	4.61	9.60E-06
CPXM2	NM_198148	4.59	1.28E-03
LOC101927787	NR_125944	4.59	7.60E-03
RDM1	NM_001034836	4.55	2.74E-04
LOC102723704	NR_125932	4.51	3.77E-02
GABBR1	NM_001319053	4.50	3.80E-07
RASSF6	NM_001270391	4.49	4.95E-04
SESN3	NM_001271594	4.48	7.57E-10
PDGFRL	NM_006207	4.48	7.35E-13
SATB1	NM_001131010	4.47	3.83E-16
C7ORF31	NM_138811	4.45	2.71E-02
CYFIP2	NM_001037333	4.45	4.93E-06
GRIP2	NM_001080423	4.43	2.89E-07
FIBIN	NM_203371	4.42	1.63E-08
LINC01429	NR_110016	4.40	1.03E-21
TNFSF10	NM_001190942	4.40	1.99E-30
LANCL3	NM_001170331	4.38	4.54E-05
RARRES3	NM_004585	4.38	2.31E-17
CCL26	NM_006072	4.36	1.12E-05
EPB41L4A	NM_022140	4.35	3.71E-13
XKRX	NM_212559	4.35	2.12E-09
SLC7A2	NM_001008539	4.35	8.42E-44
PRDM1	NM_001198	4.33	3.76E-08
HNMT	NM_001024074	4.33	6.44E-03
IQCA1	NM_001270584	4.32	2.33E-06
TNFAIP6	NM_007115	4.31	7.15E-16
TNNC1	NM_003280	4.30	3.27E-03
NOSTRIN	NM_001039724	4.28	4.50E-04
LOC105377329	XR_001741764	4.26	1.34E-02
OLFML3	NM_001286352	4.25	5.11E-05
ANGPTL2	NM_012098	4.24	2.17E-05
LOC105379109	XR_948638	4.24	3.13E-02
CLDN4	NM_001305	4.22	6.22E-09
PRR15	NM_175887	4.21	8.78E-03
SLC19A3	NM_025243	4.20	4.80E-02
CDHR5	NM_001171968	4.20	1.19E-02
MPP1	NM_001166460	4.19	4.33E-10
NIPAL1	NM_207330	4.16	3.13E-19
GLIPR1	NM_006851	4.15	6.44E-12
ALS2CL	NM_001190707	4.15	1.49E-04
RBP4	NM_001323517	4.14	4.20E-08
SLC51B	NM_178859	4.14	3.07E-02
PLEKHH2	NM_172069	4.10	1.03E-10
AS3MT	NM_020682	4.10	9.71E-11
PLEK2	NM_016445	4.09	3.13E-19
CPA5	NM_001127441	4.08	2.32E-03
MMP24	NM_006690	4.07	8.02E-19
SERPINB5	NM_002639	4.04	1.08E-04
MMP2	NM_001127891	4.04	4.67E-23
LOC105379362	XR_949653	4.03	8.14E-04
SLC2A6	NM_001145099	4.02	3.04E-22
CCL5	NM_001278736	4.02	7.75E-05
LINGO2	NM_001258282	-4.00	4.10E-21
LOC107984928	XR_001737926	-4.02	4.94E-02
UGT1A9	NM_021027	-4.05	1.01E-03
KLRK1	NM_007360	-4.08	6.16E-34
GGT7	NM_178026	-4.12	9.86E-12
STAC2	NM_198993	-4.16	1.92E-24
FOXL1	NM_005250	-4.20	6.48E-04
NLRP1	NM_001033053	-4.21	2.13E-06
PDK4	NM_002612	-4.22	9.70E-34
LOC105376346	XR_930538	-4.28	6.52E-03
ADGRG1	NM_001145770	-4.29	2.14E-22
HEY2	NM_012259	-4.30	9.82E-03
A1BG	NM_130786	-4.32	3.70E-02
ADGRG3	NM_001308360	-4.36	4.22E-03
MYHAS	NR_125367	-4.40	1.90E-02
PCDH7	NM_001173523	-4.41	3.06E-20
ANKRD18A	NM_147195	-4.46	1.97E-12
UGT1A7	NM_019077	-4.47	4.83E-04
TLE1	NM_001303103	-4.47	3.89E-04
KCTD12	NM_138444	-4.47	2.83E-19
ABCC2°	NM_000392	-4.61	1.15E-42

gene symbol	RefSeq ID	log2 fold change	padj
ST6GAL1	NM_003032	-4.63	1.06E-14
ACSL5	NM_016234	-4.75	1.11E-05
LOC101927523	NR_120624	-4.85	6.68E-03
MKX	NM_001242702	-4.96	3.90E-43
VIT	NM_001177969	-5.02	2.43E-19
ZNF718	NM_001039127	-5.13	3.76E-16
LOC284930	NR_122046	-5.14	1.01E-12
SYTL5	NM_001163334	-5.21	4.75E-35
UGT1A6	NM_001072	-5.38	2.27E-03
LOC105371291	XR_933625	-5.41	1.73E-03
DNM1	NM_001005336	-5.43	1.90E-19
ISPD	NM_001101417	-5.52	1.27E-08
LOC105369881	XR_945161	-5.58	5.04E-05
SBSPON	NM_153225	-5.68	2.63E-02
EPB41L3	NM_001281533	-5.76	1.45E-49
GUCY1A2	NM_000855	-5.80	2.12E-20
MEF2C	NM_001131005	-5.91	5.29E-09
MCTP2	NM_001159643	-5.93	9.98E-35
PHF21B	NM_001135862	-5.93	1.28E-06
ZNF91	NM_001300951	-6.03	5.26E-28
UGT1A1	NM_000463	-6.06	1.10E-02
UGT1A3	NM_019093	-6.08	1.07E-02
UGT1A4	NM_007120	-6.14	8.67E-03
P2RY6	NM_001277204	-6.15	3.97E-15
RTN4RL2	NM_178570	-6.19	4.30E-19
UGT1A5	NM_019078	-6.19	7.98E-03
LOC100128905	NR_136175	-6.33	4.32E-02
LOC102724488	XM_006718093	-6.38	3.90E-02
SPARC	NM_001309443	-6.39	7.12E-74
LOC105369688	XR_931419	-6.48	2.93E-02
MIR5009	NR_049807	-6.53	2.51E-02
A1BG-AS1	NR_015380	-6.64	2.03E-03
LOC101928080	XR_930619	-6.66	2.00E-06
HRCT1	NM_001039792	-6.68	1.62E-02
MKX-AS1	NR_121652	-6.81	1.07E-02
HPD	NM_001171993	-6.95	3.15E-53
OTOG	NM_001277269	-6.96	6.79E-07
FAM95C	NR_047651	-7.11	3.77E-03
PALMD	NM_017734	-7.12	3.43E-26
UGT8	NM_001128174	-7.40	8.02E-19
SPINK13	NM_001040129	-7.59	2.17E-20
CH17-360D5.1	NM_001278795	-7.60	2.68E-06
IGSF10	NM_001178145	-7.99	2.88E-53
NPY4R	NM_001278794	-8.28	2.24E-07
LPL	NM_000237	-8.54	1.15E-42
SLC6A15	NM_001146335	-8.58	3.40E-51
PRRX1	NM_006902	-8.84	1.58E-08
LOC105377180	XR_001740794	-8.94	6.19E-14
LOC105378220	XM_011537717	-9.03	2.54E-14
PLIN2	NM_001122	-10.24	5.15E-19
USH1C	NM_001297764	-10.61	1.62E-38
SPINK6	NM_001195290	-11.26	1.65E-08
PLAC4	NM_182832	-12.42	2.82E-02

Suppl. table S4. Differentially expressed genes in HeLa LT vs ST cells. 229 higher and 74 lower expressed genes with a log2 fold change <-4 or >4 in HeLa LT versus HeLa ST cells. The adjusted p-value was set to padj<0.05 and only genes with an RPKM >1 in the higher expressed sample were selected for this table. Genes were sorted by log2 fold change. Those genes implemented in the *TelNet* database were marked in bold. None of the genes was reported to be cell cycle-regulated in HeLa cells (Grant *et al.*, 2013).

Suppl. table S5. DESeq results of ASF1 depletion in HeLa ST cells.

gene symbol	RefSeq ID	log2 fold change	padj
MIR3975	NR_039771	8.04	3.19E-02
LOC107984532	XR_001749079	7.12	4.39E-03
MMP7	NM_002423	6.50	3.27E-03
CCR4	NM_005508	6.25	4.39E-03
KBTBD13	NM_001101362	6.15	5.15E-03
PGPEP1L	NM_001102612	5.11	4.43E-02
CCL5	NM_001278736	3.04	3.64E-05
CARD16	NM_001017534	3.00	4.93E-06
SUSD2	NM_019601	2.72	1.63E-03
NDRG4	NM_001130487	2.42	2.61E-03
TNFSF15	NM_001204344	2.36	6.47E-04
SEMA3A	NM_006080	2.35	3.85E-02
MYEOV	NM_001293291	2.22	1.64E-04
ALS2CL	NM_001190707	2.21	1.33E-02
IL7R	NM_002185	2.21	9.20E-07
EPGN	NM_001270989	2.12	5.74E-06
CD177	NM_020406	2.08	1.58E-02
LOC105371267	NR_136518	2.06	3.08E-02
LOC101059954	XR_171071	2.06	2.95E-02
IFIT2	NM_001547	2.02	2.34E-04
IL6	NM_000600	2.01	2.75E-02
OASL	NM_001261825	2.01	3.85E-04
SCG2	NM_003469	2.00	1.06E-02
OAS2	NM_001032731	1.99	3.68E-02
LOC541472	NR_131935	1.98	4.57E-02
SRPX2	NM_014467	1.87	7.93E-05
IFIT3	NM_001031683	1.84	9.60E-04
THSD4	NM_001286429	1.81	3.62E-08
LOC105369165	XR_001739464	1.81	4.28E-02
FAM9B	NM_205849	1.79	6.35E-04
LINC00882	NR_028303	1.75	1.36E-02
MGC27382	NR_027310	1.74	1.56E-02
NT5E	NM_001204813	1.73	1.72E-02
H1F0°	NM_005318	1.72	5.16E-06
RARRES3	NM_004585	1.69	4.26E-02
INPP4B	NM_001101669	1.69	1.33E-06
PARP10	NM_001317895	1.68	4.75E-04
ISG15	NM_005101	1.67	2.32E-03
ITGB2	NM_000211	1.66	1.49E-02
TMEM198	NM_001005209	1.65	3.74E-02
DHX58	NM_024119	1.64	1.37E-02
DGKI	NM_001321708	1.63	3.00E-02
LOC105378797	XR_001737670	1.62	4.46E-03
CEMIP	NM_001293298	1.60	2.61E-05
IFIT1°	NM_001270927	1.57	2.15E-02
GRB7	NM_001030002	1.56	8.51E-03
NOS1AP	NM_001126060	1.55	2.85E-02
LINC01031	NR_125789	1.54	4.37E-02
COL7A1°	NM_000094	1.52	1.36E-02
GLIS3	NM_001042413	1.48	6.31E-03
TNS4	NM_032865	1.47	5.55E-06
DDX58	NM_014314	1.46	9.98E-06
IFI44	NM_006417	1.45	3.28E-02
CPA4	NM_001163446	1.43	2.15E-02
ITGB4	NM_000213	1.41	8.10E-04
COL16A1	NM_001856	1.39	8.67E-03
FIBIN	NM_203371	1.37	4.95E-02
ABCA10	NM_080282	1.35	4.33E-03
FRY	NM_023037	1.34	7.75E-04
FBXO2	NM_012168	1.33	7.04E-05
CRABP2	NM_001199723	1.32	2.68E-04
ANPEP	NM_001150	1.32	2.37E-02
LAMB3	NM_000228	1.30	1.22E-04
FAAH2	NM_174912	1.30	5.16E-03
PPM1L	NM_001317911	1.28	6.83E-03
ST18	NM_014682	1.26	1.79E-02
SETBP1	NM_001130110	1.26	4.36E-02
CASC15	NR_015410	1.26	2.41E-02
FST	NM_006350	1.25	3.87E-02
PCED1B	NM_001281429	1.23	2.32E-02
LOC107986812	XR_001745252	1.23	2.90E-02
SNCG	NM_003087	1.21	2.70E-02
EHF	NM_001206615	1.20	2.06E-02
PLEK2	NM_016445	1.20	3.87E-02
TNFAIP6	NM_007115	-1.49	3.42E-02

Suppl. table S5. DESeq results of ASF1 depletion in HeLa ST cells. See next page for table legend.

Suppl. table S5. DESeq results of ASF1 depletion in HeLa ST cells. 74 up- and 1 downregulated genes with a log2 fold change (l2fc) <-1.2 or >1.2 for siASF1 over siCtrl in HeLa ST cells excluding deregulated genes with a l2fc <-1.6 or >1.6 for siASF1 over siCtrl in HeLa LT cells. The adjusted p-value was set to padj<0.05 and only genes with an RPKM >1 in the highest expressed sample were selected for this table. Genes were sorted by l2fc. Those genes implemented in the *TelNet* database were marked in bold, genes reported to be cell cycle-regulated in HeLa cells (Grant *et al.*, 2013) were marked with a °circle.

Suppl. table S6. DESeq results of ASF1 depletion in HeLa LT cells.

gene symbol	RefSeq ID	log2 fold change	padj
RBBP8NL	NM_080833	9.10	1.06E-13
LOC105378977	XR_948342	9.00	2.08E-04
LOC105372646	XR_936817	8.97	9.42E-08
CEACAM20	NM_001102597	8.88	2.69E-07
LOC101928362	XR_001749028	8.86	1.54E-07
IRGM	NM_001145805	8.58	2.54E-04
LOC105376956	XR_940599	8.56	1.05E-06
RHAG	NM_000324	8.47	2.48E-06
LOC107985745	XR_001738282	8.13	2.84E-10
LOC105373471	XR_001738273	7.73	3.94E-09
LOC105378649	XR_001737980	7.68	7.98E-05
LOC105377394	XR_939120	7.46	2.53E-08
LOC107985561	XR_001755499	7.39	3.98E-03
LOC107986570	XR_001743975	7.38	2.93E-04
PAEP	NM_001018048	7.36	4.41E-03
LOC101928046	XR_943988	7.28	4.93E-04
S100A9	NM_002965	7.14	8.01E-03
LINC01511	NR_125810	7.05	1.25E-06
HIST3H3	NM_003493	6.99	9.37E-04
LY86-AS1	NR_026970	6.98	1.12E-20
SLC5A4	NM_014227	6.78	2.83E-06
LOC107984272	XR_001747594	6.78	2.92E-03
LOC105370880	XR_932425	6.75	1.20E-03
LOC105369520	XR_001748413	6.72	3.32E-02
LOC105376713	XR_001751508	6.65	2.69E-03
LINC01468	NR_120641	6.64	2.41E-03
HIST1H2BA	NM_170610	6.61	1.81E-15
LOC107986116	XR_001740859	6.38	9.86E-03
HIST1H2AA	NM_170745	6.37	4.52E-05
LOC101927467	XR_245182	6.26	7.17E-05
TPO	NM_000547	5.99	1.39E-07
PSG6	NM_001031850	5.96	8.89E-04
LOC105370981	XR_001751668	5.90	1.75E-02
CD52	NM_001803	5.84	3.36E-02
LOC105374910	XR_001743950	5.68	4.80E-03
LOC105371896	XR_934982	5.62	1.21E-10
LOC100507140	NR_037886	5.61	9.90E-05
DMKN	NM_001035516	5.54	8.11E-03
KCNAB1	NM_001308217	5.51	7.01E-10
LINC01554	NR_026936	5.51	3.70E-25
LOC105369689	XR_931420	5.42	4.27E-07
LINC01091	NR_027105	5.40	4.63E-07
LOC105371619	XR_922291	5.38	4.27E-04
IL24	NM_001185156	5.36	3.46E-12
LOC107985089	XR_001753021	5.34	2.06E-02
TCN2	NM_000355	5.32	6.45E-10
CARD18	NM_021571	5.29	2.74E-02
LOC107984384	XR_001748372	5.29	2.41E-06
LINC01214	NR_110186	5.28	5.25E-04
LOC105374394	XR_001741652	5.23	1.42E-05
SMIM24	NM_001136503	5.19	8.97E-06
LOC101448202	NR_103451	5.13	1.15E-07
LOC105378668	XR_947223	5.08	3.48E-02
LOC107984545	XR_001749266	5.07	1.80E-02
LOC102724520	XR_427882	5.03	2.92E-03
LOC105374924	XR_926466	4.96	9.60E-06
MAFA	NM_201589	4.95	4.27E-13
CCBE1	NM_133459	4.94	9.42E-18
LOC101928371	NR_110236	4.86	7.85E-04
WNT11	NM_004626	4.82	8.54E-06
MLK7-AS1	NR_033882	4.80	1.12E-13
PGF	NM_001207012	4.75	1.35E-14
GAS6-AS1	NR_044995	4.73	2.99E-03

gene symbol	RefSeq ID	log2 fold change	padj
LOC105371703	NR_135673	4.71	2.94E-03
CYSLTR2	NM_001308465	4.70	5.38E-17
SLC17A1	NM_005074	4.68	7.53E-09
NPPC	NM_024409	4.64	1.62E-04
LOC101928573	XR_001744019	4.60	2.08E-02
LOC101927745	XR_001754962	4.57	2.60E-06
COL5A3	NM_015719	4.57	2.05E-11
LOC102724234	XR_427872	4.54	2.47E-03
TRIML2	NM_001303419	4.54	3.72E-14
LOC105376346	XR_930538	4.49	4.66E-02
PLIN5	NM_001013706	4.46	7.62E-11
LOC101927902	XR_001744977	4.45	4.53E-05
MMP13	NM_002427	4.45	2.35E-12
LOC105377557	XR_001741925	4.41	1.01E-03
LOC105370982	XR_001751669	4.41	1.15E-06
CCM2L	NM_080625	4.39	8.04E-05
NGFR	NM_002507	4.36	2.18E-06
LOC102800447	NR_110564	4.33	2.87E-04
ZDHHC11B	XM_017010110	4.30	4.53E-06
LOC105370969	XR_001751655	4.24	6.53E-03
CXCL13	NM_006419	4.22	3.74E-04
DLL4	NM_019074	4.09	1.06E-13
LOC105372950	XR_001738483	4.05	4.27E-03
RRAD	NM_001128850	4.03	7.30E-14
LINC01006	NR_103858	3.99	4.60E-02
LOC105376872	XR_001753496	3.94	4.95E-02
CES3	NM_001185176	3.92	1.62E-06
ANO2	NM_001278596	3.88	2.79E-08
RNF223	NM_001205252	3.86	5.91E-06
CEBPA	NM_001285829	3.86	8.26E-12
DIO3	NM_001362	3.84	1.96E-05
ATP1B2	NM_001303263	3.79	3.93E-05
LOC107983965	XM_017011612	3.78	2.37E-05
F10	NM_000504	3.78	1.87E-03
CRISPLD2	NM_031476	3.77	1.62E-20
LOC105378992	XR_001742669	3.63	2.99E-03
LOC101928004	XR_001743942	3.63	4.30E-11
SLC39A12	NM_001145195	3.60	3.28E-06
LOC105376244	XR_001746915	3.53	1.69E-05
FAM46C	NM_017709	3.52	6.47E-09
LOC100505817	NR_038340	3.51	9.38E-05
LOC107984121	XR_001744347	3.51	2.27E-02
LOC101928277	XR_001744363	3.49	6.50E-03
KCCAT333	NR_110014	3.41	3.01E-05
LOC101929450	NR_125814	3.40	6.64E-04
TCN1	NM_001062	3.37	1.07E-08
SPATA22	NM_001170695	3.34	1.54E-03
ADGRG1	NM_001145770	3.30	1.59E-12
SEMA4D	NM_001142287	3.27	2.71E-24
LOC105378314	XR_001747454	3.27	2.89E-02
LOC105374985	XR_926612	3.25	5.14E-19
LOC105370027	XR_001749346	3.25	4.64E-02
CPA2	NM_001869	3.24	7.75E-06
BIK	NM_001197	3.22	2.43E-03
LINC00589	NR_026765	3.22	2.95E-03
RND1	NM_014470	3.21	2.29E-03
AREG	NM_001657	3.19	1.05E-21
PINLYP	NM_001193621	3.18	8.16E-03
HAP1	NM_001079870	3.15	2.46E-05
A2M	NM_000014	3.14	1.38E-04
MIR711	NR_031756	3.14	2.15E-04
FOXJ1	NM_001454	3.05	3.25E-03
ADGRD1	NM_198827	3.03	2.19E-08
LOC105376755	XR_001739834	3.00	1.30E-05
TUBB3	NM_001197181	2.99	4.62E-15
NKD2	NM_001271082	2.98	3.13E-03
EPB41L3	NM_001281533	2.97	4.07E-07
LOC100288175	XR_001737597	2.97	1.45E-03
LOC107987209	XR_001750914	2.96	2.57E-03
FIBCD1	NM_001145106	2.93	5.66E-12
CTB-12O2.1	NR_109876	2.93	4.41E-02
NRIP3	NM_020645	2.90	1.38E-04
C5AR1	NM_001736	2.89	5.34E-04
FAM174B	NM_207446	2.84	8.69E-04
LOC101929475	XR_001747416	2.83	2.03E-13
LINC01239	NR_038977	2.82	2.52E-03
TRNP1	NM_001013642	2.80	2.04E-03
LOC105369332	NR_135084	2.78	2.27E-02
GALR2	NM_003857	2.74	1.57E-04
LINC01010	NR_038216	2.72	4.11E-02
LINC01399	NR_126356	2.71	8.23E-04
CCRL2	NM_001130910	2.70	8.93E-03

gene symbol	RefSeq ID	log2 fold change	padj
PILRA	NM_013439	2.69	2.00E-02
C1ORF61	NM_001320453	2.68	7.25E-03
COL11A2	NM_001163771	2.67	2.26E-02
LAMA5-AS1	NR_109922	2.66	4.12E-02
LOC105374902	XR_926428	2.65	1.24E-03
RASD1	NM_001199989	2.62	7.19E-11
PPP1R1C	NM_001080545	2.60	7.55E-06
C9	NM_001737	2.59	2.67E-04
LOC105374907	XR_926438	2.55	6.10E-03
ID2	NM_002166	2.53	2.57E-03
RNF219-AS1	NR_047001	2.48	1.85E-03
AGR2	NM_006408	2.47	2.11E-04
TUBB2A°	NM_001069	2.47	3.32E-04
SPINT1	NM_001032367	2.46	1.42E-07
LGSN	NM_001143940	2.45	2.77E-11
STXBP5-AS1	NR_034115	2.45	3.57E-03
LOC105376617	XR_001748167	2.45	1.11E-02
CASC21	NR_117099	2.45	3.94E-02
NPC1	NM_000271	2.44	1.13E-17
C5AR2	NM_001271749	2.43	6.82E-05
MFGE8	NM_001114614	2.42	8.02E-04
NPTXR	NM_014293	2.42	2.29E-04
SVOPL	NM_001139456	2.41	8.43E-03
KLF17	NM_173484	2.40	5.38E-06
NTRK1	NM_001007792	2.39	4.47E-03
LOC105376626	XR_001748179	2.38	3.56E-02
ADGRG3	NM_001308360	2.37	2.59E-02
THBS1	NM_003246	2.37	7.49E-16
KCNK6	NM_004823	2.37	1.26E-02
TNNC1	NM_003280	2.36	1.57E-02
PRRX2	NM_016307	2.34	8.95E-03
VWA7	NM_025258	2.33	1.24E-02
LOC101929710	NR_130776	2.33	1.18E-04
MAFB	NM_005461	2.33	7.65E-04
CRLF1	NM_004750	2.31	1.03E-04
NEDD9	NM_001142393	2.31	1.28E-07
KLHL3	NM_001257194	2.30	4.00E-05
CHAC1	NM_001142776	2.28	1.95E-05
ERFE	NM_001291832	2.28	1.62E-02
PSG4	NM_001276495	2.28	1.49E-05
FGFBP1	NM_005130	2.27	1.12E-03
LOC101928465	XR_244126	2.23	8.26E-04
HECTD2-AS1	NR_024467	2.19	5.73E-03
MIR3189	NR_036156	2.17	5.97E-07
TAS1R3	NM_152228	2.16	1.46E-02
CREG2	NM_153836	2.15	1.92E-02
DKK1	NM_012242	2.13	1.12E-09
AOX1	NM_001159	2.13	2.44E-04
FAM46B	NM_052943	2.12	1.14E-02
OTUD7A	NM_130901	2.12	1.63E-06
INSL4	NM_002195	2.12	7.13E-06
MYT1L	NM_001303052	2.10	1.57E-05
BMP6	NM_001718	2.10	4.06E-12
AP3B2	NM_001278511	2.07	1.71E-02
DLK2	NM_001286655	2.06	4.93E-04
HBEGF	NM_001945	2.06	2.18E-04
LOC643542	NR_033921	2.06	2.53E-02
LINGO2	NM_001258282	2.06	2.09E-02
DENND3	NM_014957	2.05	3.05E-06
COL8A1	NM_001850	2.05	2.00E-08
PFKFB4	NM_001317134	2.05	1.47E-10
LOC101928389	NR_135631	2.05	3.99E-02
BMP2°	NM_001200	2.05	1.13E-10
ADAM32	NM_001313994	2.04	2.22E-05
LOC107986931	XR_001745844	2.04	7.62E-03
LOC105379219	XR_001745785	2.03	3.47E-02
PLXNB3	NM_001163257	2.03	1.67E-03
C1S	NM_001734	2.02	1.50E-11
MST1R	NM_001244937	2.01	1.39E-03
LOC102724948	XR_001739319	2.01	3.18E-02
FBXO32	NM_001242463	2.01	2.32E-04
RGL1	NM_001297669	2.00	4.72E-04
HDAC9	NM_001204144	2.00	2.47E-03
GDF15°°	NM_004864	1.98	7.62E-11
COL1A1	NM_000088	1.98	2.19E-05
RPL13AP20	NR_003932	1.98	1.51E-02
MAPK4	NM_001292039	1.98	1.36E-08
HAS2	NM_005328	1.98	1.01E-09
CDHR5	NM_001171968	1.97	2.31E-02
GFPT2	NM_005110	1.96	3.36E-06
LOC105379109	XR_948638	1.95	1.77E-02
STYK1	NM_018423	1.94	4.19E-03

gene symbol	RefSeq ID	log2 fold change	padj
SLC41A2	NM_032148	1.94	2.84E-07
AKAP12	NM_005100	1.94	8.36E-09
SERPINE1	NM_000602	1.93	7.02E-09
ULBP2	NM_025217	1.93	6.40E-03
LOC107987138	XR_001746966	1.92	5.69E-05
CSPG4	NM_001897	1.90	3.16E-07
KREMEN2	NM_001253725	1.90	8.68E-04
MIG7	XR_001737684	1.89	2.16E-09
CMAHP	NR_002174	1.88	8.87E-04
PLIN4	NM_001080400	1.87	1.44E-03
SYNM	NM_015286	1.86	3.19E-05
LOC284561	XR_001737736	1.86	2.95E-04
TENM2	NM_001080428	1.85	3.21E-04
SNAI1	NM_005985	1.83	3.80E-05
NXPH4	NM_007224	1.83	4.40E-02
NEBL	NM_001173484	1.82	7.64E-04
LOC105373463	XR_001739316	1.82	8.40E-03
LINC01484	NR_108027	1.81	4.93E-03
IRF7	NM_001572	1.80	1.74E-02
LOC105374995	XR_001744070	1.79	4.92E-02
LRP1	NM_002332	1.78	1.03E-05
CLIP2	NM_003388	1.78	3.03E-04
SNED1	NM_001080437	1.77	9.65E-07
TSPAN10	NM_001290212	1.76	3.53E-03
PMEL	NM_001200053	1.76	9.58E-03
S100A2	NM_005978	1.75	3.26E-04
SEMA7A	NM_001146029	1.74	5.38E-03
UNC5B	NM_001244889	1.74	2.27E-03
EEF1A2	NM_001958	1.73	4.40E-06
DNER	NM_139072	1.73	4.17E-07
ADAP1	NM_001284308	1.73	3.26E-02
DCN	NM_001920	1.72	3.83E-03
PCSK9	NM_174936	1.71	1.16E-06
SYT7	NM_001252065	1.71	1.63E-02
TARID	NR_109982	1.70	3.06E-03
FAM227B	NM_152647	1.70	2.01E-02
SERPINB5	NM_002639	1.70	3.81E-03
ATP8B2	NM_001005855	1.69	4.55E-03
FAM65C	NM_001290268	1.69	1.72E-02
ACP6	NM_001323625	1.68	1.69E-02
WNT9A	NM_003395	1.68	2.36E-02
PPL	NM_002705	1.68	9.09E-06
CASC8	NR_024393	1.66	8.67E-04
KRT80	NM_001081492	1.65	3.06E-05
OLFML2A	NM_001282715	1.64	2.02E-05
LOC105372663	XR_936848	1.64	3.74E-04
MYLK4	NM_001012418	1.64	2.53E-02
STC1	NM_003155	1.64	9.42E-08
FAM222A	NM_032829	1.63	1.91E-02
SYNGR1	NM_004711	1.63	1.64E-03
PLXNA3	NM_017514	1.63	1.01E-05
F11R	NM_016946	1.63	1.60E-06
ICAM1	NM_000201	1.62	2.33E-04
EGFEM1P	NR_021485	1.62	8.08E-03
CRIM1	NM_016441	1.61	2.37E-06
MAP3K9	NM_001284230	1.61	1.19E-03
MICALL2	NM_182924	1.60	5.62E-05
HIST1H2AM°	NM_003514	-1.60	8.20E-07
HIST1H2BO	NM_003527	-1.63	3.85E-07
HIST1H3D	NM_003530	-1.64	5.37E-07
HIST2H3D	NM_001123375	-1.64	3.15E-06
OSGEPL1	NM_022353	-1.67	5.26E-05
HIST1H2BH	NM_003524	-1.67	2.08E-07
HIST2H2AC	NM_003517	-1.68	8.43E-08
SNORA74A	NR_002915	-1.68	9.64E-03
RARRES2	NM_002889	-1.69	1.12E-04
HIST1H1E	NM_005321	-1.70	4.76E-08
HIST1H1B	NM_005322	-1.70	2.95E-07
HIST1H2AB	NM_003513	-1.71	6.90E-08
HIST4H4	NM_175054	-1.72	3.52E-07
HIST1H2BJ	NM_021058	-1.72	2.90E-08
NOTUM	NM_178493	-1.74	3.24E-05
HIST1H3F	NM_021018	-1.75	3.64E-08
HIST2H2AB	NM_175065	-1.75	7.97E-07
HIST1H2BN	NM_003520	-1.76	3.96E-07
HIST1H2AK	NM_003510	-1.77	1.77E-07
HIST1H3H	NM_003536	-1.78	2.47E-08
SNORD17	NR_003045	-1.79	9.49E-05
CENPX	NM_001271006	-1.81	7.43E-08
HIST1H4B°	NM_003544	-1.82	1.42E-07
HIST1H2AL	NM_003511	-1.82	3.88E-08
HAGHL	NM_001290137	-1.87	1.63E-06

gene symbol	RefSeq ID	log2 fold change	padj
HIST1H2AD	NM_021065	-1.89	1.05E-09
HIST1H3G	NM_003534	-1.89	3.28E-09
HIST1H4K	NM_003541	-2.18	4.22E-08
LOC105379506	XR_951149	-2.41	3.73E-02
LOC107987293	XR_001754938	-2.41	3.73E-02
TYRO3P	NR_028510	-2.93	2.33E-03
RNU5D-1	NR_002755	-3.76	6.24E-03
SNORA53	NR_003015	-3.90	1.28E-20
MIR3121	NR_036067	-5.74	3.08E-05
HLA-J	NR_024240	-6.86	2.36E-37
MIR151A	NR_029892	-7.61	1.72E-03

Suppl. table S6. DESeq results of ASF1 depletion in HeLa LT cells. 284 up- and 36 downregulated genes with a log2 fold change (l2fc) <-1.6 or >1.6 for siASF1 over siCtrl in HeLa LT cells excluding deregulated genes with a l2fc <-1.2 or >1.2 for siASF1 over siCtrl in HeLa ST cells. The adjusted p-value was set to padj<0.05 and only genes with an RPKM >2 in the highest expressed sample were selected for this table. Genes were sorted by l2fc. Those genes implemented in the *TelNet* database were marked in bold, genes reported to be cell cycle-regulated in HeLa cells (Grant *et al.*, 2013) were marked with a °circle.

Suppl. table S7. DESeq results of ASF1 depleted HeLa LT cells treated with SAHA.

gene symbol	RefSeq ID	2 µM SAHA/ EtOH ctrl		0.5 µM SAHA/ EtOH ctrl	
		log2 fold change	padj	log2 fold change	padj
FABP4	NM_001442	6.71	3.24E-06	4.16	6.71E-02
HLA-DQB1	NM_001243961	6.02	1.95E-06	1.96	3.38E-05
RNASE1	NM_002933	5.84	1.86E-03	0.40	7.68E-01
LGI3	NM_139278	5.48	1.44E-11	0.84	3.95E-01
LOC105371671	XR_922391	5.45	6.38E-03	1.46	3.31E-01
DIRAS1	NM_145173	5.36	1.53E-19	0.47	4.52E-02
IL17RD	NM_001318864	5.22	4.79E-28	0.51	1.77E-03
EDA	NM_001005609	5.13	8.60E-47	1.20	5.12E-11
HPCAL4	NM_001282396	5.05	2.56E-12	1.70	5.70E-20
TNIK	NM_001161560	4.97	4.18E-11	1.03	2.31E-11
PPP4R4	NM_020958	4.93	5.45E-18	0.31	2.06E-01
CD33	NM_001082618	4.92	3.20E-07	0.36	5.59E-01
CCDC85A	NM_001080433	4.88	4.00E-20	0.96	1.50E-06
CD40	NM_001250	4.83	4.86E-08	-0.02	9.57E-01
KCNH2	NM_000238	4.82	1.73E-07	-0.17	6.81E-01
HLA-DMB	NM_002118	4.81	4.79E-28	3.68	4.06E-14
LOC102724548	XR_426710	4.70	1.78E-02	3.21	3.21E-04
NELL2	NM_001145107	4.66	1.61E-15	1.74	1.12E-39
STXBP6	NM_001304476	4.64	2.09E-06	0.86	5.81E-05
EBF1	NM_001290360	4.64	1.22E-12	0.24	4.90E-01
LOC105369563	XR_001748439	4.62	2.45E-07	1.84	9.81E-04
TMSB15A	NM_021992	4.57	1.10E-05	-0.02	9.55E-01
ZNF204P	NR_002722	4.55	4.14E-43	1.69	9.16E-14
ELSPBP1	NM_022142	4.53	7.15E-03	3.29	2.60E-02
RGS9	NM_001081955	4.49	1.26E-03	1.96	1.28E-17
GRID2	NM_001286838	4.45	2.95E-24	-0.34	1.74E-01
SLC6A12	NM_001122847	4.43	1.27E-04	-0.16	9.12E-01
AGMO	NM_001004320	4.40	5.47E-04	0.27	6.59E-01
ALOX5	NM_000698	4.37	8.70E-09	-0.11	7.07E-01
AZGP1	NM_001185	4.37	2.13E-04	2.21	4.87E-03
PRKAR2B	NM_002736	4.37	3.43E-10	0.95	1.95E-10
C2CD4C	NM_001136263	4.35	4.83E-08	-0.12	7.47E-01
RAB37	NM_001006638	4.35	1.03E-12	0.36	5.59E-01
LDLRAD4	NM_001003674	4.30	5.15E-06	-0.30	1.09E-01
PDZD4	NM_001303512	4.30	4.56E-10	1.28	1.23E-11
PURG	NM_001015508	4.30	1.55E-13	0.47	1.03E-01
CREB3L3	NM_001271995	4.28	2.75E-21	0.79	7.31E-01
OSBPL6	NM_001201480	4.28	3.67E-17	0.41	2.73E-02
FAM167A	NM_053279	4.27	7.59E-05	0.44	3.68E-01
GPR143	NM_000273	4.26	2.89E-04	0.31	8.77E-01
FXYD1	NM_001278717	4.26	2.89E-06	1.90	3.14E-03
MYCT1	NM_025107	4.26	1.75E-03	2.62	3.84E-15
DENND2C	NM_001256404	4.25	5.52E-15	0.80	3.41E-05

gene symbol	RefSeq ID	2 µM SAHA/ EtOH ctrl		0.5 µM SAHA/ EtOH ctrl	
		log2 fold change	padj	log2 fold change	padj
CGN	NM_020770	4.23	3.95E-08	0.78	3.07E-05
TMOD2	NM_001142885	4.22	3.74E-22	0.93	5.35E-05
IGF2BP2	NM_001007225	4.21	3.55E-09	0.28	1.01E-01
MYH14	NM_001077186	4.21	9.34E-04	0.29	2.12E-01
LOC105373890	XR_001739233	4.20	1.58E-02	1.11	2.31E-04
LOC105376626	XR_001748179	4.20	8.80E-05	1.64	1.87E-01
FOXD1	NM_004472	4.19	2.44E-11	-0.22	3.13E-01
PPP2R2C	NM_001206994	4.17	1.21E-05	0.57	4.56E-04
CAMSAP3	NM_001080429	4.14	5.77E-08	0.70	1.98E-02
COL5A3	NM_015719	4.13	7.72E-04	1.05	1.96E-04
CABP1	NM_001033677	4.12	2.24E-03	-0.17	9.22E-01
CRMP1	NM_001014809	4.09	5.94E-30	0.27	2.01E-01
UNC13A	NM_001080421	4.07	6.02E-08	0.65	3.95E-03
AGPAT4	NM_020133	4.07	3.77E-15	0.03	9.21E-01
FAM171A1	NM_001010924	4.07	1.89E-05	0.06	8.50E-01
C7ORF57	NM_001100159	4.03	5.90E-35	1.30	5.18E-02
HLA-F-AS1	NR_026972	4.02	1.82E-16	0.33	3.37E-01
PSG4	NM_001276495	4.02	7.17E-14	1.95	1.36E-18
PAGE2B	NM_001015038	4.01	2.45E-03	-0.27	3.28E-01
LOC107986215	XM_017008885	4.00	1.36E-04	0.62	3.90E-01
TMEM59L	NM_012109	3.99	2.06E-12	1.35	3.55E-07
LOC105379102	XR_001742829	3.97	1.09E-07	1.13	5.06E-01
SND1-IT1	NR_027330	3.96	3.05E-03	-0.16	9.52E-01
TP53I11	NM_001258320	3.95	1.04E-09	0.22	4.16E-01
LOC101929305	XR_001738364	3.95	1.34E-02	1.72	8.00E-02
CDC42EP5	NM_145057	3.91	3.83E-10	-0.37	5.84E-01
HMCN1	NM_031935	3.91	4.94E-33	0.18	4.78E-01
ADGRE1	NM_001256252	3.90	2.96E-16	1.18	1.63E-04
IGSF1	NM_001170961	3.87	1.55E-122	0.56	5.59E-01
TMEM86A	NM_153347	3.86	2.26E-32	0.56	8.30E-02
LOC101928216	XR_001737945	3.85	7.59E-07	1.02	3.38E-01
FNDC4	NM_022823	3.84	3.94E-05	0.28	5.80E-01
GPR162	NM_014449	3.83	4.91E-14	0.04	9.24E-01
KHDRBS3	NM_006558	3.82	8.84E-15	-0.21	2.40E-01
KCNK9	NM_001282534	3.81	1.20E-07	2.68	7.39E-13
RTBDN	NM_001080997	3.77	1.67E-04	1.59	1.96E-01
EPYC	NM_004950	3.77	3.74E-02	0.38	8.35E-01
LOC107986838	XR_001745337	3.77	7.32E-12	1.48	5.40E-02
ABAT	NM_000663	3.76	3.71E-08	0.82	5.51E-08
RASAL1	NM_001193520	3.76	2.48E-05	0.25	5.56E-01
SCN9A	NM_002977	3.75	3.23E-63	1.09	1.74E-08
PRKD1	NM_002742	3.74	3.04E-20	-0.17	5.20E-01
DACT3	NM_001301046	3.72	2.56E-04	1.10	2.26E-05
REEP1°	NM_001164730	3.71	3.92E-11	0.25	5.51E-01
OR51B5	NM_001005567	3.71	8.55E-06	0.87	1.53E-05
TENM1	NM_001163278	3.70	2.86E-02	1.42	1.67E-06
YPEL4	NM_145008	3.68	5.18E-09	0.34	7.21E-01
AIM1L	NM_001039775	3.66	1.69E-08	0.88	1.68E-02
ADRA1B	NM_000679	3.65	1.71E-07	0.69	2.08E-04
LOC105373891	XR_001739888	3.64	3.33E-02	1.12	5.20E-02
PIK3R1	NM_001242466	3.64	1.47E-19	-0.18	3.94E-01
SORBS1	NM_001034954	3.63	1.75E-07	0.81	1.81E-06
TPPP	NM_007030	3.61	7.34E-03	0.85	1.10E-03
LINC00922	NR_027755	3.60	4.42E-04	-0.32	8.45E-01
PTN	NM_001321386	3.60	5.55E-05	0.17	5.67E-01
MAP2	NM_001039538	3.59	2.37E-21	1.09	1.78E-14
LOC102724434	NR_130921	3.59	2.76E-21	2.55	4.80E-02
ANKRD24	NM_133475	3.57	1.38E-09	2.15	3.90E-16
WBSCR28	NM_182504	3.57	1.58E-09	1.61	2.38E-01
LOC105377706	XR_941182	3.56	4.77E-02	0.99	6.14E-01
MIR4300HG	NR_120571	3.56	5.50E-04	1.27	3.68E-01
LINC01162	NR_126381	3.55	4.41E-03	0.86	6.00E-01
C1ORF116	NM_001083924	3.55	1.84E-06	1.50	1.15E-03
TDRKH	NM_001083963	3.54	2.31E-15	0.62	2.55E-03
IGSF10	NM_001178145	3.54	2.61E-13	0.16	7.40E-01
CFAP58-AS1	NR_108036	3.52	8.67E-16	1.94	5.54E-03
ANKRD1	NM_014391	3.52	6.60E-04	1.00	3.95E-17
GPR4	NM_005282	3.51	9.82E-05	1.36	2.94E-02
CALB2	NM_001740	3.51	1.71E-03	0.04	9.14E-01
MARCH4	NM_020814	3.51	5.36E-03	0.67	1.97E-02
LOC101930114	NR_134509	3.51	2.05E-02	1.04	4.82E-01
CDH12	NM_001317227	3.50	1.58E-07	0.06	8.46E-01
PSG5	NM_001130014	3.49	5.85E-04	2.00	1.66E-03
APLP1	NM_001024807	3.48	4.25E-20	0.93	1.57E-08
ADRA2C	NM_000683	3.45	2.87E-02	0.03	9.62E-01
FLJ25758	NR_024372	3.44	1.33E-02	3.84	1.15E-01
ITGA7	NM_001144996	3.43	7.48E-04	0.73	2.23E-04
LINGO2	NM_001258282	3.42	1.87E-08	0.07	8.51E-01
SRRM3	NM_001110199	3.40	3.04E-07	0.13	7.00E-01
ADAMTS16	NM_139056	3.40	1.95E-05	0.48	1.23E-02
COL6A2	NM_001849	3.39	1.23E-08	0.15	4.19E-01

gene symbol	RefSeq ID	2 µM SAHA/ EtOH ctrl		0.5 µM SAHA/ EtOH ctrl	
		log2 fold change	padj	log2 fold change	padj
SLC29A4	NM_001040661	3.39	1.56E-09	0.04	8.95E-01
COL4A3	NM_000091	3.38	4.52E-11	0.23	8.97E-01
GRID1	NM_017551	3.38	2.02E-04	-0.32	6.23E-01
IL3RA	NM_001267713	3.38	1.45E-04	0.50	7.93E-01
SLC2A4	NM_001042	3.38	9.40E-31	0.85	7.03E-04
NEO1	NM_001172623	3.36	1.26E-26	0.25	1.90E-01
DNM1	NM_001005336	3.35	9.85E-07	-0.22	3.32E-01
ZNF467	NM_207336	3.34	3.87E-16	-0.37	5.33E-01
SEPT4	NM_001198713	3.34	5.40E-08	0.97	2.42E-02
HOMER2	NM_004839	3.33	5.68E-05	0.07	8.11E-01
BCO2	NM_001037290	3.32	4.72E-08	1.39	1.51E-04
SH2D3C	NM_001142531	3.32	8.62E-04	1.13	3.67E-03
DCN	NM_001920	3.31	8.83E-15	3.31	1.36E-01
LOC105369484	XR_948004	3.31	9.84E-07	0.32	9.08E-01
PPM1J	NM_005167	3.31	1.07E-18	1.82	2.88E-13
MAP1B	NM_001324255	3.31	3.27E-02	0.31	4.43E-02
DAW1	NM_178821	3.30	1.34E-02	2.82	7.24E-07
RGS17	NM_012419	3.30	1.02E-12	0.76	6.53E-04
SLC16A12	NM_213606	3.29	2.12E-03	2.72	1.78E-24
LOC105369438	NR_135093	3.28	1.28E-03	0.52	7.41E-01
ARFGEF3	NM_020340	3.28	2.66E-08	0.22	2.89E-01
KIAA0319	NM_001168374	3.27	4.56E-10	1.69	3.46E-04
HECTD2-AS1	NR_024467	3.26	1.30E-08	0.86	4.96E-02
CGNL1	NM_001252335	3.26	7.66E-16	0.68	1.25E-04
CHRM4	NM_000741	3.25	3.22E-07	0.98	1.79E-03
ZNF365	NM_014951	3.24	5.52E-14	1.06	6.87E-13
CYP4F12	NM_023944	3.23	2.14E-02	3.77	5.15E-06
DIRC3-AS1	NR_133642	3.23	1.34E-03	1.48	7.20E-14
RASGRP2	NM_001098670	3.23	3.54E-04	0.63	3.54E-01
C14ORF37	NM_001001872	3.22	6.74E-04	0.74	3.19E-06
NOTCH3	NM_000435	3.22	2.08E-09	0.19	3.95E-01
NRXN3	NM_001105250	3.21	1.59E-10	0.99	2.40E-02
SRPX	NM_001170750	3.21	9.23E-39	-0.28	1.08E-01
STAC2	NM_198993	3.20	4.40E-07	0.21	9.31E-01
HAPLN3	NM_001307952	3.19	3.92E-04	0.03	9.38E-01
TRNP1	NM_001013642	3.19	1.74E-05	0.25	2.74E-01
LOC105374523	XR_001741614	3.18	1.17E-02	2.54	1.62E-04
LOC105369881	XR_945161	3.17	4.50E-03	0.29	7.01E-01
LOC105371308	XR_001752232	3.16	1.06E-04	0.37	2.56E-01
SLC45A1	NM_001080397	3.16	4.02E-12	0.81	1.54E-01
LOC105373893	XR_001739889	3.16	1.81E-02	0.96	6.46E-02
LOC105375508	XR_001744984	3.16	5.49E-05	0.03	9.80E-01
DKK3	NM_001018057	3.15	8.28E-148	0.55	1.76E-04
NXN	NM_001205319	3.14	3.14E-09	0.03	9.11E-01
TMEM63C	NM_020431	3.13	5.84E-04	1.15	3.15E-06
CHRD	NM_001304472	3.12	4.73E-04	-0.19	6.55E-01
KLC3	NM_177417	3.12	4.20E-03	1.03	8.41E-04
PHOSPHO1	NM_001143804	3.11	5.70E-28	1.27	7.27E-04
LINC00431	NR_126378	3.11	6.51E-03	1.47	1.68E-01
ATP1A3	NM_001256213	3.09	4.49E-02	1.57	7.75E-12
GPRIN3	NM_198281	3.09	1.39E-21	1.18	5.01E-07
NR3C2	NM_000901	3.08	8.62E-07	-0.10	7.66E-01
TMC3-AS1	NR_120365	3.07	9.39E-05	1.09	1.41E-05
SLC17A7	NM_020309	3.07	4.31E-03	1.04	1.12E-02
KANK3	NM_198471	3.07	1.08E-03	1.08	3.21E-04
MAST1	NM_014975	3.06	2.05E-26	1.19	3.53E-05
LOC105373592	XR_001739684	3.06	2.24E-02	0.26	6.86E-01
ATP8B2	NM_001005855	3.06	2.19E-14	0.26	1.91E-01
MIR6124	NR_106739	3.05	2.83E-02	0.52	4.71E-01
RTN4RL2	NM_178570	3.05	4.11E-24	0.27	6.52E-01
S1PR1	NM_001320730	3.05	1.31E-22	1.61	6.41E-04
LOC101927880	XR_001747321	3.04	2.11E-07	-0.32	7.81E-01
SEMA6B	NM_032108	3.03	1.41E-06	0.18	3.75E-01
TNFRSF9	NM_001561	3.03	4.40E-06	0.90	1.64E-06
IQUB	NM_001282855	3.03	1.59E-15	1.04	1.87E-02
LHFP	NM_005780	3.03	1.28E-03	-0.23	4.99E-01
NTNG2	NM_032536	3.03	9.64E-03	0.39	9.09E-02
REEP2	NM_001271803	3.02	3.15E-35	0.47	7.00E-02
PTX3	NM_002852	3.01	4.13E-09	0.38	6.03E-01
SLC2A9	NM_001001290	3.01	3.93E-02	0.17	8.90E-01
CADM4	NM_145296	3.00	1.23E-21	0.06	8.29E-01
HMSD	NM_001123366	2.99	3.06E-04	0.98	3.17E-01
LINC01170	NR_125774	2.98	8.35E-05	-0.47	5.39E-01
PRR16°	NM_001300783	2.97	4.59E-18	-0.15	8.77E-01
RGL1	NM_001297669	2.96	1.82E-06	0.54	1.34E-03
SULT2B1	NM_004605	2.96	5.99E-08	0.78	4.21E-01
ABCA3	NM_001089	2.96	1.18E-23	0.91	1.00E-04
LOC105374678	XR_001742406	2.95	5.92E-04	0.07	9.71E-01
RAB3B	NM_002867	2.95	9.67E-03	-0.11	6.95E-01
LOC107984502	XR_001749075	2.95	1.25E-05	0.07	9.32E-01
LYPD5	NM_001031749	2.94	8.69E-08	2.21	4.38E-09

gene symbol	RefSeq ID	2 µM SAHA/ EtOH ctrl		0.5 µM SAHA/ EtOH ctrl	
		log2 fold change	padj	log2 fold change	padj
MAN1C1	NM_001289010	2.94	9.54E-08	0.43	2.02E-01
TSPAN9	NM_001168320	2.94	3.15E-07	0.23	3.03E-01
GALNT12	NM_024642	2.94	1.65E-29	0.50	2.70E-01
TNFAIP8L3	NM_001311175	2.93	1.90E-03	1.25	1.68E-01
HMGA2	NM_001300918	2.93	2.33E-02	0.03	9.32E-01
TMCC2	NM_001242925	2.92	2.44E-12	1.20	5.04E-10
SEPT5	NM_001009939	2.92	4.77E-35	0.23	2.30E-01
PMEL	NM_001200053	2.92	1.12E-11	1.66	5.26E-04
FGF13	NM_001139498	2.91	2.03E-04	-0.05	9.27E-01
LOC100506113	XR_001748304	2.91	1.59E-08	0.36	7.93E-01
NPL	NM_001200050	2.90	2.67E-05	0.47	1.24E-01
CREB5	NM_001011666	2.90	3.73E-09	0.36	5.78E-01
DCDC1	NM_181807	2.90	4.99E-14	1.45	2.02E-03
LOC107001062	NR_134500	2.89	8.12E-03	0.09	9.65E-01
ADAMTS10	NM_001282352	2.89	3.61E-20	-0.21	4.74E-01
SPOCK3	NM_001040159	2.89	1.78E-31	-0.15	8.38E-01
LOC255187	NR_122044	2.89	1.42E-02	-0.60	5.52E-01
CCDC69	NM_015621	2.88	1.19E-08	0.74	8.35E-06
RARB	NM_000965	2.88	1.81E-06	1.40	2.13E-17
LINC01098	NR_028342	2.88	1.05E-03	1.38	3.00E-01
RDH12	NM_152443	2.87	7.33E-03	1.24	1.43E-02
PCDH1	NM_001278613	2.87	1.32E-29	3.01	1.94E-43
LOC101928419	XR_241794	2.86	1.71E-04	2.11	6.82E-02
ARHGAP44	NM_001321164	2.86	3.61E-28	0.43	6.08E-02
LOC101928599	XR_001750839	2.85	6.55E-08	-0.12	8.85E-01
MAPK8IP2	NM_012324	2.84	1.18E-05	2.09	2.70E-13
SYNPO2	NM_001128933	2.84	8.25E-07	2.26	9.64E-05
AHNAK2	NM_138420	2.84	3.43E-13	0.01	9.66E-01
MFGE8	NM_001114614	2.83	1.59E-06	0.22	2.19E-01
TSPAN33	NM_178562	2.82	1.27E-33	0.92	2.06E-05
NRG2	NM_001184935	2.82	3.27E-03	1.79	5.34E-06
CLCN4	NM_001256944	2.82	1.15E-16	0.49	9.64E-03
LRRC17°	NM_001031692	2.82	4.60E-02	0.78	1.65E-01
ATP7B	NM_000053	2.82	1.79E-14	0.58	1.30E-02
KLLN	NM_001126049	2.82	3.86E-11	0.08	9.70E-01
SLC9A9	NM_173653	2.81	4.57E-43	0.95	1.39E-04
LOC105378800	XR_947517	2.81	2.58E-02	3.63	1.11E-02
ATP8A1	NM_001105529	2.81	3.84E-23	0.58	3.15E-05
ARMC12	NM_001286574	2.80	4.42E-09	0.38	7.19E-01
YBX2	NM_015982	2.78	1.21E-05	0.65	6.10E-02
CDS1	NM_001263	2.76	4.27E-24	1.26	5.69E-10
RBM20	NM_001134363	2.76	7.91E-10	0.33	3.40E-01
LOC105373215	XR_001738537	2.75	2.00E-03	-0.11	8.99E-01
SLC2A12	NM_145176	2.75	1.99E-57	-0.15	4.91E-01
LOC283352	NR_104172	2.75	3.23E-03	0.58	6.91E-03
LOC107986606	XR_001744176	2.74	5.74E-06	2.51	2.78E-04
LOC102546294	NR_105057	2.74	1.06E-26	0.94	1.15E-01
LINC00707	NR_038291	2.74	2.72E-04	0.32	8.13E-01
ICA1	NM_001136020	2.74	7.33E-06	-0.08	9.11E-01
CCL20	NM_001130046	2.73	4.69E-02	3.51	1.08E-15
SAMD14	NM_001257359	2.73	2.89E-05	1.11	2.88E-03
FRMD5	NM_001286490	2.72	2.44E-04	0.00	9.95E-01
CNBD1	NM_173538	2.71	2.19E-03	0.11	9.39E-01
MAP1A	NM_002373	2.69	3.10E-07	0.50	9.00E-03
LOC105369349	XR_950211	2.68	1.01E-02	0.22	8.87E-01
OR1J2	NM_054107	2.68	1.31E-05	0.72	2.58E-02
LOC101927947	XR_001741892	2.68	2.93E-02	1.05	7.28E-03
VPS37D	NM_001077621	2.68	2.79E-07	0.08	8.86E-01
CETN4P	NR_024041	2.68	3.80E-07	1.20	2.69E-01
CYTH4	NM_001318024	2.67	3.23E-02	1.86	1.55E-06
C2ORF70	NM_001105519	2.66	3.43E-07	0.83	3.83E-01
CTB-12O2.1	NR_109876	2.66	2.22E-02	0.19	8.25E-01
GALNT18	NM_198516	2.66	3.32E-09	0.90	3.38E-08
LOC102724895	XR_430113	2.65	1.39E-03	4.18	3.99E-07
LOC107986824	XR_001745287	2.65	8.50E-03	-0.14	9.08E-01
LARGE2	NM_001300721	2.64	5.98E-14	-0.01	9.79E-01
EEPD1	NM_030636	2.64	4.82E-06	0.70	2.83E-03
CTTNBP2	NM_033427	2.64	2.39E-07	-0.19	6.97E-01
LOC107985325	XR_001754012	2.62	1.54E-03	1.39	1.41E-02
PAG1	NM_018440	2.61	6.23E-07	1.32	6.48E-10
MAK	NM_001242385	2.61	1.32E-02	0.53	5.03E-01
LOC105373369	XR_001755974	2.61	2.50E-11	0.00	9.99E-01
LOC105373463	XR_001739316	2.61	3.13E-04	0.15	9.07E-01
MYZAP	NM_001018100	2.60	3.92E-50	1.10	5.49E-09
RTN4RL1	NM_178568	2.60	2.64E-04	0.19	9.14E-01
MATN3	NM_002381	2.60	1.60E-05	-0.49	7.36E-02
LOC101927252	XR_001739825	2.60	2.52E-04	0.37	7.07E-01
LOC107985339	XR_001753852	2.60	1.24E-07	2.55	4.39E-02
DNAH11	NM_001277115	2.60	1.66E-32	0.44	4.12E-01
HOXA1	NM_005522	2.59	6.05E-06	0.63	4.73E-02
HDAC9	NM_001204144	2.59	6.65E-05	0.17	4.89E-01

gene symbol	RefSeq ID	2 µM SAHA/ EtOH ctrl		0.5 µM SAHA/ EtOH ctrl	
		log2 fold change	padj	log2 fold change	padj
CCDC148	NM_001301684	2.59	1.79E-03	1.62	1.87E-13
LOC554206	NR_038379	2.59	3.95E-08	1.08	4.42E-01
DIRAS3	NM_004675	2.58	1.38E-12	-0.18	9.20E-01
MIR137HG	NR_046105	2.58	4.56E-07	0.19	8.11E-01
CRLF1	NM_004750	2.57	8.92E-06	1.23	1.69E-05
LOC105372424	XR_935996	2.57	1.35E-06	-0.03	9.76E-01
AREG	NM_001657	2.56	1.37E-02	1.82	5.38E-15
TJP3	NM_001267560	2.56	2.84E-10	1.15	4.26E-06
PELI2	NM_021255	2.56	9.20E-10	-0.10	7.40E-01
LOC107986884	XR_001745703	2.55	4.30E-02	2.41	4.13E-04
SEPT5-GP1BB	NR_037611	2.55	3.22E-30	0.22	2.53E-01
PALM3	NM_001145028	2.54	1.29E-04	0.71	1.39E-01
LINC01057	NR_104131	2.54	6.02E-04	-0.02	9.76E-01
STAT4	NM_001243835	2.54	2.50E-08	0.65	5.95E-01
TPPP3	NM_015964	2.53	1.44E-03	-0.16	9.39E-01
SCIN	NM_001112706	2.53	1.86E-05	0.42	3.29E-01
BEX2	NM_001168399	2.52	9.02E-10	0.54	1.74E-02
LINC01182	NR_121681	2.52	4.20E-06	-0.02	9.86E-01
KCTD12	NM_138444	2.52	3.99E-07	0.02	9.70E-01
TMEM232	NM_001039763	2.52	3.03E-09	0.85	3.57E-02
PSG10P	NR_026824	2.52	8.93E-03	1.96	1.09E-01
LOC105369344	XR_001748261	2.52	1.42E-13	-0.08	9.65E-01
LOC107986412	XR_001742638	2.51	3.01E-02	2.69	8.44E-02
NMRAL2P	NR_033752	2.51	4.39E-12	-0.11	9.26E-01
PRRT3	NM_001318871	2.51	5.43E-16	0.59	1.17E-02
LOC105375746	XR_001746072	2.51	2.40E-02	0.76	2.38E-01
GBP2	NM_004120	2.50	1.30E-32	0.25	5.44E-01
DPF3	NM_001280542	2.50	2.49E-08	0.80	1.52E-01
CPM	NM_001005502	2.49	6.51E-11	0.74	7.64E-03
LINC00871	NR_102699	2.48	1.01E-02	0.18	9.49E-01
IQGAP2	NM_001285460	2.48	5.93E-05	1.64	4.28E-17
GIPR	NM_000164	2.48	1.56E-05	0.24	8.21E-01
SMIM1	NM_001163724	2.48	2.01E-19	0.30	7.56E-01
GRB14	NM_001303422	2.47	3.96E-34	0.57	1.66E-02
RPLP0P2	NR_002775	2.47	7.34E-03	1.92	2.12E-19
KCNIP4	NM_001035003	2.47	1.84E-02	1.52	1.46E-02
KIF21B	NM_001252100	2.47	2.63E-08	0.84	2.08E-05
NRTN	NM_004558	2.46	6.65E-14	-0.09	8.99E-01
DNM3	NM_001136127	2.46	2.92E-07	1.87	1.39E-37
CHODL	NM_001204174	2.46	4.19E-02	1.19	1.25E-03
NR2F2-AS1	NR_102743	2.46	1.06E-03	0.69	2.20E-03
RASD2	NM_014310	2.45	1.17E-03	1.13	1.34E-03
PTK7	NM_001270398	2.45	1.27E-08	-0.02	9.61E-01
OLFM2	NM_001304347	2.45	4.86E-06	0.46	4.78E-02
LINC01461	NR_125761	2.45	8.25E-04	0.74	5.05E-01
LOC105369949	XR_001749294	2.45	1.14E-04	1.40	1.47E-02
PLEKHB1	NM_001130033	2.45	3.64E-06	0.20	6.38E-01
PTHLH	NM_002820	2.43	2.14E-05	0.45	2.57E-01
LOC107987105	XR_001746865	2.43	1.65E-05	0.81	4.64E-01
NMNAT2	NM_015039	2.42	5.15E-07	1.70	1.20E-22
LOC101927967	NR_110288	2.42	3.45E-02	0.50	4.39E-01
DNAJC28	NM_001040192	2.41	3.92E-11	0.57	2.90E-01
CASZ1	NM_001079843	2.41	6.86E-05	0.64	1.03E-02
FBLN5	NM_006329	2.41	4.00E-20	0.42	3.52E-01
C10ORF113	NM_001010896	2.41	3.00E-03	1.52	9.02E-02
STK11	NM_000455	2.41	4.27E-11	0.00	9.88E-01
IL18	NM_001243211	2.40	2.70E-12	0.66	2.67E-08
KCNH3	NM_001314030	2.39	1.58E-12	0.97	1.91E-09
LOC105375751	XR_001746076	2.39	1.01E-03	0.24	5.42E-01
LOC105372281	XR_936336	2.39	3.19E-08	0.62	3.70E-01
EML5	NM_183387	2.39	1.02E-21	0.39	6.61E-01
ATL1	NM_001127713	2.39	9.71E-04	-0.05	8.91E-01
EEF1A2	NM_001958	2.39	5.78E-09	0.21	2.21E-01
PDZD7	NM_001195263	2.38	3.97E-14	1.64	4.97E-08
LOC105376615	XR_001748166	2.38	2.73E-03	0.13	9.25E-01
LOC105373805	NR_136318	2.38	6.79E-03	0.46	8.16E-01
LINC01399	NR_126356	2.38	2.70E-02	0.36	2.87E-02
BMF	NM_001003940	2.37	1.46E-08	-0.29	3.24E-01
JAG2	NM_002226	2.37	1.04E-24	0.01	9.84E-01
SYTL2	NM_001162951	2.37	3.84E-06	0.85	8.74E-11
LOC105378992	XR_001742669	2.37	3.94E-03	0.03	9.41E-01
PITPNM3	NM_001165966	2.37	6.30E-09	-0.51	8.77E-02
SCAMP5	NM_001178111	2.37	1.36E-29	0.74	8.57E-04
LMO1	NM_001270428	2.36	3.23E-03	0.44	7.30E-01
MAPK8IP1	NM_005456	2.36	1.10E-08	1.03	4.63E-11
SAMD11	NM_152486	2.36	9.26E-07	-0.15	6.59E-01
IL1A	NM_000575	2.36	1.36E-04	2.02	1.14E-05
LOC105377732	XR_001743000	2.35	4.23E-02	1.70	1.75E-06
NKILA	NR_131157	2.34	8.85E-18	0.94	1.40E-10
LINC00936	NR_028138	2.34	2.31E-25	1.16	1.48E-03
KCNJ2	NM_000891	2.34	1.99E-45	0.50	6.13E-01

gene symbol	RefSeq ID	2 µM SAHA/ EtOH ctrl		0.5 µM SAHA/ EtOH ctrl	
		log2 fold change	padj	log2 fold change	padj
DAPK1	NM_001288729	2.33	5.77E-08	-0.02	9.74E-01
DNER	NM_139072	2.33	2.00E-08	1.01	1.05E-01
PLCL1	NM_006226	2.33	2.90E-04	-0.34	8.11E-01
HS6ST3	NM_153456	2.32	1.86E-17	0.87	1.83E-01
DNAAF3	NM_001256714	2.32	1.71E-15	1.66	4.02E-11
CACNA1G	NM_001256324	2.31	1.02E-08	0.88	3.95E-04
CCDC110	NM_001145411	2.31	3.19E-29	1.64	2.23E-03
AFDN°	NM_001040000	2.31	6.46E-20	0.11	5.83E-01
TRPM4	NM_001195227	2.31	3.79E-31	0.10	7.46E-01
PPFIBP2	NM_001256568	2.30	1.95E-03	0.43	1.34E-01
STMN3	NM_001276310	2.30	1.03E-04	1.10	1.18E-10
MORN3	NM_173855	2.30	2.53E-06	0.22	8.93E-01
DNAH2	NM_001303270	2.30	2.78E-06	0.43	5.49E-01
PGM5P2	NR_002836	2.30	7.72E-06	0.32	6.24E-01
STARD5	NM_181900	2.29	2.68E-08	-0.36	4.51E-01
SNPH	NM_001318234	2.29	1.62E-12	0.63	2.81E-04
PLCXD2	NM_001185106	2.29	2.03E-12	0.88	3.10E-11
LINC01619	NR_046159	2.29	3.50E-03	0.07	8.81E-01
COL4A4	NM_000092	2.28	7.67E-05	0.09	7.78E-01
MMP9	NM_004994	2.28	3.31E-02	0.51	1.01E-01
MIR4260	NR_036213	2.28	2.99E-06	0.88	4.28E-02
PRSS16	NM_005865	2.28	1.49E-09	0.00	9.96E-01
LOC100288798	NR_125377	2.28	3.46E-02	0.77	1.28E-01
SLC27A1	NM_198580	2.28	1.01E-11	0.24	3.06E-01
HS1BP3-IT1	NR_046836	2.28	4.02E-03	0.06	9.73E-01
IL12A	NM_000882	2.28	1.28E-03	1.01	2.01E-01
GNAO1	NM_020988	2.27	1.07E-08	0.46	1.16E-01
LOC105378482	XR_001747585	2.27	2.85E-04	-0.13	9.15E-01
SYT7	NM_001252065	2.26	1.80E-07	1.67	4.75E-13
MTUS2	NM_001033602	2.26	3.05E-28	0.89	3.58E-03
SLC1A1	NM_004170	2.25	1.56E-30	0.97	2.72E-04
CITED1	NM_001144885	2.25	1.39E-02	0.85	2.56E-01
CTSV	NM_001201575	2.25	1.24E-07	0.31	1.65E-01
FER1L4	NR_119376	2.24	3.54E-04	0.44	4.69E-01
FAM129A	NM_052966	2.24	1.50E-15	-0.73	6.23E-01
SH2D5	NM_001103160	2.24	8.65E-19	-0.21	2.95E-01
LOC105373044	NR_134631	2.23	1.47E-02	-0.39	7.42E-01
EML6	NM_001039753	2.23	8.56E-15	0.21	4.03E-01
NECTIN1	NM_002855	2.23	4.29E-26	0.14	7.18E-01
LOC105378316	XR_945981	2.22	4.75E-02	0.65	6.12E-01
LOC105377199	XR_001755529	2.22	4.23E-05	1.50	4.33E-04
LOC107986198	XR_001741448	2.22	3.32E-02	1.96	7.83E-06
GLI2	NM_005270	2.22	4.49E-12	-0.45	9.11E-02
CREG2	NM_153836	2.22	1.48E-05	0.15	8.81E-01
SERPINI1	NM_001122752	2.22	1.74E-13	1.71	8.74E-07
PRSS3	NM_001197097	2.22	2.02E-02	2.61	2.03E-02
GSDMB	NM_001042471	2.22	1.07E-09	0.46	2.15E-01
CAPN5	NM_004055	2.22	3.60E-03	0.18	5.17E-01
CCDC3	NM_001282658	2.21	1.32E-02	0.91	3.59E-12
CYFIP2	NM_001037333	2.21	4.64E-37	0.87	1.73E-10
MYH10	NM_001256012	2.21	5.75E-22	0.09	6.90E-01
SLC44A3	NM_001114106	2.21	3.61E-10	0.69	1.85E-03
TUB	NM_003320	2.20	1.58E-17	-0.15	6.26E-01
LINC01411	NR_125806	2.19	3.46E-02	1.37	2.54E-16
MGC27382	NR_027310	2.19	4.47E-03	0.18	9.15E-01
NLGN1	NM_014932	2.19	4.69E-05	-0.07	8.75E-01
CHSY3	NM_175856	2.19	1.03E-08	-0.23	3.65E-01
LOC105375716	XR_001746038	2.19	2.97E-02	0.26	7.31E-01
CTSH	NM_001319137	2.19	4.71E-16	-0.02	9.69E-01
DUSP9	NM_001318503	2.19	3.41E-18	-0.56	8.28E-02
LOC105377700	XR_001742961	2.18	5.19E-03	0.29	6.92E-01
LRRC75A	NM_001113567	2.18	5.93E-05	0.11	8.48E-01
MIR6843	NR_106902	2.17	3.85E-03	0.45	7.82E-01
ANG	NM_001097577	2.17	7.15E-20	0.69	2.20E-02
ARHGAP26	NM_001135608	2.17	7.16E-06	0.53	3.53E-03
AOX1	NM_001159	2.17	1.12E-03	-0.09	8.10E-01
SLC38A3	NM_006841	2.17	1.66E-03	-0.03	9.84E-01
LOC102723648	XR_001744105	2.17	1.24E-09	0.17	9.18E-01
ELOVL7	NM_001104558	2.16	1.66E-03	0.34	1.58E-01
HID1	NM_030630	2.16	2.50E-08	1.26	1.54E-02
DES	NM_001927	2.15	3.85E-06	0.95	2.12E-02
LOC107983953	XM_006715813	2.15	4.37E-02	-0.46	7.05E-01
JMJD1C-AS1	NR_027182	2.15	4.41E-17	0.22	7.08E-01
LOC101930275	XR_428319	2.15	6.14E-09	-0.20	6.97E-01
TGFB2-AS1	NR_046268	2.15	8.57E-06	0.78	4.80E-01
LOC105374888	XR_926394	2.15	1.09E-06	2.46	9.66E-05
LOC283140	NR_126004	2.14	5.83E-10	0.80	9.13E-05
LOC101927421	NR_109882	2.14	3.61E-02	4.86	8.54E-28
GNG4	NM_001098721	2.14	1.18E-02	-0.35	5.38E-01
GATM	NM_001321015	2.14	2.13E-03	1.11	2.49E-01
GPR155	NM_001033045	2.13	5.99E-39	1.26	4.25E-07

gene symbol	RefSeq ID	2 µM SAHA/ EtOH ctrl		0.5 µM SAHA/ EtOH ctrl	
		log2 fold change	padj	log2 fold change	padj
MKLN1-AS	NR_125364	2.13	5.74E-52	0.79	3.66E-02
NEBL	NM_001173484	2.12	1.32E-04	1.07	1.73E-09
LOC148709	NR_002929	2.12	6.62E-06	1.26	7.57E-02
ARL14EPL	NM_001195581	2.11	3.10E-02	3.50	4.07E-05
LOC105371932	XM_017025492	2.11	2.13E-14	1.04	2.53E-02
LOC105369791	XR_001749167	2.11	2.68E-04	0.47	4.60E-01
LOC107987295	XR_001754961	2.10	2.73E-03	-0.26	7.44E-01
KLHL3	NM_001257194	2.10	4.77E-02	-0.37	6.25E-01
LOC105373428	XR_922797	2.10	2.95E-06	0.95	2.12E-02
LOC100130370	NM_001272086	2.09	1.72E-04	-0.56	6.11E-01
LOC101928424	NR_135053	2.09	3.23E-04	0.88	5.98E-01
MURC	NM_001018116	2.09	8.75E-17	0.39	5.41E-01
BAIAP3	NM_001199096	2.09	2.59E-02	0.62	2.72E-02
LRGUK	NM_144648	2.09	1.03E-06	0.95	2.96E-02
STON1-GTF2A1L	NM_001198593	2.09	3.20E-11	0.21	4.16E-01
ADTRP	NM_001143948	2.08	1.13E-10	1.97	4.93E-13
GPC2	NM_152742	2.08	1.66E-17	0.64	1.83E-02
LURAP1L-AS1	NR_125775	2.08	3.20E-08	0.57	1.46E-02
HOXD8	NM_001199746	2.08	8.68E-08	0.28	4.05E-01
MAPRE3	NM_001303050	2.07	2.93E-20	0.98	3.87E-05
LOC105372353	XR_935896	2.07	2.03E-09	1.16	7.20E-02
PDE5A	NM_001083	2.07	2.20E-19	0.10	6.61E-01
C1QL4	NM_001008223	2.07	2.15E-02	0.15	6.56E-01
KREMEN1	NM_001039570	2.07	1.38E-17	0.19	4.91E-01
SCN1B	NM_001037	2.06	3.46E-13	0.31	4.45E-01
ADAMTS7	NM_014272	2.06	4.50E-10	-0.29	6.70E-01
SPATA6	NM_001286238	2.06	2.75E-19	0.15	6.30E-01
AMZ1	NM_001284355	2.06	1.30E-03	-0.12	9.09E-01
FAM131C	NM_182623	2.06	7.39E-08	0.92	3.23E-01
FKBP1B	NM_001322963	2.06	9.39E-16	-0.26	5.67E-01
LOC105373303	XR_001755938	2.05	7.68E-08	-0.20	8.53E-01
LOC105369165	XR_001739464	2.05	9.65E-03	-0.36	5.86E-01
LOC107985284	XR_001753854	2.05	2.40E-02	0.49	6.57E-01
CLU	NM_001831	2.05	2.89E-07	0.64	1.41E-05
PFKFB1	NM_001271804	2.05	3.22E-07	0.54	5.80E-01
RAP2C-AS1	NR_110410	2.05	5.65E-32	0.59	1.31E-01
CASC11	NR_117101	2.04	1.87E-08	-0.01	9.97E-01
BAIAP2-AS1	NR_026857	2.04	4.72E-24	0.30	2.08E-01
FAM47E	NM_001136570	2.04	1.03E-07	-0.19	8.26E-01
STON1	NM_001198595	2.04	1.78E-09	0.16	5.52E-01
MICAL2	NM_001282663	2.03	4.87E-14	0.58	5.20E-05
GATA5	NM_080473	2.03	1.67E-03	-0.70	6.28E-01
C1ORF228	NM_001145636	2.03	1.89E-06	0.19	8.02E-01
CFL1P1	NR_028492	2.03	1.73E-08	1.50	3.08E-02
UBASH3B	NM_032873	2.02	1.12E-04	0.05	8.72E-01
LOC105370348	XR_931705	2.02	6.00E-07	0.14	9.31E-01
LOC102724623	NR_125826	2.02	5.48E-03	-0.32	4.78E-01
LOC285692	NR_027112	2.02	2.53E-03	-0.04	9.72E-01
LOC105375186	XR_927096	2.02	1.60E-02	0.72	5.96E-01
PTGFR	NM_000959	2.02	2.09E-07	0.03	9.49E-01
LRP1	NM_002332	2.02	3.47E-05	-0.13	5.37E-01
RAB6B	NM_016577	2.00	6.21E-27	0.68	4.69E-03
P4HA3	NM_001288748	2.00	2.98E-09	0.46	4.58E-01
BORCS7-ASMT	NR_037644	-2.00	1.93E-32	-0.75	1.15E-03
MIR4635	NR_039778	-2.01	2.29E-07	-2.03	4.36E-02
GPER1	NM_001039966	-2.02	2.09E-16	-1.20	3.37E-03
PARP10	NM_001317895	-2.03	9.35E-54	-1.17	2.60E-10
KCTD15	NM_001129994	-2.13	7.42E-40	-1.10	1.35E-09
ABHD14A	NM_015407	-2.13	9.33E-19	-0.92	5.61E-02
EMP3	NM_001313905	-2.17	2.79E-37	-0.88	1.49E-08
OLFML3	NM_001286352	-2.17	3.42E-09	-0.56	1.75E-03
PCBD1	NM_000281	-2.17	9.36E-11	-0.71	8.22E-06
C1QTNF6	NM_031910	-2.23	3.48E-80	-0.20	7.18E-01
CTSS	NM_001199739	-2.24	2.93E-04	-0.41	7.52E-01
NDUFB2	NM_004546	-2.27	5.85E-21	-0.40	3.80E-02
FAIM	NM_001033030	-2.37	9.18E-33	-1.15	2.66E-03
DUS3L	NM_001161619	-2.48	9.65E-34	-0.71	2.81E-04
NMI	NM_004688	-2.53	1.56E-22	-1.34	2.25E-06
GTF3C6	NM_138408	-2.53	3.01E-19	-1.42	4.38E-09
SLC16A6	NM_001174166	-2.54	1.79E-39	0.06	9.75E-01
LOC105372233	XR_936223	-2.55	1.32E-29	-0.74	2.44E-01
UFC1	NM_016406	-2.56	3.73E-26	-1.16	2.60E-12
PSMB10	NM_002801	-2.56	1.65E-43	-0.99	1.67E-06
PHF11	NM_001040443	-2.64	1.23E-39	-1.37	4.30E-04
PMF1-BGLAP	NM_001199661	-2.65	1.80E-25	-1.23	8.18E-12
APOL6	NM_030641	-2.69	3.88E-99	-1.38	5.62E-10
PMF1	NM_001199653	-2.73	7.10E-26	-1.25	8.47E-12
AS3MT	NM_020682	-2.84	1.02E-21	-0.30	8.61E-01
IFIT2	NM_001547	-2.93	5.14E-34	0.26	8.25E-01
SLC16A14	NM_152527	-3.10	6.05E-139	0.41	7.33E-01
MYLK3	NM_001308301	-3.20	2.67E-25	0.54	6.88E-01

gene symbol	RefSeq ID	2 µM SAHA/ EtOH ctrl		0.5 µM SAHA/ EtOH ctrl	
		log2 fold change	padj	log2 fold change	padj
ADI1	NM_001306077	-3.26	2.14E-59	-0.92	2.30E-07
DDX60	NM_017631	-3.57	6.87E-63	-0.34	4.07E-01
ISG15	NM_005101	-3.64	8.93E-28	-0.13	7.47E-01
IFIT3	NM_001031683	-3.65	1.99E-49	-0.32	7.10E-01
NUPR1	NM_001042483	-3.84	3.39E-14	-1.06	1.26E-05
OASL	NM_001261825	-4.07	1.37E-22	-1.04	4.29E-04
IFI44	NM_006417	-4.30	1.11E-41	0.02	9.86E-01

Suppl. table S7. DESeq results of ASF1 depleted HeLa LT cells treated with SAHA. 501 up- and 35 downregulated genes with a log2 fold change (l2fc) <-2.0 or >2.0 for 2 µM SAHA over EtOH ctrl were identified, while the l2fc of 0.5 µM SAHA over EtOH ctrl was either not statistical significant or in the same direction. The adjusted p-value was set to padj<0.05 and genes with an RPKM >1 in the highest expressed sample were selected for this table. Genes were sorted by l2fc (2 µM SAHA over EtOH ctrl). Those genes implemented in the *TelNet* database were marked in bold, genes reported to be cell cycle-regulated in HeLa cells (Grant *et al.*, 2013) were marked with a °circle.

Suppl. table S8. DESeq results of type II survivor formation in budding yeast.

gene symbol	RefSeq ID	log2 fold change	padj
YER078W-A	NM_001184548	3.47	2.56E-04
YPL185W	NC_001148	2.82	1.55E-03
YLR101C	NC_001144	2.18	1.29E-02
YPR108W-A	NM_001184581	2.05	6.77E-03
YER079W	NM_001178970	1.80	1.53E-03
YER158W-A	-	1.79	1.32E-04
ALD6	NM_001183875	1.21	1.25E-08
PGM2	NM_001182605	1.05	4.54E-03
YFR052C-A	-	1.03	3.39E-02
VID24	NM_001178453	0.98	8.44E-03
YLR108C	NM_001181995	0.97	5.83E-03
ALD4	NM_001183794	0.92	3.64E-03
TIR1	NM_001178902	-0.92	2.31E-05
ARN2	NM_001179127	-0.99	1.15E-07
FIT3	NM_001183803	-1.00	4.35E-08
TPO2	NM_001181267	-1.02	8.44E-03
FRE4	NM_001183237	-1.07	4.49E-02
FIT2	NM_001183802	-1.14	2.54E-10
YMR013W-A	NC_001145	-1.22	1.15E-12
YAL037W	NM_001178182	-1.31	3.41E-03
EDS1	NM_001178381	-1.32	1.38E-02
YJL047C-A	NM_001184635	-1.37	2.83E-13
COS12	NM_001181129	-1.42	5.83E-03
YBR113W	NC_001134	-1.93	2.56E-02
FIT1	NM_001180842	-1.95	2.65E-14
YMR317W	NM_001182830	-2.10	8.79E-09
YGR270C-A	-	-4.34	1.51E-04

The table shows significantly deregulated genes with a log2 fold change <-0.9 or >0.9 and padj <0.05. Genes were sorted by log2 fold change. Those genes implemented in the *TelNet* database were marked in bold.

Danksagung

Ich möchte allen danken, die mich während der Zeit der Doktorarbeit begleitet und unterstützt haben.

Ganz besonders gilt dieser Dank Prof. Dr. Karsten Rippe für die Betreuung der Arbeit als Doktorvater und Erstgutachter, für den anhaltenden Optimismus, für kontinuierliche Motivation und umfassende Unterstützung in jeglicher Hinsicht. Vielen Dank für Deine Geduld, für Deine Zeit und Mühen.

Ein besonderer Dank geht auch an Prof. Dr. Brian Luke für die Übernahme des Zweitgutachters, die Teilnahme an meinen TAC-Meetings, für hilfreiche Diskussionen mit viel Enthusiasmus.

Herzlichen Dank an Prof. Dr. Ursula Kummer und Prof. Harald Herrmann-Lerdon für die Bereitschaft, Teil meiner Prüfungskommission zu sein und insbesondere Prof. Dr. Ursula Kummer für die Übernahme des Prüfungsvorsitzes.

Vielen Dank auch an Prof. Dr. Christoph Plass für das Interesse an meiner Arbeit und die hilfreiche Teilnahme an meinen TAC-Meetings.

Ein großer Dank geht an alle Mitarbeiter der DKFZ und Bioquant Core Facilities sowie an unsere Partnergruppen, insbesondere an Dr. Felix Bestvater, Dr. Steffen Schmitt Dr. Markus Eich, Dr. Rainer Will, Dr. Stephan Wolf, Dr. Angela Schulz, Dr. Holger Erfle, Dr. Manuel Gunkel, Dr. Thomas Höfer, Dr. Andres Florez, PD Dr. Karl Rohr, Dr. Stefan Wörz, Yu Qiang, Dr. Sharib Ali, Lina Sieverling, Rainer König und Bettina Balk für die Bereitstellung von Geräten und Mikroskopen, für fachliche Diskussionen und für die gute Zusammenarbeit.

Ich möchte der Studienstiftung des deutschen Volkes, der Graduiertenschule des DKFZ (Helmholtz International Graduate School) und dem Bundesministerium für Bildung und Forschung (BMBF) für die Finanzierung meiner Arbeit danken.

Ein riesiger Dank geht an die Leitung der Kindertagesstätte, *Die Wichtel*, und Erzieherinnen der blauen Gruppe insbesondere Alessandra Monti Kost, Rosalinda Usselmann, Lisa Stephan, Margarete Götz, Gudrun Lange-Hahn, Sabina Jaehnke, Melis Tepeli, Tabea Poerting, Caro Sauter, Carolin Heck und Sascha Dreßel für die umfassende Betreuung meiner Tochter in einer unglaublich vertrauensvollen Umgebung, die die Fortführung meiner Arbeit erst ermöglicht haben.

Herzlichen Dank an alle ehemaligen und aktuellen Kollegen in der Arbeitsgruppe Rippe für eine lockere Atmosphäre, für die allgemeine Hilfsbereitschaft, für die rege Beteiligung an fachlichen Diskussionen,

für lustige Cocktail-Abende, gemeinsame Kaffee-Pausen und für viele, viele Kuchen. Ein großer Dank geht an Katha und Sarah für die Einführung in die Welt der Telomere. Vielen lieben Dank an Caro für die unersetzliche Hilfe bei meinen Experimenten, insbesondere im letzten Jahr. Herzlichen Dank an Fabian für die geduldige Erörterung aller kleinen und großen Fragen. Ich danke Armin, Alexandra und ganz besonders Inn für das kritische Lesen dieser Arbeit! Vielen Dank an Nick und Sofie für die Unterstützung bei Computer- und Clusterproblemen sowie bei der Bearbeitung von allerlei Formularen und Regularien. Danke auch an Markus, Lara, Lukas, Sabrina, Verena, Kathi, Anne, Maïwen, Philipp, Jana Mo, Jana He, Jana Tü, Jorge, Teresa, Katharina, Andre, Nathalie und Michael. Cheers!

Meinen lieben Dank an meine Freunde, die mich auf dem Weg der Promotion moralisch begleitet und unterstützt haben. Vielen Dank für motivierende Worte, Ablenkungen in den richtigen Momenten, alle Aufmunterungen, für lange Telefonate und offene Ohren.

Das größte Dankeschön allerdings geht an meine Familie, für die immerwährende Unterstützung. Insbesondere meiner Mutter bin ich sehr dankbar für ihre verständnisvolle Art und den fortwährenden Rückhalt. Meiner Tochter Lina danke ich für ihre Frohnatur und positive Energie. Mein aufrichtigster Dank geht an Philipp, für einfach Alles! Ohne Dich wäre ich jetzt nicht an diesem Punkt meines Lebens. Danke, dass Du immer für mich da bist, auch in Phasen der Frustration. Danke, dass Du immer an mich geglaubt hast und mir den Rücken freigehalten hast, ganz besonders in letzter Zeit.

Vielen Dank!